การเตรียมและความเป็นพิษต่อเซลล์ของอนุพันธ์เอ็กเทนาสซิดิน 770 จากเพรียงหัวหอม *Ecteinascindia thurstoni* ของไทย

นายวิทยา โล้วตั้งกิจเจริญ

วิทยานิพนธ์นี้เป็นส่วนหนึ่งของการศึกษาตามหลักสูตรปริญญาเภสัชศาสตรมหาบัณฑิต
สาขาวิชาเภสัชเวท ภาควิชาเภสัชเวทและเภสัชพฤกษศาสตร์
คณะเภสัชศาสตร์ จุฬาลงกรณ์มหาวิทยาลัย
ปีการศึกษา 2556
ลิขสิทธิ์ของจุฬาลงกรณ์มหาวิทยาลัย

PREPARATION AND CYTOTOXICITY OF ECTEINASCIDIN 770 DERIVATIVES FROM THE THAI TUNICATE *ECTEINASCIDIA THURSTONI*

Mr. Witaya Lowtangkitcharoen

A Thesis Submitted in Partial Fulfillment of the Requirements
for the Degree of Master of Science in Pharmacy Program in Pharmacognosy
Department of Pharmacognosy and Pharmaceutical Botany
Faculty of Pharmaceutical Sciences
Chulalongkorn University
Academic Year 2013

Thesis Title	PREPARATION AND CYTOTOXICITY OF ECTEINASCIDIN 770 DERIVATIVES FROM THE THAI TUNICATE *ECTEINASCIDIA THURSTONI*
By	Mr. Witaya Lowtangkitcharoen
Field of Study	Pharmacognosy
Thesis Advisor	Khanit Suwanborirux, Ph.D.
Thesis Co-Advisor	Assistant Professor Taksina Chuanasa, Ph.D.

Accepted by the Faculty of Pharmaceutical Sciences, Chulalongkorn University in Partial Fulfillment of the Requirements for the Master's Degree

.....Dean of the Faculty of Pharmaceutical Sciences

(Assistant Professor Rungpetch Sakulbumrungsil, Ph.D.)

THESIS COMMITTEE

.....Chairman

(Professor Kittisak Likhitwitayawuid, Ph.D.)

.....Thesis Advisor

(Khanit Suwanborirux, Ph.D.)

.....Thesis Co-Advisor

(Assistant Professor Taksina Chuanasa, Ph.D.)

.....Examiner

(Supakarn Chamni, Ph.D.)

.....Examiner

(Assistant Professor Pithi Chanvorachote, Ph.D.)

.....External Examiner

(Ploenthip Puthongking, Ph.D.)

วิทยา โล้วตั้งกิจเจริญ : การเตรียมและความเป็นพิษต่อเซลล์ของอนุพันธ์เอ็กเทนาสซิดิน 770 จากเพรียงหัวหอม *Ecteinascindia thurstoni* ของไทย. (PREPARATION AND CYTOTOXICITY OF ECTEINASCIDIN 770 DERIVATIVES FROM THE THAI TUNICATE *ECTEINASCIDIA THURSTONI*) อ.ที่ปรึกษาวิทยานิพนธ์หลัก: อ. ดร.คณิต สุวรรณบริรักษ์, อ.ที่ปรึกษาวิทยานิพนธ์ร่วม: ผศ. ดร.ทักษิณา ชวนอาษา, 167 หน้า.

สารเอ็กเทนาสซิดิน 743 (Et 743) เป็นแอลคาลอยด์ในกลุ่มทริสเตตราไฮโดรไอโซควิโนลิน ที่แยกได้จากเพรียงหัวหอมในทะเลแคริบเบียนชนิด *Ecteinascidia turbinata* สารชนิดนี้ได้รับการอนุมัติจาก European Medicines Agency เพื่อใช้เป็นยาบำบัดโรคมะเร็งเนื้อเยื่ออ่อนและมะเร็งรังไข่ที่กลับมาเป็นซ้ำ ต่อมาได้มีการแยกสารเอ็กเทนาสซิดิน 770 (Et 770) ซึ่งเป็นสารเสถียรในปริมาณสูงจากเพรียงหัวหอมในไทยชนิด *E. thurstoni* โดยการเติมโพแทสเซียมไซยาไนด์ ก่อนกระบวนการสกัดแยกสาร ในการศึกษาครั้งนี้ได้ปรับปรุงความเป็นพิษต่อเซลล์มะเร็งของสาร Et 770 โดยมุ่งเน้นการดัดแปลงโครงสร้างทางเคมี ที่ตำแหน่ง 2'-*N* ของ C-subunit ของสาร Et 770 ผ่านสารมัธยันตร์ 18,6'-*O*-bisallyl Et 770 ทำให้สามารถเตรียมอนุพันธ์ 2'-*N*-acyl Et 770 ได้ทั้งสิ้น ๙ ชนิด และนำไปประเมินความเป็นพิษต่อเซลล์มะเร็ง ๓ ชนิด ได้แก่ เซลล์มะเร็งลำไส้ใหญ่ HCT116 เซลล์มะเร็งปอด QG56 และ เซลล์มะเร็งต่อมลูกหมาก DU145 พบว่าอนุพันธ์เหล่านี้มีความเป็นพิษต่อเซลล์สูงมาก มีค่า IC_{50} ที่ความเข้มข้นระดับนาโนโมลาร์ โดยสาร 2'-*N*-(4"-fluorocinnamoyl) Et 770 เป็นสารที่มีความเป็นพิษต่อเซลล์สูงที่สุดในกลุ่มสารอนุพันธ์ที่เตรียมได้ โดยมีความเป็นพิษต่อเซลล์มะเร็งลำไส้ใหญ่ HCT116 มากกว่าสารตั้งต้น Et 770 ประมาณ ๗๐ เท่า สารอนุพันธ์ใหม่ชนิดนี้จึงมีความน่าสนใจในการพัฒนาเป็นสารต้านเซลล์มะเร็งในลำดับถัดไป

ภาควิชา	เภสัชเวทและเภสัชพฤกษศาสตร์	ลายมือชื่อนิสิต .....
สาขาวิชา	เภสัชเวท	ลายมือชื่อ อ.ที่ปรึกษาวิทยานิพนธ์หลัก .....
ปีการศึกษา	2556	ลายมือชื่อ อ.ที่ปรึกษาวิทยานิพนธ์ร่วม .....

5476245833 : MAJOR PHARMACOGNOSY
KEYWORDS: ECTEINASCIDIN 770 / ECTEINASCIDIA THURSTONI / 2'-N-ACYL DERIVATIVES / CYTOTOXICITY

WITAYA LOWTANGKITCHAROEN: PREPARATION AND CYTOTOXICITY OF ECTEINASCIDIN 770 DERIVATIVES FROM THE THAI TUNICATE *ECTEINASCIDIA THURSTONI*. ADVISOR: KHANIT SUWANBORIRUX, Ph.D., CO-ADVISOR: ASST. PROF. TAKSINA CHUANASA, Ph.D., 167 pp.

Ecteinascidin 743 (Et 743), a *tris*-tetrahydroisoquinoline alkaloid isolated from the Caribbean tunicate *Ecteinascidia turbinata*, has been approved by European Medicines Agency as a new anticancer drug for the patients with soft tissue sarcoma and relapsed ovarian cancer. The stabilized ecteinascidin 770 (Et 770) was recently isolated in large yield from the Thai tunicate *E. thurstoni* by pretreatment with potassium cyanide. To improve the cytotoxicity of Et 770, the chemical modification has been particularly focused at the 2'-*N* position on the C-subunit of Et 770. Nine new 2'-*N*-acyl Et 770 derivatives were prepared from Et 770 *via* the intermediate 18,6'-*O*-bisallyl Et 770 in acceptable yields. The synthesized derivatives were evaluated for cytotoxicity against three human solid carcinoma cell lines, including colorectal carcinoma (HCT116), human lung carcinoma (QG56), and human prostate carcinoma (DU145) cell lines and exhibited excellent cytotoxicity with IC_{50} at nanomolar concentrations. Among them, 2'-*N*-(4''-fluorocinnamoyl) Et 770 displayed the most potent cytotoxicity with approximately 70-fold higher potency to HCT116 than the parent Et 770. Therefore, this new derivative is a promising lead for further development as a new anticancer agent.

Department:	Pharmacognosy and Pharmaceutical Botany	Student's Signature .....
		Advisor's Signature .....
Field of Study:	Pharmacognosy	Co-Advisor's Signature .....
Academic Year:	2013	

ACKNOWLEDGEMENTS

I would like to express my appreciation to my thesis advisor, Dr.Khanit Suwanborirux, and my thesis co-advisor, Assistant Professor Dr.Taksina Chuanasa, for their valuable advices, continual guidance, kindness, and understanding throughout this research study.

I would like to acknowledge Professor Dr.Naoki Saito of Meiji Pharmaceutical University, Japan for supporting my research in Japan and I am appreciated for his helpful discussions and suggestions.

I would like to thank all of my thesis committee, for their valuable suggestions and discussions.

I would like to thank the Pharmaceutical Research Instrument Center, Faculty of Pharmaceutical Sciences, Chulalongkorn University and the Analytical Center, Meiji Pharmaceutical University for supporting research facilities. I am grateful to the Phuket Marine Biological Center (PMBC) for supporting the SCUBA equipment. I would like to thank Dr.Nobuo Shimma of Chugai Pharmaceutical Company Research Center for conducting cytotoxicity assay.

I would like to thank all staff members of the Department of Pharmacognosy and Pharmaceutical Botany, Faculty of Pharmaceutical Sciences, Chulalongkorn University, for assistance in research facilities.

I am grateful to Mr. Mitsuhiro Tsujimoto, Miss Nanae Mori, Miss Punyisa Ngankaranatikarn, and all my friends at Chulalongkorn University and Meiji Pharmaceutical University who have shared happy time together.

Finally, I would like to express my special and deepest appreciation to my family for their love, understanding and encouragement.

CONTENTS

Page

LIST OF TABLES

PAGE

LIST OF FIGURES

PAGE

LIST OF SCHEMES

PAGE

ABBREVIATIONS AND SYMBOLS

%	= Percentage
$[M+H]^+$	= Pseudomolecular ion or protonated molecular ion
$[\alpha]_D^t$	= Specific rotation at t °C and Sodium D line (589 nm)
µg	= Microgram
µl	= Microliter
^{13}C NMR	= Carbon-13 Nuclear Magnetic Resonance
^{1}H NMR	= Proton Nuclear Magnetic Resonance
$^{1}H,^{1}H$ COSY	= Homonuclear (Proton-Proton) Correlation Spectroscopy
2D NMR	= Two Dimentional Nuclear Magnetic Resonance
A	= Adenine
A375	= Human malignant melanoma
A549	= Human lung adenocarcinoma
AcOH	= Acetic acid
br	= Broad (for NMR spectra)
C	= Cytosine
calcd	= Calculated
CC	= Column chromatography
CD	= Circular dichroism
$CDCl_3$	= Deuterated chloroform
CH_2Cl_2	= Dichloromethane
$CHCl_3$	= Chloroform
cm	= Centimeter
cm^{-1}	= Reciprocal centimeter (unit of wave number)
d	= Doublet (for NMR spectra)

dd = Double doublets, doublet of doublets (for NMR spectra)

dq = Double quartets, doublet of quartets (for NMR spectra)

dt = Double triplets, doublet of triplets (for NMR spectra)

DEPT = Distortionless Enhancement by Polarization Transfer

DMAP = *N*,*N*-4-Dimethylaminopyridine

DNA = Deoxyribose Nucleic Acid

DU145 = Human prostate carcinoma

e.g. = exempli gratia (for example)

eq = Equivalent

et. al. = Et alia (and other)

EtOAc = Ethyl acetate

eV = Electron volt

ε = Molar absorptivity

FABMS = Fast Atom Bombardment Mass Spectrometry

FT-IR = Fourier Transform Infrared

g = Gram

G = Guanine

HCT116 = Human colorectal carcinoma cell line

HMBC = ^{1}H-detected Heteronuclear Multiple Bond Correlation

HR = High Resolution

hr. = Hour

HSQC = Heteronuclear Single Quantum Coherence

Hz = Hertz

IC_{50} = Median inhibitory concentration

IR = Infrared

J	= Coupling constant
KBr	= Potassium bromide
kg	= Kilogram
l	= Liter
m	= Multiplet (for NMR spectra)
m/z	= Mass to charge ratio
MeOH	= Methanol
mg	= Milligram
MHz	= Mega Hertz
ml	= Milliliter
mM	= Millimolar
MS	= Mass spectrum
NER	= Nucleotide Excision Repair
nM	= Nanomolar
nm	= Nanometer
NMR	= Nuclear Magnetic Resonance
No.	= Number
NOESY	= Nuclear Overhauser Enhancement Spectroscopy
NRPS	= Nonribosomal Peptide Synthetase
°C	= Degree Celsius
PC-3	= Human prostate carcinoma
ppm	= Part per million
q	= Quartet (for NMR spectra)
QG56	= Human lung carcinoma
ROESY	= Rotating Frame Nuclear Overhauser Effect Spectroscopy

s	= Singlet (for NMR spectra)
sp.	= Species
T	= Thymidine
t	= Triplet (for NMR spectra)
td	= Triplet of doublets (for NMR spectra)
TC-NER	= Transcription-Coupled Nucleotide Excision Repair
TLC	= Thin Layer Chromatography
UV	= Ultraviolet
wt	= Weight
XPG	= Xeroderma Pigmentosum Complementation Group G
α	= Alpha
β	= Beta
δ	= Chemical shift

CHAPTER I

INTRODUCTION

For several decades, marine organisms have been known as a new source of anticancer drugs. One of them, ecteinascidin 743 (Et 743, **1**, Figure 1), a *tris*-tetrahydroisoquinoline alkaloid isolated from the Caribbean tunicate *Ecteinascidia turbinata* (Rinehart *et al.,* 1990), is the anticancer drug which has been approved by European Medicines Agency (EMA) for using in the patients with relapsed ovarian cancer (EMA, 2004) and advanced soft tissue sarcoma (EMA, 2007) under the trade name Yondelis® (Trabectedin).

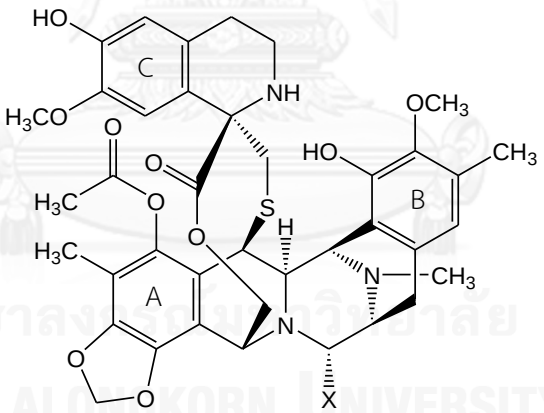

Et 743 **(1)**: X = OH
Et 770 **(2)**: X = CN

Figure 1. Chemical structures of the ecteinascidins.

The chemical structure of Et 743 consists of 3 subunits of tetrahydroisoquinoline (A-, B- and C-subunits) and an α-carbinolamine functional group. The core chemical structure of Et 743 (A- and B-subunits) is closely related to

the tetrahydroisoquinoline natural product antitumor agents such as saframysins (Arai *et al*., 1977; Yazawa *et al*., 1982; Lown *et al*., 1983), safracins (Ikeda *et al*., 1983), renieramycins (Frinke *et al*., 1982; Davidson, 1992; Suwanborirux *et al*., 2003; Amnouypol *et al*., 2004), and jorumycin (Fontana *et al*., 2000) as shown in Figure 2.

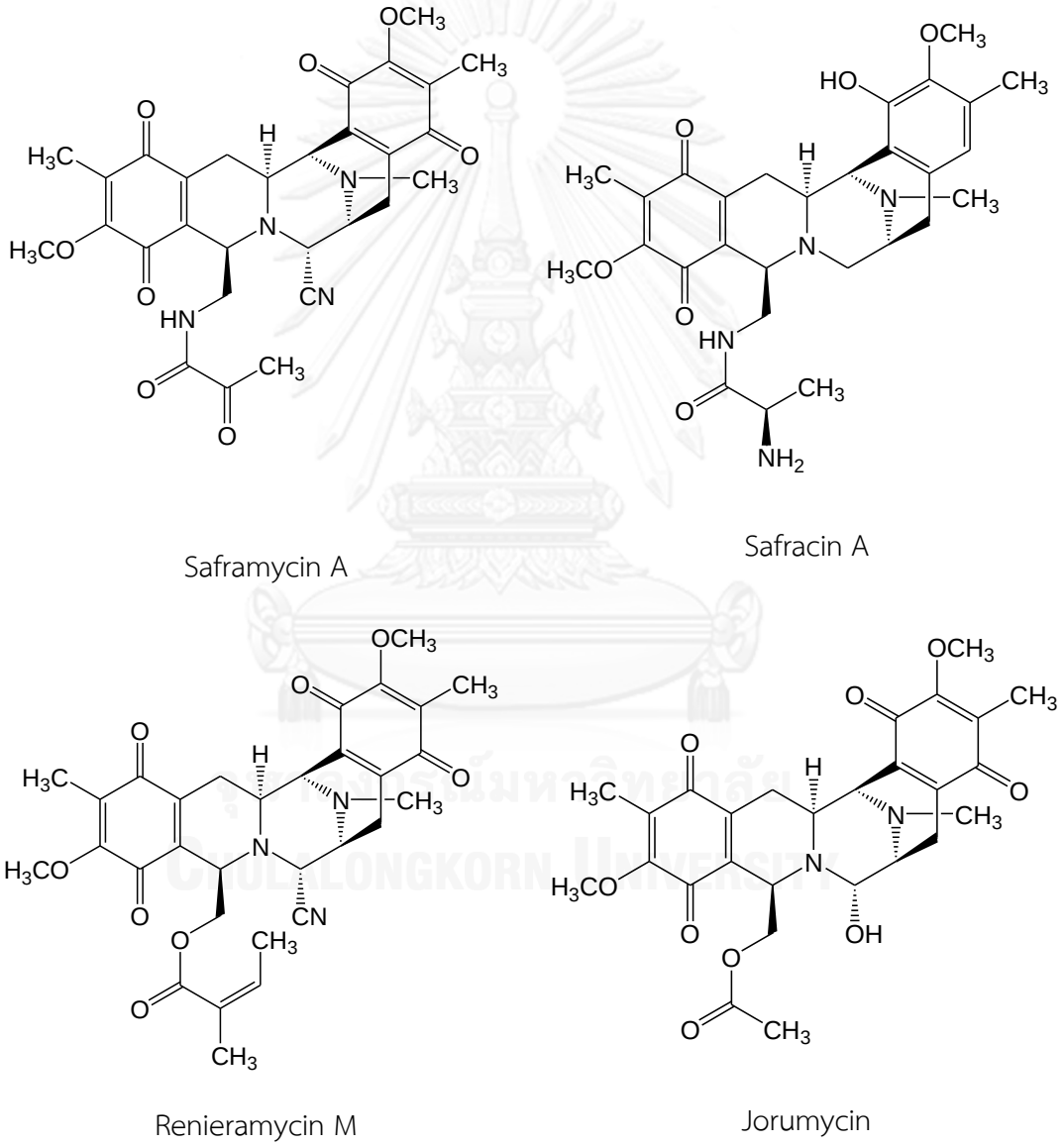

Figure 2. Representatives of the tetrahydroisoquinoline antitumor agents.

Et 743 inhibits cancer cells by DNA sequence-selective alkylation between the α-carbinolamine group and the exocyclic 2-amino (*N*2) group of guanine (G) base in the duplex DNA minor groove (Pommier *et al.,* 1996). The formation of Et 743-DNA adducts bends the DNA structure towards the major groove opposite to the adducts located in the minor groove (Zewail-Foote and Hurley 1999). The NMR-based studies of the Et 743 and DNA interaction have shown that the A-, B-subunits and α-carbinolamine group are sequence binding recognition (Moore *et al*., 1997; Seaman *et al*., 1998). Interestingly, the C-subunit, which is perpendicular to the A-, B-subunits and protrudes from the duplex DNA binding sites (Sakai *et al*., 1992; Moore *et al*., 1997; Seaman *et al*., 1998). The C-subunit might be related to its binding affinity between the DNA and Et 743 (David-Cordonnier *et al.,* 2005) and interaction with different DNA-binding proteins located in the DNA adduct area, possibly the xeroderma pigmentosum complementation group G (XPG), a member of the Nucleotide Excision Repair (NER) system (Takebayashi *et al*., 2001; Herrero *et al*., 2006; Guirouilh-Barbat *et al*., 2009). The α-carbinolamine group is not only structurally crucial for the DNA-alkylation but also causing the compound unstabiliy. Suwanborirux group succeeded in isolating a large amount of the stable ecteinascidin 770 (Et 770, **2**, Figure 1) from the Thai tunicate *E. thurstoni* by pretreatment with potassium cyanide before the extraction process (Suwanborirux *et al.,* 2002). To improve its cytotoxicity, the chemical modification of Et 770 has been focused. The first modification, the synthesis of 6'-*O*-acyl Et 770 derivatives, showed not much different cytotoxicity from the parent compound. However, the serendipitous discovery of 2'-*N*-(indole-3-carbonyl) Et 770 expressed 2-6 times higher cytotoxicity in various cancer cell lines (Puthongking *et al*., 2006). The next modification, the

preparation of new 2'-*N*-acyl Et 770 derivatives was investigated based on a three-step transformation including: a) 18,6'-*O*-bisallyl protection, b) 2'-*N*-acylation, and c) removing of the allyl protecting group (Figure 3, Saktrakulkla *et al*., 2011). Most of them showed potent cytotoxicity on human solid tumor cell lines. It was found that the nitrogen-containing heterocyclic and cinnamoyl derivatives showed 10 times higher cytotoxicity than Et 770 (Saktrakulkla *et al.,* 2011).

The previous studies showed that the modification at 2'-*N* position significantly improved cytotoxicity compared to the parent compound Et 770. This study aims to investigate additional 2'-*N*-acyl Et 770 derivatives by using new acyl groups containing high electronegative element, naphthoyl or fluorocinnamoyl moieties. Ten proposed 2'-*N*-acyl Et 770 derivatives are summarized in Table 1.

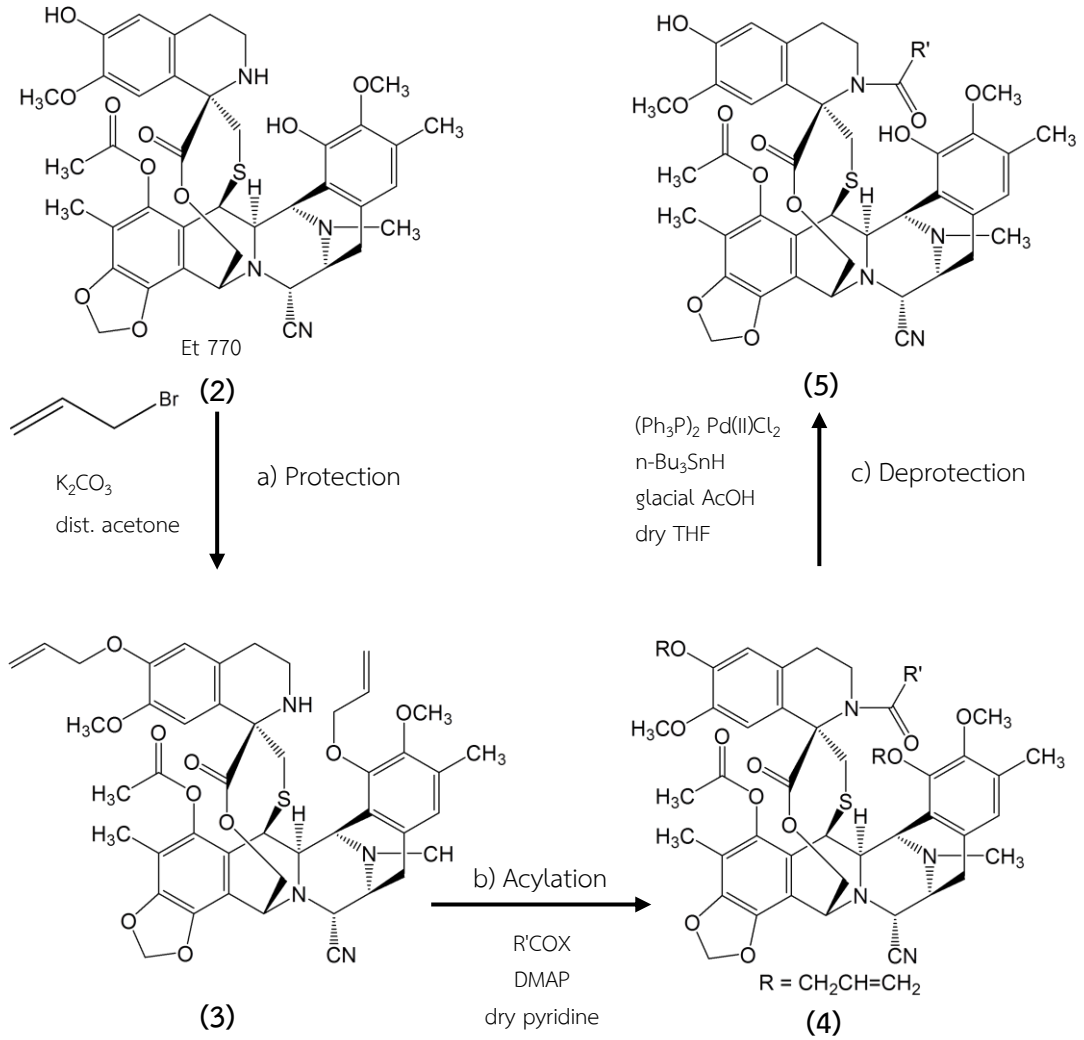

Figure 3. The three-step transformation for preparation of 2'-*N*-acyl Et 770 derivatives.

Table 1. Chemical structures of 2'-*N*-acyl Et 770 derivatives prepared in this study.

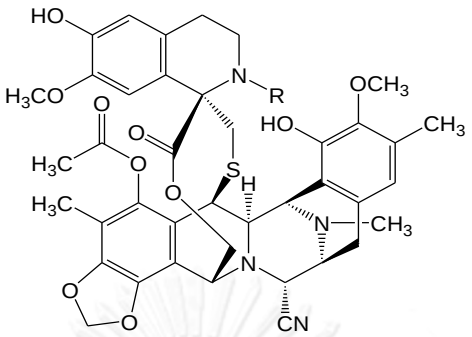

Compounds	R	Compounds	R
5a	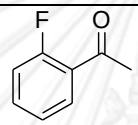	5f	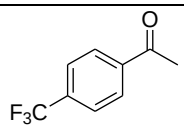
5b	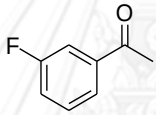	5g	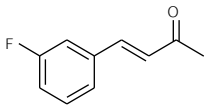
5c	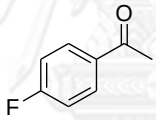	5h	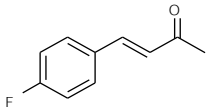
5d	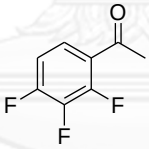	5i	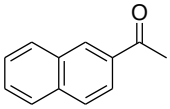
5e	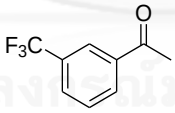	5j	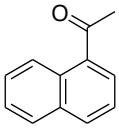

CHAPTER II

LITERATURE REVIEW

1. Characteristics of Tunicates

Tunicates are marine animals classified in the phylum Chordata, subphylum Urochordata. The most familiar tunicates are sea squirts or ascidians (class Ascidiacea). The tunicates are fouling organisms attached to hard surfaces, or anchored in soft sediments. The sac-like soft body is surrounded by a thick test, or tunic, often transparent or translucent and varying in consistency from gelatinous to leathery. The tunic, for which the tunicates are named, is secreted by the body wall of the adult animal and is composed of cellulose, an almost unique occurrence of that material in the animal kingdom. The tunicates are filter feeders by using a ciliated, sieve-like sac to filter water typically flowing through the mouth, or incurrent siphon. Food is filtered from water and passed into a U-shaped gut. Filtered water is expelled through a second opening, the excurrent siphon. Nearly all species reproduce sexually and are hermaphroditic. The tunicates produce eggs in the oviduct and release the free-swimming tadpole larvae from the atrium. Tadpole larvae clearly display the fundamental chordate characters of gill slits, a dorsal nerve cord, a notochord, and a well-developed post-anal tail. They also have an eye. Tadpole larvae do not feed but only swim to find a suitable surface on which to settle and undergo a drastic metamorphosis into the adult form. Some tunicates asexually reproduce by budding to colonies, joined at their bases by slender stolons

or embedded in a common tunic material (Brusca and Brusca, 2003; Castro and Huber, 2013).

Figure 4. A Photograph of the tunicate *Ecteinascidia thurstoni*.

The collected Thai tunicate in this work was identified by Dr.Teruaki Nishikawa of Nagoya University Museum as *Ecteinascidia thurstoni* Herdman, 1981 (Figure 4) and the taxa of this genus was given by Kott (2003) as follows.

Kingdom: Animalia

Phylum: Chordata

Subphylum: Urochodata

Class: Ascidiaces

Order: Phlebobrancia

Family: Perophoridae

Genus: Ecteinascidia

Species: *Ecteinascidia thurstoni* Herdman, 1981

2. Anticancer Agents from Marine Tunicates

Many anticancer agents derived from marine organisms were evaluated in Phase I, II, and III clinical studies for example dolastatin-10 from sea hare *Dolabella* sp. (Margolin *et al*., 2002) and bryostatin-1 from bryozoans *Bugula neritina* (Haas *et al*., 2003). Among them, the cytotoxic agents produced by the tunicates have reached clinical trials as antitumor agents included didemnin B (**6**), aplidine (**7**), and Et 743 (**1**).

Didemnin B (**6**, Figure 5) is a cyclic depsipeptide isolated from the tunicate *Trididemnum solidum* (Rinehart *et al*., 1987). It has shown impressive antitumor activity in human tumor models *in vitro* as well as in tumors growing in athymic mice (Geldof *et al*., 1999). Detailed mechanistic study revealed that didemnin B inhibits the synthesis of RNA, DNA and it binds non-competitively to palmitoyl protein thioesterase (Vera and Joullie, 2002). The impressive *in vitro* and *in vivo* biological activities of the didemnins resulted in the first human clinical trials in the U.S. of a marine natural product against cancer. Consequently, didemnin B was submitted to several Phase I and Phase II clinical trials against previously treated non-small cell lung cancer (Shin *et al*., 1991), breast cancer (Benvenuto *et al*., 1992), small-cell lung cancer (Shin *et al*., 1994), non-Hodgkin's lymphoma (Goss *et al*., 1995; Kucuk *et al*., 2000) and metastatic melanoma (Hochster *et al*., 1999).

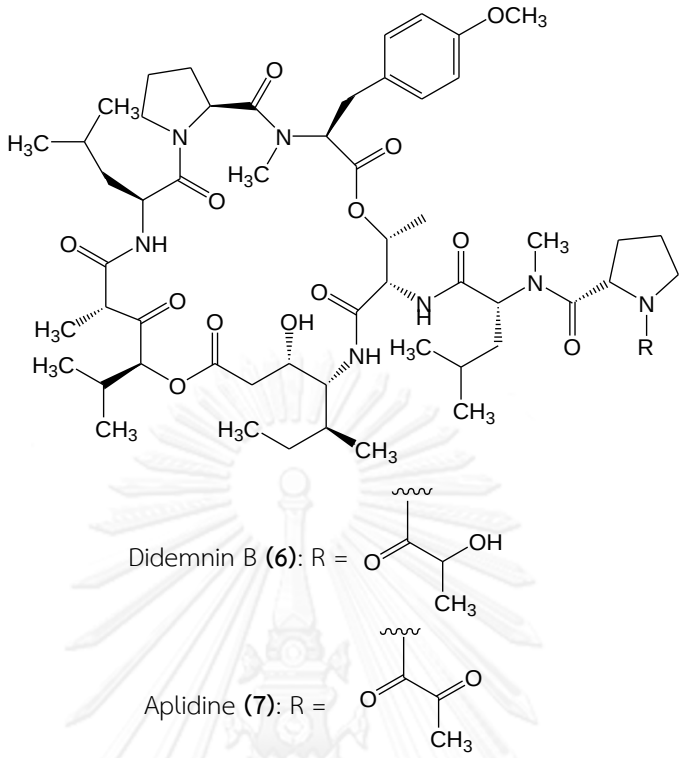

Figure 5. Structures of didemnin B and aplidine.

Another depsipeptide, aplidine (dehydrodidemnin B, **7**, Figure 5) was isolated from the tunicate *Aplidium albicans* (Schmitz and Yasumoto, 1991) and contained the same amino acids building block as didemnin B, but its molecular formula differs from that of didemnin B by 2 hydrogen atoms, indicating the replacement of the lactic acid side chain of didemnin B by the pyruvyl side chain in aplidine. Aplidine was proved to be a fovourable substitute for didemnin B, since it appeared to be less toxic and even more effective than didemnin B, with a broad spectrum of activity both *in vitro* and *in vivo* against various tumor types (Urdiales *et al*., 1996; Rinehart, 2000; Lobo *et al*., 1997). Mechanistic study of aplidine revealed that it interferes the synthesis of DNA, proteins and induces G1–G2 cell cycle arrest (Erba *et al*., 2002). Aplidine exhibited cytotoxicity by inhibition of the ornithine decarboxylase,

which is an enzyme that critical in the process of tumor formation and growth and angiogenesis. Furthermore, it inhibited the expression of the vascular endothelial growth factor gene, having antiangiogenic effects (Taraboletti *et al*., 2004). On the basis of promising pre-clinical data aplidine entered into phase I clinical trials in Spain, Canada, UK, and France for the treatment of solid tumors, and non-Hodgkin's lymphoma (Rinehart, 2000; Maroun *et al*., 2006; Armand *et al*., 2001; Cuadrado *et al*., 2003). Recently this compound entered into Phase II clinical trials in patients with metastatic non-cell lung carcinoma (Peschel *et al*., 2007), unresectable advanced renal cell carcinoma (Schoffski *et al*., 2009), relapsed/refractory non-Hodgkin's lymphoma (Ribrag *et al*., 2013), and advanced melanoma (Plummer *et al*., 2013).

3. The Tetrahydroisoquinoline Antitumor Agents

Several naturally occurring tetrahydroisoquinolines have been isolated from actinomycetes and marine organisms such as sponges, nudibranchs and tunicates. The basic structure of tetrahydroisoquinoline compounds is structurally characterized by the presence of the tetrahydroisoquinoline ring system which fused, varied with oxidation states, substitution patterns and additional fragments to distinguish several subfamilies of natural products. Tetrahydroisoquinoline compounds exhibited potent cytotoxic activities, for example (Figure 6) cyanocycline A (Hill *et al*., 1991), quinocarcin (Tomita *et al*., 1984; Katoh and Terashima, 1996), saframycin A (Arai *et al*., 1980), renieramycin M (Halim *et al*., 2011), jorumycin (Fontana *et al*., 2000), and ecteinascidin 743 (Powan *et al*., 2013). Among them, ecteinascidin 743 displayed promising anticancer drug property in nanomolar concentration (Rinehart *et al*., 2000; Jimeno *et al*., 2004; Powan *et al*., 2013) and is now authorized in the European

Union as for the treatment of patients with relapsed ovarian cancer (EMA, 2004) and advanced soft tissue sarcoma (EMA, 2007).

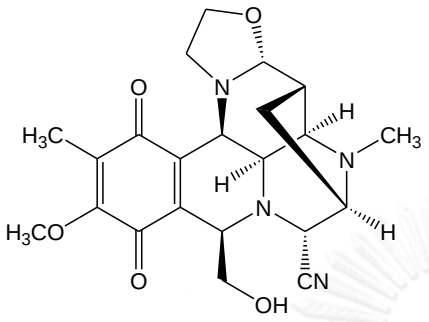

Cyanocycline A

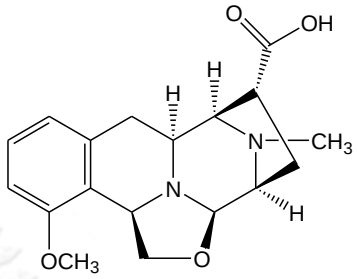

Quinocarcin

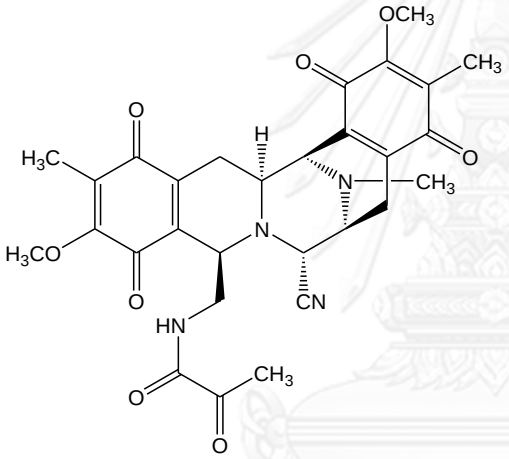

Saframycin A

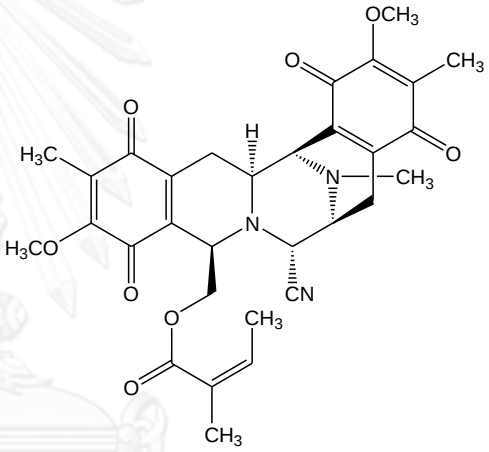

Renieramycin M

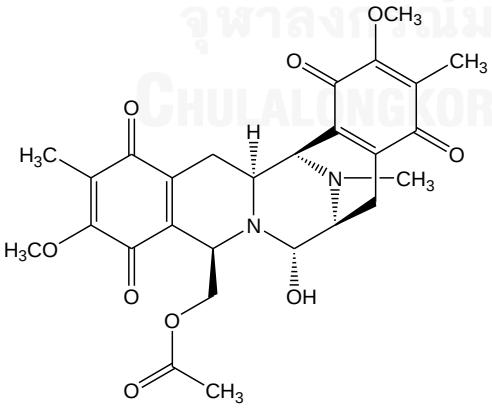

Jorumycin

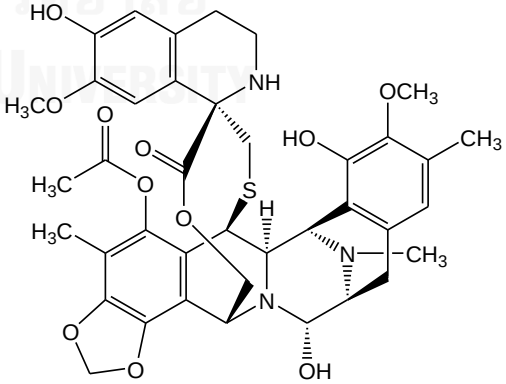

Ecteinascidin 743

Figure 6. Structures of representative tetrahydroisoquinoline antitumor agents.

4. Isolation and Structure Determination of the Ecteinascidins

The first isolation and structural characterization of six new chemical entities called ecteinascidins (Ets) 729, 743, 745, 759A, 759B and 770 was reported by the Rinehart group in 1990 from *Ecteinascidia turbinata*, a tunicate found in the Caribbean Sea, of which Et 743 was the most abundant representative (0.0001% yield). The structures of Ets 729 and 743 with the relative stereochemistry were elucidated later by Rinehart (1990) and Wright (1990) groups. In 1992, Rinehart *et al*. reported the structures of Ets 722, 736, and 734 N12-oxide, later in 1996, four putative biosynthetic precursors, Ets 594, 596, 597 and 583, were also isolated. The novel and unique structure of the ecteinascidins consists of a monobridged penta-cyclic skeleton composed of two fused tetrahydroisoquinoline rings (A- and B-subunits) linked to a 10-membered lactone bridge through a benzylic sulfide linkage. Most ecteinascidins have an additional tetrahydroisoquinoline or tetrahydro-β-carboline ring (C-subunit) attached to the rest of the structure through a spiro-ring. This is one of the features distinguishing these molecules from the saframycin, safracin, and renieramycin families isolated from bacteria and sponges. However, all of the ecteinascidins were unfortunately unstable, and it is quite difficult to obtain these natural products with large amount for evaluating cytotoxic activity. In 2002, Suwanborirux *et al*. isolated the stable ecteinascidins, Ets 770 and 786, from the KCN-pretreated Thai tunicate, *Ecteinascidia thurstoni* (Suwanborirux *et al*., 2002). The structures of ecteinascidins are summarized in Figure 7.

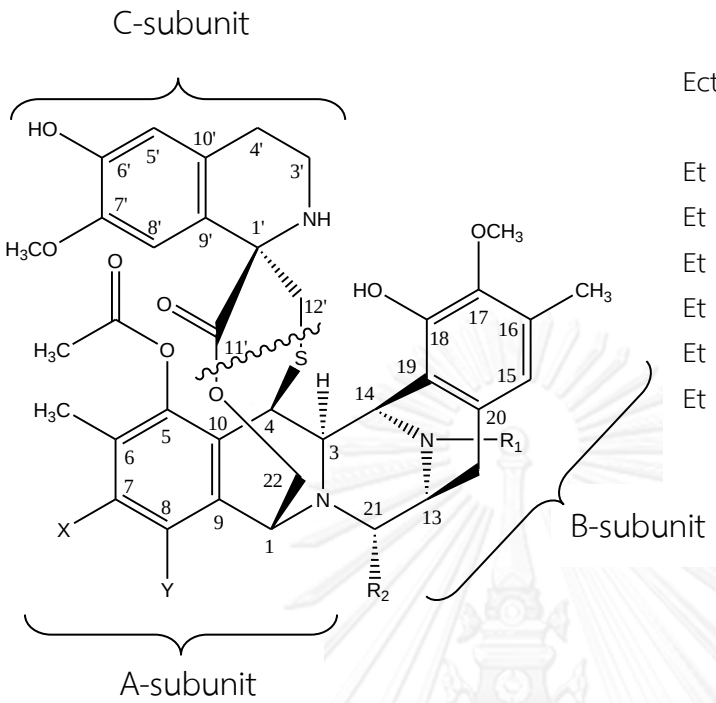

Ecteinascidin 743-type

XY = -O-CH_2-O-

Et 743: R_1= CH_3, R_2= OH

Et 770: R_1= CH_3, R_2= CN

Et 745: R_1= CH_3, R_2= H

Et 759B: R_1= CH_3, R_2= OH, S-oxide

Et 786: R_1= CH_3, R_2= OH, S-oxide

Et 729: R_1= H, R_2= OH

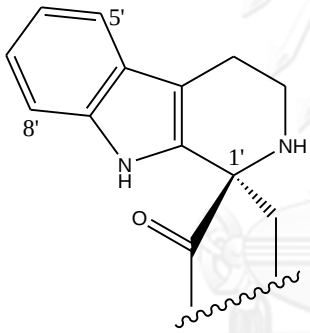

Ecteinascidin 736-type

XY = -O-CH_2-O-

Et 722: R_1= H, R_2= OH

Et 736: R_1= CH_3, R_2= OH

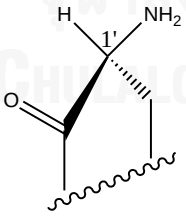

Et 597: R_1= CH_3, R_2= OH, X= OCH_3, Y= OH

Et 583: R_1= H, R_2= OH, X= OCH_3, Y= OH

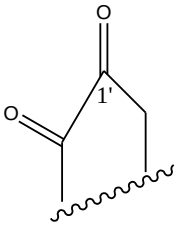

Et 594: R_1= CH_3, R_2= OH, XY= -O-CH_2-O-

Et 596: R_1= CH_3, R_2= OH, X= OCH_3, Y= OH

Figure 7. Structures of the ecteinascidins.

The structures of ecteinascidins were determined by extensive NMR and mass spectral (MS) studies. At first, the positive ion High Resolution Fast Atom Bombardment MS (HR-FABMS) technique showed the most abundant protonated molecular ion (*m/z*) of Et 743 at 744.2591 $[M+H]^+$ in agreement with the molecular formula $C_{39}H_{42}N_3O_{10}S$. Analysis of FABMS/MS data (Figure 8, Rinehart *et al*., 1990) was critical in locating the three nitrogen atoms in three subunits of similar size and composition, differing mainly in the numbers of oxygens. The B-subunit appeared to be identical with a subunit in safracin B (Ikeda *et al*., 1983) since the ^{13}C and ^{1}H chemical shifts were nearly the same and the key FABMS peaks at *m/z* 204 and 218 were also prominent, which was confirmed by HMBC spectroscopy (Figure 9, Rinehart *et al*., 1990). The A-subunit was constructed from HMBC correlations and demonstrated to connect to the B-subunit by the FABMS/MS ion at *m/z* 495. The C-subunit was also identified by HMBC correlations, which was assigned to join to the other two subunits by the mass fragment ions at *m/z* 250 and 224 to yield a complete structure for Et 743.

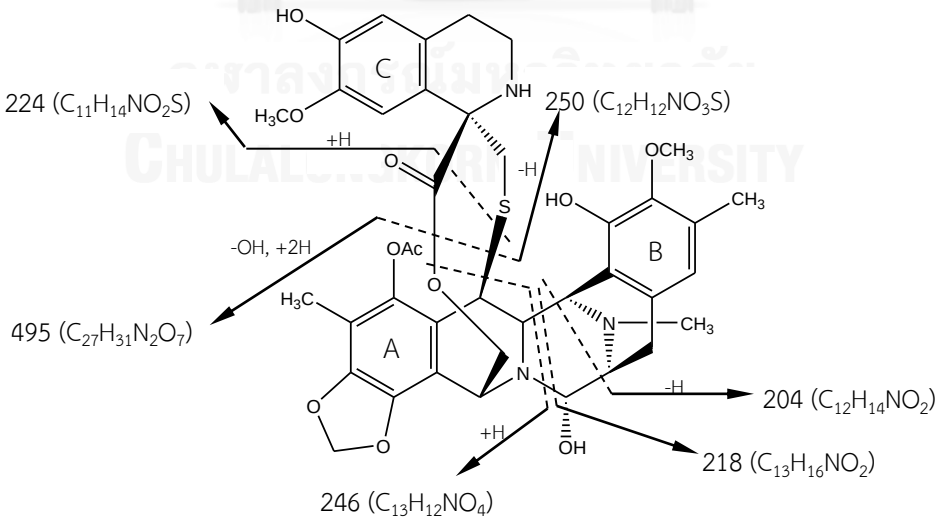

Figure 8. Fragmentations in FABMS/MS of Et 743 (Rinehart *et al*., 1990).

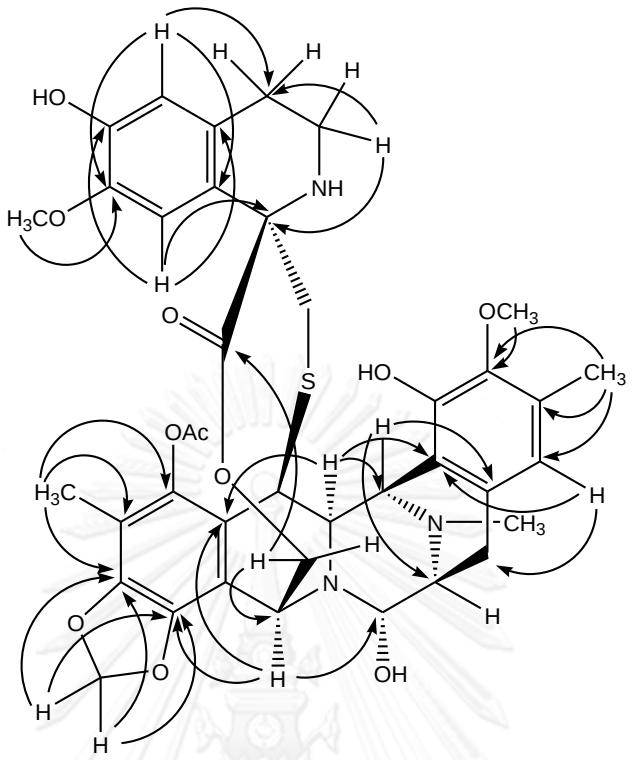

Figure 9. HMBC correlations of Et 743 (Rinehart *et al*., 1990).

The relative stereochemistry was proposed by 2-dimentional rotating-frame Overhauser enhancement spectroscopy (2D ROESY) (Sakai *et al*., 1996). The structure of Et 743 was unambiguously confirmed by X-ray crystallography of its relatives, 21-*O*-methyl- N^{12}-formyl-Et 729 and Et 734 N^{12}-oxide, (Sakai *et al*., 1992) as shown in Figure 10. The molecular shape is highly compact and three large principal planar groups are observed in the three-dimensional structure corresponding to three aromatic units, which are nearly perpendicular to each other. The absolute configuration of Et 743 was assigned by NOE correlations on ROESY spectrum as 1*R*, 2*R*, 3*R*, 4*R*, 11*R*, 13*S*, 21*S*, 1'*R* (Sakai *et al*., 1996; Sainz-Diaz *et al*., 2003).

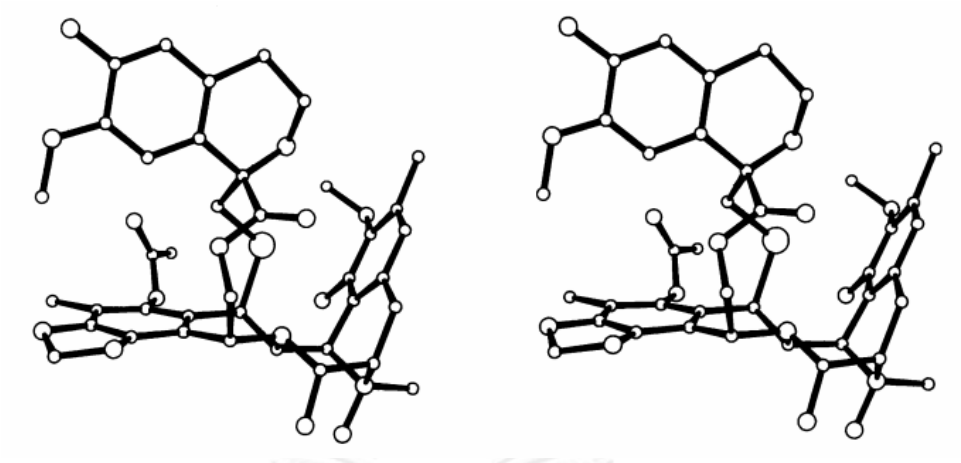

Figure 10. Stereoscopic X-ray crystallographic structure of 21-*O*-methyl-N^{12}-formyl Et 729 and Et 734 N^{12}-oxide (Sakai *et al*., 1992).

5. Biosynthesis of the Ecteinascidins

The chemical structure of most ecteinascidins is formed by a two-fused tetrahydroisoquinoline ring (A- and B-subunits) which linked to another ring system, either tetrahydroisoquinoline or tetrahydro-β-carboline, forming a spiro ten-membered lactone bridge through a benzylic sulfide linkage (Sakai *et al*., 1996). The basic structure of the ecteinascidins, A- and B-subunits, is the same as that of the saframycins and safracins, which was isolated from cultured *Streptomyces* species (Arai *et al*., 1977; Ikeda *et al*., 1983). This suggested that ecteinascidins may share biosynthetic origins of the A- and B-subunits with those of saframycins.

The biosynthetic origins of saframycin A have been elucidated by the use of isotopically labeled substrates (Mikami *et al.,* 1985). It has been proposed that the dimeric quinone skeletons common to all the saframycins are derived directly from two tyrosine molecules. The remaining carbons of the tetrahydroisoquinoline system and the pyruvoyl amide side chain are derived from glycine and alanine,

respectively. The *O*- and *C*-methyl and one *N*-methyl carbons were determined to derive from methionine (Figure 11, Mikami *et al.,* 1985).

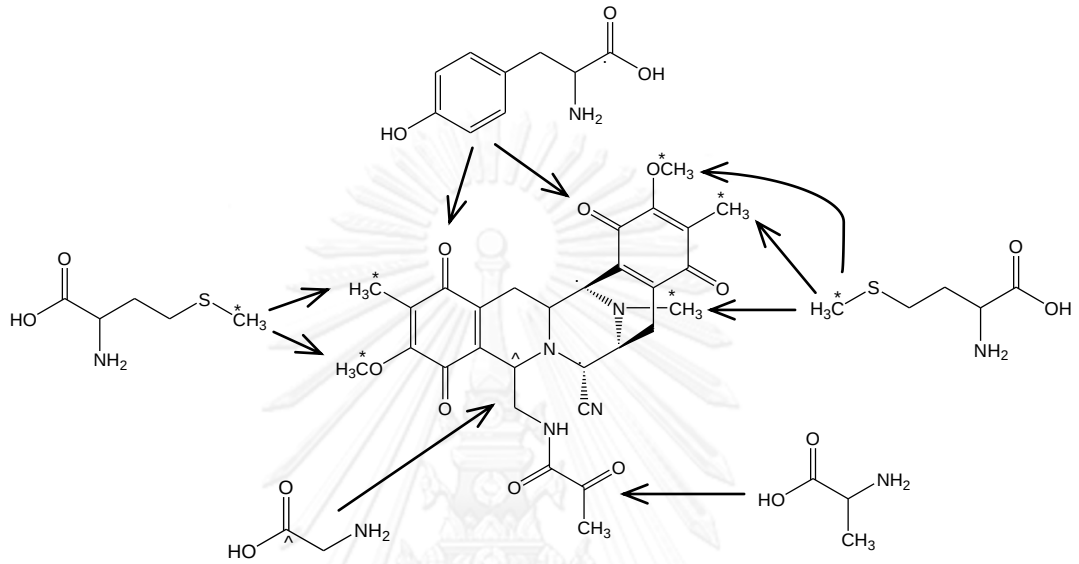

Figure 11. Biosynthetic origins of saframycin A (Mikami *et al*., 1985).

The biogenetic pathways of the ecteinascidins as proposed for the A- and B-subunits are most likely formed by condensation (Pictet-Spengler reaction) of two tyrosine building blocks (Kerr and Miranda 1995), then derived to a tyrosine-diketopiperazine intermediate which then oxidized to DOPA-diketopiperazine (Jeedigunta *et al.,* 2000). The tetrahydroisoquinoline ring in the B-subunit is closed by condensation with a serine- (or glycine-) derived aldehyde as in the case of the related saframycins. *S*-Adenosyl methionine is the likely source of methyl groups at *C*-6, *O*-7, *C*-16, *O*-17, and *N*-12. The sequence of the oxidation, methylation, and acetylation at the aromatic rings is not yet clear. The present study offers the side chain alcohol at *C*-22 being acylated by cysteine, followed by oxidation and addition

(or substitution) at *C*-4 by the SH group of the side chain with closure of the 10-membered lactone ring. Transamination at *C*-1 forms an oxo derivative, then oxidation of the 7-OCH_3 to form the methylenedioxy group. The C-subunit was performed by the electrophilic ketone are condensed in a Pictet-Spengler reaction with a dopamine derivative to form the third tetrahydroisoquinoline group in Et 743 or with tryptamine to form the tetrahydro-β-carboline group in Et 736 (Kerr and Miranda, 1995; Sakai *et al*., 1996; Rinehart, 2000). The proposed biosynthetic pathway of the ecteinascidins is shown in Figure 12.

In 2011, Rath and co-worker used molecular biology techniques to identify and characterize the biosynthetic pathway of Et 743. This study proposed that Et 743 was produced by *Candidatus Endoecteinascidia frumentensis*, the marine bacterial symbiont of *E. turbinata*, through nonribosomal peptide synthetase (NRPS) modules. The proposed NRPS biosynthetic pathway of Et 743 is shown in Figure 13.

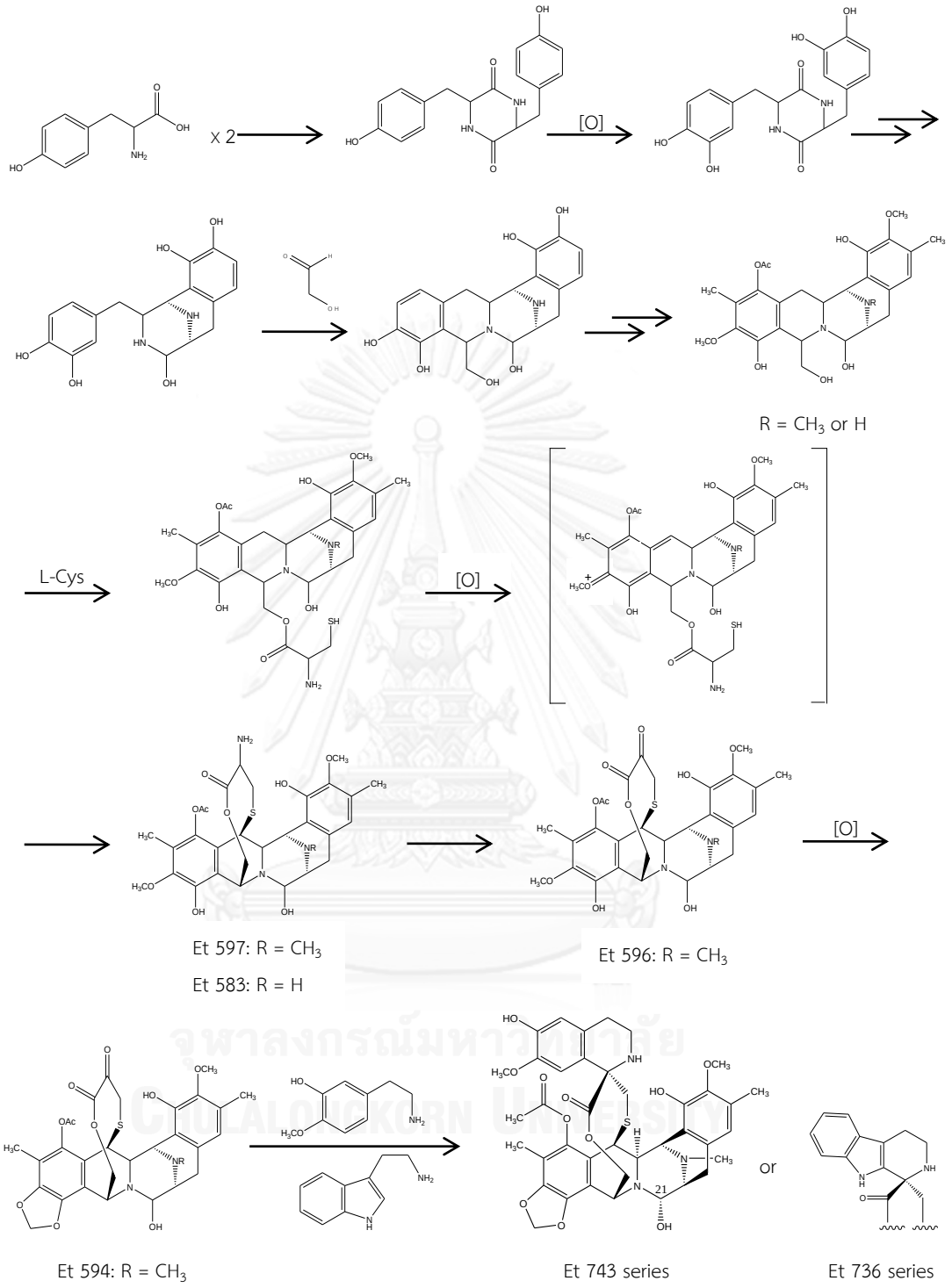

Figure 12. Proposed biosynthetic pathway of the ecteinascidins (modified from Kerr and Miranda, 1995; Sakai *et al*., 1996; Jeedigunta *et al.,* 2000; Rinehart, 2000).

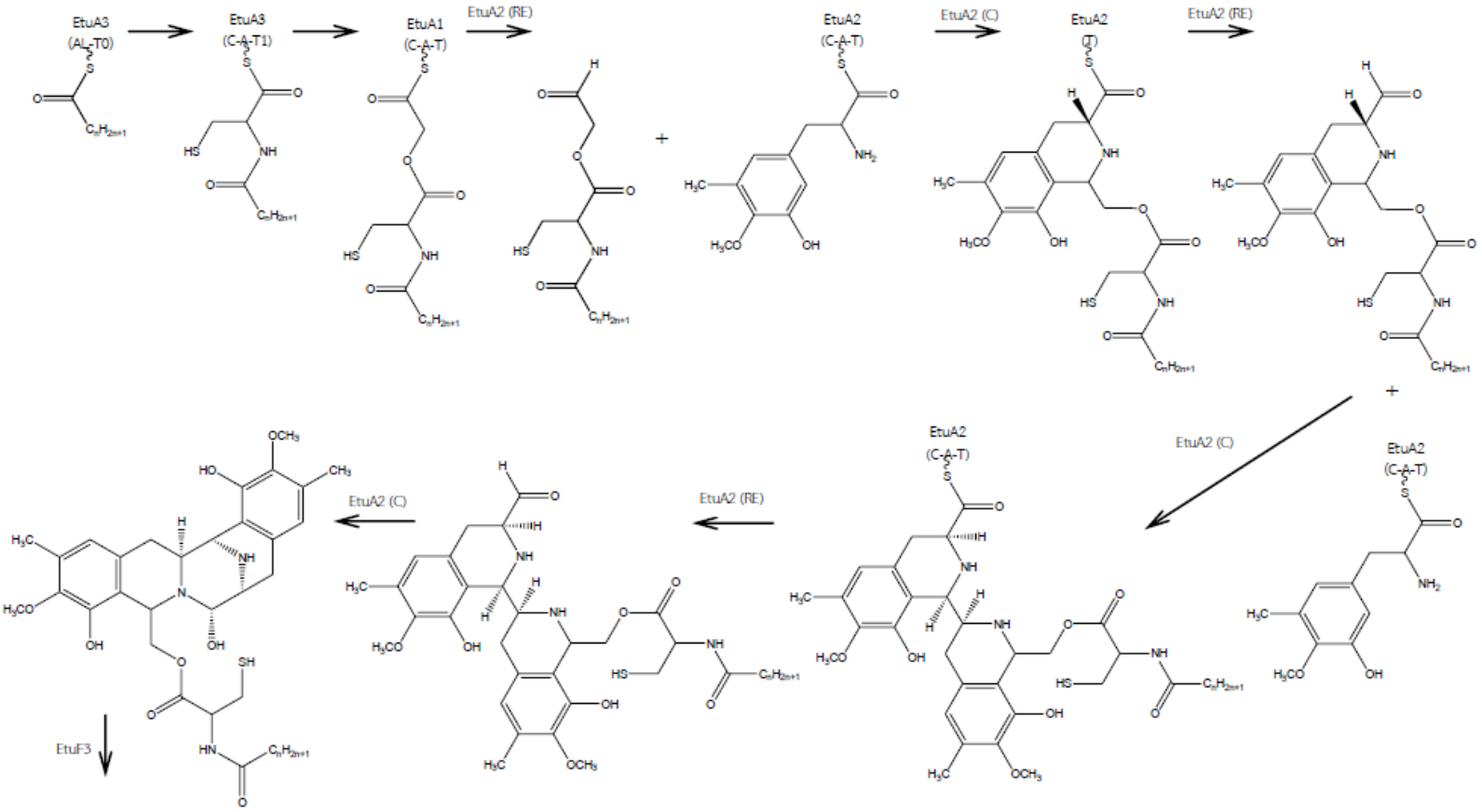

Figure 13. Proposed NRPS biosynthetic pathway of Et 743. Names relate to proposed function for each protein: EtuA, NRPS with domains illustratrated; EtuF, fatty acid biosynthesis; EtuO, monoxygenase (Rath *et al.,* 2011).

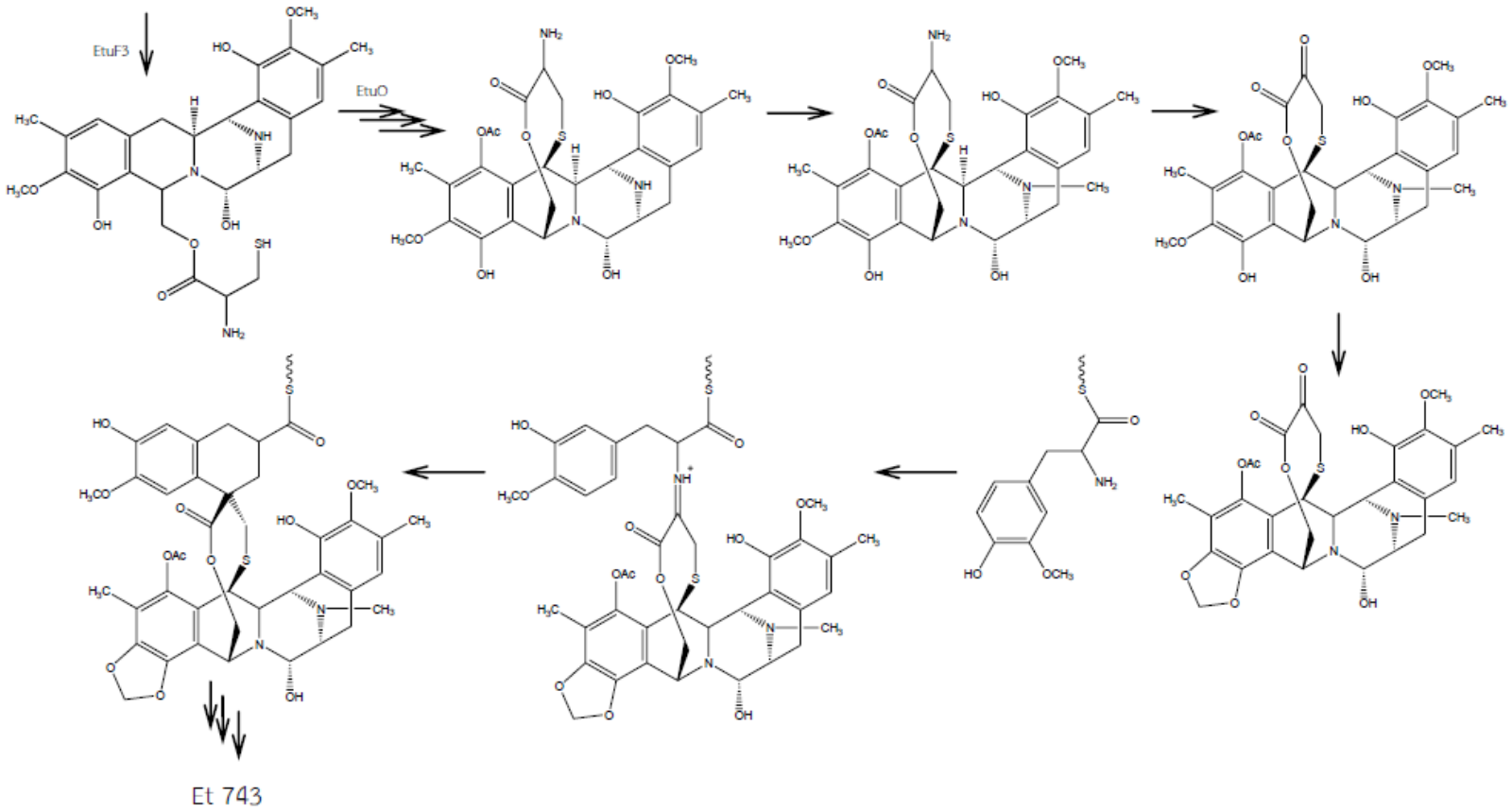

Figure 13. (continued).

6. The Mechanism of Action for Cytotoxic Activity of the Ecteinascidins

Ecteinascidin 743 is the first of a new class of DNA binding agents with a complex, transcription-targeted mechanism of action. The mechanism of action of the ecteinascidins was first reported in 1992 (Sakai *et al.,* 1992). Interaction of the ecteinascidins with DNA has been proposed on the basis of X-ray crystallography and the molecular modeling by using the DNA heptamer d(TTGGGAA) with the middle G as the target base for the alkylation reaction of Et. It has been shown that the A-subunit stacked on the backbone of DNA on one side of the minor groove and the C-subunit stacked on the backbone on the other side of the minor groove (Figure 14). Later, a model of Et 743 covalently bound to 6G*N*2 of the $[d(CGTAAGCTTACG)]_2$ oligonucleotide using solvated molecular dynamics was generated (Moore *et al*., 1997). The resulting model as shown in Figure 15 is generally consistent with the existing theoretical models.

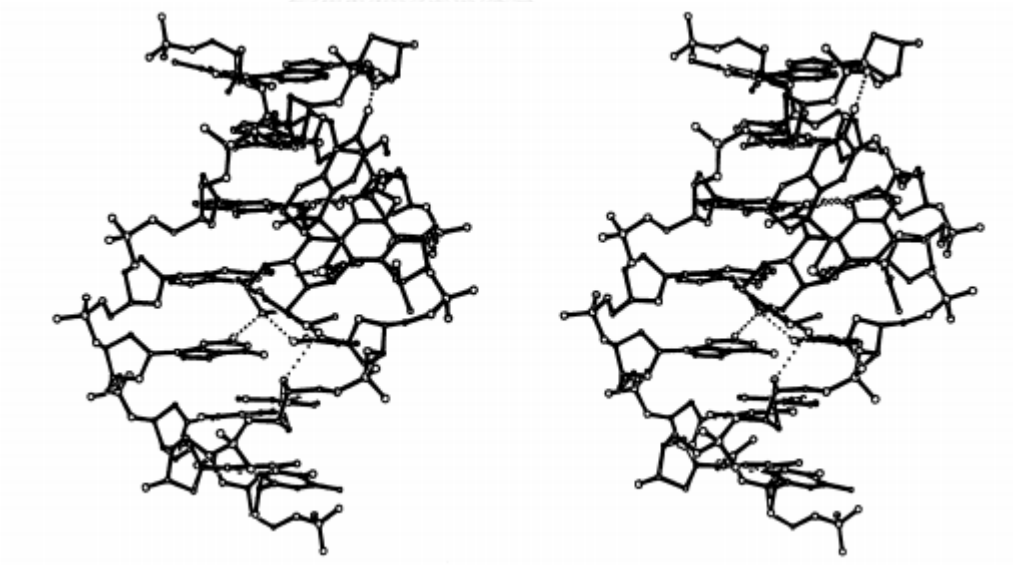

Figure 14. A model of the Et-DNA adduct produced by a computer modeling study (Sakai *et al*., 1992).

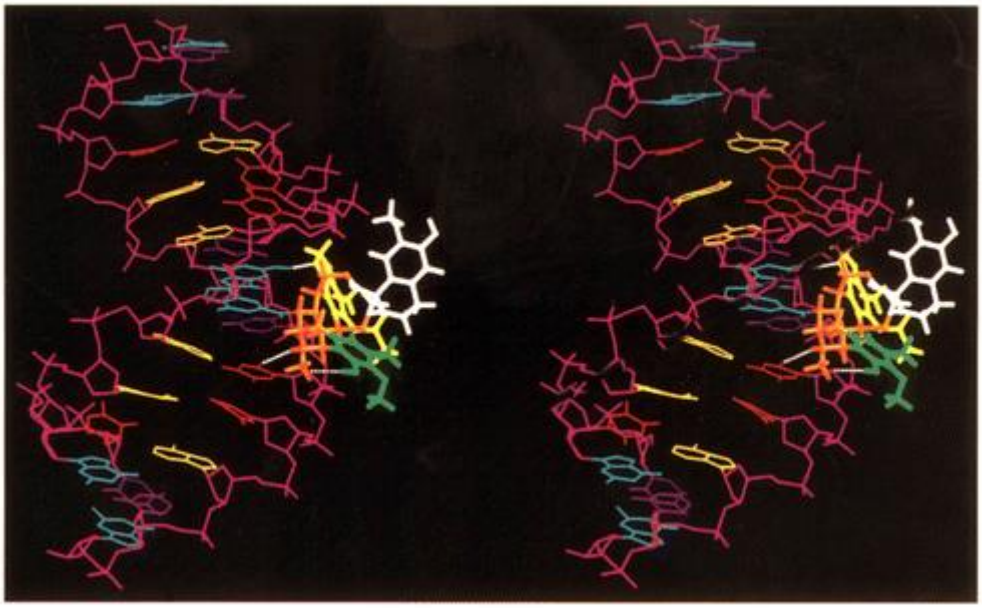

Figure 15. Stereoview of Et 743-oligonucleotide adduct derived from molecular dynamics analysis (Moore *et al*., 1997). [The model depicts the orientations of A-subunit (yellow), B-subunit (green) and C-subunit (white) and their interaction with the adenine (gold), thymidine (red), guanine (cyan) and cytosine (purple) residues in the minor groove of the 12-mer oligonucleotide].

Et 743 inhibited the cancer cell by DNA sequence-selective alkylation between carbinolamine functional group and exocyclic 2-amino (*N*2) group of guanine base in the duplex DNA minor groove (Pommier *et al.,* 1996). The chemical reaction leading to the guanine *N*2 alkylation was proposed to result from an intramolecular acid-catalyzed dehydration of the carbinolamine moiety (Figure 16, Moore *et al*., 1998), resulting in the formation of an electrophilic iminium, which is the DNA-reactive intermediate (Moore *et al*., 1998). The formation of Et 743-DNA adducts bends the DNA structure towards the major groove opposite to adducts located in the minor groove (Figure 17) (Zewail-Foote and Hurley, 1999).

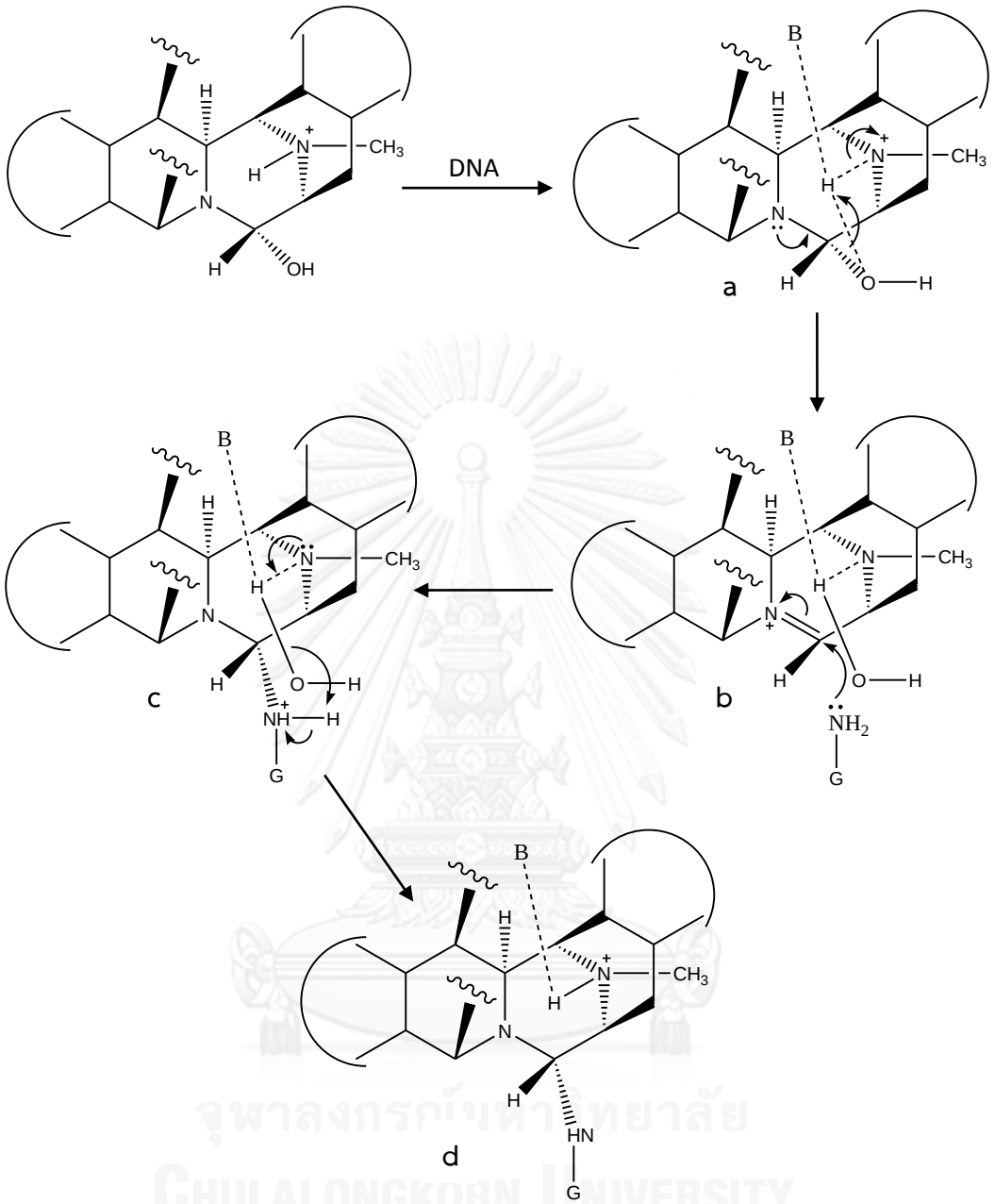

Figure 16. Proposed mechanism for the catalytic activation of the ecteinascidin carbinolamine prior to covalent bond formation with *N*2 of guanine. The 12-NH of the carbinolamine (**a**) catalyzes the dehydration of *C*21, yielding the iminium ion (**b**). Nucleophillic attack by G*N*2 on **b** results in the expulsion of the transiently bound H_2O, which contains the proton released by guanine *N*2 (**c**). The resulting adduct (**d**) retains a protonated *N*12. Hydrogen bonds are depicted by dotted lines, and B corresponds to a DNA base hydrogen bond acceptor (Moore *et al*., 1998).

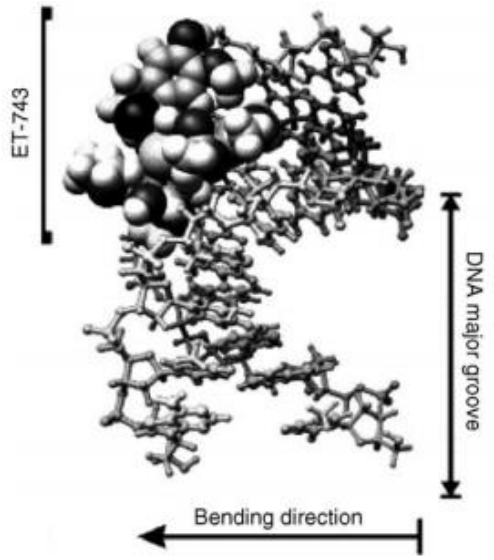

Figure 17. Stereoisomer view of Et 743 alkylated to *N*2 position of guanine in the DNA minor groove, the alkylation produces a bend toward the DNA major groove (Soares *et al*., 2005).

The high-field NMR-based study of the Et 743/DNA interaction has shown that the A- and B-subunits and the α-carbinolamine group are sequence binding recognition (Moore *et al*., 1997; Seaman *et al*., 1998). The resulting adduct is additionally stabilized through van der Waals interactions and hydrogen bonds between the A- and B-subunits, with neighboring nucleotides in the same or opposite strand of the DNA double helix (Figure 18, Seaman *et al*., 1998), thus creating the equivalent to a functional interstrand crosslink. In fact, hydrogen bonding rules seem to determine the DNA-binding sequence specificity of Et 743, with a guanine located in the central position of triplets 5′-purine-GC and 5′-pyrimidine-GG. Therefore, favored triplets are TGG, CGG, AGC, and GGC sequences, whereas AGC is completely refractory (Pommier *et al*., 1996; Seaman *et al*., 1998). The relationship between DNA sequences and hydrogen bonds that related to binding affinity of Et 743 are concluded in Figure 19.

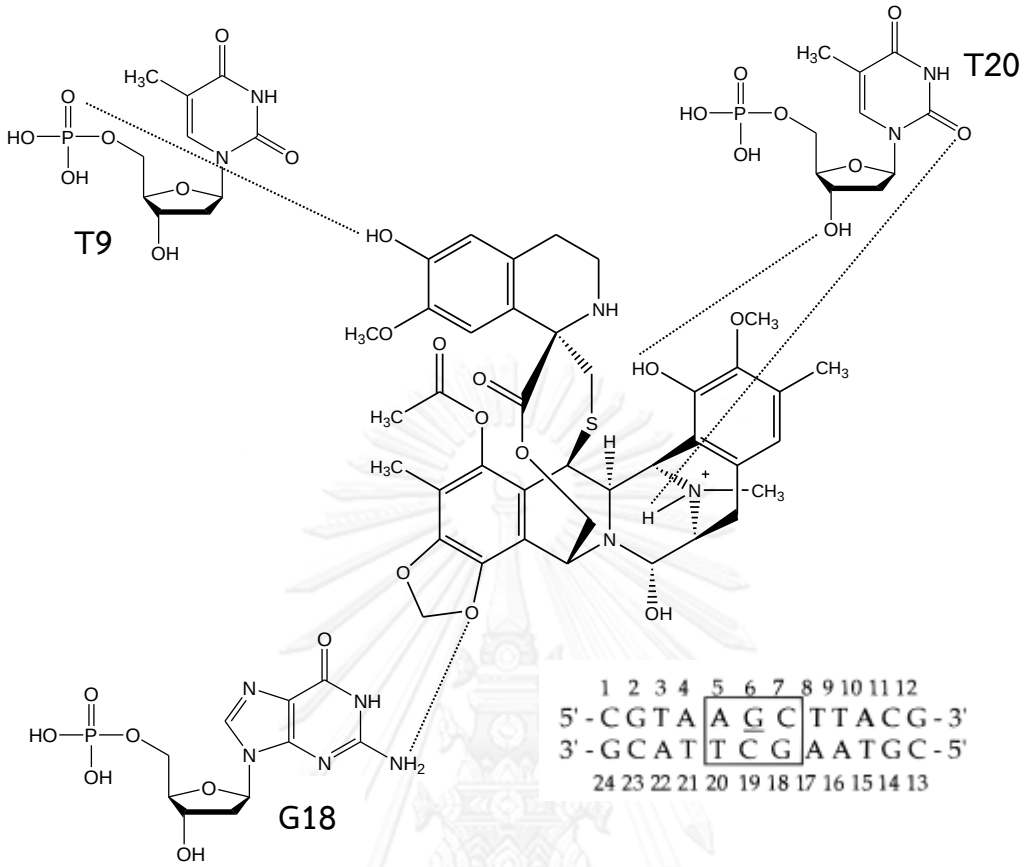

Figure 18. Sites of Et 743 and 12-mer oligonucleotide hydrogen-bonding interaction (modified from Seaman *et al*., 1998). H-bond represented by a dot line.

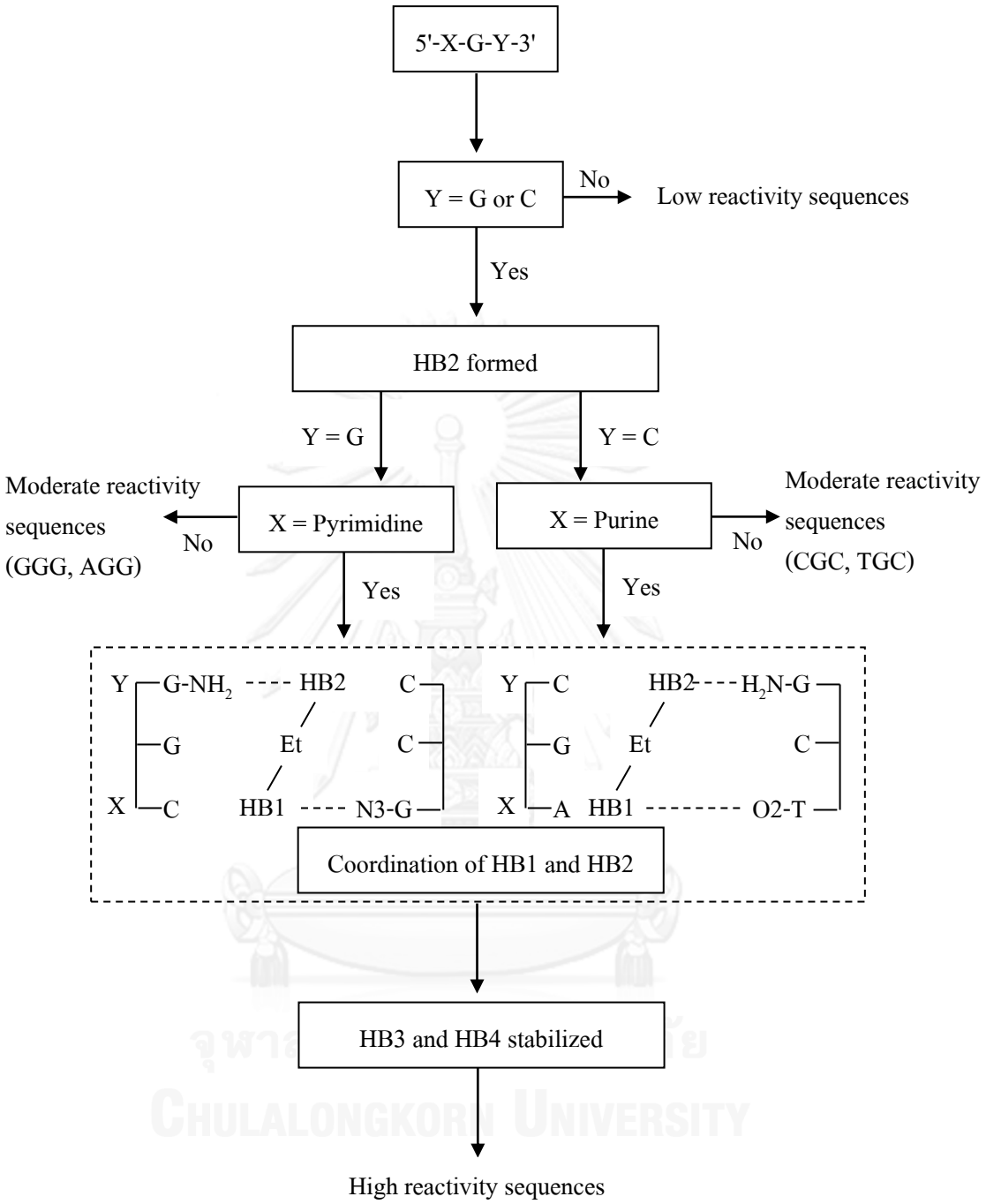

Figure 19. The relationship between DNA sequences and hydrogen bonding that related to reactivity of Et 743 (Seaman *et al*., 1998).

Interestingly, the C-subunit, which is perpendicular to the A- and B-subunits and protrudes from the duplex DNA binding sites (Sakai *et al*., 1992; Moore *et al*., 1997; Seaman *et al*., 1998), might be related to binding affinity between the DNA and Et 743 (David-Cordonnier *et al*., 2005) and interacting with different DNA-binding proteins located in the DNA adduct area. One of these proteins is XPG, a member of the Nucleotide Excision Repair (NER) system (Takebayashi *et al*., 2001; Zewail-Foote *et el*., 2001; Soares *et al*., 2005; Herrero *et al*., 2006; Guirouilh-Barbat *et al*., 2009) (Figure 20). Under these circumstances, Et 743 affects the activity of the Transcription-Coupled Nucleotide Excision Repair (TC-NER) system. In the absence of Et 743, TC-NER recognizes and removes DNA lesions from transcribed strands of expressed genes. This is followed by removal of the DNA segment containing the lesion and gap polymerization using the intact strand as the template. In the presence of Et 743, the TC-NER machinery is recruited into the DNA adduct region in an attempt to correct the DNA lesion but is blocked, creating strong cytotoxic complexes that will induce double strand DNA breaks and cell death (Takebayashi *et al*., 2001). Thus, while all other known DNA-interacting agents require a deficient NER mechanism to exert their activity, Et 743 needs a proficient NER system to exert its cytotoxic activity (Damia *et al*., 2001; Erba *et al*., 2001; Soares *et al*., 2005).

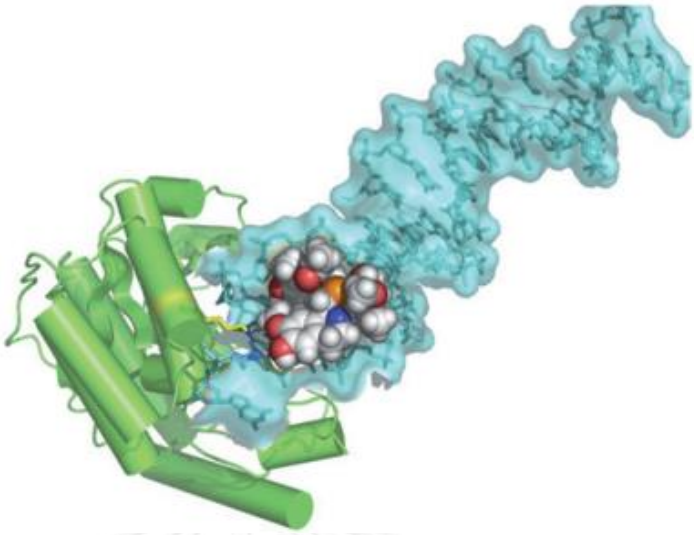

Figure 20. Binding of Et 743 to the complex DNA-XP**G** (Cuevas and Francesch, 2009)**.**

7. Structure Modification of the Ecteinascidins

The ecteinascidins are known as cytotoxic compounds from marine tunicates. To improve its biological activity, chemical modification of the ecteinascidins has been focused. One of the simple ecteinasdin analogues named phthalascidin (**8**) was synthesized and the structure-activity relationships were summarized as illustrated in Figure 21 (Martinez *et al*., 1999). The phthalascidin is an ecteinascidin-like compound that replaced the C-subunit by a phthalimide group. As mentioned earlier, the C-subunit of Et 743 protrudes from the minor groove of the double helix when the drug is bound to DNA (Sakai *et al*., 1992; Moore *et al*., 1997; Seaman *et al*., 1998). It has also been shown that modifying the C-subunit changes ability to inhibit cell division. On the other hand, it was found that the antiproliferative activity on human solid cancer cell lines (A549 lung adenocarcinoma, HCT116 colon carcinoma, A375 malignant melanoma and PC-3 prostate carcinoma) of phthalascidin is greater than Et

743 (Table 2, Martinez *et al*., 1999). These results showed that structure modification of Et 743 at the C-subunit might improve its biological activity.

Table 2. Antiproliferative activity of Et 743 and phthalascidin.

Compounds	Antiproliferative activity (IC_{50} in nM)			
	A549	HCT116	A375	PC-3
Et 743	1.00	0.50	0.15	0.70
Phthalascidin (**8**)	0.95	0.38	0.17	0.55

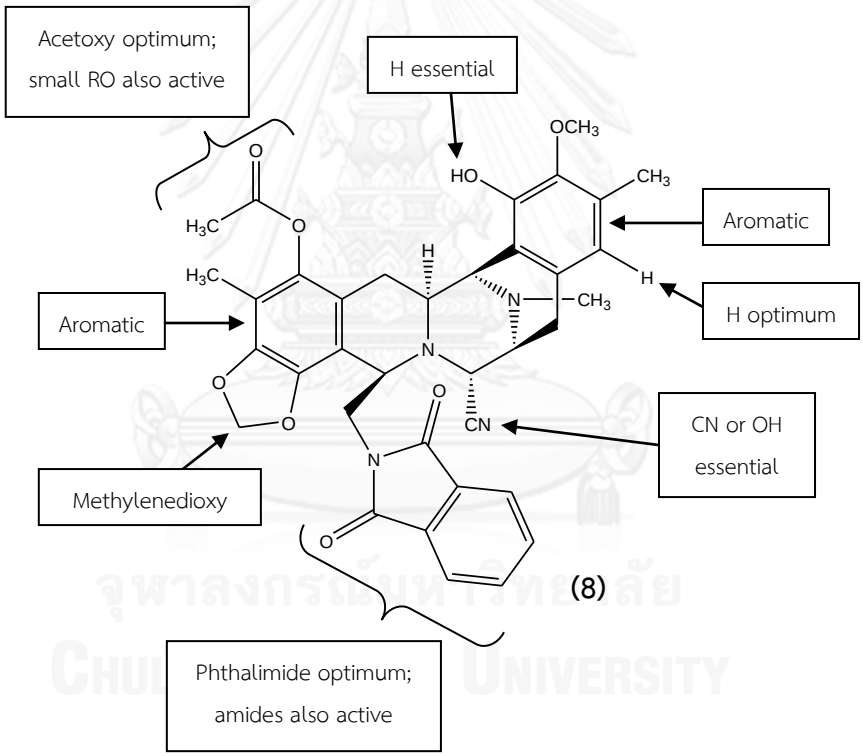

Figure 21. Structure of phthalascidin and its structure-activity summary (Martinez *et al*., 1999).

The second modification, of the ecteinascidins has been investigated at the 6'-OH position of the C-subunit of the stable Et 770 (Puthongking *et al*., 2006). The cytotoxicity on human solid cancer cell lines (HCT116 colon carcinoma, QG56 lung

carcinoma, and DU145 prostate carcinoma) of the 6'-*O*-acyl Et 770 derivatives, showed not much different from the parent compound Et 770. However, the serendipitous discovery of the 2'-*N*-(indole-3-carbonyl) Et 770 (**5k**, Figure 22) expressed 2-6 times higher cytotoxicity in various cancer cell lines (Table 3).

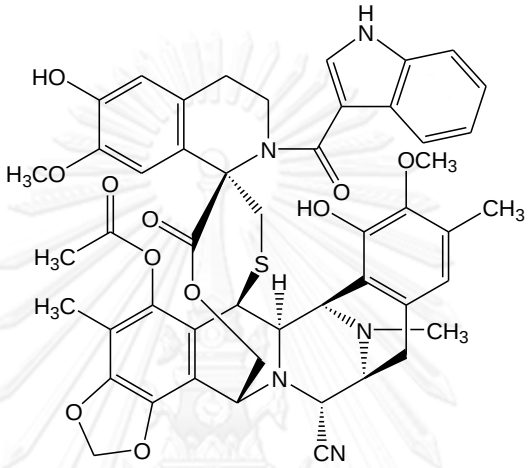

(5k)

Figure 22. Sturcture of 2'-*N*-(indole-3-carbonyl) Et 770.

Table 3. Cytotoxicity of Et 770 and 2'-*N*-indole-3-carbonyl Et 770.

Compounds	Cytotoxicity (IC_{50} in nM)		
	HCT116	QG56	DU145
Et 770	0.40	1.8	0.66
2'-*N*-Indole-3-carbonyl Et 770 (**5k**)	0.07	0.53	0.37

The next modification, Saktrakulkla *et al*. (2011) investigated other 2'-*N*-acyl Et 770 derivatives based on a three-step transformation including: a) 18,6'-*O*-bisallyl protection, b) 2'-*N*-acylation, and c) removing of the allyl protecting group (Figure 3). Most of them showed potent cytotoxicity on human solid tumor cell lines and found

that the nitrogen-containing heterocyclic derivatives e.g. 2'-*N*-(6''-quinolinecarbonyl) Et770 (**5l**) and cinnamoyl derivatives e.g. 2'-*N*-(cinnamoyl) Et 770 (**5m**) showed 10 times higher cytotoxicity than Et 770 (Table 4). The previous studies showed that the modification of 2'-*N* position of the C-subunit played a key role to improve cytotoxicity of the parent compound Et 770.

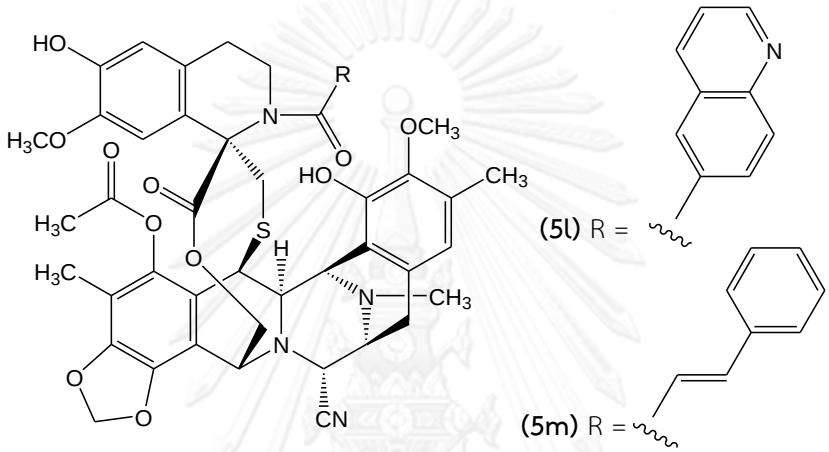

Figure 23. Structures of some 2'-*N*-acyl Et 770 derivatives.

Table 4. Cytotoxicity of Et 770 and its 2'-*N*-acyl derivatives.

Compounds	Cytotoxicity (IC_{50} in nM)		
	HCT116	QG56	DU145
Et 770	0.60	2.4	0.81
2'-*N*-(6''-Quinolinecarbonyl) Et770 (**5l**)	0.045	0.15	0.043
2'-*N*-(Cinnamoyl) Et 770 (**5m**)	0.053	0.33	0.24

CHAPTER III

EXPERIMENTAL

1. Animal Material

The tunicate was identified by Dr. T. Nishikawa of Nagoya University Museum as *Ecteinascidia thustoni* Herdman 1981. The sample was collected by scuba diving at 1-5 meters deep on the East coast of Phuket Island, Thailand. The collection was done during May 2012. The sample was stored frozen at -20°C until use.

2. General Experimental Procedures

2.1 Chromatography

2.1.1 Thin-Layer Chromatography

Technique	: One dimension, ascending
Adsorbent	: Silica gel 60 F_{254} (Merck)
Layers thickness	: 250 μm
Distance	: 5 cm
Temperature	: Room temperature (25-30°C)
Detection	: 1) Ultraviolet light at wavelengths of 254 and 365 nm 2) Spraying with anisaldehyde-sulfuric acid reagent and heating until colors developed

2.1.2 Column Chromatography

2.1.2.1 Flash Column Chromatography

Adsorbent : Silica gel 60 (No. 1.09385) particle size 0.040-0.063 mm (230-400 mesh ASTH) (Merck)

Packing method : The adsorbent was packed by the wet method. The adsorbent was mixed with the eluent into a free-flowing suspension and poured into the column. The eluent was drained and the adsorbent was evenly settled by compressed air or low pressure (about 2 psi). The flow rate was adjusted at 1-2 ml/minute by compressed air and the stopcock.

Sample loading : The sample was dissolved in a small amount of the eluent and then applied gently on top of the column.

Detection : Fractions were monitored by TLC technique.

2.1.2.2 Quick Column Chromatography

Adsorbent : Silica gel 60 (No. 1.07734) particle size 0.063-0.200 mm (70-230 mesh ASTH) (Merck)

Packing method : The adsorbent was packed by the wet method. The adsorbent was mixed with the eluent into a free-flowing suspension and poured into the sintered glass funnel used as the column. The eluent was drained and the adsorbent was evenly settled under reduced pressure using an aspirator as a membrane pump.

Sample loading : The sample was dissolved in a small amount of organic solvent, mixed with a small quantity of Kieselgurh, triturated, dried and then placed gently on top of the column. The elution was generated under reduced pressure using an aspirator as a membrane pump.

Detection : Fractions were monitored by TLC technique.

2.1.2.3 Gel Filtration Chromatography

Gel filter : Sephadex LH-20 (Pharmacia Biotech AB)

Packing method : Sephadex gel was suspended in the eluent and kept overnight to swell prior to use. The slurry of adsorbent was poured into the column and allowed to settle before use.

Sample loading : The sample was dissolved in a small volume of eluent and loaded on top of the column.

Detection : Fractions were monitored by TLC technique.

2.2 Spectroscopy

2.2.1 Infrared Spectrometry

Infrared (IR) spectra were obtained on a Shimadzu FT-IR 8200PC spectrophotometer (Meiji Pharmaceutical University) or a Perkin Elmer Spectrum One FT-IR spectrometer (Chulalongkorn University).

2.2.2 Mass Spectrometry

The FABMS and HR-FABMS spectra were recorded on a JEOL JMS-700 instrument with a direct inlet system operating at 70 eV (Meiji Pharmaceutical University).

2.2.3 Proton and Carbon Nuclear Magnetic Resonance Spectroscopy

Proton and carbon nuclear magnetic resonance (^{1}H- and ^{13}C-NMR), DEPT 90 and 135, HMQC, HMBC, and ^{1}H, ^{1}H-COSY spectra were obtained on a JEOL JNM-ECA500 FT-NMR spectrometer operating at 500 MHz for ^{1}H and 125 MHz for ^{13}C (Analytical Center of Meiji Pharmaceutical University) and on a Bruker Avance DPX-300 FT-NMR spectrometer operating at 300 MHz for ^{1}H and 75 MHz for ^{13}C (Pharmaceutical Research Instrument Center, Faculty of Pharmaceutical Sciences, Chulalongkorn University).

The solvent for NMR measurement was deuterated chloroform ($CDCl_3$). Chemical shifts were recorded in ppm scale and the coupling constants were recorded in Hz using the chemical shifts of the residue in NMR solvents or TMS as the internal standard. Proton-detected heteronuclear correlations were measured using HMQC (optimized for $^{1}J_{HC}$ = 145 Hz) and HMBC (optimized for $^{n}J_{HC}$ = 4 and 8 Hz) pulse sequences.

2.3 Physical Properties

2.3.1 Optical Rotation

Optical rotations were measured on a Horiba-SEPA instrument (Meiji Pharmaceutical University) and on a Perkin Elmer 341 polarimeter (Chulalongkorn University).

2.3.2 Circular Dichroism Spectroscopy

Circular dichroism (CD) spectra were measured on a Jasco J-820 spectropolarimeter (Meiji Pharmaceutical University) and on a Jasco J-715 spectropolarimeter (Chulalongkorn University).

3. Chemical Reagents

Allyl Bromide	(TCI)
Deuterated Chloroform ($CDCl_3$)	(Aldrich, Euriso-top)
N,*N*-4-Dimethylaminopyridine (DMAP)	(Aldrich, Fluka)
m-Fluorobenzoyl Chloride	(TCI)
o-Fluorobenzoyl Chloride	(TCI)
p-Fluorobenzoyl Chloride	(TCI)
tran-3-Fluorocinnamic Acid	(Kanto)
4-Fluorocinnamoyl Chloride	(Aldrich)
Glacial Acetic Acid	(Merck)
1-Naphthoyl Chloride	(Wako)
2-Naphthoyl Chloride	(Wako)

Potassium Carbonate (KBr)	(Nacalai-tesque)
Potassium Cyanide (KCN)	(Kanto)
Tetramethylsilane (TMS)	(Merck)
Tributyltin Hydride (Bu_3SnH)	(TCI)
2,3,4-Trifluorobenzoyl Chloride	(TCI)
m-Trifluoromethylbenzoyl Chloride	(TCI)
p-Trifluoromethylbenzoyl Chloride	(TCI)
bis-(Triphenylphosphine)-Palladium(II) Dichloride	(TCI)

4. Solvents

All solvents were used either analytical or laboratory grade, and redistilled prior to use. For chemical reaction, acetone and pyridine were dried with molecular sieve type 4 Å. Tetrahydrofuran was refluxed in the presence of sodium and freshly distilled prior to use.

5. Extraction and Isolation of Ecteinascidin 770 from the Thai Tunicate *Ecteinascidia thurstoni*

The tunicate sample (65 kg, wet wt) was homogenized, and then a phosphate buffer solution (45 l) was added to the homogenized suspension until pH 7.0±0.2. Potassium cyanide solution (10% KCN) was added to the homogenized suspension to get the final concentration of 10 mM KCN, and the suspension was stirred for 5 hours. Then, the sample suspension was macerated with methanol (5 times, 20 l each) and filtered. The filtrate was concentrated to obtain the aqueous mathanolic

part, which was further partitioned with ethyl acetate to give a dark-brown residue (38.87 g, Scheme 1).

The residue (38.87 g) was subjected to quick column chromatography (column diameter = 13 cm, silica gel 250 g) using a gradient elution of hexane-ethyl acetate 3:1 to 1:3, ethyl acetate and methanol, respectively. Forty-two fractions (300 ml each) were collected and combined based on TLC pattern (Silica gel GF, hexane-ethyl acetate) to obtain 5 fractions (ET1-ET5). The TLC pattern of the fraction ET3 (3.61 g) showing Et compounds was re-fractionated with quick column chromatography (column diameter = 7 cm, silica gel 63 g) using a gradient elution of hexane-ethyl acetate 2:1 to 1:2, ethyl acetate and methanol, respectively. Thirty-nine fractions (100 ml each) were collected and combined based on TLC pattern (Silica gel GF, hexane-ethyl acetate 3:7) to obtain 7 fractions (ET3-1 to ET3-7). Fractions ET3-3 and ET3-4 which contained Et compounds were isolated by gel filtration chromatography (Sephadex LH 20, column diameter = 2.5 cm, height = 70 cm, using methanol as the eluting solvent). Forty fractions (10 ml each) were collected and combined based on TLC pattern (Silica gel GF, hexane-ethyl acetate 3:7) to obtain 4 fractions (ET1s-ET4s). Fraction ET2s which contained the crude mixture of Et 770 and Et 786 was precipitated in co-solvent of dichloromethane-methanol to give the pale yellow precipitates (280.8 mg) and mother liquor (337.9 mg). Then the precipitates (280.8 mg) and mother liquor (337.9 mg) were separated by a silica gel flash column using an isocratic elution of dichloromethane-ethyl acetate (2:3). The sub-fractions were combined according to their TLC pattern to afforded pale yellow precipitates of Et 770 from fractions ET2p and ET2m. Fractions ET2p and ET2m were combined and

crystallized in co-solvent of dichloromethane-methanol to give colorless crystals of Et 770 (258.2 mg, 3.97 x 10^{-4} % of wet wt) as shown in Scheme 2.

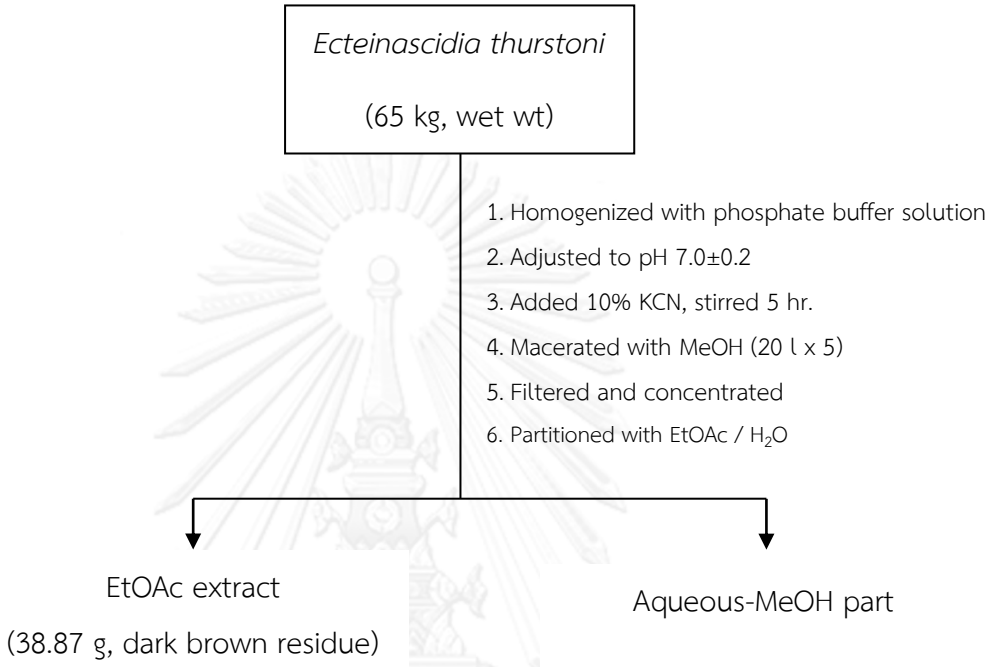

Scheme 1. Extraction of *Ecteinasidia thurstoni* collected in May 2012.

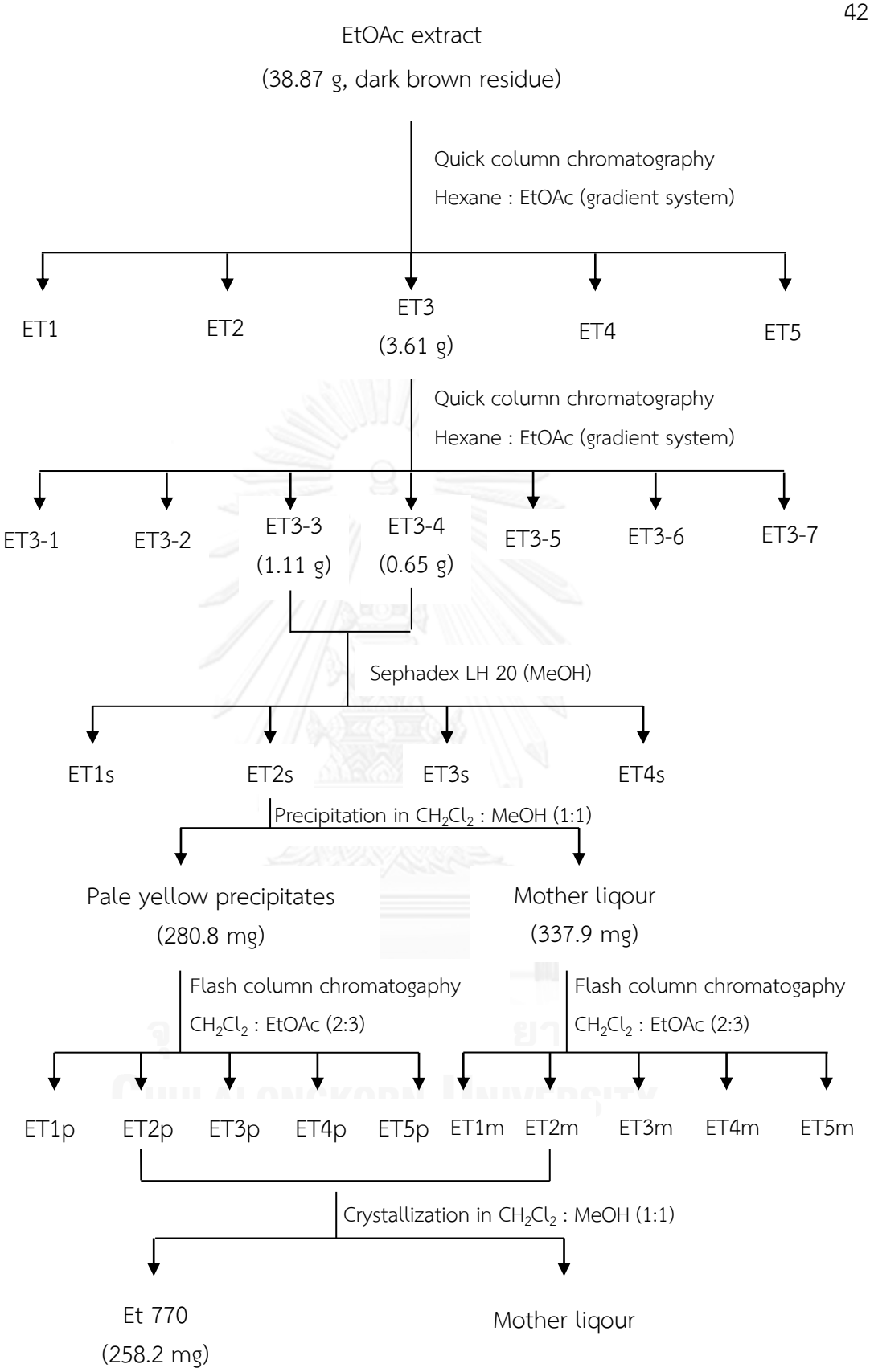

Scheme 2. Isolation of Et 770 from *Ecteinascidia thurstoni* collected in May 2012.

Et 770 (2)

Colorless crystal (258.2 mg, 4.0 x 10^{-4} % of wet animal)

^{1}H-NMR: δ ppm *see* Table 5, Figure 29

^{13}C-NMR: δ ppm *see* Table 5, Figure 30

FAB-MS: *m/z* 771 $[M+H]^+$

HR-FABMS: *m/z* 771.2693 $[M+H]^+$; calcd for $C_{40}H_{43}N_4O_{10}S$, 771.2700

IR (KBr) cm^{-1}: 3530, 3500, 2940, 1770, 1740, 1630, 1595, 1478

$[\alpha]_D^{24}$: -58.5 (c=1.0, $CHCl_3$)

CD $\Delta\varepsilon$ nm (c=13.0 μM, methanol, 24°C): 0 (306), -12.0 (289), 0 (270), 12.8 (254), 0 (242), -51.0 (221)

6. Preparation of the 2'-*N*-acyl Et 770 Derivatives

6.1 Preparation of the Allyl-protected Et 770 (18,6'-*O*-bisallyl Et 770)

Et 770 (232.6 mg, 0.30 mmole) was dissolved in acetone (60 ml), then the solution was added K_2CO_3 (1.04 g, 25 eq) and stirred for 5 minutes at 0°C. Allyl bromide (522.7 μl, 20 eq) was added dropwise over 20 minutes to the vigorously stirred mixture at 0°C. After the reaction suspension was stirred for 1 hour at 0°C, the reaction flask was further stirred at room temperature for 18 hours. Then, the reaction mixture was filtered and concentrated *in vacuo*, the residue was diluted with water (50 ml) and extracted with $CHCl_3$ (5 x 50 ml). The combined organic layers were washed with brine (50 ml), dried with anhydrous Na_2SO_4 and concentrated *in vacuo*. The crude extract was separated by a silica gel flash column using gradient elution of benzene-EtOAc 15:1 to 1:1 and 0:1 to provide 18,6'-*O*-bisallyl Et 770 (**3**, 234.5 mg) in 77.5% yield.

18,6'-*O*-bisallyl Et 770 (3)

Colorless amorphous powder (234.5 mg, 77.5% yield)

^{1}H-NMR: δ ppm *see* Table 6, Figure 31

^{13}C-NMR: δ ppm *see* Table 6, Figure 32

FAB-MS: *m/z* 851 $[M+H]^+$ (Figure 33)

HR-FABMS: *m/z* 851.3328 $[M+H]^+$; calcd for $C_{46}H_{51}N_4O_{10}S$, 851.3326

IR (KBr) cm^{-1}: 3437, 2932, 2855, 1769, 1742, 1518, 1458 (Figure 34)

$[\alpha]_D^{16}$: -55.3 (c=0.47, $CHCl_3$)

CD $\Delta\varepsilon$ nm (c=11.7 μM, methanol, 23°C): 8.0 (210), -89.3 (220), 0 (239), 23.4 (254), 0 (276), -10.8 (292) (Figure 35)

6.2 Preparation of the 18,6'-*O*-bisallyl-2'-*N*-acyl Et 770 Derivatives

Ten of 18,6'-*O*-bisallyl-2'-*N*-acyl Et 770 derivatives (**4a**-**4j**) were prepared by the general procedure. The starting material, 18,6'-*O*-bisallyl Et 770, (about 0.02 mmole, about 15-16 mg) and DMAP (0.5-5 eq) was dissolved in pyridine (1.5 ml), and then the solution was stirred 5 minutes at 0°C. The corresponding acid chloride (15-50 eq) was slowly poured into the stirred cold solution. After the reaction solution was stirred for 30 minutes at 0°C, the reaction was continuously stirred at room temperature until the TLC showed disappearance of the starting material. After the solvent was removed *in vacuo*, the residue was diluted with water (10 ml) and extracted with CH_2Cl_2 or $CHCl_3$ (5 x 15 ml). The combined organic layer was washed with brine (40 ml), dried, and concentrated *in vacuo* to give a residue. The residue was purified by silica gel flash column chromatography using an appropriate eluent to give the corresponding purified product.

18,6'-*O*-bisallyl-2'-*N*-(2''-fluorobenzoyl) Et 770 (4a)

Pale yellow amorphous powder (15.2 mg, 86.9% yield)

^{1}H-NMR: δ ppm *see* Table 8, Figure 36

^{13}C-NMR: δ ppm *see* Table 8, Figure 37

FAB-MS: *m/z* 973 $[M+H]^+$ Figure 38

HR-FABMS: *m/z* 973.3494 $[M+H]^+$; calcd for $C_{53}H_{54}N_4FO_{11}S$, 973.3494

IR (KBr) cm^{-1}: 3524, 2932, 2226, 1759, 1518, 1449, 1256 (Figure 39)

$[\alpha]_D^{27}$: -64.7 (c=0.94, $CHCl_3$)

CD $\Delta\varepsilon$ nm (c=10.3 μM, methanol, 23°C): -19.5 (203), -97.3 (217), 0 (240), 13.3 (256), 0 (281), -8.1 (294) (Figure 40)

18,6'-*O*-bisallyl-2'-*N*-(3''-fluorobenzoyl) Et 770 (4b)

Pale yellow amorphous powder (15.5 mg, 88.6% yield)

^{1}H-NMR: δ ppm *see* Table 9, Figure 41

^{13}C-NMR: δ ppm *see* Table 9, Figure 42

FAB-MS: *m/z* 973 $[M+H]^+$ Figure 43

HR-FABMS: *m/z* 973.3494 $[M+H]^+$; calcd for $C_{53}H_{54}N_4FO_{11}S$, 973.3494

IR (KBr) cm^{-1}: 2926, 2853, 2226, 1763, 1748, 1585, 1445 (Figure 44)

$[\alpha]_D^{27}$: -72.7 (c=1.0, $CHCl_3$)

CD $\Delta\varepsilon$ nm (c=10.3 μM, methanol, 27°C): 17.8 (207), 0 (210), -363.0 (216), 0 (223), 10.4 (239), 50.5 (254) (Figure 45)

18,6'-*O*-bisallyl-2'-*N*-(4''-fluorobenzoyl) Et 770 (4c)

Pale yellow amorphous powder (17.2 mg, 98.3% yield)

^{1}H-NMR: δ ppm *see* Table 10, Figure 46

^{13}C-NMR: δ ppm *see* Table 10, Figure 47

FAB-MS: *m/z* 973 $[M+H]^+$ Figure 48

HR-FABMS: *m/z* 973.3502 $[M+H]^+$; calcd for $C_{53}H_{54}N_4FO_{11}S$, 973.3494

IR (KBr) cm^{-1}: 2930, 2226, 1736, 1659, 1603, 1508, 1258 (Figure 49)

$[\alpha]_D^{25}$: -69.1 (c=1.0, $CHCl_3$)

CD Δε nm (c=10.3 μM, methanol, 27°C): 0 (210), -65.8 (213), 0 (219), 1.4 (220), -150.4 (229), 149.5 (255) (Figure 50)

18,6'-*O*-bisallyl-2'-*N*-(2'',3'',4''-trifluorobenzoyl) Et 770 (4d)

Colorless amorphous powder (14.5 mg, 80.1% yield)

^{1}H-NMR: δ ppm *see* Table 11, Figure 51-52

^{13}C-NMR: δ ppm *see* Table 11, Figure 53

FAB-MS: *m/z* 1008 $[M+H]^+$ Figure 54

HR-FABMS: *m/z* 1009.3298 $[M+H]^+$; calcd for $C_{53}H_{52}N_4F_3O_{10}S$, 1009.3306

IR (KBr) cm^{-1}: 3437, 2925, 2225, 1760, 1510, 1194 (Figure 55)

$[\alpha]_D^{25}$: -56.9 (c=0.58, $CHCl_3$)

CD Δε nm (c=10.9 μM, methanol, 22°C): 2.9 (210), -2.4 (216), -0.6 (226), 0.8 (256) (Figure 56)

18,6'-*O*-bisallyl-2'-*N*-(3''-trifluoromethylbenzoyl) Et 770 (4e)

Pale yellow amorphous powder (18.4 mg, 100% yield)

^{1}H-NMR: δ ppm *see* Table 12, Figure 57

^{13}C-NMR: δ ppm *see* Table 12, Figure 58

FAB-MS: *m/z* 1023 $[M+H]^+$ Figure 59

HR-FABMS: *m/z* 1023.3458 $[M+H]^+$; calcd for $C_{54}H_{54}N_4F_3O_{11}S$, 1023.3462

IR (KBr) cm^{-1}: 2932, 2226, 1763, 1748, 1520, 1487, 1331 (Figure 60)

$[\alpha]_D^{16}$: -55.1 (c=0.83, $CHCl_3$)

CD Δε nm (c=9.8 μM, methanol, 21°C): -10.7 (204), -119.3 (216), 0 (244), 17.6 (225), 0 (280), -8.7 (292) (Figure 61)

18,6'-*O*-bisallyl-2'-*N*-(4''-trifluoromethylbenzoyl) Et 770 (4f)

Pale yellow amorphous powder (18.4 mg, 100% yield)

^{1}H-NMR: δ ppm *see* Table 13, Figure 62

^{13}C-NMR: δ ppm *see* Table 13, Figure 63

FAB-MS: *m/z* 1023 $[M+H]^+$ (Figure 64)

HR-FABMS: *m/z* 1023.3458 $[M+H]^+$; calcd for $C_{54}H_{54}N_4F_3O_{11}S$, 1023.3462

IR (KBr) cm^{-1}: 2932, 2226, 1763, 1663, 1611, 1582, 1410 (Figure 65)

$[\alpha]_D^{25}$: -59.6 (c=0.67, $CHCl_3$)

CD Δε nm (c=9.8 μM, methanol, 23°C): -20.6 (204), -142.5 (216), 0 (245), 19.5 (256), 0 (280), -9.8 (294), 0 (304) (Figure 66)

18,6'-*O*-bisallyl-2'-*N*-(3''-fluorocinnamoyl) Et 770 (4g)

Pale yellow amorphous powder (11.0 mg, 61.1% yield)

^{1}H-NMR: δ ppm *see* Table 14, Figure 67

^{13}C-NMR: δ ppm *see* Table 14, Figure 68

FAB-MS: *m/z* 999 $[M+H]^+$ (Figure 69)

HR-FABMS: *m/z* 999.3655 $[M+H]^+$; calcd for $C_{55}H_{56}N_4FO_{11}S$, 999.3650

IR (KBr) cm^{-1}: 2934, 2225, 1759, 1659, 1518, 1447, 1260 (Figure 70)

$[\alpha]_D^{26}$: -32.4 (c=0.63, $CHCl_3$)

CD Δε nm (c=10.0 μM, methanol, 27°C): 0 (203), 27.8 (207), 0 (212), -260.0 (216), 0 (245), 22.1 (254), 0 (277) (Figure 71)

18,6'-*O*-bisallyl-2'-*N*-(4''-fluorocinnamoyl) Et 770 (4h)

Pale yellow amorphous powder (17.1 mg, 95.0% yield)

^{1}H-NMR: δ ppm *see* Table 15, Figure 72

^{13}C-NMR: δ ppm *see* Table 15, Figure 73

FAB-MS: *m/z* 999 $[M+H]^+$ (Figure 74)

HR-FABMS: *m/z* 999.3649 $[M+H]^+$; calcd for $C_{55}H_{56}N_4FO_{11}S$, 999.3650

IR (KBr) cm^{-1}: 2934, 2872, 2592, 2226, 1759, 1508, 1416 (Figure 75)

$[\alpha]_D^{25}$: -33.2 (c=0.95, $CHCl_3$)

CD Δε nm (c=10.0 μM, methanol, 23°C): 0 (203), 65.4 (207), 0 (212), -254.6 (223), 0 (246), 44.6 (254), 0 (269) (Figure 76)

18,6'-*O*-bisallyl-2'-*N*-(2''-naphthoyl) Et 770 (4i)

Pale yellow amorphous powder (14.7 mg, 81.2% yield)

^{1}H-NMR: δ ppm *see* Table 16, Figure 77

^{13}C-NMR: δ ppm *see* Table 16, Figure 78

FAB-MS: *m/z* 1005 $[M+H]^+$ (Figure 79)

HR-FABMS: *m/z* 1005.3743 $[M+H]^+$; calcd for $C_{57}H_{57}N_4O_{11}S$, 1005.3745

IR (KBr) cm^{-1}: 2930, 2226, 1761, 1748, 1518, 1464, 1445 (Figure 80)

$[\alpha]_D^{26}$: -43.9 (c=0.83, $CHCl_3$)

CD $\Delta\varepsilon$ nm (c=10.0 μM, methanol, 23°C): -8.2 (201), -44.5 (215), 0 (246), 4.8 (256), 0 (283), -1.4 (292), 0 (299) (Figure 81)

18,6'-*O*-bisallyl-2'-*N*-(1''-naphthoyl) Et 770 (4j)

Pale yellow amorphous powder (15.3 mg, 84.5% yield)

^{1}H-NMR: δ ppm *see* Table 17, Figure 82

^{13}C-NMR: δ ppm *see* Table17, Figure 83

FAB-MS: *m/z* 1005 $[M+H]^+$ (Figure 84)

HR-FABMS: *m/z* 1005.3749 $[M+H]^+$; calcd for $C_{57}H_{57}N_4O_{11}S$, 1005.3745

IR (KBr) cm^{-1}: 2926, 2225, 1761, 1747, 1655, 1518, 1445 (Figure 85)

$[\alpha]_D^{25}$: -67.5 (c=0.56, $CHCl_3$)

CD $\Delta\varepsilon$ nm (c=10.7 μM, methanol, 22°C): -2.6 (216), 2.1 (207), -0.9 (226), 0.1 (251), -0.4 (291) (Figure 86)

6.3 Deallylation of the 18,6'-*O*-bisallyl-2'-*N*-acyl Et 770 Derivatives

Nine of the 2'-*N*-acyl Et 770 derivatives (**5a**-**5i**) were prepared by the following procedure. Tributyltin hydride (16.5 eq) was added dropwise over 10 minutes to a vigorously stirred solution of the 18,6'-*O*-bisallyl-2'-*N*-acyl Et 770 derivative, $(Ph_3P)_2Pd(II)Cl_2$ (0.6 eq), and glacial AcOH (37.5 eq) in dry THF (4 ml) at 25°C, and the mixture was stirred at 25°C for 1-4 hours. And then, the mixture was diluted with water (10 ml), made alkaline with 5% aqueous $NaHCO_3$, and extracted with $CHCl_3$ (3 x 30 ml). The combined extracts were washed with 5% aqueous $NaHCO_3$, dried, and concentrated *in vacuo* to give a residue. The residue was purified by silica gel column chromatography using an appropriate eluent to give the corresponding purified product.

2'-*N*-(2''-fluorobenzoyl) Et 770 (5a)

Pale yellow amorphous powder (6.4 mg, 69.6% yield)

^{1}H-NMR: δ ppm *see* Table 19, Figure 87

^{13}C-NMR: δ ppm *see* Table 19, Figure 88

FAB-MS: *m/z* 893 $[M+H]^+$ (Figure 89)

HR-FABMS: *m/z* 893.2875 $[M+H]^+$; calcd for $C_{47}H_{46}N_4FO_{11}S$, 893.2868

IR (KBr) cm^{-1}: 3422, 2922, 2853, 2228, 1744, 1512, 1464 (Figure 90)

$[\alpha]_D^{19}$: -47.7 (c=0.41, $CHCl_3$)

CD $\Delta\varepsilon$ nm (c=8.92 μM, methanol, 25°C): -46.8 (216), 0 (243), 5.5 (252), 0 (270), -3.1 (280), -5.7 (291), 0 (303) (Figure 91)

2'-*N*-(3''-fluorobenzoyl) Et 770 (5b)

Pale yellow amorphous powder (8.0 mg, 87.0% yield)

^{1}H-NMR: δ ppm *see* Table 20, Figure 92

^{13}C-NMR: δ ppm *see* Table 20, Figure 93

FAB-MS: *m/z* 893 $[M+H]^+$ (Figure 94)

HR-FABMS: *m/z* 893.2869 $[M+H]^+$; calcd for $C_{47}H_{46}N_4FO_{11}S$, 893.2868

IR (KBr) cm^{-1}: 3443, 2928, 2228, 1751, 1657, 1587, 1437 (Figure 95)

$[\alpha]_D^{25}$: -59.1 (c=0.56, $CHCl_3$)

CD Δε nm (c=11.2 μM, methanol, 27°C): -29.5 (203), -150.7 (216), 0 (242), 20.5 (253), 0 (269), -17.2 (286), 0 (300) (Figure 96)

2'-*N*-(4''-fluorobenzoyl) Et 770 (5c)

Pale yellow amorphous powder (8.2 mg, 89.1% yield)

^{1}H-NMR: δ ppm *see* Table 21, Figure 97

^{13}C-NMR: δ ppm *see* Table 21, Figure 98

FAB-MS: *m/z* 893 $[M+H]^+$ (Figure 99)

HR-FABMS: *m/z* 893.2872 $[M+H]^+$; calcd for $C_{47}H_{46}N_4FO_{11}S$, 893.2868

IR (KBr) cm^{-1}: 3445, 2930, 2226, 1759, 1655, 1508, 1464 (Figure 100)

$[\alpha]_D^{25}$: -67.7 (c=0.51, $CHCl_3$)

CD Δε nm (c=10.2 μM, methanol, 25°C): 0 (203), 34.3 (206), 0 (211), -360.0 (221), 0 (242), 63.0 (253), 0 (268) (Figure 101)

2'-*N*-(2'',3'',4''-trifluorobenzoyl) Et 770 (5d)

Colorless amorphous powder (3.4 mg, 31.5% yield)

^{1}H-NMR: δ ppm *see* Table 22, Figure 102

^{13}C-NMR: δ ppm *see* Table 22, Figure 103

FAB-MS: *m/z* 928 $[M+H]^+$ (Figure 104)

HR-FABMS: *m/z* 929.2683 $[M+H]^+$; calcd for $C_{47}H_{44}N_4F_3O_{10}S$, 929.2680

IR (KBr) cm^{-1}: 3436, 2925, 2854, 1759, 1629, 1462, 1196 (Figure 105)

$[\alpha]_D^{25}$: -45.6 (c=0.09, $CHCl_3$)

CD Δε nm (c=19.4 μM, methanol, 22°C): 1.8 (201), -4.2 (216), -2.3 (226), 0.7 (251) (Figure 106)

2'-*N*-(3''-trifluoromethylbenzoyl) Et 770 (5e)

Pale yellow amorphous powder (7.4 mg, 80.4% yield)

^{1}H-NMR: δ ppm *see* Table 23, Figure 107

^{13}C-NMR: δ ppm *see* Table 23, Figure 108

FAB-MS: *m/z* 943 $[M+H]^+$ (Figure 109)

HR-FABMS: *m/z* 943.2839 $[M+H]^+$; calcd for $C_{48}H_{46}N_4F_3O_{11}S$, 943.2836

IR (KBr) cm^{-1}: 3449, 2934, 2228, 1751, 1659, 1514, 1464 (Figure 110)

$[\alpha]_D^{22}$: -37.8 (c=0.49, $CHCl_3$)

CD Δε nm (c=10.6 μM, methanol, 23°C): 4.9 (202), 0 (203), -87.8 (218), 0 (245), 12.0 (255), 0 (276), -10.0 (294) (Figure 111)

2'-*N*-(4''-trifluoromethylbenzoyl) Et 770 (5f)

Pale yellow amorphous powder (6.1 mg, 66.3% yield)

^{1}H-NMR: δ ppm *see* Table 24, Figure 112

^{13}C-NMR: δ ppm *see* Table 24, Figure 113

FAB-MS: *m/z* 943 $[M+H]^+$ (Figure 114)

HR-FABMS: *m/z* 943.2845 $[M+H]^+$; calcd for $C_{48}H_{46}N_4F_3O_{11}S$, 943.2836

IR (KBr) cm^{-1}: 3435, 2931, 2243, 1751, 1661, 1591, 1464 (Figure 115)

$[\alpha]_D^{20}$: -53.6 (c=0.38, $CHCl_3$)

CD Δε nm (c=10.6 μM, methanol, 23°C): -2.3 (204), -66.3 (217), 0 (245), 8.4 (255), 0 (273), -7.7 (291), 0 (310) (Figure 116)

2'-*N*-(3''-fluorocinnamoyl) Et 770 (5g)

Pale yellow amorphous powder (6.0 mg, 65.2% yield)

^{1}H-NMR: δ ppm *see* Table 25, Figure 117

^{13}C-NMR: δ ppm *see* Table 25, Figure 118

FAB-MS: *m/z* 919 $[M+H]^+$ (Figure 119)

HR-FABMS: *m/z* 919.3029 $[M+H]^+$; calcd for $C_{49}H_{48}N_4FO_{11}S$, 919.3025

IR (KBr) cm^{-1}: 3437, 2934, 2226, 1757, 1655, 1584, 1447 (Figure 120)

$[\alpha]_D^{25}$: -23.6 (c=0.37, $CHCl_3$)

CD Δε nm (c=10.9 μM, methanol, 25°C): 0 (203), 29.8 (206), 0 (212), -213.4 (216), 0 (245), 15.6 (252), 0 (265) (Figure 121)

2'-*N*-(4''-fluorocinnamoyl) Et 770 (5h)

Pale yellow amorphous powder (8.1 mg, 52.5% yield)

^{1}H-NMR: δ ppm *see* Table 26, Figure 122

^{13}C-NMR: δ ppm *see* Table 26, Figure 123

FAB-MS: *m/z* 919 $[M+H]^+$ (Figure 124)

HR-FABMS: *m/z* 919.3028 $[M+H]^+$; calcd for $C_{49}H_{48}N_4FO_{11}S$, 919.3024

IR (KBr) cm^{-1}: 3447, 2932, 2226, 1759, 1657, 1508, 1420 (Figure 125)

$[\alpha]_D^{19}$: -28.4 (c=0.54, $CHCl_3$)

CD Δε nm (c=10.9 μM, methanol, 23°C): -7.4 (207), -87.5 (216), 0 (246), 6.5 (252), 0 (264), -13.2 (286), 0 (297) (Figure 126)

2'-*N*-(2''-naphthoyl) Et 770 (5i)

Pale yellow amorphous powder (4.7 mg, 56.6% yield)

^{1}H-NMR: δ ppm *see* Table 27, Figure 127

^{13}C-NMR: δ ppm *see* Table 27, Figure 128

FAB-MS: *m/z* 925 $[M+H]^+$ (Figure 129)

HR-FABMS: *m/z* 925.3128 $[M+H]^+$; calcd for $C_{51}H_{49}N_4O_{11}S$, 925.3121

IR (KBr) cm^{-1}: 3443, 2932, 2228, 1751, 1653, 1516, 1464 (Figure 130)

$[\alpha]_D^{23}$: -36.5 (c=0.29, $CHCl_3$)

CD Δε nm (c=10.8 μM, methanol, 23°C): -9.8 (202), -52.5 (217), 0 (249), 5.8 (256), 0 (277), -4.5 (291), 0 (300) (Figure 131)

7. Cytotoxicity Assay

The cytotoxicity of the synthesized ecteinascidin derivatives were evaluated by the antiproliferative assay using three human cancer cell lines (HCT116 colorectal carcinoma, QG56 human lung carcinoma and DU145 human prostate carcinoma). A single-cell suspension of each cell line (2×10^3 cells/well) was added to the serially diluted test compounds in a microplate. The cell line was then cultured for 4 days. Cell growth was measured with a cell counting kit (DOJINDO, Osaka, Japan). IC_{50} was expressed as the concentration at which cell growth was inhibited by 50% compared with untreated control.

CHAPTER IV

RESULTS AND DISCUSSION

1. Extraction and Isolation of Ecteinascidin 770 from the Thai Tunicate *Ecteinascidia thurstoni*

Ecteinascidin 743 (Et 743, **1**) is a potent marine-derived antitumor compound isolated from the Caribbean tunicate *Ecteinascidia turbinata*, and is currently approved by European Medicines Agency for using in the patients with advanced soft tissue sarcoma (EMA, 2007) and relapsed ovarian cancer (EMA, 2009). Due to the **α-**carbinolamine functionality in the structure, Et 743 was unstable during extraction and isolation processes causing low yield results. Thus, the KCN-pretreated strategy was applied to isolate the ecteinascidin-type compounds of which the labile **α-**carbinolamine group was converted to the more stable **α-**cyanoamine group. In 2002, Suwanborirux *et al*. succeeded in isolating a large amount of the stable ecteinascidin 770 (Et 770, **2**) from the Thai tunicate *E. thurstoni* by using the KCN-pretreated strategy. This strategy provides the advantage of increasing the yield of ecteinascidins.

The Thai tunicate *E. thurstoni* was collected from Phuket Island in the southern part of Thailand. The identification and characterization of this tunicate were conducted, mainly on the basic of its morphological characteristic by Dr.Teruaki Nishikawa of Nagoya University Museum, Japan. However, the distribution information of the Thai tunicate is unclear, therefore our collection has been conducted following the blooming period. For this research, the tunicate collection was done in during May 2012 and the sample was stored frozen until use.

The homogenized tunicate sample (65 kg, wet wt) was pretreated with potassium cyanide and macerated with methanol to afford an aqueous emulsion, upon filtration and concentration. The emulsion was further partitioned with ethyl acetate to give the crude ethyl acetate extract as a dark brown residue (38.87 g), which was respectively fractionated with silica gel quick column chromatography, Sephadex LH-20 gel filtration, and silica gel flash column chromatography, to give the crude Et 770. Then the crude product was crystallized with co-solvent of dichloromethane-methanol to give colorless crystals of Et 770 (258.2 mg, 4.0×10^{-4}% of wet animal). The isolation yield of Et 770 is comparable to that of the previous study (6.0×10^{-4}% of wet animal) (Suwanborirux *et al*., 2002) whereas the ecteinascidins isolated from the Caribbean tunicate *E. turbinata* were obtained in lower yields (1.0×10^{-4}% to 1.0×10^{-5}% yield of wet animal) (Rinehart *et al*., 1990). The isolation process of Et 770 is summarized in Scheme 3. The isolated Et 770 was structurally elucidated by comparison its NMR spectral data with the authentic sample (Suwanborirux *et al*., 2002), which was identical in all respects (Table 5). The obtained Et 770 was further used as the synthetic starting material for this study.

Ecteinascidia thurstoni
(65 kg, wet wt)

-Homogenized with phosphate buffer solution
-Adjusted to pH 7.0±0.2
-Added 10% KCN, stirred 5 hr.
-Macerated with MeOH (20 l x 5)
-Filtered and concentrated
-Partitioned with EtOAc/H_2O

EtOAc extract
(38.87 g, dark brown residue)

Aqueous-MeOH part

1. Quick CC.; silica gel, gradient of Hexane : EtOAc (3:1-1:3)
2. Sephadex LH 20; MeOH
3. Flash CC.; silica gel, CH_2Cl_2 : EtOAc (2:3)

Crude Et 770

Crystallized with CH_2Cl_2 : MeOH (1:1)

Colorless crystal of Et 770
(258.2 mg)

Scheme 3. The extraction and isolation of Et 770 from *Ecteinascidia thurstoni.*

Table 5. 500 MHz ^{1}H- and 125 MHz ^{13}C-NMR data of Et 770 in $CDCl_3$.

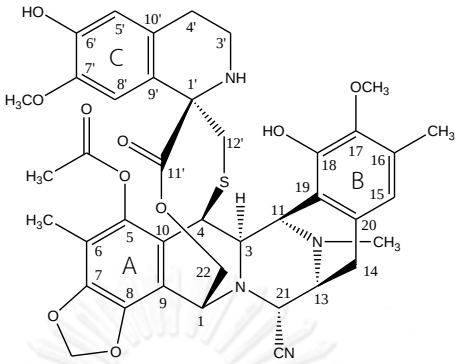

No.	δ_H in ppm (*J* in Hz)	δ_C in ppm	No.	δ_H in ppm (*J* in Hz)	δ_C in ppm
1	4.32 br s	61.2	4'	2.60 m	28.8
3	3.51 d (4.9)	59.7		2.42 dt (15.9, 3.4)	
4	4.57 br s	41.9	5'	6.46 s	114.2
5	-	141.4	6'	-	144.6
6	-	113.4	7'	-	144.4
7	-	145.3	8'	6.44 s	109.9
8	-	140.2	9'	-	125.8
9	-	114.1	10'	-	129.2
10	-	121.2	11'	-	172.6
11	4.28 dd (4.9, 1.2)	54.8	12'	2.35 br	42.3
13	3.41 m	54.7		2.15 m	
14	2.91, 2H, br d (7.6)	24.2	18-OH	5.77 s	
15	6.60 s	120.7	6'-OH	5.59 br s	
16	-	129.4	OCH_2O	6.04 d (1.2)	102.0
17	-	143.1		5.97 d (1.2)	
18	-	147.9	17-OCH_3	3.78 s	60.4
19	-	118.4	7'-OCH_3	3.60 s	55.2
20	-	130.8	5-OCO$\underline{CH_3}$	2.26 s	20.4
21	4.18 d (2.8)	59.6	12-NCH_3	2.19 s	41.6
22	5.01 d (11.6)	60.1	6-CH_3	2.04 s	9.7
	4.12 dd (11.6, 2.0)		16-CH_3	2.32 s	15.8
1'	-	64.6	5-OCO	-	168.2
3'	3.11 br t	39.7	21-CN	-	118.7
	2.79 m				

2. Preparation of 18,6'-*O*-bisallyl Et 770

The reactive 18- and 6'-OHs of Et 770 were protected by treating with 25 equivalents of K_2CO_3 and 20 equivalents of allyl bromide at room temperature for 18 hours to provide 18,6'-*O*-bisallyl Et 770 (**3**) in 77.5% yield. The mechanism of reaction has been proposed that the lone pair electrons of oxygen atoms at 18 and 6' positions undergo nucleophilic attack to the electrophilic carbons of allyl bromides in K_2CO_3 as base. The allylation mechanism to produce 18,6'-*O*-bisallyl Et 770 is shown in Figure 24.

The chemical structure of the bisallylated product (**3**) was mainly determined based on HR-FABMS and NMR spectral data. The HR-FABMS data of **3** (Figure 33) presented a pseudomolecular ion $[M+H]^+$ at *m/z* 851.3328, corresponding to the molecular formula $C_{46}H_{50}N_4O_{10}S+H^+$ (calcd 851.3326). The ^{1}H- and ^{13}C-NMR spectra (Table 6, Figures 31-32) of **3** showed the characteristic signals similar to those of Et 770. In addition, the proton and carbon signals of two allyllic groups were observed in regions of δ_H 4.35-6.10 ppm (Figure 52) and δ_C 69.6-134.6 ppm, along with the disappearance of the 18-OH (δ_H 5.77) and 6'-OH (δ_H 5.59) signals as follows: δ_H 5.99/δ_C 133.2 (6'-OCH$_2$<u>CH</u>=CH$_2$), δ_H 5.31, 5.22/δ_C 117.8 (6'-OCH$_2$CH=<u>CH$_2$</u>), δ_H 4.49/δ_C 69.6 (6'-O<u>CH$_2$</u>CH=CH$_2$), δ_H 6.10/δ_C 134.6 (18-OCH$_2$<u>CH</u>=CH$_2$), δ_H 5.45, 5.25/δ_C 116.7 (18-OCH$_2$CH=<u>CH$_2$</u>), and δ_H 4.80, 4.35/δ_C 72.9 (18-O<u>CH$_2$</u>CH=CH$_2$). Moreover, the downfield shifts of the carbon signals of the aromatic rings B (C-15 to C-20) and C (C-5' to C-10') compared to those of Et 770 were the useful information to confirm the nucleophilic substitution at the phenolic hydroxyls by the allyl groups. The allyl substitutions at C-6' and C-18 were confirmed by HMBC correlations (Figure 25) of the allyl methylene protons 6'-O<u>CH$_2$</u> and 18-O<u>CH$_2$</u> to the aromatic carbons (C-6', δ_C 147.0 and

C-18, δ_C 150.6), respectively. Importantly, assignments for all protons and carbons of the 18,6'-*O*-bisallyl Et 770 was identical to the authentic compound (Saktrakulkla *et al*., 2011).

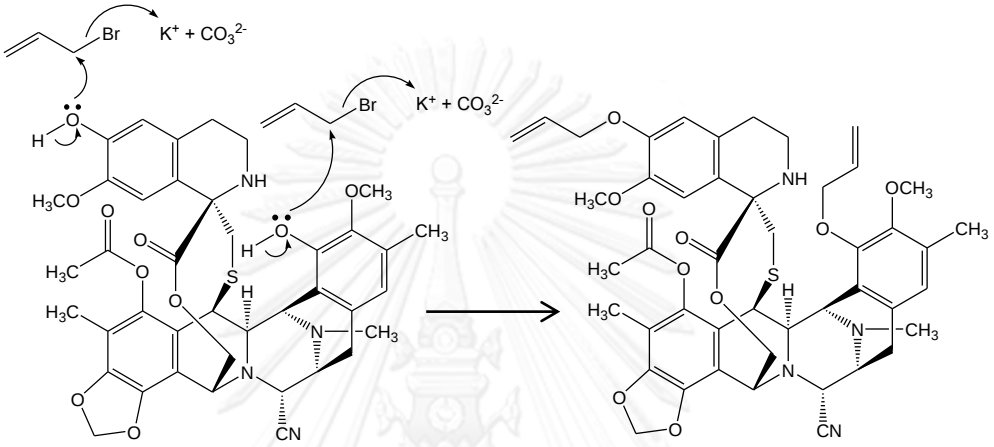

Figure 24. The allylation mechanism to prepare 18,6'-*O*-bisallyl Et 770.

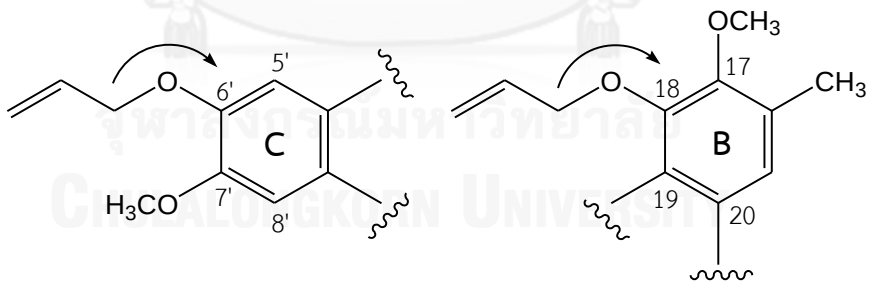

Figure 25. Partial HMBC correlations of 18,6'-*O*-bisallyl Et 770.

Table 6. 500 MHz ^{1}H- and 125 MHz ^{13}C-NMR data of 18,6'-*O*-bisallyl Et 770 in $CDCl_3$.

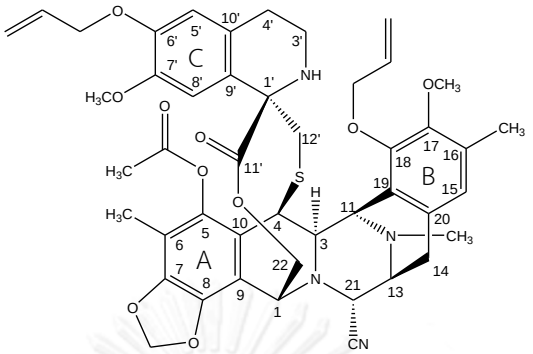

No.	δ_H in ppm (*J* in Hz)	δ_C in ppm	No.	δ_H in ppm (*J* in Hz)	δ_C in ppm
1	4.33 br s	61.2	6'	-	147.0
3	3.52 br d (4.0)	59.8	7'	-	147.0
4	4.54 br s	41.9	8'	6.48 br s	110.9
5	-	141.3	9'	-	126.5
6	-	113.3	10'	-	128.3
7	-	145.4	11'	-	172.5
8	-	140.2	12'	2.33 br s	42.0
9	-	114.0		2.14 br d	
10	-	121.2	6'-$OCH_2\underline{CH}=CH_2$	5.99 ddt (17.1, 10.7, 5.2)	133.2
11	4.25 d (4.0)	55.1	6'-$OCH_2CH=\underline{CH_2}$	5.31 dq (17.1, 1.3)	117.8
13	3.43 dd (8.2, 1.4)	54.7		5.22 dq (10.7, 1.3)	
14	2.95, 2H, d (8.2)	24.2	6'-$O\underline{CH_2}CH=CH_2$	4.49, 2H, d (5.2)	69.6
15	6.79 s	124.5	18-$OCH_2\underline{CH}=CH_2$	6.10 ddt (17.1, 10.4, 5.2)	134.6
16	-	131.3	18-$OCH_2CH=\underline{CH_2}$	5.45 dq (17.1, 1.5)	116.7
17	-	148.9		5.25 dq (10.4, 1.5)	
18	-	150.6	18-$O\underline{CH_2}CH=CH_2$	4.80 dd (12.6, 5.2)	72.9
19	-	124.7		4.35 dd (12.6, 5.2)	
20	-	130.3	OCH_2O	6.05 d (1.2)	101.9
21	4.19 d (1.4)	59.3		5.98 d (1.2)	
22	5.02 d (11.3)	59.8	17-OCH_3	3.83 s	59.4
	4.13 d (11.3)		7'-OCH_3	3.61 s	55.2
1'	-	64.6	5-$OCO\underline{CH_3}$	2.24 s	20.3
3'	3.12 m	39.6	12-NCH_3	2.20 s	41.7
	2.81 br t		6-CH_3	2.04 s	9.7
4'	2.63 m	28.9	16-CH_3	2.29 s	15.8
	2.49 br t (15.9)		5-OCO	-	168.1
5'	6.41 s	113.2	21-CN	-	118.1

3. Preparation of the 18,6'-*O*-bisallyl-2'-*N*-acyl Et 770 Derivatives

Ten 18,6'-*O*-bisallyl-2'-*N*-acyl Et 770 derivatives (**4a**-**4j**) were synthesized in 61.1–100 % yields (Table 7) by treating 18,6'-*O*-bisallyl Et 770 with the corresponding acyl acid chlorides (15-50 eq) and a catalytic amount (0.5-5 eq) of 4-dimethylaminopyridine (DMAP) in dry pyridine at room temperature for several hours. Ten aromatic acyl acid chlorides in this study included, four fluorine-substituted benzoyl chlorides, two trifluoromethyl-substituted benzoyl chlorides, two fluorine-substituted cinnamoyl chlorides, and two napthoyl chlorides. The mechanism of reaction has been proposed that the acyl acid chloride is activated to an active form by DMAP. After that, the electrophilic carbonyl carbon undergoes nucleophilic attack by the lone pair electrons of 2'-*N* and forms an amide bond in the final step. The acylation mechanism to prepare the 18,6'-*O*-bisallyl-2'-*N*-acyl Et 770 derivatives is shown in Figure 26.

The HR-FABMS spectra (Figures 38, 43, 48, 54, 59, 64, 69, 74, 79, and 84) of the synthesized products (**4a**-**4j**) presented the pseudo-molecular ions $[M+H]^+$ corresponding to the molecular formulae of the expected products as summarized in Table 7. Assignments for all protons and carbons of the compounds were mainly accomplished by extensive analyses through 1D-NMR and 2D-NMR measurements. The ^{1}H- and ^{13}C-NMR spectra (Figures 36, 37, 41, 42, 46, 47, 51, 53, 57, 58, 62, 63, 67, 68, 72, 73, 77, 78, 82, and 83) of the 18,6'-*O*-bisallyl-2'-*N*-acyl Et 770 derivatives showed characteristic signals similar to those of 18,6'-*O*-bisallyl Et 770. The additional signals of the corresponding aromatic acyl moiety and the downfield shifts of C-1' (δ_C 68-70 ppm) and C-3' (δ_C 44-46 ppm) implied the 2'-*N* acylation. Importantly, the 2'-*N* substitutions were confirmed by HMBC correlations from methylene protons of C-3'

position to the acyl carbonyl carbons (Figure 27). The NMR spectral data of the bisallyl 2'-*N*-acylated products are shown in Tables 8-17.

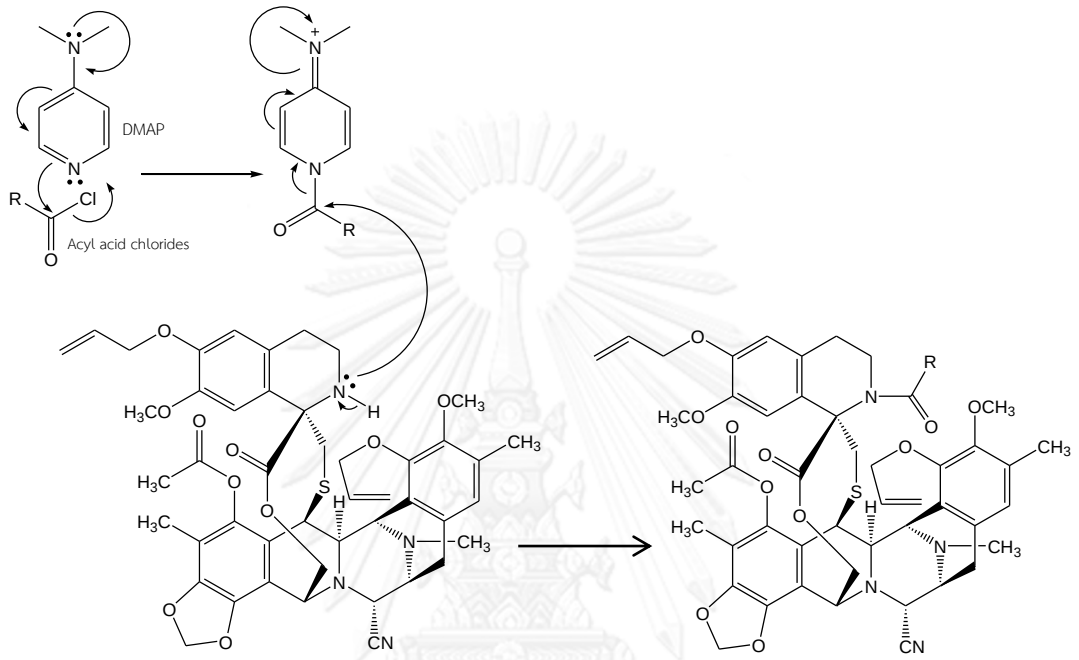

Figure 26. The acylation mechanism catalyzed by DMAP.

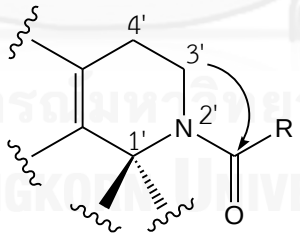

Figure 27. A partial HMBC correlation of the 18,6'-*O*-bisallyl-2'-*N*-acyl Et 770 derivatives.

Table 7. The summary of yields and HR-FABMS data of the 18,6'-*O*-bisallyl-2'-*N*-acyl Et 770 derivatives.

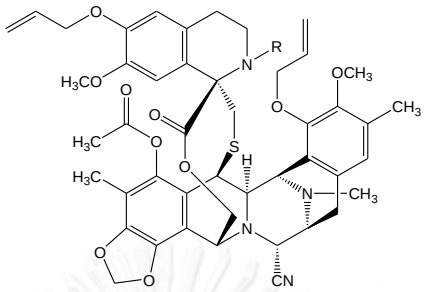

Compounds	R	%Yield	*m/z* (HR-FABMS)
4a	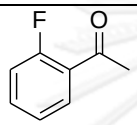	86.9	973.3494 $[M+H]^+$; calcd for $C_{53}H_{54}N_4FO_{11}S$, 973.3494
4b	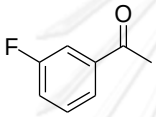	88.6	973.3494 $[M+H]^+$; calcd for $C_{53}H_{54}N_4FO_{11}S$, 973.3494
4c	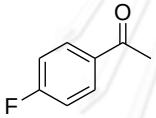	98.3	973.3502 $[M+H]^+$; calcd for $C_{53}H_{54}N_4FO_{11}S$, 973.3494
4d	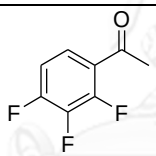	80.1	1009.3298 $[M+H]^+$; calcd for $C_{53}H_{52}N_4F_3O_{10}S$, 1009.3306
4e	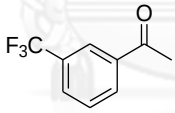	100	1023.3458 $[M+H]^+$; calcd for $C_{54}H_{54}N_4F_3O_{11}S$, 1023.3462
4f	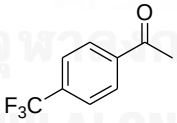	100	1023.3458 $[M+H]^+$; calcd for $C_{54}H_{54}N_4F_3O_{11}S$, 1023.3462
4g	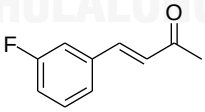	61.1	999.3655 $[M+H]^+$; calcd for $C_{55}H_{56}N_4FO_{11}S$, 999.3650
4h	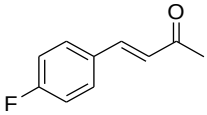	95.0	999.3649 $[M+H]^+$; calcd for $C_{55}H_{56}N_4FO_{11}S$, 999.3650
4i	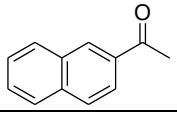	81.2	1005.3743 $[M+H]^+$; calcd for $C_{57}H_{57}N_4O_{11}S$, 1005.3745
4j	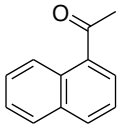	84.5	1005.3749 $[M+H]^+$; calcd for $C_{57}H_{57}N_4O_{11}S$, 1005.3745

Table 8. 500 MHz ^{1}H- and 125 MHz ^{13}C-NMR data of 18,6'-*O*-bisallyl-2'-*N*-(2''-fluorobenzoyl) Et 770 in $CDCl_3$.

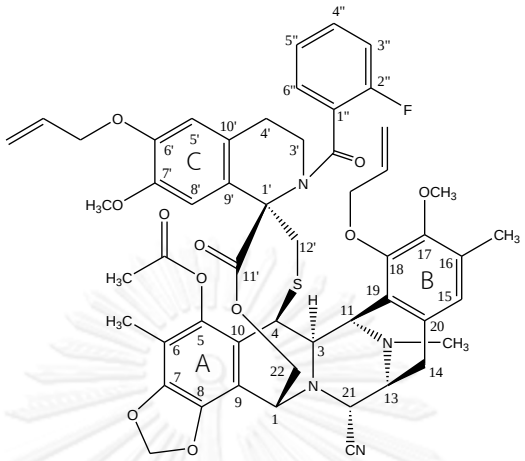

No.	δ_H in ppm (*J* in Hz)	δ_C in ppm	No.	δ_H in ppm (*J* in Hz)	δ_C in ppm
1	4.37 s	60.5	11'	-	166.1
3	3.56 d (4.8)	61.0	12'	3.50 br s	39.2
4	4.64 br s	42.2		2.51 br s	
5	-	141.4	1''	-	125.7
6	-	112.7	2''	-	161.2
7	-	145.4	3''	7.13 t like (8.6)	116.0
8	-	140.9	4''	7.38 t like	130.0
9	-	113.6	5''	7.26 t like	124.3
10	-	122.6	6''	7.41 q like (6.6)	131.2
11	4.23 dd (5.4, 1.4)	55.4	6'-$OCH_2\underline{CH}=CH_2$	5.99 ddt (17.3, 10.7, 5.3)	133.1
13	3.45 m	54.8	6'-$OCH_2CH=\underline{CH_2}$	5.32 dq (17.3, 1.5)	117.9
14	2.96, 2H, d (8.5)	24.8		5.21 dq (10.7, 1.5)	
15	6.58 s	124.7	6'-$O\underline{CH_2}CH=CH_2$	4.49, 2H, dt (5.3, 1.5)	69.6
16	-	131.2	18-$OCH_2\underline{CH}=CH_2$	6.08 ddt (17.2, 10.7, 5.4)	134.7
17	-	148.7	18-$OCH_2CH=\underline{CH_2}$	5.44 dd (17.2, 1.5)	116.6
18	-	150.2		5.21 dq (10.7, 1.5)	
19	-	124.4	18-$O\underline{CH_2}CH=CH_2$	4.79 ddt (12.8, 5.4, 1.5)	72.9
20	-	130.0		4.30 ddt (12.8, 5.4, 1.5)	
21	4.16 d (2.2)	59.4	OCH_2O	6.07 d (1.4)	102.0
22	4.64 br s	60.7		5.98 d (1.4)	
	4.48 br d (10.3)		17-OCH_3	3.77 s	59.4
1'	-	70.5	7'-OCH_3	3.62 s	55.2
3'	3.50, 2H, br s	45.6	5-$OCO\underline{CH_3}$	2.29 s	20.2
4'	2.41, 2H, m	29.4	12-NCH_3	2.14	41.8
5'	6.35 s	112.7	6-CH_3	2.05	9.7
6'	-	147.1	16-CH_3	1.80	15.6
7'	-	147.4	2'-NCO	-	168.9
8'	6.35 s	111.1	5-OCO	-	168.3
9'	-	127.9	21-CN	-	118.3
10'	-	126.5			

Table 9. 500 MHz ^{1}H- and 125 MHz ^{13}C-NMR data of 18,6'-*O*-bisallyl-2'-*N*-(3''-fluorobenzoyl) Et 770 in $CDCl_3$.

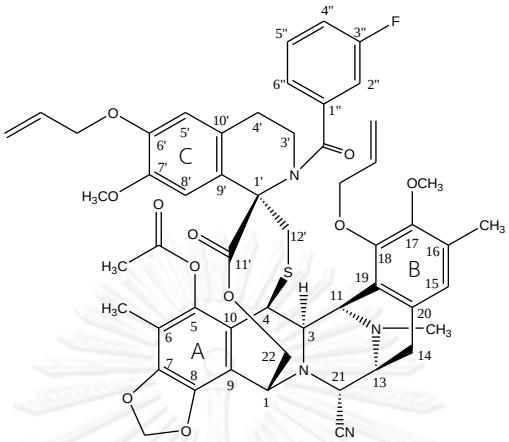

No.	δ_H in ppm (*J* in Hz)	δ_C in ppm	No.	δ_H in ppm (*J* in Hz)	δ_C in ppm
1	4.33 s	60.4	11'	-	169.4
3	3.59 br s	60.9	12'	3.58 d (15.3)	39.3
4	4.63 br	42.0		2.30 d (15.3)	
5	-	141.2	1''	-	139.2
6	-	112.6	2''	7.21-7.15 (overlapped)	115.2
7	-	145.5	3''	-	162.4
8	-	141.3	4''	7.21-7.15 (overlapped)	117.2
9	-	113.2	5''	7.43 td (8.0, 5.7)	130.2
10	-	122.3	6''	7.25 d (8.0)	123.8
11	4.22 dd (4.1, 1.4)	55.4	6'-$OCH_2\underline{CH}=CH_2$	5.98 ddt (17.2, 10.5, 5.4)	133.1
13	3.45 m	54.8	6'-$OCH_2CH=\underline{CH_2}$	5.32 dq (17.2, 1.5)	117.9
14	2.86 br d (17.3)	24.9		5.22 dq (10.5, 1.5)	
	3.00 dd (17.3, 9.4)		6'-$O\underline{CH_2}CH=CH_2$	4.48, 2H, dt (5.4, 1.6)	69.6
15	6.61 br s	124.6	18-$OCH_2\underline{CH}=CH_2$	6.09 ddt (17.2, 10.7, 5.4)	134.7
16	-	131.3	18-$OCH_2CH=\underline{CH_2}$	5.43 dq (17.2, 1.5)	116.8
17	-	148.7		5.23 dq (10.7, 1.5)	
18	-	150.4	18-$O\underline{CH_2}CH=CH_2$	4.78 ddt (12.8, 5.4, 1.5)	72.9
19	-	124.4		4.29 ddt (12.8, 5.4, 1.5)	
20	-	130.0	OCH_2O	6.09 d (1.3)	102.1
21	4.13 d (2.3)	59.5		6.09 d (1.3)	
22	4.51, 2H, br	60.4	17-OCH_3	3.72 s	59.4
1'	-	69.0	7'-OCH_3	3.66 s	55.2
3'	3.50, 2H, m	45.6	5-$OCO\underline{CH_3}$	2.29 s	20.2
4'	2.40, 2H, m	29.1	12-NCH_3	2.14 s	41.8
5'	6.35 br s	112.8	6-CH_3	2.04 s	9.7
6'	-	147.1	16-CH_3	1.80 s	15.3
7'	-	147.4	2'-NCO	-	171.2
8'	6.53 br s	111.2	5-OCO	-	168.3
9'	-	128.1	21-CN	-	118.2
10'	-	125.8			

Table 10. 500 MHz ^{1}H- and 125 MHz ^{13}C-NMR data of 18,6'-*O*-bisallyl-2'-*N*-(4''-fluorobenzoyl) Et 770 in $CDCl_3$.

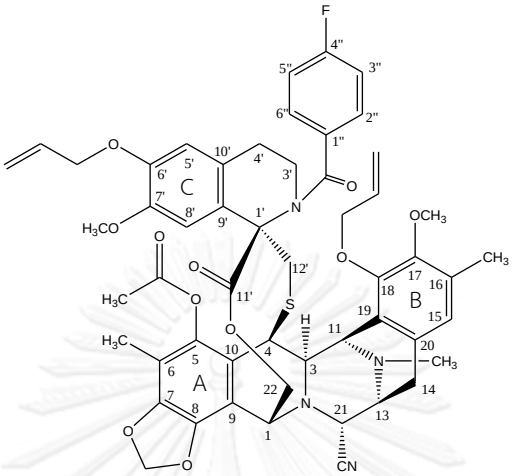

No.	δ_H in ppm (*J* in Hz)	δ_C in ppm	No.	δ_H in ppm (*J* in Hz)	δ_C in ppm
1	4.30 s	60.3	10'	-	125.7
3	3.60 br d (4.8)	60.9	11'	-	169.4
4	4.61 br s	41.8	12'	3.52 d (15.6)	39.6
5	-	141.1		2.30 d (15.6)	
6	-	112.5	1''	-	132.9
7	-	145.5	2''	7.48 dd (8.6, 5.5)	130.6
8	-	141.5	3''	7.15 t (8.6)	115.4
9	-	113.0	4''	-	163.9
10	-	122.1	5''	7.15 t (8.6)	115.4
11	4.22 dd (4.8, 1.3)	55.4	6''	7.48 dd (8.6, 5.5)	130.6
13	3.44 br d (9.3)	54.8	6'-$OCH_2\underline{CH}=CH_2$	5.99 ddt (17.2, 10.5, 5.4)	133.1
14	2.97 dd (17.2, 9.3)	25.0	6'-$OCH_2CH=\underline{CH_2}$	5.32 dq (17.2, 1.5)	117.8
	2.81 br d (17.2)			5.22 dq (10.5, 1.5)	
15	6.57 br s	124.4	6'-$O\underline{CH_2}CH=CH_2$	4.48, 2H, dt (5.4, 1.5)	69.6
16	-	131.1	18-$OCH_2\underline{CH}=CH_2$	6.08 ddt (17.2, 10.5, 5.4)	134.6
17	-	148.6	18-$OCH_2CH=\underline{CH_2}$	5.44 dq (17.2, 1.5)	116.8
18	-	150.5		5.23 dq (10.5, 1.5)	
19	-	124.5	18-$O\underline{CH_2}CH=CH_2$	4.78 ddt (12.8, 5.5, 1.5)	73.0
20	-	130.1		4.29 ddt (12.8, 5.4, 1.5)	
21	4.10 d (2.0)	59.6	OCH_2O	6.10 d (1.5)	102.1
22	4.61 br s	60.4		6.01 d (1.5)	
	4.43 br d (11.0)		17-OCH_3	3.73 s	59.4
1'	-	68.6	7'-OCH_3	3.66 s	55.2
3'	3.49, 2H, t (6.0)	45.5	5-$OCO\underline{CH_3}$	2.29 s	20.2
4'	2.39, 2H, m	29.0	12-NCH_3	2.14 s	41.8
5'	6.34 s	112.8	6-CH_3	2.04 s	9.7
6'	-	147.0	16-CH_3	1.85 br s	15.6
7'	-	147.3	2'-NCO	-	172.0
8'	6.58 br s	111.3	5-OCO	-	168.3
9'	-	128.2	21-CN	-	118.1

Table 11. 300 MHz ^{1}H- and 75 MHz ^{13}C-NMR data of 18,6'-*O*-bisallyl-2'-*N*-(2",3",4"-trifluorobenzoyl) Et 770 in $CDCl_3$.

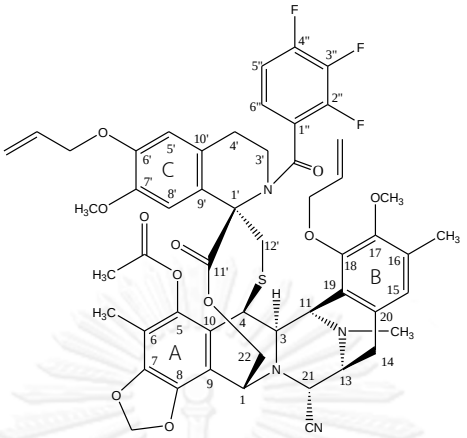

No.	δ_H in ppm (*J* in Hz)	δ_C in ppm	No.	δ_H in ppm (*J* in Hz)	δ_C in ppm
1	4.35 br s	60.4	10'	-	126.0
3	3.56 br s	60.9	11'	-	168.3
4	4.67 br	42.2	12'	3.50 br	39.0
5	-	140.9		2.49 d (14.7)	
6	-	112.6	1"	-	
7	-	145.5	2"	-	
8	-	141.4	3"	-	
9	-	113.4	4"	-	
10	-	122.4	5"	7.05 br s	112.8
11	4.22 m	55.4	6"	7.07 br s	123.3
13	3.50 br	54.9	6'-$OCH_2\underline{CH}=CH_2$	5.96 ddt (17.1, 10.5, 5.4)	133.0
14	2.98 br d (17.7)	24.9	6'-$OCH_2CH=\underline{CH_2}$	5.29 dq (17.1, 1.5)	117.9
	2.89 br d (17.7)			5.20 dq (10.5, 1.5)	
15	6.52 s	123.2	6'-$O\underline{CH_2}CH=CH_2$	4.46, 2H, br d (5.4)	69.7
16	-	131.2	18-$OCH_2\underline{CH}=CH_2$	6.05 ddt (17.1, 10.5, 5.4)	134.7
17	-	148.8	18-$OCH_2CH=\underline{CH_2}$	5.41 dq (17.1, 1.5)	116.8
18	-	150.2		5.20 dq (10.5, 1.5)	
19	-	124.6	18-$O\underline{CH_2}CH=CH_2$	4.76 dd (12.9, 5.1)	72.9
20	-	130.0		4.27 m	
21	4.14 br s	59.4	OCH_2O	6.05 d (0.6)	102.1
22	4.64 br s	60.6		5.96 d (0.6)	
	4.24 m		17-OCH_3	3.72 s	59.4
1'	-	70.5	7'-OCH_3	3.59 s	55.2
3'	3.45, 2H, br	45.5	5-$OCO\underline{CH_3}$	2.26 s	20.3
4'	2.37 dt (16.2, 4.2)	29.3	12-NCH_3	2.12 s	41.8
	2.49 br		6-CH_3	2.01 s	9.8
5'	6.33 s	112.6	16-CH_3	1.79 s	15.6
6'	-	147.5	2'-NCO	-	168.8
7'	-	147.2	5-OCO	-	164.0
8'	6.33 s	111.0	21-CN	-	118.1
9'	-	127.7			

Table 12. 500 MHz ^{1}H- and 125 MHz ^{13}C-NMR data of 18,6'-*O*-bisallyl-2'-*N*-(3''-trifluoromethylbenzoyl) Et 770 in $CDCl_3$.

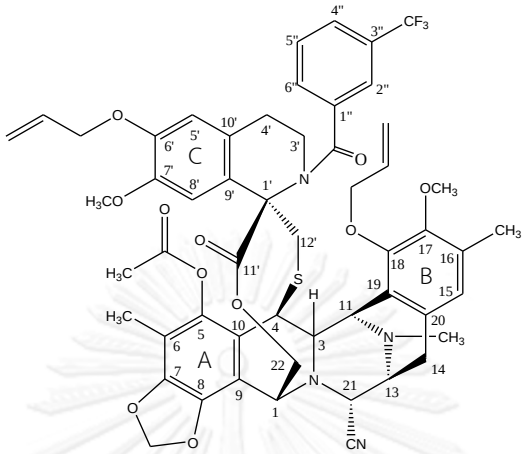

No.	δ_H in ppm (*J* in Hz)	δ_C in ppm	No.	δ_H in ppm (*J* in Hz)	δ_C in ppm
1	4.37 s	60.6	9'	-	127.8
3	3.56 d (5.1)	60.9	10'	-	126.0
4	4.65 br s	42.2	11'	-	169.4
5	-	141.1	12'	3.63, 2H, d (15.4)	39.0
6	-	112.6	1''	-	138.1
7	-	145.5	2''	7.79 s	125.1
8	-	141.3	3''	-	130.9
9	-	113.4	4''	7.77 d (7.7)	126.8
10	-	122.4	5''	7.62 t (7.7)	129.0
11	4.22 dd (5.1, 1.4)	55.3	6''	7.67 d (7.7)	131.6
13	3.46 d (9.7)	54.8	3''-CF_3	-	123.8
14	2.98 dd (17.3, 9.3)	24.7	6'-$OCH_2\underline{CH}=CH_2$	5.99 ddt (17.3, 10.6, 5.4)	133.1
	2.87 d (17.3)		6'-$OCH_2CH=\underline{CH_2}$	5.32 dq (17.3, 1.5)	117.9
15	6.44 s	124.3		5.22 dq (10.6, 1.5)	
16	-	131.2	6'-$O\underline{CH_2}CH=CH_2$	4.49, 2H, dt (5.4, 1.5)	69.6
17	-	148.7	18-$OCH_2\underline{CH}=CH_2$	6.07 ddt (17.4, 10.6, 5.4)	134.7
18	-	150.3	18-$OCH_2CH=\underline{CH_2}$	5.43 dq (17.4, 1.5)	116.7
19	-	124.3		5.22 dq (10.6, 1.5)	
20	-	130.0	18-$O\underline{CH_2}CH=CH_2$	4.77 ddt (12.7, 5.4, 1.4)	72.9
21	4.17 d (2.2)	59.6		4.28 ddt (12.7, 5.4, 1.4)	
22	4.65 br s	60.5	OCH_2O	6.09 d (1.3)	102.0
	4.40 br d (9.4)			6.00 d (1.3)	
1'	-	70.1	17-OCH_3	3.73 s	59.6
3'	3.58 m	46.2	7'-OCH_3	3.65 s	55.2
	3.44 m		5-$OCO\underline{CH_3}$	2.30 s	20.2
4'	2.47 ddd (16.1, 10.1, 5.8)	29.1	12-NCH_3	2.13 s	41.8
	2.34 dd (16.1, 4.2)		6-CH_3	2.05 s	9.7
5'	6.35 s	112.6	16-CH_3	1.58 s	15.1
6'	-	147.2	2'-NCO	-	170.4
7'	-	147.4	5-OCO	-	168.2
8'	6.46 s	111.2	21-CN	-	118.2

Table 13. 500 MHz ^{1}H- and 125 MHz ^{13}C-NMR data of 18,6'-*O*-bisallyl-2'-*N*-(4''-trifluoromethylbenzoyl) Et 770 in $CDCl_3$.

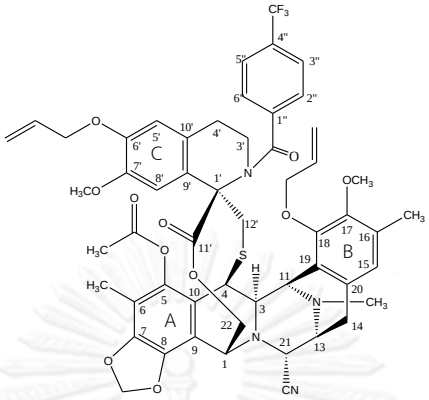

No.	δ_H in ppm (*J* in Hz)	δ_C in ppm	No.	δ_H in ppm (*J* in Hz)	δ_C in ppm
1	4.35 s	60.5	10'	-	125.8
3	3.58 d (6.0)	60.9	11'	-	169.3
4	4.65 br s	42.0	12'	3.59 d (14.7)	39.2
5	-	141.2		2.45 d (14.7)	
6	-	112.7	1"	-	140.6
7	-	145.5	2"	7.58 d (7.9)	128.5
8	-	141.3	3"	7.73 d (7.9)	125.4
9	-	113.2	4"	7.58 d (7.9)	132.0
10	-	122.3	5"	7.73 d (7.9)	125.4
11	4.22 dd (6.0, 1.5)	55.4	6"	-	128.5
13	3.46 d (9.3)	54.8	4"-CF_3	-	123.8
14	2.99 dd (17.2, 9.3)	24.9	6'-$OCH_2\underline{CH}=CH_2$	5.99 ddt (17.2, 10.6, 5.4)	133.1
	2.86 d (17.2)		6'-$OCH_2CH=\underline{CH_2}$	5.32 dq (17.2, 1.4)	117.9
15	6.53 s	124.5		5.23 dq (10.5, 1.4)	
16	-	131.1	6'-$O\underline{CH_2}CH=CH_2$	4.49, 2H, dt (5.4, 1.4)	69.6
17	-	148.7	18-$OCH_2\underline{CH}=CH_2$	6.07 ddt (17.2, 10.5, 5.4)	134.7
18	-	150.4	18-$OCH_2CH=\underline{CH_2}$	5.44 dq (17.2, 1.4)	116.8
19	-	124.6		5.23 dq (10.5, 1.4)	
20	-	130.0	18-$O\underline{CH_2}CH=CH_2$	4.78 ddt (12.8, 5.4, 1.4)	72.9
21	4.13 d (1.9)	59.6		4.29 ddt (12.8, 5.4, 1.4)	
22	4.58 br s	60.6	OCH_2O	6.09 d (1.1)	102.1
	4.46 br d (10.3)			6.00 d (1.1)	
1'	-	69.6	17-OCH_3	3.70 s	59.4
3'	3.50, 2H, m	45.7	7'-OCH_3	3.65 s	55.2
4'	2.45 ddd (16.2, 8.9, 6.8)	29.1	5-$OCO\underline{CH_3}$	2.30 s	20.2
	2.36 dd (16.2, 5.0)		12-NCH_3	2.13 s	41.8
5'	6.35 s	112.7	6-CH_3	2.05 s	9.7
6'	-	147.2	16-CH_3	1.70 s	15.5
7'	-	147.4	2'-NCO	-	170.8
8'	6.48 s	111.2	5-OCO	-	168.3
9'	-	127.9	21-CN	-	118.1

Table 14. 500 MHz ^{1}H- and 125 MHz ^{13}C-NMR data of 18,6'-*O*-bisallyl-2'-*N*-(3''-fluorocinnamoyl) Et 770 in $CDCl_3$.

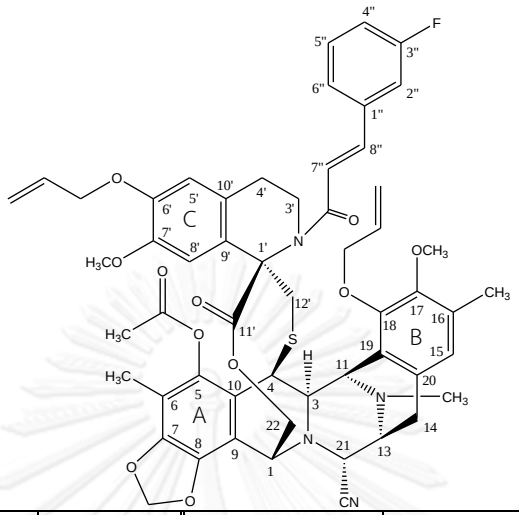

No.	δ_H in ppm (*J* in Hz)	δ_C in ppm	No.	δ_H in ppm (*J* in Hz)	δ_C in ppm
1	4.33 br s	60.3	12'	3.48 d (15.4)	39.1
3	3.57 br d (5.0)	60.8		2.32 d (15.4)	
4	4.62 br s	41.9	1''	-	137.7
5	-	141.3	2''	7.24 td (7.8, 2.3)	113.7
6	-	112.8	3''	-	163.1
7	-	145.4	4''	7.08 tt (7.8, 2.3)	116.4
8	-	140.8	5''	7.38 td (7.8, 5.8)	130.4
9	-	113.6	6''	7.29 td (7.8, 2.3)	123.7
10	-	122.3	7''	6.76 d (15.6)	122.3
11	4.22 dd (5.0, 1.1)	55.3	8''	7.34 d (15.6)	140.0
13	3.42 m	54.8	6'-$OCH_2\underline{CH}=CH_2$	5.98 ddt (17.5, 10.7, 5.4)	133.1
14	2.92, 2H, d (5.4)	24.7	6'-$OCH_2CH=\underline{CH_2}$	5.31 dq (17.5, 1.5)	117.9
15	6.60 s	124.4		5.22 dq (10.7, 1.5)	
16	-	130.9	6'-$O\underline{CH_2}CH=CH_2$	4.64, 2H, dt (5.4, 1.5)	69.7
17	-	148.6	18-$OCH_2\underline{CH}=CH_2$	6.09 ddt (17.2, 10.9, 4.5)	134.7
18	-	150.3	18-$OCH_2CH=\underline{CH_2}$	5.45 dq (17.2, 1.4)	116.6
19	-	124.4		5.23 dq (10.9, 1.4)	
20	-	130.2	18-$O\underline{CH_2}CH=CH_2$	4.79 ddt (10.9, 4.5, 1.4)	72.9
21	4.12 d (2.5)	59.7		4.31 dd (10.9, 4.5)	
22	4.63 br d (10.5)	61.0	OCH_2O	6.06 d (1.3)	102.0
	4.28 br d (10.5)			5.98 d (1.3)	
1'	-	69.7	17-OCH_3	3.83 s	59.4
3'	3.71, 2H, m	43.8	7'-OCH_3	3.61 s	55.1
4'	2.57, 2H, t (6.0)	29.1	5-$OCO\underline{CH_3}$	2.30 s	20.3
5'	6.37 s	112.8	12-NCH_3	2.15 s	41.8
6'	-	147.1	6-CH_3	2.04 s	9.7
7'	-	147.5	16-CH_3	1.99 s	16.1
8'	6.32 s	110.7	2'-NCO	-	167.0
9'	-	128.6	5-OCO	-	168.3
10'	-	126.3	21-CN	-	118.3
11'	-	169.0			

Table 15. 500 MHz ^{1}H- and 125 MHz ^{13}C-NMR data of 18,6'-*O*-bisallyl-2'-*N*-(4''-fluorocinnamoyl) Et 770 in $CDCl_3$.

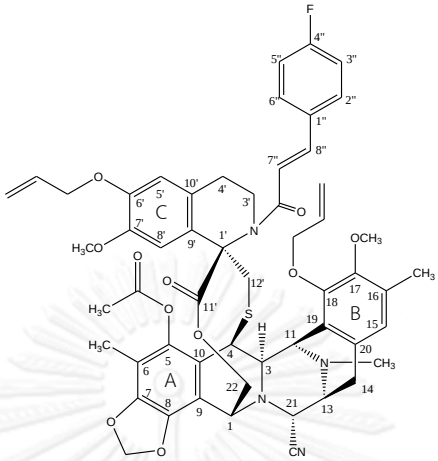

No.	δ_H in ppm (*J* in Hz)	δ_C in ppm	No.	δ_H in ppm (*J* in Hz)	δ_C in ppm
1	4.33 br s	60.3	12'	3.49 d (15.4)	39.1
3	3.57 br d (5.0)	60.8		2.36 d (15.4)	
4	4.61 br s	41.9	1"	-	131.6
5	-	141.3	2"	7.52 dd (8.6, 5.4)	129.3
6	-	112.8	3"	7.11 t (8.6)	116.0
7	-	145.4	4"	-	163.4
8	-	140.8	5"	7.11 t (8.6)	116.0
9	-	113.6	6"	7.52 dd (8.6, 5.4)	129.3
10	-	122.3	7"	6.69 d (15.5)	120.6
11	4.22 dd (5.0, 1.4)	55.3	8"	7.36 d (15.5)	140.2
13	3.41 m	54.8	6'-$OCH_2\underline{CH}=CH_2$	5.98 ddt (17.3, 10.7, 5.4)	133.2
14	2.92, 2H, d (5.4)	24.7	6'-$OCH_2CH=\underline{CH_2}$	5.31 dq (17.3, 1.6)	117.6
15	6.59 s	124.4		5.22 dq (10.7, 1.6)	
16	-	130.9	6'-$O\underline{CH_2}CH=CH_2$	4.49, 2H, dt (5.4, 1.4)	69.7
17	-	148.5	18-$OCH_2\underline{CH}=CH_2$	6.09 ddt (17.1, 10.5, 5.3)	134.7
18	-	150.3	18-$OCH_2CH=\underline{CH_2}$	5.45 dq (17.1, 1.5)	116.6
19	-	124.4		5.23 dq (10.5, 1.5)	
20	-	130.2	18-$O\underline{CH_2}CH=CH_2$	4.79 ddt (11.3, 3.7, 1.5)	72.9
21	4.11 d (2.6)	59.7		4.32 dd (11.3, 5.3)	
22	4.62 br d (11.1)	60.9	OCH_2O	6.06 d (1.3)	102.0
	4.29 br d (11.1)			5.98 d (1.3)	
1'	-	69.6	17-OCH_3	3.83 s	59.4
3'	3.72, 2H, t (6.2)	43.7	7'-OCH_3	3.61 s	55.1
4'	2.57, 2H, t (6.2)	29.1	5-$OCO\underline{CH_3}$	2.30 s	20.3
5'	6.32 s	112.8	12-NCH_3	2.14 s	41.8
6'	-	147.1	6-CH_3	2.04 s	9.7
7'	-	147.5	16-CH_3	1.97 s	16.1
8'	6.37 s	110.7	2'-NCO	-	167.3
9'	-	128.6	5-OCO	-	168.3
10'	-	126.3	21-CN	-	118.2
11'	-	169.0			

Table 16. 500 MHz ^{1}H- and 125 MHz ^{13}C-NMR data of 18,6'-*O*-bisallyl-2'-*N*-(2''-naphthoyl) Et 770 in $CDCl_3$.

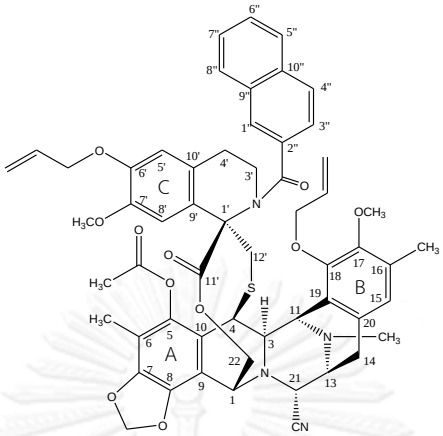

No.	δ_H in ppm (*J* in Hz)	δ_C in ppm	No.	δ_H in ppm (*J* in Hz)	δ_C in ppm
1	4.35 s	60.5	11'	-	169.7
3	3.59 d (5.1)	60.9	12'	3.67 overlapped	39.2
4	4.62 br	42.0		2.43 br s	
5	-	141.3	1"	8.00 br s	128.5
6	-	112.7	2"	-	134.4
7	-	145.5	3"	7.55 dd (8.4, 1.3)	125.4
8	-	141.3	4"	7.96-7.92 (overlapped)	127.9
9	-	113.2	5"	7.96-7.92 (overlapped)	127.8
10	-	122.4	6"	7.60-7.57 (overlapped)	127.2
11	4.22 dd (5.6, 1.5)	55.4	7"	7.60-7.57 (overlapped)	126.6
13	3.47 d (7.9)	54.9	8"	7.96-7.92 (overlapped)	128.6
14	3.02 dd (17.4, 9.0)	24.9	9"	-	132.8
	2.94 d (17.4)		10"	-	134.1
15	6.53 br s	124.5	6'-$OCH_2\underline{CH}=CH_2$	5.98 ddt (17.2, 10.5, 5.4)	133.1
16	-	131.3	6'-$OCH_2CH=\underline{CH_2}$	5.31 dq (17.2, 1.5)	117.8
17	-	148.6		5.21 dq (10.5, 1.5)	
18	-	150.3	6'-$O\underline{CH_2}CH=CH_2$	4.56, 2H, dt (5.4, 1.5)	69.6
19	-	124.3	18-$OCH_2\underline{CH}=CH_2$	6.06 ddt (17.2, 10.5, 5.5)	134.7
20	-	129.9	18-$OCH_2CH=\underline{CH_2}$	5.42 dq (17.2, 1.5)	116.7
21	4.17 br s	59.5		5.21 dq (10.5, 1.5)	
22	4.62 br	60.4	18-$O\underline{CH_2}CH=CH_2$	4.76 ddt (12.8,5.5, 1.5)	72.9
	4.50 br d (11.6)			4.26 ddt (12.8, 5.5, 1.5)	
1'	-	69.5	OCH_2O	6.10 d (1.3)	102.0
3'	3.67 overlapped	45.9		6.00 d (1.3)	
	3.50 ddd (14.1, 8.9, 5.2)		17-OCH_3	3.69 s	59.4
4'	2.45 ddd (15.6, 9.5, 6.1)	29.1	7'-OCH_3	3.67 s	55.2
	2.34 d (15.6)		5-$OCO\underline{CH_3}$	2.30 s	20.2
5'	6.33 s	112.7	12-NCH_3	2.13 s	41.8
6'	-	147.0	6-CH_3	2.05 s	9.7
7'	-	147.3	16-CH_3	1.40 s	15.1
8'	6.53 br s	111.3	2'-NCO	-	172.5
9'	-	128.2	5-OCO	-	168.3
10'	-	126.1	21-CN	-	118.2

Table 17. 500 MHz ^{1}H- and 125 MHz ^{13}C-NMR data of 18,6'-*O*-bisallyl-2'-*N*-(1''-naphthoyl) Et 770 in $CDCl_3$.

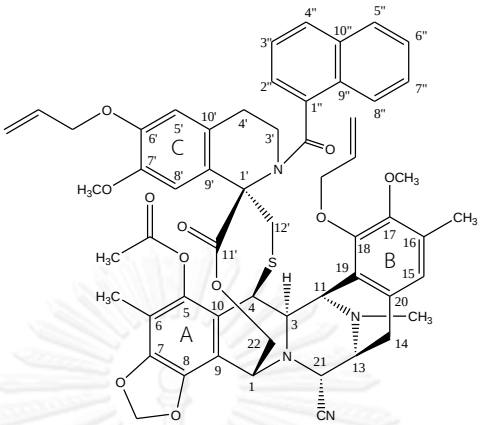

No.	δ_H in ppm (*J* in Hz)	δ_C in ppm	No.	δ_H in ppm (*J* in Hz)	δ_C in ppm
1	4.40 br s	60.3	11'	-	169.4
3	3.57 br s	60.9	12'	3.62 d (15.2)	40.2
4	4.67 br s	42.1		3.52 d (15.2)	
5	-	141.5	1''	-	135.3
6	-	112.6	2''	7.92 m	128.1
7	-	145.5	3''	7.50 m	125.2
8	-	141.3	4''	7.59 m	126.2
9	-	113.4	5''	7.67 m	127.2
10	-	122.7	6''	7.40 m	125.8
11	4.25 d (3.4)	55.4	7''	7.50 m	125.2
13	3.49 m	54.9	8''	7.92 m	129.7
14	3.03 br s	25.1	9''	-	129.0
	3.00 br s		10''	-	133.2
15	6.33 s	124.7	6'-$OCH_2\underline{CH}=CH_2$	5.98 ddt (18.8, 10.9, 5.4)	133.1
16	-	131.6	6'-$OCH_2CH=\underline{CH_2}$	5.32 dd (18.8, 1.4)	117.9
17	-	148.6		5.22 dq (10.9, 1.4)	
18	-	150.3	6'-$O\underline{CH_2}CH=CH_2$	4.48 br d (5.4)	69.6
19	-	124.1	18-$OCH_2\underline{CH}=CH_2$	6.08, 2H, ddt (18.6, 10.5, 5.4)	134.8
20	-	129.7	18-$OCH_2CH=\underline{CH_2}$	5.44 br d (18.6)	116.7
21	4.18 br s	59.9		5.22 dd (10.5, 1.4)	
22	4.59 br s	61.2	18-$O\underline{CH_2}CH=CH_2$	4.77 ddt (12.7, 5.4, 1.4)	72.9
	4.51 br s			4.29 dd (12.7, 5.4)	
1'	-	71.3	OCH_2O	6.09 d (1.3)	102.1
3'	3.62 overlapped	45.0		6.02 d (1.3)	
	3.30 m		17-OCH_3	3.78 s	59.3
4'	2.37 br s	29.7	7'-OCH_3	3.66 s	55.3
	2.29 m		5-$OCO\underline{CH_3}$	2.31	20.3
5'	6.33 s	112.7	12-NCH_3	2.15 s	41.8
6'	-	147.2	6-CH_3	2.05 s	9.8
7'	-	147.4	16-CH_3	1.57 s	15.7
8'	6.46 s	111.3	2'-NCO	-	170.1
9'	-	128.3	5-OCO	-	168.4
10'	-	126.3	21-CN	-	118.2

4. Preparation of the 2'-*N*-acyl Et 770 Derivatives

The allyl groups of 18,6'-*O*-bisallyl-2'-*N*-acyl Et 770 derivatives (**4a**-**4j**) were converted to the free hydroxyl groups by 16.5 equivalents of tributyltin hydride (n-Bu_3SnH) (Dangles *et al*., 1987) with $(Ph_3P)_2Pd(II)Cl_2$ (0.6 eq) as a catalyst for hydrostannolytic cleavage in the presence of glacial AcOH (37.5 eq), a proton donor, in THF at 25 ^{o}C for 1–4 hours to provide the 2'-*N*-acyl Et 770 derivatives (**5a**-**5i**) in 31.1–89.1 % yields (Table 18). The mechanism of action has been proposed that the allyl groups were cleavage by $(Ph_3P)_2Pd(0)$, which is formed by reduction of $(Ph_3P)_2Pd(II)Cl_2$ by n-Bu_3SnH. In the catalytic process, $(Ph_3P)_2Pd(0)$ reacts with the allyl groups to give the allyl-palladium(II) complexs, then reacts with n-Bu_3SnH to produce the –$OSnBu_3$ functional groups and propene. After that, the –$OSnBu_3$ functional groups were hydrolyzed by glacial AcOH to provide the free hydroxyl groups. The deallylation mechanism to produce the 2'-*N*-acyl Et 770 derivatives is shown in Figure 28.

Preparations of nine 18,6'-*O*-bisallyl-2'-*N*-acyl Et 770 derivatives (**5a**-**5i**) were achieved *via* the deallylation process. In contrast, the 18,6'-*O*-bisallyl-2'-*N*-(1''-Napthoyl) Et 770 (**4j**) was unable to be removed the allyl groups from structure, that may result from unsuitable chemical reaction. The structures of these compounds were elucidated by the interpretation of HR-FABMS and NMR spectral data. The HR-FABMS spectra (Figures 89, 94, 99, 104, 109, 114, 119, 124, and 129) of these products presented the pseudomolecular ions $[M+H]^+$ corresponding to the molecular formulae of the expected products (Table 18). The ^{1}H- and ^{13}C-NMR spectra (Figures 87, 88, 92, 93, 97, 98, 102, 103, 107, 108, 112, 113, 117, 118, 122, 123, 127, and 128) of the deallylated derivatives showed characteristic signals similar to those of the

parent 18,6'-*O*-bisallyl-2'-*N*-acyl Et 770 except the disappearance of the allyl signals along with the appearance of the 18-OH (around δ_H 5.70-5.77) and 6'-OH (around δ_H 5.47-5.51) signals. This evidence implied that the allyl groups were completely removed and replaced by the phenolic hydroxyl protons. The NMR spectral data of the 2'-*N*-acylated products are shown in Tables 18-27.

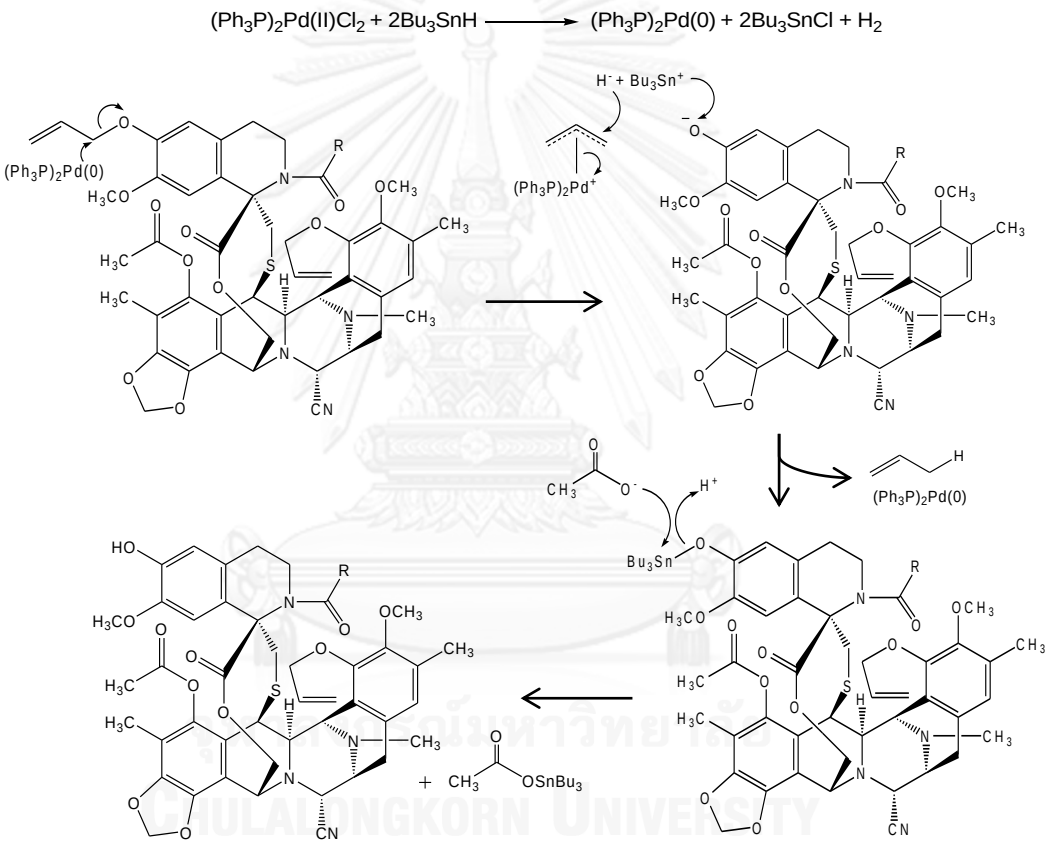

Figure 28. The deallylation mechanism by palladium-catalyzed hydrostannolytic cleavage.

Table 18. The summary of yields and HR-FABMS data of the 2'-*N*-acyl Et 770 derivatives.

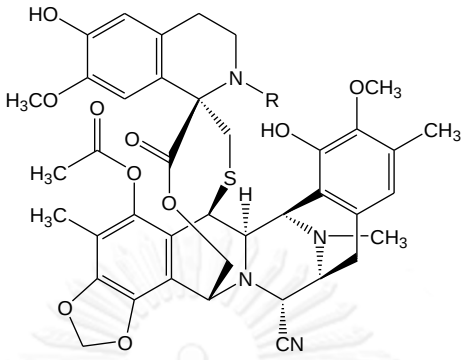

Compounds	R	%Yield	*m/z* (HR-FABMS)
5a	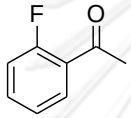	69.6	893.2875 $[M+H]^+$; calcd for $C_{47}H_{46}N_4FO_{11}S$, 893.2868
5b	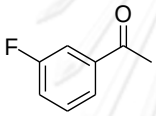	87.0	893.2869 $[M+H]^+$; calcd for $C_{47}H_{46}N_4FO_{11}S$, 893.2868
5c	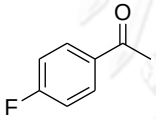	89.1	893.2872 $[M+H]^+$; calcd for $C_{47}H_{46}N_4FO_{11}S$, 893.2868
5d	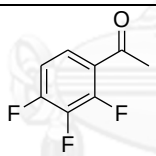	31.5	929.2683 $[M+H]^+$; calcd for $C_{47}H_{44}N_4F_3O_{10}S$, 929.2680
5e	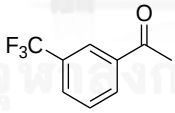	80.4	943.2839 $[M+H]^+$; calcd for $C_{48}H_{46}N_4F_3O_{11}S$, 943.2836
5f	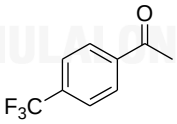	66.3	943.2845 $[M+H]^+$; calcd for $C_{48}H_{46}N_4F_3O_{11}S$, 943.2836
5g	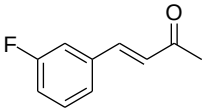	65.2	919.3029 $[M+H]^+$; calcd for $C_{49}H_{48}N_4FO_{11}S$, 919.3025
5h	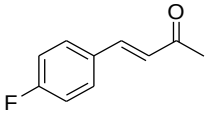	65.2	919.3028 $[M+H]^+$; calcd for $C_{49}H_{48}N_4FO_{11}S$, 919.3024
5i	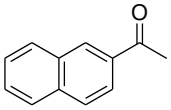	56.6	925.3128 $[M+H]^+$; calcd for $C_{51}H_{49}N_4O_{11}S$, 925.3121

Table 19. 500 MHz ^{1}H- and 125 MHz ^{13}C-NMR data of 2'-*N*-(2''-fluorobenzoyl) Et 770 in $CDCl_3$.

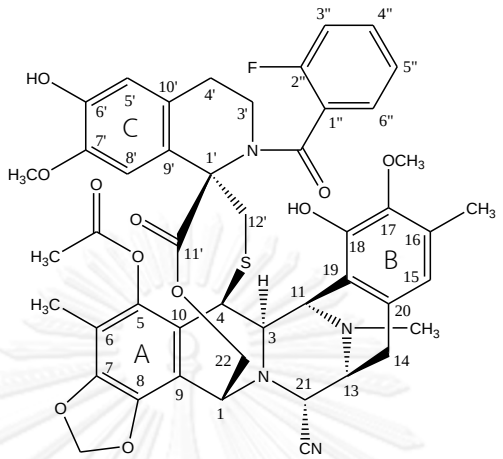

No.	δ_H in ppm (*J* in Hz)	δ_C in ppm	No.	δ_H in ppm (*J* in Hz)	δ_C in ppm
1	4.37 s	60.4	6'	-	144.7
3	3.56 d (4.5)	61.1	7'	-	144.9
4	4.67 br s	42.1	8'	6.43 s	110.3
5	-	141.4	9'	-	127.2
6	-	112.6	10'	-	125.8
7	-	145.4	11'	-	166.2
8	-	141.1	12'	3.58 br s	39.4
9	-	113.6		2.33 br s	
10	-	122.6	1"	-	125.7
11	4.26 dd (5.1, 1.4)	55.0	2"	-	161.2
13	3.45 m	54.8	3"	7.12 t like (8.2)	116.0
14	2.97 dd (17.3, 9.1)	24.8	4"	7.32 br	129.3
	2.90 d (17.3)		5"	7.24 br	124.3
15	6.39 s	121.1	6"	7.42 q like (5.8)	131.0
16	-	129.3	18-OH	5.73 s	
17	-	144.7	6'-OH	5.49 s	
18	-	147.4	OCH_2O	6.09 d (1.3)	102.0
19	-	117.9		5.99 d (1.3)	
20	-	130.5	17-OCH_3	3.71 s	60.2
21	4.14 d (2.2)	59.8	7'-OCH_3	3.66 s	55.3
22	4.67, 2H, br s	60.9	5-OCO$\underline{CH_3}$	2.33 s	20.3
1'	-	70.5	12-NCH_3	2.14	41.8
3'	3.47 br s	45.3	6-CH_3	2.05	9.8
	3.44 m		16-CH_3	1.82	15.5
4'	2.52 m	29.1	2'-NCO	-	169.1
	2.40 m		5-OCO	-	168.4
5'	6.35 s	113.8	21-CN	-	118.3

Table 20. 500 MHz ^{1}H- and 125 MHz ^{13}C-NMR data of 2'-*N*-(3''-fluorobenzoyl) Et 770 in $CDCl_3$.

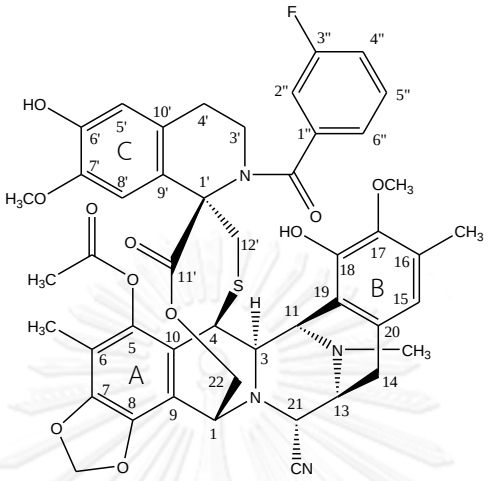

No.	δ_H in ppm (*J* in Hz)	δ_C in ppm	No.	δ_H in ppm (*J* in Hz)	δ_C in ppm
1	4.33 s	60.3	6'	-	144.8
3	3.58 s	61.0	7'	-	144.7
4	4.66 br s	41.8	8'	6.55 s	110.4
5	-	141.2	9'	-	127.3
6	-	112.6	10'	-	126.6
7	-	145.5	11'	-	169.5
8	-	141.5	12'	3.58 br d (15.0)	39.4
9	-	113.1		2.39 d (15.0)	
10	-	122.2	1''	-	139.1
11	4.26 dd (4.9, 1.3)	55.3	2''	7.15 d (8.8)	115.2
13	3.45 m	54.8	3''	-	162.4
14	2.99 dd (17.4, 9.3)	25.0	4''	7.19 m	117.2
	2.83 d (17.4)		5''	7.42 td (7.8, 5.7)	130.2
15	6.42 s	120.9	6''	7.25 d (7.8)	123.8
16	-	129.4	OCH_2O	6.10 d (1.4)	102.1
17	-	143.0		6.00 d (1.4)	
18	-	147.5	18-OH	5.74 s	
19	-	117.8	6'-OH	5.50 s	
20	-	130.4	17-OCH_3	3.69 s	60.1
21	4.11 d (2.2)	59.8	7'-OCH_3	3.63 s	55.0
22	4.58 br s	60.7	5-OCO$\underline{CH_3}$	2.33 s	20.3
	4.47 br d (10.5)		12-NCH_3	2.14 s	41.7
1'	-	69.7	6-CH_3	2.03 s	9.8
3'	3.47 m	45.6	16-CH_3	1.82 s	15.3
	3.41 m		2'-NCO	-	171.3
4'	2.40, 2H, m	28.8	5-OCO	-	168.4
5'	6.42 s	113.9	21-CN	-	118.2

Table 21. 500 MHz ^{1}H- and 125 MHz ^{13}C-NMR data of 2'-*N*-(4''-fluorobenzoyl) Et 770 in $CDCl_3$.

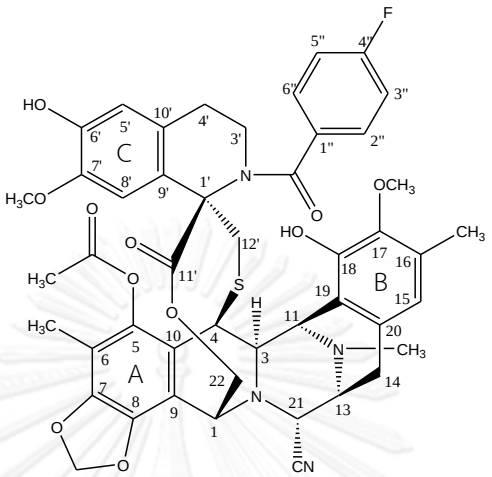

No.	δ_H in ppm (*J* in Hz)	δ_C in ppm	No.	δ_H in ppm (*J* in Hz)	δ_C in ppm
1	4.31 s	60.2	7'	-	144.7
3	3.59 d (4.7)	61.0	8'	6.59 br s	110.4
4	4.64 br s	41.7	9'	-	127.4
5	-	141.1	10'	-	126.5
6	-	112.5	11'	-	169.6
7	-	143.0	12'	3.53 d (15.3)	39.7
8	-	141.6		2.33 d (15.3)	
9	-	113.0	1''	-	132.9
10	-	122.1	2''	7.46 dd (8.7, 5.6)	130.6
11	4.25 dd (4.7, 1.4)	55.0	3''	7.14 t (8.7)	115.4
13	3.43 d (9.3)	54.8	4''	-	163.9
14	2.97 dd (17.2, 9.3)	25.0	5''	7.14 t (8.7)	115.4
	2.78 br d (17.3)		6''	7.46 dd (8.7, 5.6)	130.6
15	6.37 br s	120.7	18-OH	5.77 s	
16	-	129.2	6'-OH	5.51 br s	
17	-	145.5	OCH_2O	6.11 d (1.3)	102.1
18	-	147.7		6.01 d (1.3)	
19	-	118.0	17-OCH_3	3.70 s	60.1
20	-	130.6	7'-OCH_3	3.66 s	55.3
21	4.08 d (1.9)	59.9	5-OCO$\underline{CH_3}$	2.32 s	20.3
22	4.64 br s	60.6	12-NCH_3	2.14 s	41.7
	4.40 br d (10.7)		6-CH_3	2.04 s	9.8
1'	-	69.7	16-CH_3	1.88 s	15.6
3'	3.45, 2H, m	45.5	2'-NCO	-	172.0
4'	2.38, 2H, m	28.7	5-OCO	-	168.4
5'	6.41 s	113.9	21-CN	-	118.2
6'	-	144.8			

Table 22. 300 MHz ^{1}H- and 75 MHz ^{13}C-NMR data of 2'-*N*-(2'',3'',4''-trifluorobenzoyl) Et 770 in $CDCl_3$.

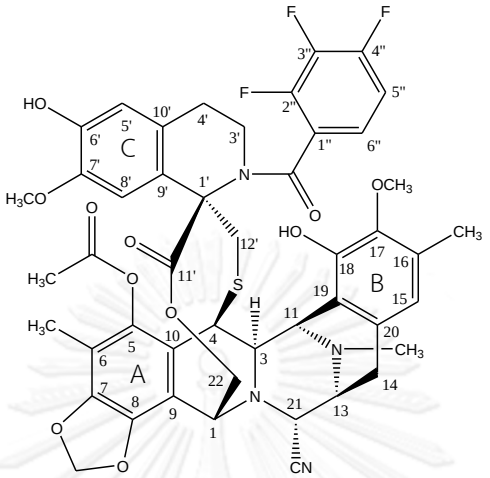

No.	δ_H in ppm (*J* in Hz)	δ_C in ppm	No.	δ_H in ppm (*J* in Hz)	δ_C in ppm
1	4.34 s	60.4	6'	-	145.0
3	3.54 br s	61.1	7'	-	144.9
4	4.67 br s	42.0	8'	6.36 s	110.2
5	-	141.4	9'	-	128.8
6	-	112.7	10'	-	126.8
7	-	145.5	11'	-	168.4
8	-	141.2	12'	3.55 d (15.0)	39.2
9	-	113.4		2.50 d (15.0)	
10	-	122.4	1''	-	
11	4.24 d (4.8)	55.0	2''	-	
13	3.41 m	54.8	3''	-	
14	2.95 dd (17.4, 8.7)	24.9	4''	-	
	2.84 d (17.4)		5''	7.04 br	112.7
15	6.33 s	120.9	6''	7.06 br	123.5
16	-	129.1	18-OH	5.72 s	
17	-	143.0	6'-OH	5.47 s	
18	-	147.4	OCH_2O	6.06 d (0.9)	102.0
19	-	118.1		5.97 d (0.9)	
20	-	130.6	17-OCH_3	3.66 s	60.2
21	4.11 d (1.8)	59.8	7'-OCH_3	3.65 s	55.4
22	4.60, 2H, m	61.1	5-OCO$\underline{CH_3}$	2.32 s	20.4
1'	-	70.3	12-NCH_3	2.11 s	41.8
3'	3.43 m	45.5	6-CH_3	2.02 s	9.8
	3.41 m		16-CH_3	1.82 s	15.5
4'	2.41 m	29.1	2'-NCO	-	169.3
	2.35 m		5-OCO	-	169.0
5'	6.42 s	113.8	21-CN	-	118.3

Table 23. 500 MHz ^{1}H- and 125 MHz ^{13}C-NMR data of 2'-*N*-(3''-trifluoromethylbenzoyl) Et 770 in $CDCl_3$.

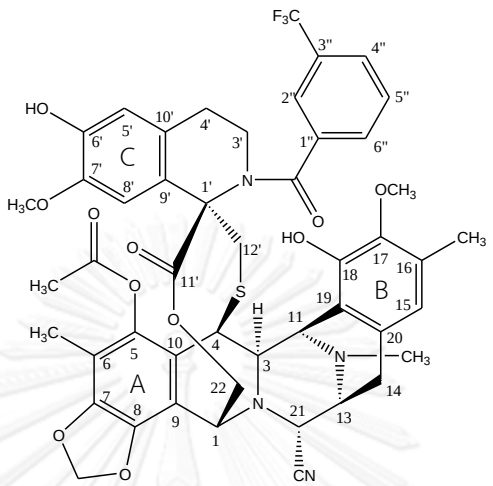

No.	δ_H in ppm (*J* in Hz)	δ_C in ppm	No.	δ_H in ppm (*J* in Hz)	δ_C in ppm
1	4.36 s	60.5	6'	-	144.8
3	3.56 d (4.8)	61.0	7'	-	144.9
4	4.67 br s	42.0	8'	6.47 s	110.4
5	-	141.3	9'	-	127.1
6	-	112.6	10'	-	126.8
7	-	145.5	11'	-	169.6
8	-	141.3	12'	3.64 d (15.4)	39.1
9	-	113.3		2.51 d (15.4)	
10	-	122.3	1"	-	138.0
11	4.25 dd (5.1, 1.4)	54.9	2"	7.76 s	125.2
13	3.45 d (9.2)	54.8	3"	-	130.9
14	2.97 dd (17.5, 9.2)	24.7	4"	7.76 d (7.8)	126.9
	2.84 d (17.5)		5"	7.61 t (7.8)	129.0
15	6.24 s	120.7	6"	7.65 d (7.8)	131.6
16	-	129.3	3"-CF_3	-	123.8
17	-	143.0	18-OH	5.70 s	
18	-	147.5	6'-OH	5.49 s	
19	-	117.8	OCH_2O	6.10 d (1.1)	102.0
20	-	130.4		6.00 d (1.1)	
21	4.15 d (2.3)	59.6	17-OCH_3	3.69 s	60.1
22	4.61 br d (10.5)	60.7	7'-OCH_3	3.64 s	55.3
	4.47 br d (10.5)		5-OCO$\underline{CH_3}$	2.33 s	20.4
1'	-	70.0	12-NCH_3	2.13 s	41.7
3'	3.53 m	46.3	6-CH_3	2.05 s	9.8
	3.40 ddd (14.5, 9.9, 4.8)		16-CH_3	1.60 s	15.0
4'	2.45 ddd (16.0, 9.9, 6.1)	28.9	2'-NCO	-	170.5
	2.33 dd (16.0, 4.2)		5-OCO	-	168.3
5'	6.42 s	113.8	21-CN	-	118.2

Table 24. 500 MHz ^{1}H- and 125 MHz ^{13}C-NMR data of 2'-*N*-(4''-trifluoromethylbenzoyl) Et 770 in $CDCl_3$.

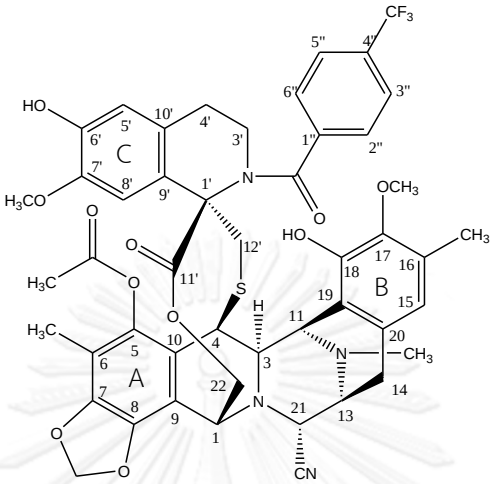

No.	δ_H in ppm (*J* in Hz)	δ_C in ppm	No.	δ_H in ppm (*J* in Hz)	δ_C in ppm
1	4.34 s	60.4	7'	-	144.9
3	3.58 m	61.0	8'	6.50 s	110.3
4	4.67 br s	41.9	9'	-	127.1
5	-	141.3	10'	-	126.6
6	-	112.6	11'	-	169.4
7	-	143.0	12'	3.60 d (15.3)	39.2
8	-	141.4		2.44 d (15.3)	
9	-	113.2	1"	-	140.6
10	-	122.2	2"	7.56 d (7.9)	128.5
11	4.25 dd (4.9, 1.5)	55.0	3"	7.72 d (7.9)	125.4
13	3.46 d (9.3)	54.8	4"	7.56 d (7.9)	132.0
14	2.99 dd (17.3, 9.4)	25.0	5"	7.72 d (7.9)	125.4
	2.83 d (17.3)		6"	-	128.5
15	6.33 s	120.8	4"-CF_3	-	123.8
16	-	129.2	18-OH	5.71 s	
17	-	145.5	6'-OH	5.49 s	
18	-	147.6	OCH_2O	6.10 d (1.5)	102.1
19	-	118.0		6.01 d (1.5)	
20	-	130.4	17-OCH_3	3.69 s	60.1
21	4.12 d (2.3)	59.9	7'-OCH_3	3.62 s	55.3
22	4.52, 2H, br s	60.8	5-OCO$\underline{CH_3}$	2.33 s	20.4
1'	-	69.4	12-NCH_3	2.13 s	41.7
3'	3.45, 2H, m	45.7	6-CH_3	2.05 s	9.8
4'	2.42 dt (16.2, 4.8)	28.9	16-CH_3	1.73 s	15.4
	2.36 ddd (16.2, 9.1, 6.4)		2'-NCO	-	170.9
5'	6.42 s	113.8	5-OCO	-	168.4
6'	-	144.8	21-CN	-	118.2

Table 25. 500 MHz ^{1}H- and 125 MHz ^{13}C-NMR data of 2'-*N*-(3''-fluorocinnamoyl) Et 770 in $CDCl_3$.

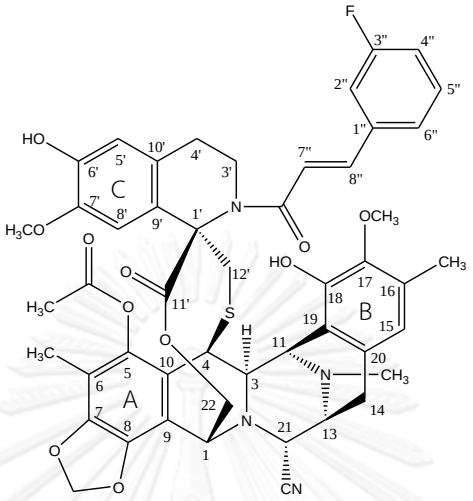

No.	δ_H in ppm (*J* in Hz)	δ_C in ppm	No.	δ_H in ppm (*J* in Hz)	δ_C in ppm
1	4.33 br s	60.2	8'	6.34 s	109.9
3	3.56 br d (4.7)	60.9	9'	-	127.8
4	4.60 br s	41.9	10'	-	127.2
5	-	141.3	11'	-	169.1
6	-	112.6	12'	3.50 d (15.0)	39.2
7	-	145.4		2.33 d (15.0)	
8	-	140.9	1"	-	137.7
9	-	113.6	2"	7.22 td (7.9, 2.2)	113.8
10	-	122.3	3"	-	163.1
11	4.25 dd (4.7, 1.4)	54.9	4"	7.07 tt (7.9, 2.2)	116.4
13	3.41 m	54.7	5"	7.38 td (7.9, 5.8)	130.4
14	2.91, 2H, d (5.4)	24.7	6"	7.27 td (7.9, 2.2)	123.6
15	6.41 s	120.7	7"	6.75 d (15.6)	122.3
16	-	129.1	8"	7.30 d (15.6)	140.0
17	-	142.9	18-OH	5.77 s	
18	-	147.5	6'-OH	5.49 s	
19	-	117.9	OCH_2O	6.07 d (1.5)	102.0
20	-	130.7		5.98 d (1.5)	
21	4.10 d (2.6)	60.0	17-OCH_3	3.77 s	60.2
22	4.61 br d (10.5)	61.1	7'-OCH_3	3.65 s	55.3
	4.32 br d (10.5)		5-OCO$\underline{CH_3}$	2.33 s	20.4
1'	-	69.7	12-NCH_3	2.15 s	41.7
3'	3.68 m	43.9	6-CH_3	2.04 s	9.8
	3.68 m		16-CH_3	2.01 s	16.0
4'	2.56, 2H, t (5.7)	28.9	2'-NCO	-	167.0
5'	6.45 s	113.6	5-OCO	-	168.4
6'	-	144.8	21-CN	-	118.3
7'	-	144.8			

Table 26. 500 MHz ^{1}H- and 125 MHz ^{13}C-NMR data of 2'-*N*-(4''-fluorocinnamoyl) Et 770 in $CDCl_3$.

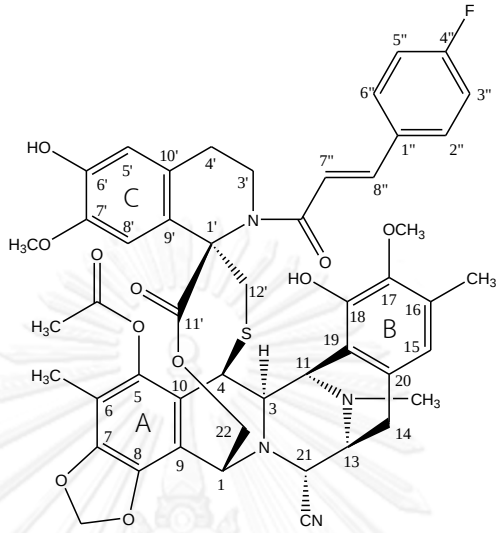

No.	δ_H in ppm (*J* in Hz)	δ_C in ppm	No.	δ_H in ppm (*J* in Hz)	δ_C in ppm
1	4.32 br s	60.2	8'	6.40 s	109.9
3	3.56 d (4.5)	60.8	9'	-	127.9
4	4.60 br s	41.8	10'	-	127.2
5	-	141.3	11'	-	169.1
6	-	112.6	12'	3.51 d (14.8)	39.2
7	-	145.3		2.34 d (14.8)	
8	-	140.9	1"	-	131.6
9	-	113.6	2"	7.50 dd (8.7, 5.2)	129.3
10	-	122.3	3"	7.10 t (8.7)	116.0
11	4.25 dd (4.5, 1.2)	54.9	4"	-	164.3
13	3.41 m	54.7	5"	7.10 t (8.7)	116.0
14	2.90, 2H, d (8.5)	24.7	6"	7.50 dd (8.7, 5.2)	129.3
15	6.44 s	120.7	7"	6.68 d (15.6)	120.6
16	-	129.1	8"	7.33 d (15.6)	140.1
17	-	142.9	18-OH	5.73 s	
18	-	147.5	6'-OH	5.49 s	
19	-	117.9	OCH_2O	6.06 d (1.4)	102.0
20	-	130.7		5.97 d (1.4)	
21	4.10 d (2.8)	60.0	17-OCH_3	3.77 s	60.2
22	4.60 br d (11.3)	61.1	7'-OCH_3	3.64 s	55.2
	4.32 br d (11.3)		5-OCO$\underline{CH_3}$	2.33 s	20.4
1'	-	69.6	12-NCH_3	2.15 s	41.7
3'	3.68, 2H, t (6.1)	43.9	6-CH_3	2.03 s	9.7
4'	2.56, 2H, t (6.1)	28.9	16-CH_3	2.00 s	16.0
5'	6.34 s	113.8	2'-NCO	-	167.3
6'	-	144.8	5-OCO	-	168.4
7'	-	144.8	21-CN	-	118.3

Table 27. 500 MHz ^{1}H- and 125 MHz ^{13}C-NMR data of 2'-*N*-(2"-naphthoyl) Et 770 in $CDCl_3$.

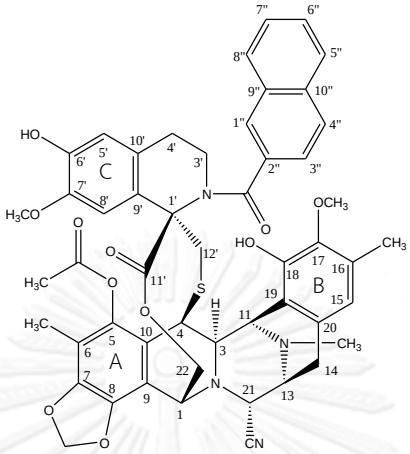

No.	δ_H in ppm (*J* in Hz)	δ_C in ppm	No.	δ_H in ppm (*J* in Hz)	δ_C in ppm
1	4.35 br s	60.4	8'	6.54 br s	110.4
3	3.59 d (5.1)	61.0	9'	-	127.5
4	4.68 br s	41.9	10'	-	126.9
5	-	141.2	11'	-	169.8
6	-	112.6	12'	3.71 br	39.3
7	-	142.9		2.44 br d (13.2)	
8	-	141.4	1"	7.97 br s	128.5
9	-	113.2	2"	-	134.3
10	-	122.3	3"	7.53 dd (8.5, 1.4)	125.4
11	4.25 dd (5.1, 1.5)	55.0	4"	7.96-7.91 (overlapped)	127.9
13	3.47 d (7.9)	54.8	5"	7.96-7.91 (overlapped)	127.8
14	3.02 dd (17.4, 9.3)	25.0	6"	7.61-7.56 (overlapped)	127.2
	2.91 d (17.4)		7"	7.61-7.56 (overlapped)	126.6
15	6.42 s	120.8	8"	7.96-7.91 (overlapped)	128.7
16	-	129.4	9"	-	132.8
17	-	145.5	10"	-	134.1
18	-	147.5	18-OH	5.70 s	
19	-	117.9	6'-OH	5.49 br s	
20	-	130.3	OCH_2O	6.11 d (1.4)	102.1
21	4.16 br s	59.8		6.01 d (1.4)	
22	4.56, 2H, br s	60.7	17-OCH_3	3.71 s	60.1
1'	-	69.4	7'-OCH_3	3.67 s	55.3
3'	3.71 br	46.1	5-OCO$\underline{CH_3}$	2.34 s	20.4
	3.46 m		12-NCH_3	2.13 s	41.7
4'	2.44 ddd (15.7, 9.4, 6.4)	28.9	6-CH_3	2.06 s	9.8
	2.34 d (15.7)		16-CH_3	1.41 s	15.1
5'	6.33 br s	113.8	2'-NCO	-	172.6
6'	-	144.7	5-OCO	-	168.3
7'	-	144.8	21-CN	-	118.3

5. Cytotoxic Activity

The synthesized ecteinascidin derivatives were tested for *in vitro* cytotoxicity with three representative human solid carcinoma cell lines including; human colon carcinoma (HCT116), human lung carcinoma (QG56), and human prostate carcinoma (DU145) using the standard MTT assay. The IC_{50} cytotoxic values of Et 770 derivatives obtained were generally in nM order as shown in Tables 28 and 29.

The 18,6'-*O*-bisallyl-2'-*N*-acyl Et770 intermediates (**4a**-**4j**) exhibited dramatically decreased cytotoxicity, compared with the parent Et 770 (Table 28). The reduction in potency of those 18,6'-*O*-bisallyl protected compounds may result from the lack of hydrogen donor bonding at the 6'-OH (C-subunit) and 18-OH (B-subunit) positions, which ultimately decreased the DNA-binding affinity (Seaman *et al*., 1998). This result confirmed the previous studies that cytotoxicity of the 18,6'-*O*-disubstituted Et 770 derivatives also dramatically decreased (Puthongking *et al*., 2006; Saktrakulkla *et al*., 2011).

Table 28. Cytotoxicity of 18,6'-*O*-bisallyl-2'-*N*-acyl Et 770 derivatives.

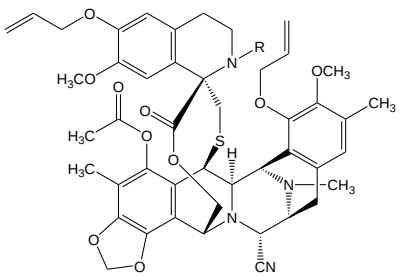

Compounds	R	Cytotoxicity (IC_{50} nM)		
		HCT116	QG56	DU145
Et 770	H	0.71	1.60	1.60
4a	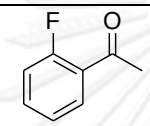	1.20×10^3	1.40×10^3	1.70×10^3
4b	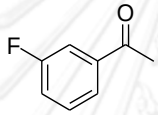	0.95×10^3	1.50×10^3	1.60×10^3
4c	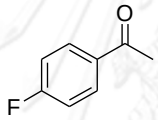	0.28×10^3	0.75×10^3	0.33×10^3
4d	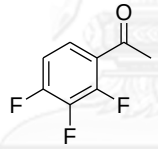	0.22×10^3	0.71×10^3	0.31×10^3
4e	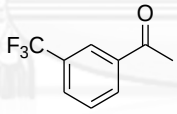	1.80×10^3	$>2.0 \times 10^3$	$>2.0 \times 10^3$
4f	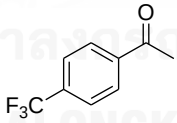	1.30×10^3	$>2.0 \times 10^3$	$>2.0 \times 10^3$
4g	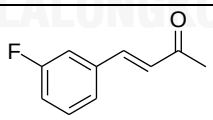	0.24×10^3	0.29×10^3	0.41×10^3
4h	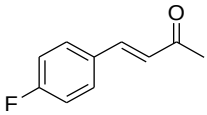	0.28×10^3	0.75×10^3	0.33×10^3
4i	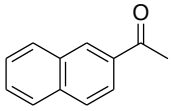	0.29×10^3	0.51×10^3	1.40×10^3
4j	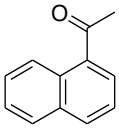	$>2.0 \times 10^3$	$>2.0 \times 10^3$	$>2.0 \times 10^3$

After the serendipitous discovery of 2'-*N*-indole-3-carbonyl Et 770 (**5k**) displaying 4-fold more potent cytotoxicity than Et 770 (Puthongking *et al*., 2006), this interesting result influenced us to continuously investigate cytotoxic activity of a series of 2'-*N*-acyl Et 770 derivatives (Saktrakulkla *et al*., 2011). The cytotoxic data of twenty-one 2'-*N*-aromatic acyl Et 770 derivatives prepared from the previous study (Puthongking *et al.,* 2006; Saktrakulkla *et al*., 2011) and this study are summarized in Table 29. In general, cytotoxicities of almost 2'-*N*-aromatic acyl Et770 derivatives were significantly more potent than Et 770.

Six compounds (**5a**–**5f**) containing a 2'-*N*-benzoyl group with different fluorinated substituents displayed up to 5-fold higher equipotent cytotoxicity except the 2'-*N*-*meta*-fluorobenzoyl derivative (**5b**) displaying 4-fold less cytotoxicity than Et 770. The 2'-*N*-benzoyl Et 700 itself (**5n**) showed similar cytotoxicity to Et 770 while the 2'-*N*-*ortho*- and 2'-*N*-*para*-substituted benzoyl derivatives (**5a, 5c,** and **5f**) were more potent than the 2'-*N*-*meta*-substituted ones (**5b** and **5e**). In contrast, it was observed that the 2'-*N*-*meta*-nitro substituted benzoyl (**5o**) was approximately twice as potent as **5n** while the 2'-*N*-*para*-nitro substituted benzoyl (**5p**) exhibited similar potency. The larger aromatic acyl group such as 2'-*N*-naphthoyl Et 770 (**5i**) also exhibited equipotent cytotoxicity to Et 770. However, the nitrogen-heterocyclic acyl derivatives (**5l** and **5q**-5t) exhibited 5- to 10- fold higher cytotoxicity than the corresponding aromatic acyl derivatives (**5n** and **5i**), respectively. Among them, compound **5l** consisting of a 6''-quinolinecarbonyl moiety which was the most potent derivatives exhibited approximately 10- to 40-fold higher cytotoxicity than Et 770. It exhibited very potent inhibitory activity against HCT116 and DU145 cell lines with IC_{50} values of 0.04 nM and QG56 cell line with with IC_{50} value of 0.16 nM.

We paid our attempt to explore cytotoxicity of 2'-*N*-cinnamoyl Et 770 (**5m**), two 2'-*N*-(fluorocinnamoyl) (**5g**-**5h**), and one 2'-*N*-(*p*-nitrocinnamoyl) Et 770 (**5u**) derivatives which were the extended carbon chain of the benzoyl **5n** and structurally more flexible than the naphthoyl **5i**. All compounds displayed considerably increased cytotoxicity compared to **5i** and **5n**. It is noteworthy that 2'-*N*-(4''-fluorocinnamoyl) Et 770 (**5h**) was the most potent of all prepared derivatives at approximately 10- to 70-fold more potent than the parent Et 770 toward the three cancer cell lines. It exhibited extremely potent activity against HCT116, QG56 and DU145 cell lines with IC_{50} values of 0.01, 0.12, and 0.04 nM, respectively.

The increase in potency of the 2'-*N*-aromatic acyl Et 770 derivatives might be related to the C-subunit properties. It is well known that all biologically active ecteinascidins bind to the minor groove of DNA with preference for GC-rich triplets and subsequently form covalent adducts with the *N*2 of guanine through its iminium intermediate (Pommier *et al*., 1996; Moore *et al*., 1997; Seaman *et al*., 1998). Moreover, the C-subunit protruding from the DNA backbone (Sakai *et al*., 1992; Moore *et al*., 1997; Seaman *et al*., 1998) may serve as a hook for trapping different DNA-binding proteins surrounding the ecteinascidins-DNA adduct complex (Takebayashi *et al*., 2001; Herrero *et al*., 2006; Guirouilh-Barbat *et al*., 2009). Therefore, the modification at the 2'-*N* position of the C-subunit might affect the trapping affinity of these compounds to these proteins, probably the xeroderma pigmentosum G (XPG) protein, a member of the nucleotide excision repair system (Takebayashi *et al*., 2001; Soares *et al*., 2005; Herrero *et al*., 2006; Guirouilh-Barbat *et al*., 2009).

On the other hand, the characteristic effects of fluorine and fluoroalkyl substituent on the fluorinated compounds are important to its physico-chemical properties and biological activities. In 2001, Smart described the influence of fluorination on hydrogen-bonding, lipophilicity, and steric effects that affect compound absorption and distribution. A part of interesting conclusion is that aromatic fluorination always increases lipophilicity, which might be involved in the cell transfer ability of fluorinated compounds (Smart, 2001). Therefore, the increased cytotoxicity of the 2'-*N*-(acyl fluoride) Et 770 derivatives may result from its physico-chemical property change.

Table 29. Cytotoxicity of the 2'-*N*-aromatic Et 770 derivatives.

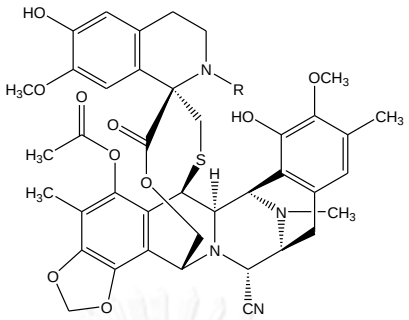

Compounds	R	Cytotoxicity (IC_{50} nM)		
		HCT116	QG56	DU145
Et 770	H	0.71	1.60	1.60
5k*	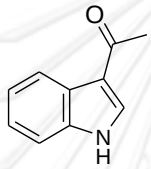	0.16	0.46	0.45
5a	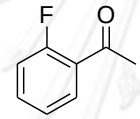	0.23	0.55	0.47
5b	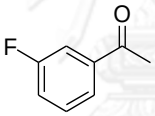	1.20	2.70	6.10
5c	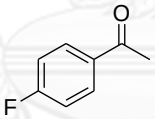	0.20	0.41	0.43
5d	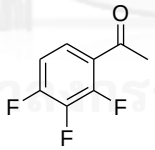	0.28	0.93	0.53
5e	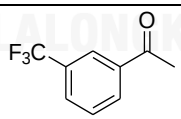	0.21	0.48	0.39
5f	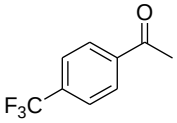	0.12	0.51	0.39
5n*	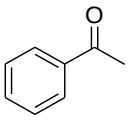	0.37	1.00	1.00

*data for **5k**-**5u** are from Saktrakulkla *et al*., 2011.

Table 29. (continued)

Compounds	R	Cytotoxicity (IC_{50} nM)		
		HCT116	QG56	DU145
5o*	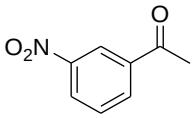	0.14	0.43	0.73
5p*	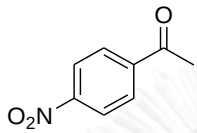	0.38	1.10	1.00
5q*	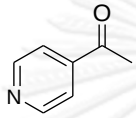	0.05	0.20	0.30
5r*	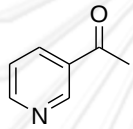	0.13	0.40	0.72
5i	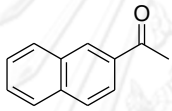	0.64	1.20	1.50
5l*	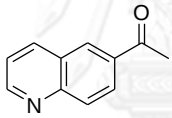	0.05	0.16	0.04
5s*	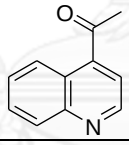	0.07	0.23	0.16
5t*	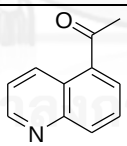	0.09	0.36	0.92
5m*	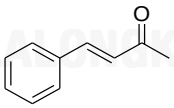	0.05	0.33	0.24
5g	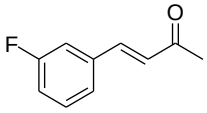	0.12	0.32	0.39
5h	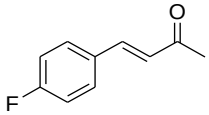	0.01	0.12	0.04
5u*	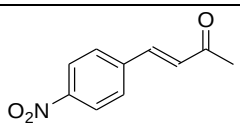	0.60	2.40	0.81

*data for **5k**-**5u** are from Saktrakulkla *et al*., 2011.

CHAPTER V

CONCLUSION

This investigation was aimed to isolate Et 770 from the Thai tunicate *Ecteinascidia thurstoni* and to prepare the additional 2'-*N*-acyl Et 770 derivatives for cytotoxicity evaluation.

In this study, the stable Et 770 was isolated from the Thai tunicate in a large quantity (234.5 mg, 4.0 x 10^{-4}% yield of tunicate wet wt) by the KCN-pretreated method followed by a sequence of several chromatographic techniques.

Nine 2'-*N*-aromatic Et 770 derivatives (**5a**-**5i**) were prepared from the obtained Et 770 *via* a three-step transformation including: a) 18,6'-*O*-bisallyl protection, b) 2'-*N*-acylation, and c) 18,6'-*O*-bisallyl deprotection. The protection step, the reactive 18- and 6'-OHs of Et 770 were protected by using allyl bromide and K_2CO_3 to provide 18,6'-*O*-bisallyl Et 770 (**3**) in 77.5% yield. The chemical structure of bisallyl product was mainly determined based on HR-FABMS and NMR spectral data and comparison of chemical shifts to the authentic compound. The appearance of the allyl-proton signals along with the disappearance of the 18-OH and 6'-OH signals implied the substitutions at the phenolic hydroxyls by the allyl groups.

The 18,6'-*O*-bisallyl-2'-*N*-acyl Et 770 derivatives (**4a**-**4j**) were synthesized by treating 18,6'-*O*-bisallyl Et 770 (**3**) with the corresponding acyl acid chlorides and DMAP in dry pyridine. The additional signals of the corresponding aromatic acyl moiety were shown in ^{1}H- and ^{13}C-NMR spectra. In additional, the chemical structures

of these compounds were proved by the long-range HMBC correlations from 3'-methylene protons to the additional acyl carbons.

The last step, bisallyl deprotection, the allyl groups were converted to the hydroxyl groups by palladium-catalyzed hydrostannolytic cleavage with n-Bu_3SnH in the presence of glacial AcOH, to provide the 2'-*N*-acyl Et 770 derivatives (**5a**-**5i**). The disappearance of the allyl signals along with the appearance of the 18-OH and 6'-OH signals implied that the allyl groups were completely removed and replaced by the phenolic hydroxyl protons.

Cytotoxicities of the synthesized compounds were evaluated on human solid carcinoma including HCT116, QG56, and DU145. The 18,6'-*O*-bisallyl-2'-*N*-acyl Et 770 derivatives (**4a**-**4j**) exhibited significantly decreasing cytotoxicity, compared with the parent Et 770. On the other hand, most of the 2'-*N*-aromatic compounds (**5a**-**5i**) showed higher cytotoxicity than the parent compound. Among them, the 2'-*N*-(4''-fluorocinnamoyl) Et 770 (**5h**) was the most potent cytotoxicity on these cancer cell lines and shown approximately 70-fold higher cytotoxicity to HCT116 than the parent Et 770. The potent cytotoxicity of this compound is opening the opportunity for future candidate for the anticancer agent. Future studies are essential to understand the molecular basis for the extraordinary cytotoxicity of the next generation ecteinascidins as the new anticancer agent.

REFERENCES

Amnuoypol, S., K. Suwanborirux, S. Pummangura, A. Kubo, C. Tanaka and N. Saito (2004). "Chemistry of renieramycins. Part 5. Structure elucidation of renieramycin-type derivatives O, Q, R, and S from Thai marine sponge *Xestospongia* species pretreated with potassium cyanide." Journal of Natural Products **67**(6): 1023-1028.

Arai, T., K. Takahashi, K. Ishiguro and Y. Mikami (1980). "Some chemotherapeutic properties of two new antitumor antibiotics, saframycins A and C." GANN Japanese Journal of Cancer Research **71**(6): 790-796.

Arai, T., T. Takahashi and A. Kubo (1977). "New antibiotics, saframycin A, B, C, D and E." Journal of Antibiotics **30**(11): 1015-1018.

Armand, J. P., *et al*. (2001). "Phase I and pharmacokinetic study of aplidine (apl) given as a 24-hours continuous infusion every other week (q2w) in patients (pts) with solid tumor (st) and lymphoma (NHL)." Proceedings American Society of Clinical Oncology **20**: 120a (Abstr).

Benvenuto, J. A., *et al*. (1992). "Phase II clinical and pharmacological study of didemnin B in patients with metastatic breast cancer." Investigational New Drugs **10**: 113-117.

Brusca, R. C. and G. J. Brusca (2003). Invertebrates 2nd ed. Sunderland: Sinauer Associates.

Castro, P. and M. E. Huber (2013). Marine Biology 9th ed. New York: McGrow-Hill.

Caudrado, A., *et al*. (2003). "Aplidin induces apoptosis in human cancer cells via glutathione depletion and sustained activation of the epidermal growth factor receptor, Src, JNK, and p38 MAPK." Journal of Biological Chemistry **278**(1): 241-250.

Cuevas, C. and A. Francesch (2009). "Development of Yondelis® (trabectedin, ET-743). A semisynthetic process solves the supply problem." Natural Product Reports **26**: 322-337.

Damia, G., *et al*. (2001). "Unique pattern of ET-743 activity in different cellular systems with defined deficiencies in DNA-repair pathways." International Journal of Cancer **92**(4): 583-588.

Dangles, O., F. Guibe, G. Balavoine, S. lavielle and A. Marquet (1987). "Selective cleavage of the allyloxycarbonyl groups through palladium-catalyzed hydrostannolysis with tributyltin hydride, application to the selective protection-deprotection of amino acid derivatives and in peptide synthesis." Journal of Organic Chemistry **52**(22): 4984-4993.

David-Cordonnier, M. H., *et al*. (2005). "DNA and non-DNA targets in the mechanism of action of the antitumor drug trabectedin." Chemistry and Biology **12**: 1201-1210.

Davidson, B. S. (1992). "Renieramycin G, a new alkaloid from the sponge *Xestospongia caycedoi*." Tetrahedron Letters **33**(26): 3721-3724.

Erba, E., *et al*. (2001). "Ecteinascidin-743 (ET-743), a natural marine compound, with a unique mechanism of action." European Journal of Cancer **37**: 97-105.

Erba, E., *et al*. (2002). "Cell cycle phase perturbations and apoptosis in tumor cells induced by aplidine." British Journal of Cancer **86**:1510-1517.

European Medicines Agency (EMA) (2004). Public summary of opinion on orphan designation trabectedin for the treatment of ovarian cancer[Online]. Available From: http://www.ema.europa.eu/ema [2014, April 17]

European Medicines Agency (EMA) (2007). Public summary of positive opinion for orphan designation of ecteinascidin 743 for the treatment of soft tissue sarcoma[Online]. Available From: http://www.ema.europa.eu/ema [2014, April 17]

Fontana, A., P. Cavaliere, S. Wahidulla, C. G. Naik and G. Cimino (2000). "A new antitumor isoquinoline alkaloids from the marine nudibranch *Jorunna funebris*." Tetrahedron **56**: 7305-7308.

Frincke, J. M. and D. J. Faulkner (1982). "Antimicrobial metabolites of the sponge *Reniera* sp." Journal of the American Chemical Society **104**(1): 265-269.

Geldof, A. A., S. C. Mastbergen, R. E. C. Henrar and G. T. Faircloth (1999). "Cytotoxicity and neurocytotoxicity of new marine anticancer agents evaluated using in vitro assays." Cancer Chemotherapy and Pharmacology **44**: 312-318.

Goss, G., *et al*. (1995). "Didemnin B in favorable histology non-Hodgkin's lymphoma: a phase II study of the National Cancer Institute of Canada Clinical Trials Group." Investigational New Drugs **13**: 257-260.

Guirouilh-Barbat, J., S. Antony and Y. Pommier (2009). "Zalypsis (PM00104) is a potent inducer of γ-H2Ax foci and reveals the importance of the C ring of trabectedin for transcription-coupled repair inhibition." American Association for Cancer Research **8**(7): 2007-2014.

Haas, N. B., *et al*. (2003). "Weekly bryostatin-1 in metastatic renal cell carcinoma: a Phase II study." Clinical Cancer Research **9**(1): 109-114.

Halim, H., P. Chunhacha, K. Suwanborirux and P. Chanvorachote (2011). "Anticancer and antimestastatic activities of renieramycin M, a marine tetrahydroisoquinoline alkaloid, in human non-small cell lung cancer cells." Anticancer Research **31**: 193-202.

Herrero, A. B., C. Martin-Castellanos, E. Marco, F. Gago and S. Moreno (2006). "Cross-talk between nucleotide excision and homologous recombination DNA repair pathways in the mechanism of action of antitumor trabectedin." Cancer Research **66**(16): 8155-8162.

Hill, G. C., T. P. Wunz, N. E. MacKenzie, P. R. Gooley and W. A. Remers (1991). "Computer simulation of the binding of naphthyridinomycin and cyanocycline A to DNA." Journal of Medicinal Chemistry **34**: 2079-2088.

Hochster, H., R. Oratz, D. S. Ettinger and E. Borden (1999). "A phase II study of didemnin B (NSC 325319) in advanced malignant melanoma: an Eastern Cooperative Oncology Group study (PB687)." Investigational New Drugs **16**: 259-263.

Ikeda, Y., *et al*. (1983). "Safracins, new antitumor antibiotics I. producing organism, fermentation and isolation." Journal of Antibiotics **36**(10): 1279-1283.

Jeedigunta, S., J. M. Krenisky and R. G. Kerr (2000). "Diketopiperazines as advanced intermediates in the biosynthesis of ecteinascidins." Tetrahedron **56**: 3303-3307.

Jimeno, J., G. Faircloth, J. M. F. Sousa-Faro P. Scheuer and K. L. Rinehart (2004). "New marine derived anticancer therapeutics- A journey from the sea to clinical trials." Marine Drugs **2**(1): 14-29.

Katoh, T. and S. Terashima (1996). "Synthesis and cytotoxic of natural (-)-quinocarcin and its related compounds." Pure and Applied Chemistry **68**(3): 703-706.

Kerr, R. G. and N. F. Miranda (1995). "Biosynthetic studies of ecteinascidins in the marine tunicate *Ecteinascidia turbinata*." Journal of Natural Products **58**(10): 1618-1621.

Kucuk, O., *et al*. (2000). "Phase II trial of didemnin B in previously treated non-Hodgkin's lymphoma: an Eastern Cooperative Oncology Group (ECOG) Study." American Journal of Clinical Oncology **23**: 273-277.

Lobo, C., *et al*. (1997). "Effect of dehydrodidemnin B on human colon carcinoma cell lines." Anticancer Research **17**: 333-336.

Lown, J. W., C. C. Hanstock, A. V. Joshua, T. Arai and K. Takahashi (1983). "Structure and conformation of saframycin R determined by high field ^{1}H and ^{13}C NMR and its interactions with DNA in solution." Journal of Antibiotics **36**(9): 1184-1194.

Margolin, K., *et al*. (2002). "Dolastatin-10 in metastatic melanoma: a Phase II and pharmacokinetic trial of the California Cancer Consortium." Investigational New Drugs **19**(4): 335-440.

Maroun, J.A., *et al*. (2006). "Phase I study of aplidine in a daily x 5 one-hour infusion every 3 weeks in patients with solid tumors refractory to standard therapy. A National Cancer Institute of Canada Clinical Trials Group study: NCIC CTG IND 115." Annals of Oncology **17**(9): 1371-1378.

Martinez, E. J., T. Owa, S. L. Schreiber and E. J. Corey (1999) "Phthalascidin, a synthetic antitumor agent with potency and mode of action comparable to ecteinascidin 743."

Proceedings of the National *Academy* of Sciences of the *United States* of America **96**: 3496-3501.

Mikami, Y., *et al*. (1985). "Biosynthetic studies on saframycin A, a quinine antitumor antibiotic produced by *Streptomyces lavendulae*." Journal of Biological Chemistry **260**(1): 344-348.

Moore, B. M., F. C. Seaman, L. H. Hurley (1997). "NMR-based model of an ecteinascidin 743-DNA adduct." Journal of the American Chemical Society **119**(23): 5475-5476.

Moore, B. M., F. C. Seaman, R. T. Wheelhouse and L. H. Hurley (1998). "Mechanism for the catalytic activation of ecteinascidin 743 and its subsequent alkylation of guanine N2." Journal of the American Chemical Society **120**(10): 2490-2491.

Peschel, C., *et al*. (2007). "Phase II study of plitidepsin in pretreated patients with locally advanced or metastatic non-small cell lung cancer." Lung Cancer **60**(3): 374-380.

Plummer, R., *et al*. (2013). "Phase I-II study of plitidepsin and dacarbazine as first-line therapy for advanced melanoma." British Journal of Cancer **109**: 1451-1459.

Pommier, Y., G. Kohlhagen, C. Baily, M. Waring, A. Mazumder and K. W. Kohn, (1996). "DNA sequence- and structure-selective alkylation of guanine N2 in the DNA minor groove by ecteinascidin 743, a potent antitumor compound from the Caribbean tunicate *Ecteinascidia turbinata*." Biochemistry **35**(41): 13303-13309.

Powan, P., N. Saito, K. Suwanborirux and P. Chanvorachote (2013). "Ecteinascidin 770, a tetrahydroisoquinoline alkaloid, sensitizes human lung cancer cells to anoikis." Anticancer Research **33**(2): 505-512.

Puthongking, P., C. Patarapanich, S. Amnuoypol, K. Suwanborirux, A. Kubo and N. Saito (2006). "Chemistry of ecteinascidins. Part 2. Preparation of 6'-*O*-acyl derivatives of stable ecteinascidin and evaluation of cytotoxicity." Chemical and Pharmaceutical Bulletin **54**(7): 1010-1016.

Rath, C. M., *et al*. (2011). "Meta-omic characterization of the marine invertebrate microbial consortium that produces the chemotherapeutic natural product ET-743." ACS Chemical biology **6**: 1244-1256.

Ribrag, V., *et al*. (2013). "Multicenter phase II study of plitidepsin in patients with relapsed/refractory non-Hodgkin's lymphoma." Haematologica **98**(3); 357-363.

Rinehart, K. L. (2000). "Antitumor compounds from tunicates." Medicinal Research Reviews **20**: 1-27.

Rinehart, K. L., *et al*. (1990). "Ecteinascidins 729, 743, 745, 759A, 759B and 770: potent antitumor agents from the Caribbean tunicate *Ecteinascidia turbinata.*" Journal of Organic Chemistry **55**(15): 4512-4515.

Rinehart, K., J. Gloer, J. Cook, J. Carter, S. Mizsak and T. Scahill (1987). "Structure of the didemnins, antiviral and cytotoxic depsipeptides from a Caribbean tunicate." Journal of the American Chemical Society **103**: 1857-1859.

Sainz-Diaz, C. I., I. Manzanares, A. Francesch and J. Garcia-Ruiz (2003). "The potent anticancer compound ecteinascidin-743 (ET-743) as its 2-propanol disolvate." Acta Crystallographica Section C: Crystal Structure Communications **59**(4): o197-o198.

Sakai, R., E. A. Jares-Erijman, I. Manzanares, M. V. S. Elipe and K. L. Rinehart (1996). "Ecteinascidins: Putative biosynthetic precursors and absolute stereochemistry." Journal of the American Chemistry Society **118**: 9017-9023.

Sakai, R., K. L. Rinehart, Y. Guan and A. H. J. Wang (1992). "Additional antitumor ecteinascidins from a Caribbean tunicate: crystal structure and activities *in vivo*." Proceedings of the National Academy of Sciences of the United States of America **89**: 11456-11460.

Saktrakulkla, P., *et al.* (2011). "Chemistry of ecteinascidins. Part 3: Preparation of 2'-*N*-acyl derivatives of ecteinascidin 770 and evaluation of cytotoxicity." Bioorganic and Medicinal Chemistry **19**(15): 4421-4436.

Schmitz, F. J. and T. Yasumoto (1991). "The 1990 United States-Japan seminar on bioorganic marine chemistry, meeting report." Journal of Natural Products **54**(6): 1469-1490.

Schoffski, P., *et al*. (2009). "Phase II randomized study of plitidepsin (aplidin), alone or in association with L-carnitine, in patients with unresectable advanced renal cell carcinoma." Marine Drugs **7**(1): 57-70.

Seaman, F. C. and L. H. Hurley (1998). "Molecular basis for the DNA sequence selectivity of ecteinascidin 736 and 743: evidence for the dominant role of direct readout via hydrogen bonding." Journal of the American Chemical Society **120**(50): 13028-13041.

Shin, D. M., *et al*. (1991). "Phase I/II clinical trial of didemnin B in non-small-cell lung cancer: neuromuscular toxicity is dose-limiting." Cancer Chemotherapy and Pharmacology **29**: 145-149.

Shin, D. M., *et al*. (1994). "Phase II clinical trial of didemnin B in previously treated small cell lung cancer." Investigational New Drugs **12**: 243-249.

Smart, B. E. (2001). "Fluorine substituent effects (on bioactivity)." Journal of Fluorine Chemistry **109**: 3-11.

Soares, D. G., N. P. Poletto, D. Bonatto, M. Salvador, G. Schwartsmann and J. A. P. Henriques (2005). "Low cytotoxicity of ecteinascidin 743 in yeast lacking the major endonucleolytic enzymes of base and nucleotide excision repair pathways." Biochemical Pharmacology **70**: 59-69.

Suwanborirux, K., *et al*. (2003). "Chemistry of renieramycins. Part 3. Isolation and structure of stabilized renieramycin type derivatives possessing antitumor activity from Thai sponge *Xestospongia* species, pretreated with potassium cyanide." Journal of Natural Products **66**(11): 1441-1446.

Suwanborirux, K., K. Charupant, S. Amnuoypol, S. Pummangura, A. Kubo and N. Saito (2002). "Ecteinascidins 770 and 786 from the Thai tunicate *Ecteinascidia thurstoni*." Journal of Natural Products **65**(6): 935-937.

Takebayashi, Y., *et al*. (2001). "Antiproliferative activity of ecteinascidin 743 is dependent upon transcription-coupled nucleotide-excision repair." Nature Medicine **7**(8): 961-966.

Taraboletti, G., *et al*. (2004). "Antiangiogenic activity of aplidine, a new agent of marine origin." British Journal of Cancer **90**(12): 2418-2424.

Tomita, F., K. Takahashi and T. Tamaoki (1984). "Quinocarcin, a novel antitumor antibiotic. III: mode of action." Journal of Antibiotics **37**(10): 1268-1272.

Urdiales, J. L., *et al*. (1996). "Antiproliferative effect of dehydrodidemnin B (DDB), a depsipeptide isolated from Mediterranean tunicates." Cancer Letters **102**: 31-37.

Vera, M. D. and M. M. Joullie (2002). "Natural products as probes of cell biology: 20 years of didemnin research." Medicinal Research Reviews **22**(2): 102-145.

Wright, A. E., D. A. Forleo, G. P. Gunawardana, S. P. Gunasekera, F. E. Koehn and O. J. McConnell (1990). "Antitumor tetrahydroisoquinoline alkaloids from the colonial ascidian *Ecteinascidia turbinata*." Journal of Organic Chemistry **55**(15): 4508-4512.

Yazawa, K., T. Asaoka, K. Takahashi, Y. Mikami and T. Arai (1982). "Bioconversions of saframycin A specific to some genera of actinomycetes." Journal of Antibiotics **35**(7): 915-917.

Zewail-Foote, M. and L. H. Hurley (1999). "Ecteinascidin 743: a minor groove alkylator that bends DNA toward the major groove." Journal of Medicinal Chemistry **42**(14): 2493-2497.

Zewail-Foote, M., V. S. Li, H. Kohn, D. Bearss, M. Guzman and L. H. Hurley (2001). "The inefficiency of incisions of ecteinascidin 743–DNA adducts by the UvrABC nuclease and the unique structural feature of the DNA adducts can be used to explain the repair-dependent toxicities of this antitumor agent." Chemistry and Biology **8**(11): 1033-1049.

APPENDIX

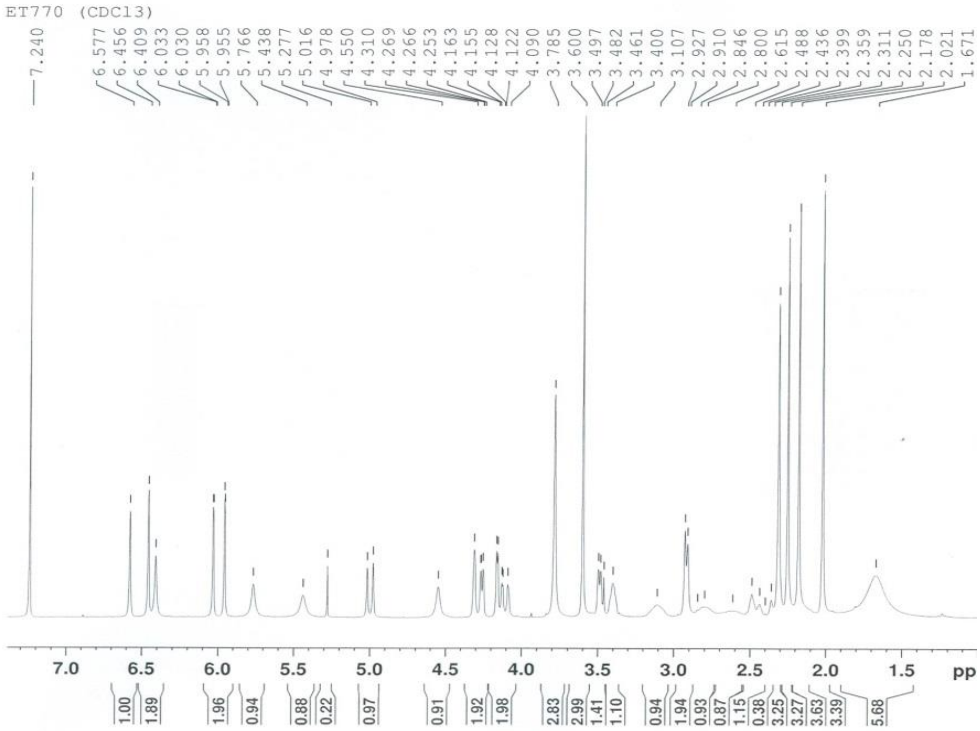

Figure 29. The ^{1}H-NMR spectrum of Et 770 (300 MHz, $CDCl_3$).

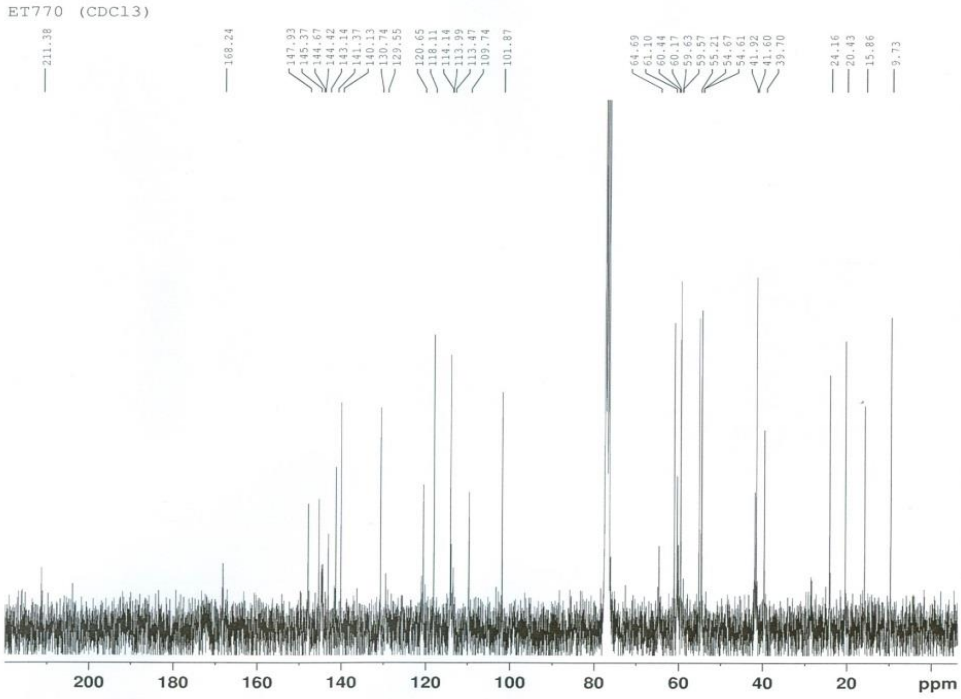

Figure 30. The ^{13}C-NMR spectrum of Et 770 (75 MHz, $CDCl_3$).

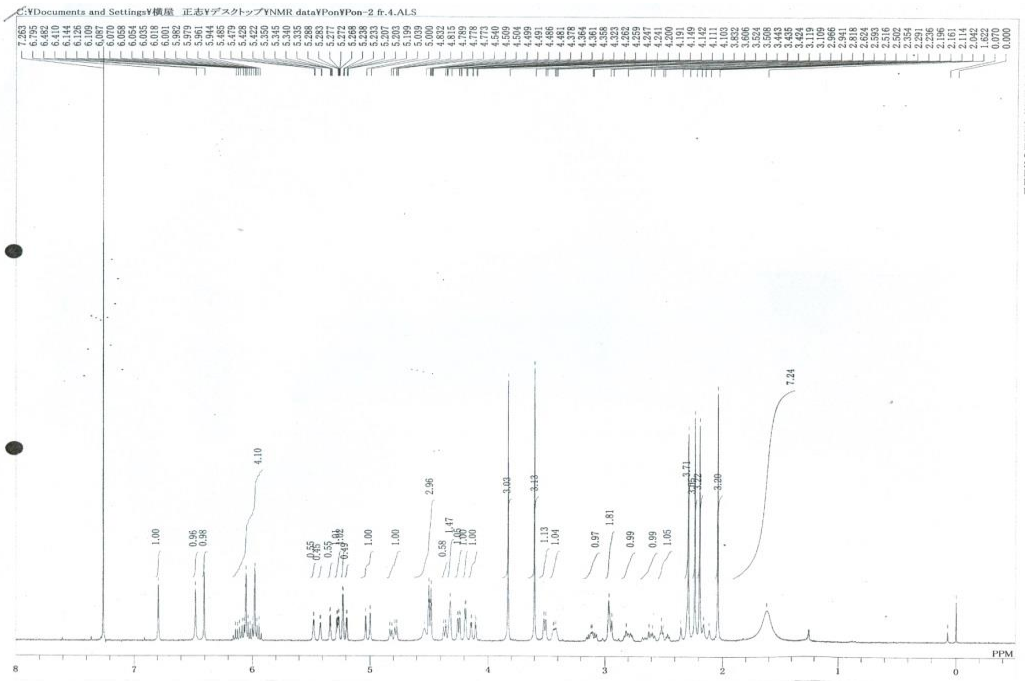

Figure 31. The ^{1}H-NMR spectrum of 18,6'-*O*-bisallyl Et 770 (500 MHz, $CDCl_3$).

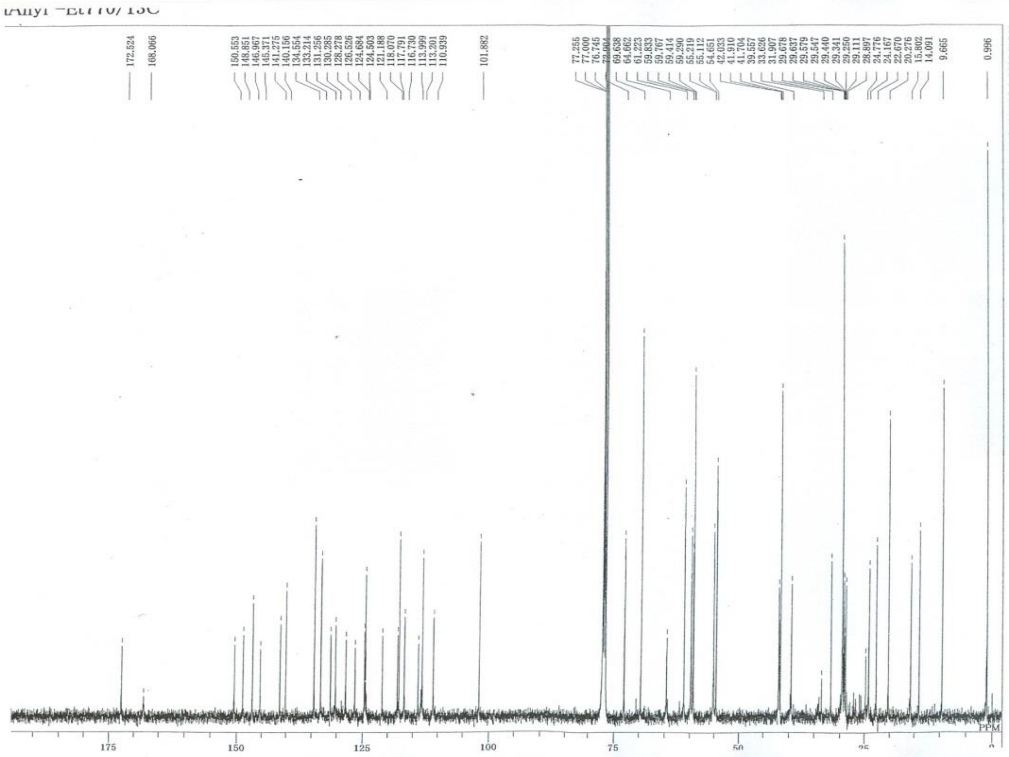

Figure 32. The ^{13}C-NMR spectrum of 18,6'-*O*-bisallyl Et 770 (125 MHz, $CDCl_3$).

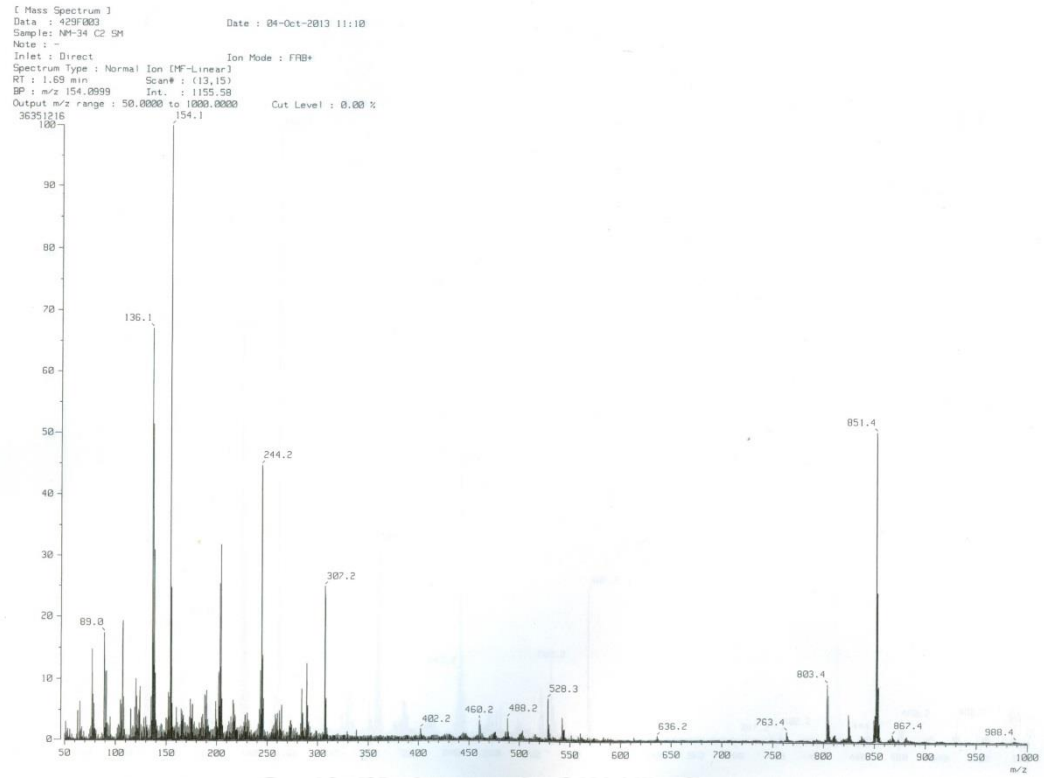

Figure 33. The FAB-Mass spectrum of 18,6'-*O*-bisallyl Et 770.

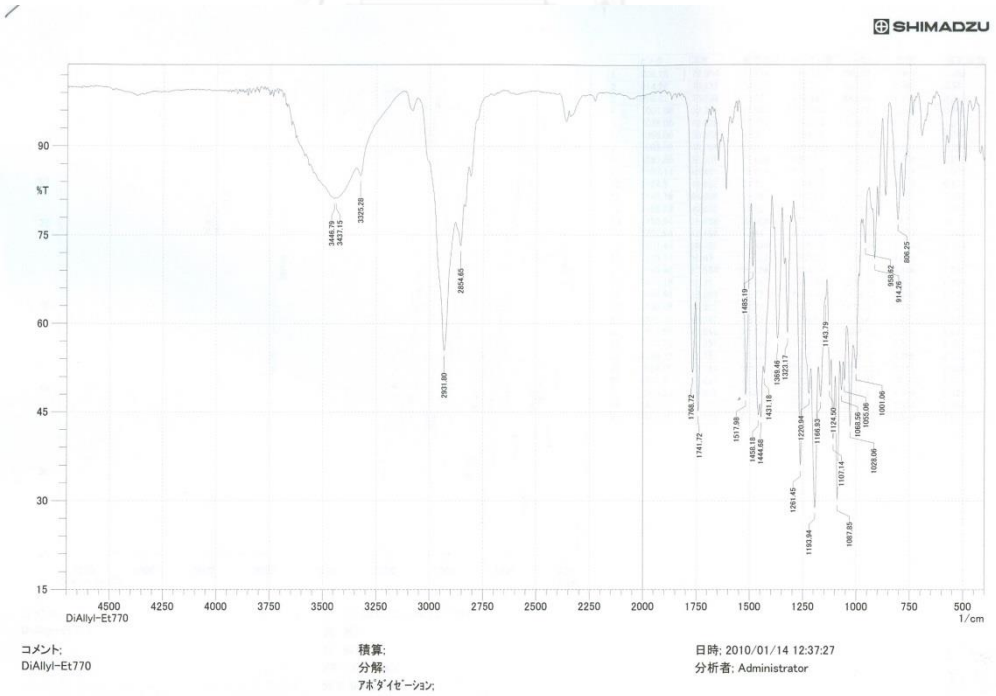

Figure 34. The IR spectrum (in KBr) of 18,6'-*O*-bisallyl Et 770.

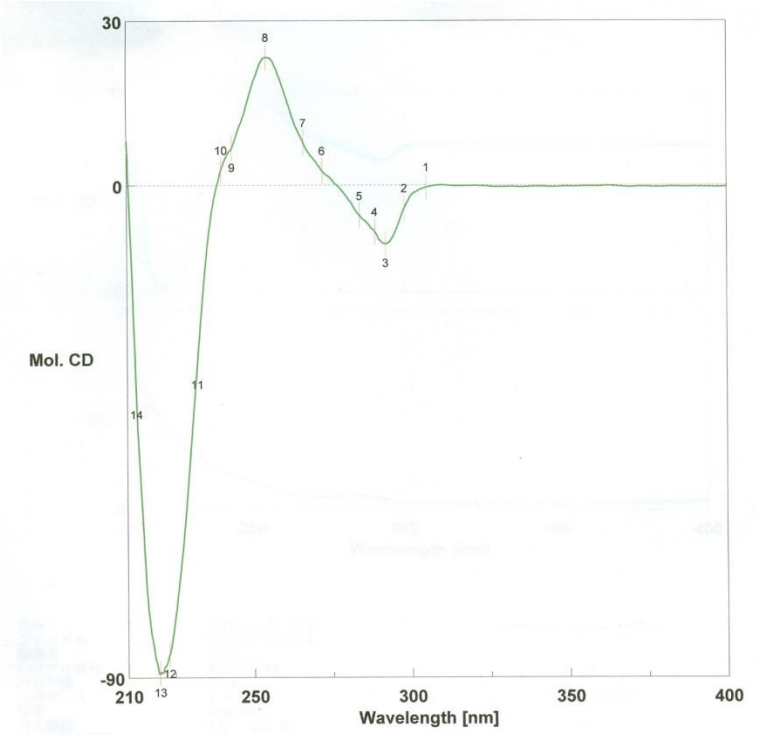

日時	2010/05/27 12:26
測定者	toriumi
ファイル名	DiAllyl Et770_s
試料名	DiAllyl Et770
コメント	DiAllyl Et770

No.	nm	Mol. CD	No.	nm	Mol. CD	No.	nm	Mol. CD
1	305.00	-0.391589	2	298.00	-4.18144	3	292.00	-10.7461
4	288.60	-8.51421	5	283.80	-5.56822	6	272.00	2.62681
7	266.00	7.77123	8	254.20	23.3864	9	243.40	6.74136
10	240.00	2.75179	11	232.20	-32.9172	12	223.00	-85.6931
13	220.00	-89.1188	14	212.80	-38.3267			

Figure 35. The CD spectrum of 18,6'-*O*-bisallyl Et 770.

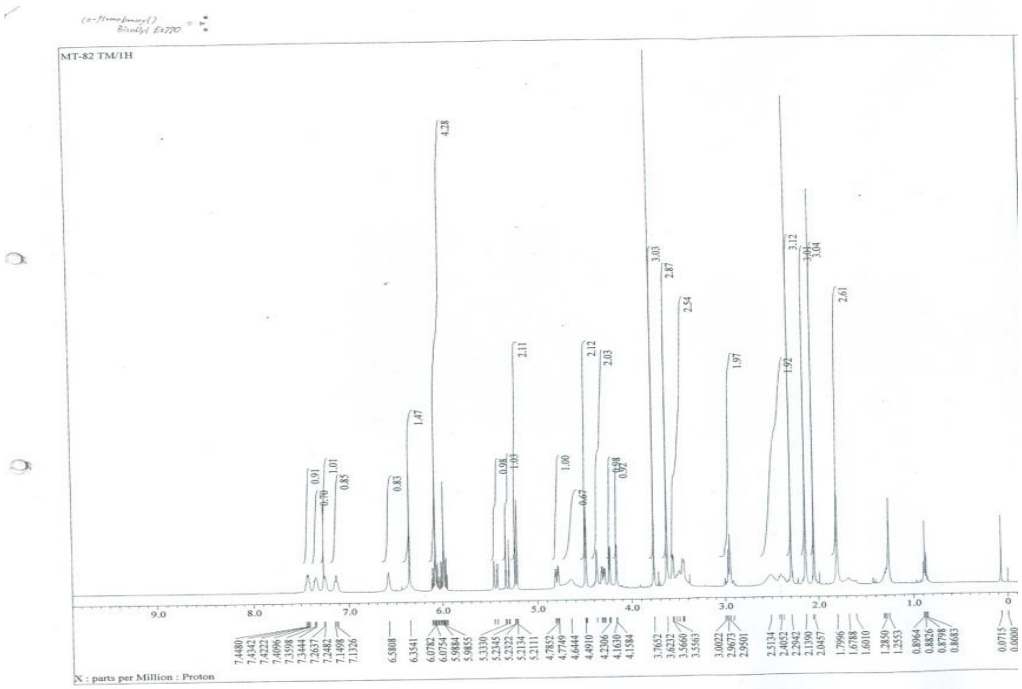

Figure 36. The ^{1}H-NMR spectrum of 18,6'-*O*-bisallyl-2'-*N*-(2''-fluorobenzoyl) Et 770 (500 MHz, $CDCl_3$).

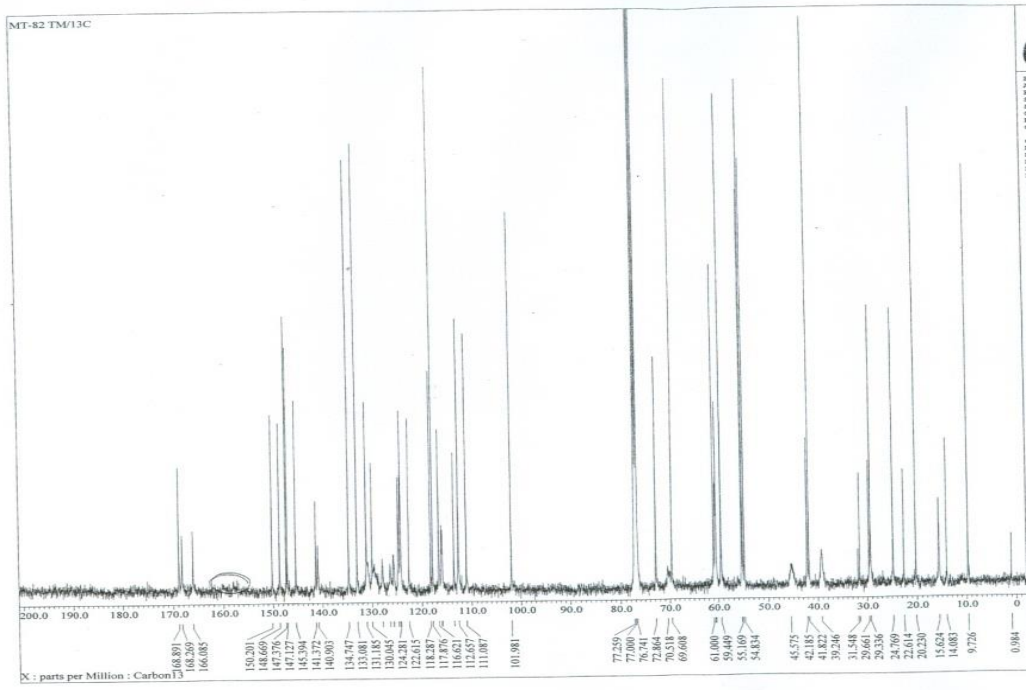

Figure 37. The ^{13}C-NMR spectrum of 18,6'-*O*-bisallyl-2'-*N*-(2''-fluorobenzoyl) Et 770 (125 MHz, $CDCl_3$).

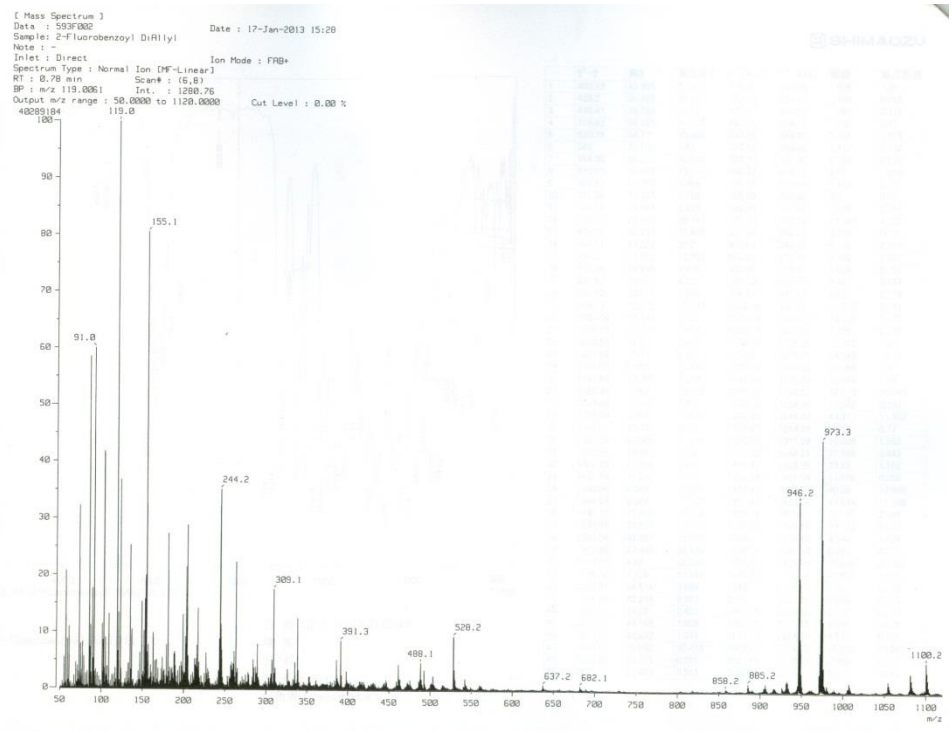

Figure 38. The FAB-Mass spectrum of 18,6'-*O*-bisallyl-2'-*N*-(2''-fluorobenzoyl) Et 770.

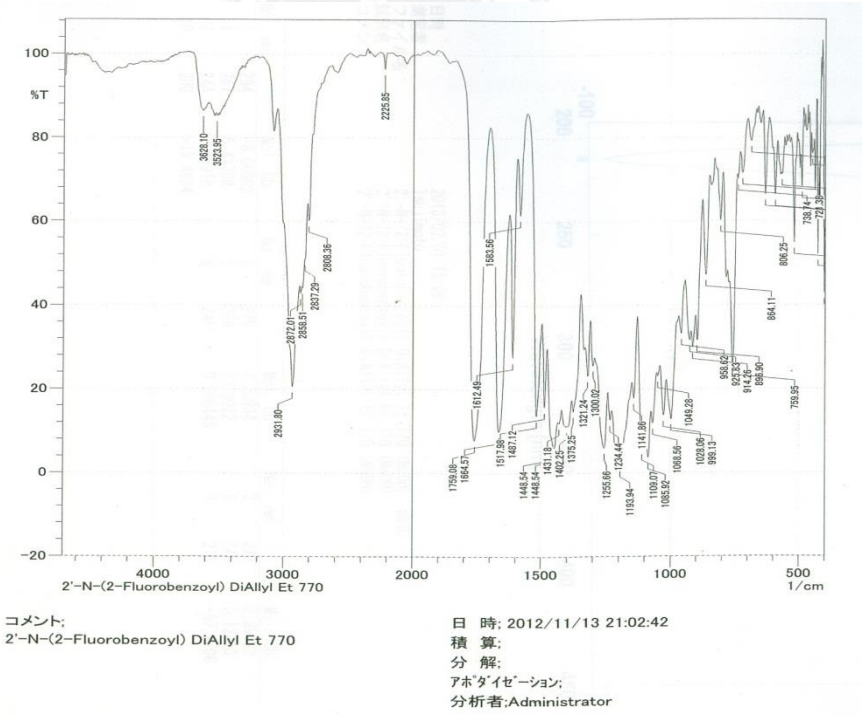

Figure 39. The IR spectrum (in KBr) of 18,6'-*O*-bisallyl-2'-*N*-(2''-fluorobenzoyl) Et 770.

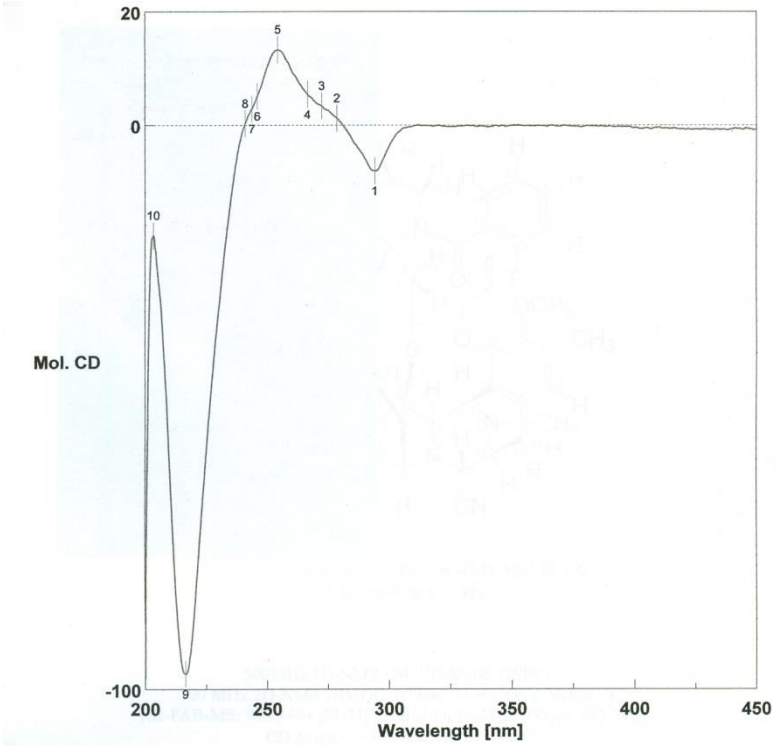

日時	2013/02/01 15:09
測定者	Tsujimoto
ファイル名	2'-N-(2-Fluorobenzoyl) DiAllyl Et 770 (MeOH) 修正
試料名	2'-N-(2-Fluorobenzoyl) DiAllyl Et 770 (MeOH)
コメント	2'-N-(2-Fluorobenzoyl) DiAllyl Et 770 (MeOH)

No.	nm	Mol. CD	No.	nm	Mol. CD	No.	nm	Mol. CD
1	294	-8.06002	2	279	1.20934	3	272	3.39092
4	267	5.41708	5	254	13.3022	6	246	5.12803
7	244	2.88918	8	241	0.296446	9	216	-97.2706
10	203	-19.4834						

Figure 40. The CD spectrum of 18,6'-*O*-bisallyl-2'-*N*-(2"-fluorobenzoyl) Et 770.

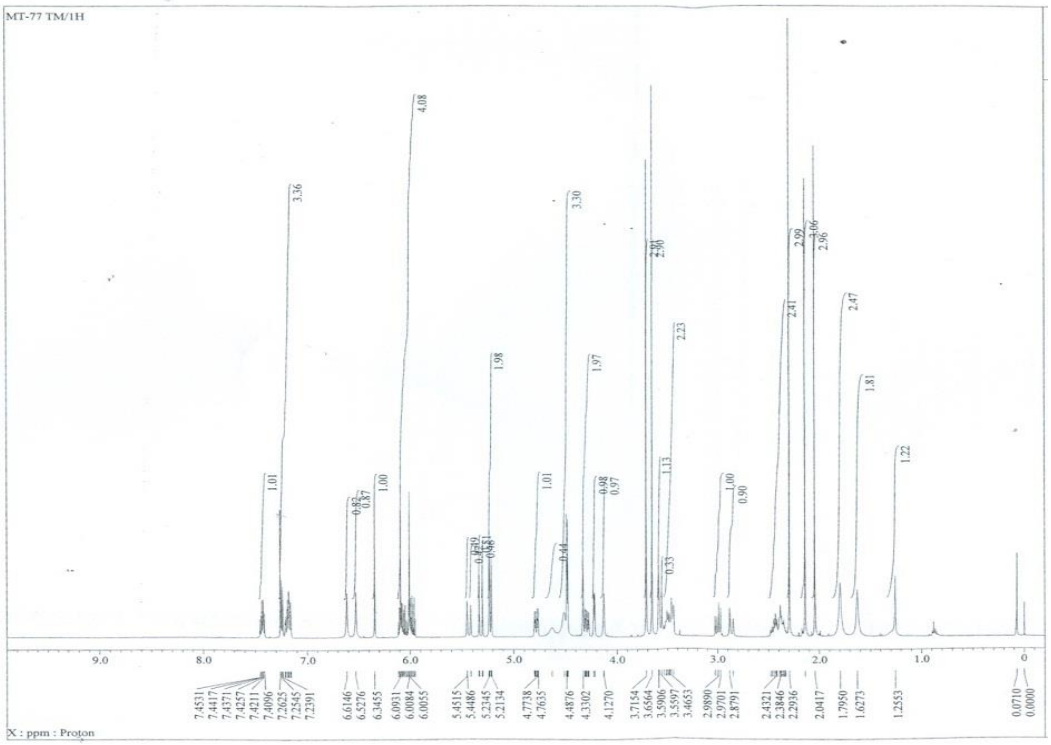

Figure 41. The ^{1}H-NMR spectrum of 18,6'-*O*-bisallyl-2'-*N*-(3''-fluorobenzoyl) Et 770 (500 MHz, $CDCl_3$).

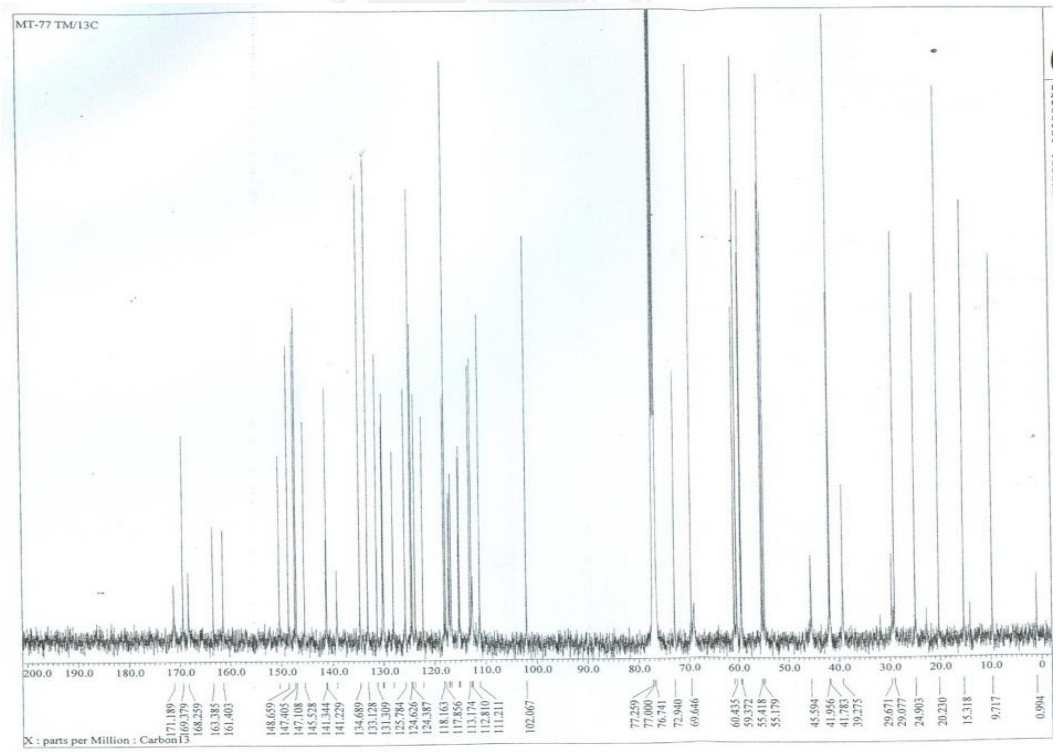

Figure 42. The ^{13}C-NMR spectrum of 18,6'-*O*-bisallyl-2'-*N*-(3''-fluorobenzoyl) Et 770 (125 MHz, $CDCl_3$).

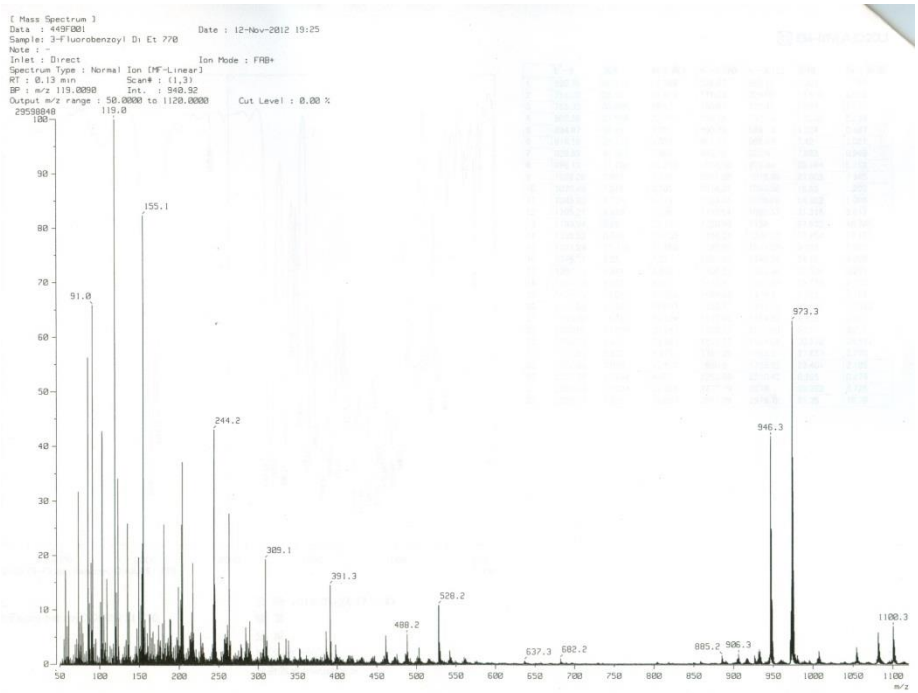

Figure 43. The FAB-Mass spectrum of 18,6'-*O*-bisallyl-2'-*N*-(3"-fluorobenzoyl) Et 770.

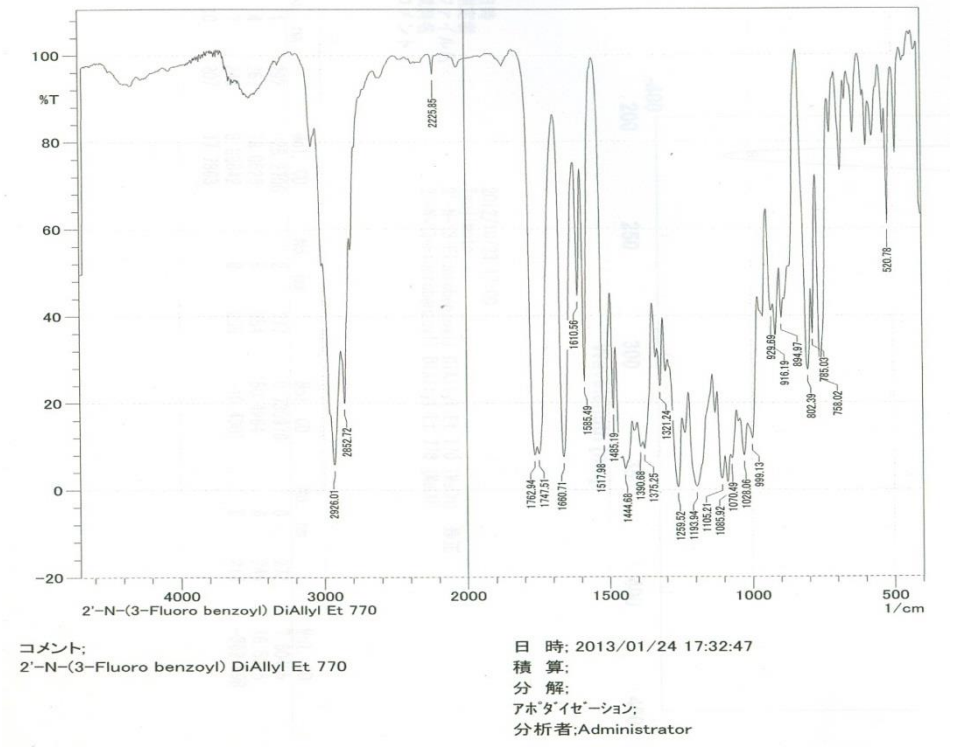

Figure 44. The IR spectrum (in KBr) of 18,6'-*O*-bisallyl-2'-*N*-(3"-fluorobenzoyl) Et 770.

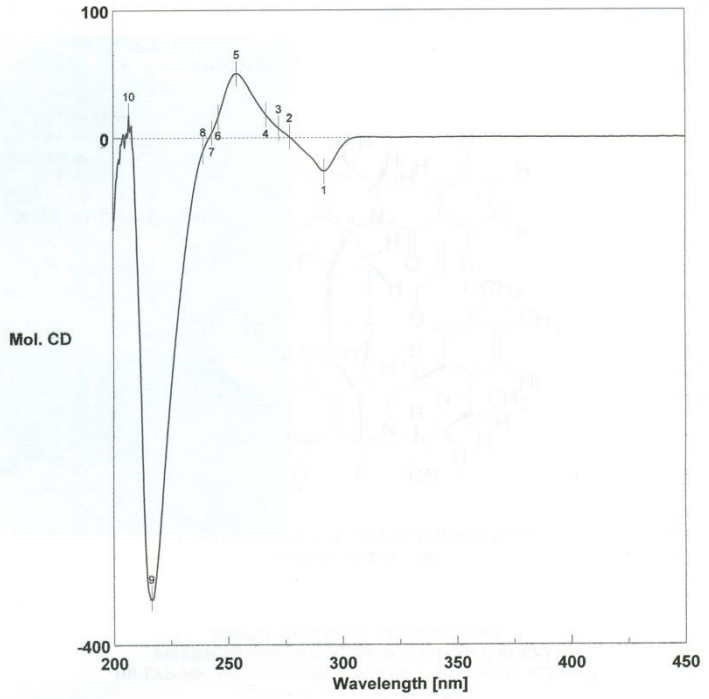

日時 2012/10/23 17:00
測定者 Tsujimoto
ファイル名 2'-N-(3-Fluorobenzoyl) DiAllyl Et 770 (MeOH) 修正
試料名 2'-N-(3-Fluorobenzoyl) DiAllyl Et 770 (MeOH)
コメント

No.	nm	Mol. CD	No.	nm	Mol. CD	No.	nm	Mol. CD
1	292	-26.2706	2	277	0.730976	3	272	7.60485
4	267	18.0528	5	254	50.4964	6	246	16.5375
7	243	3.89842	8	239	-10.4301	9	216	-362.998
10	207	17.7863						

Figure 45. The CD spectrum of 18,6'-*O*-bisallyl-2'-*N*-(3''-fluorobenzoyl) Et 770.

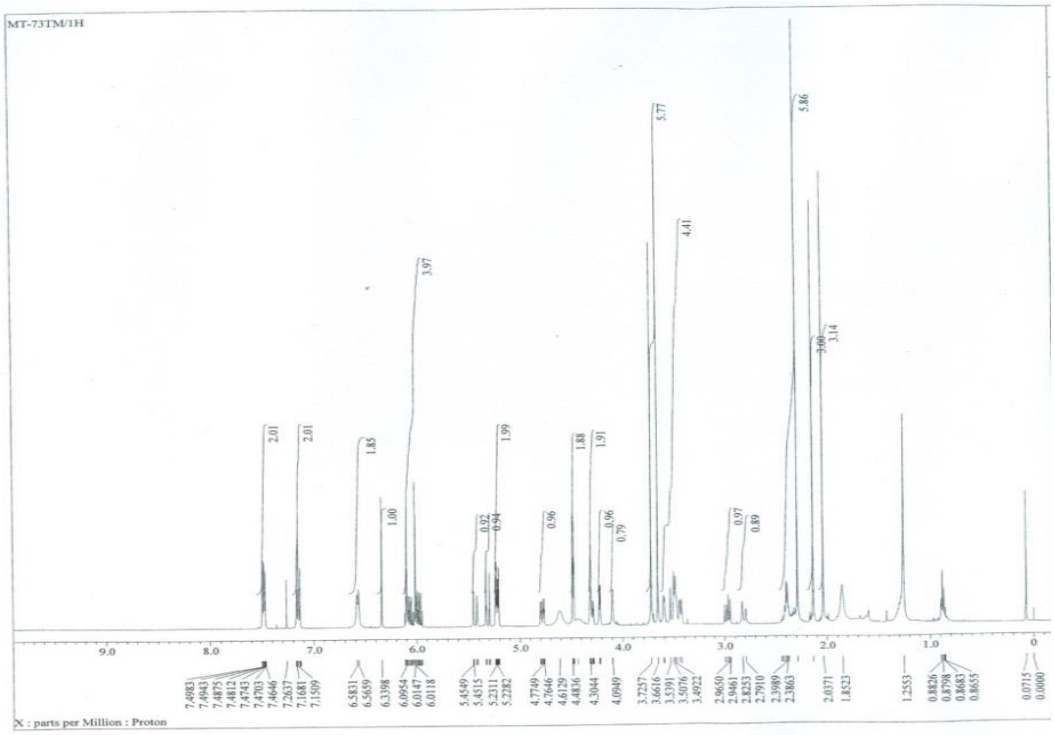

Figure 46. The ^{1}H-NMR spectrum of 18,6'-*O*-bisallyl-2'-*N*-(4''-fluorobenzoyl) Et 770 (500 MHz, $CDCl_3$).

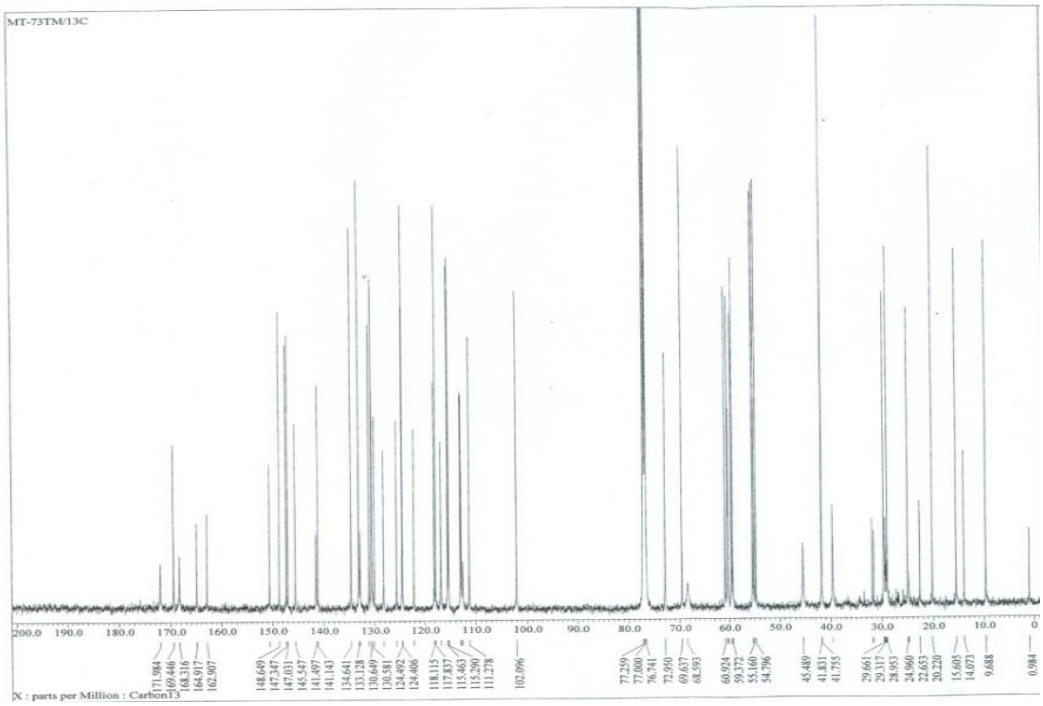

Figure 47. The ^{13}C-NMR spectrum of 18,6'-*O*-bisallyl-2'-*N*-(4''-fluorobenzoyl) Et 770 (125 MHz, $CDCl_3$).

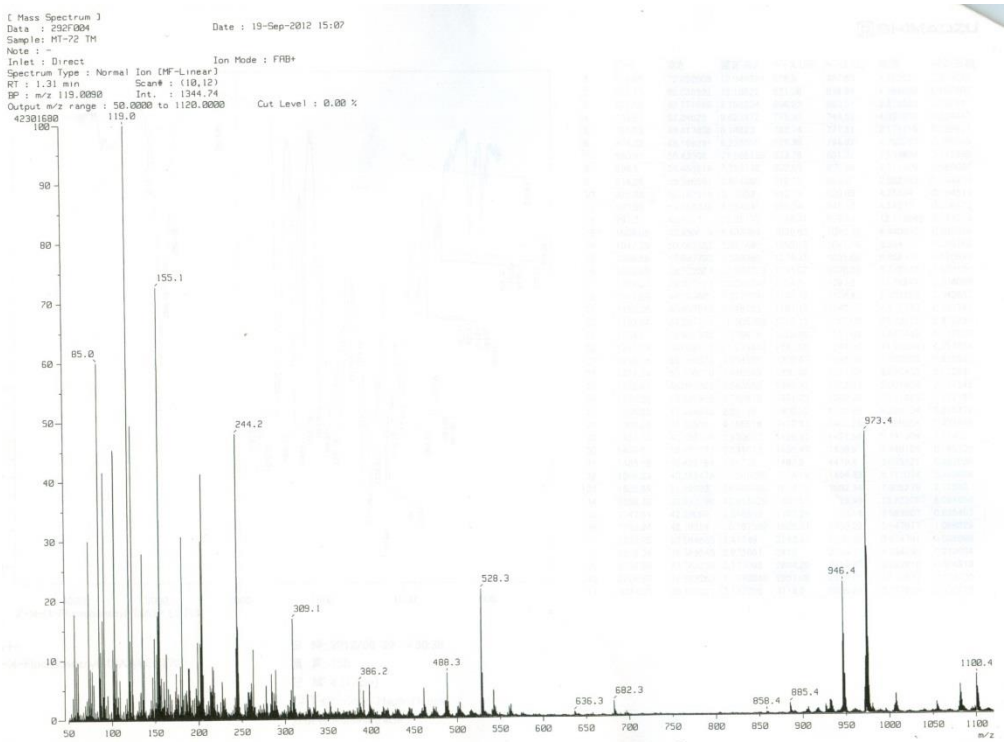

Figure 48. The FAB-Mass spectrum of 18,6'-*O*-bisallyl-2'-*N*-(4''-fluorobenzoyl) Et 770.

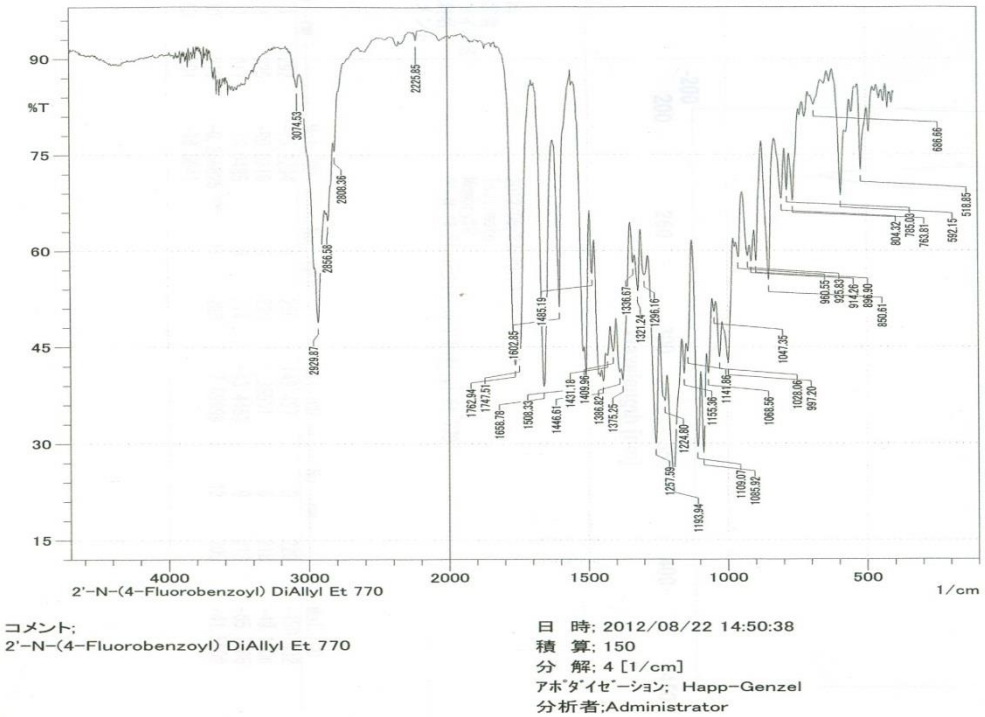

Figure 49. The IR spectrum (in KBr) of 18,6'-*O*-bisallyl-2'-*N*-(4''-fluorobenzoyl) Et 770.

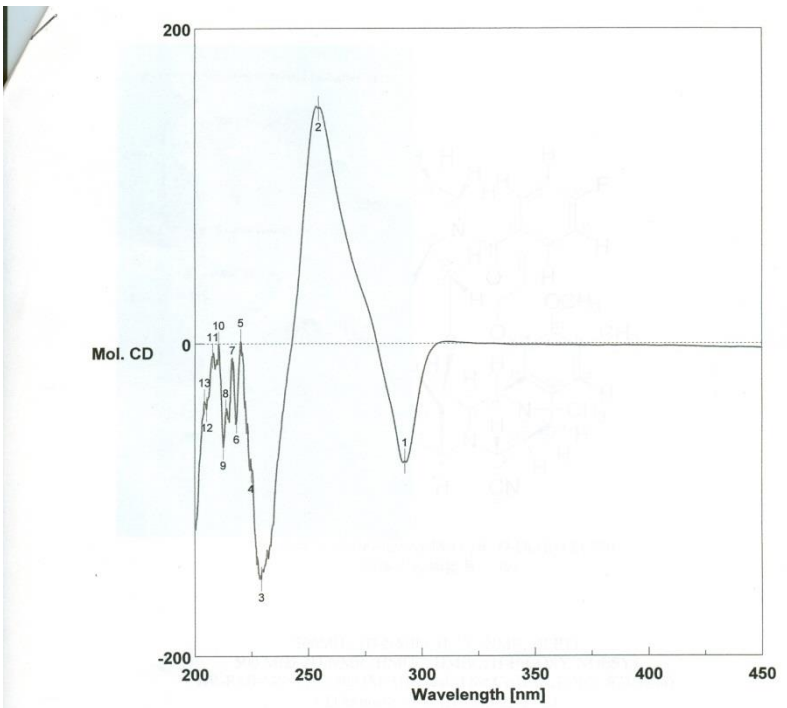

日時 2012/08/22 20:24
測定者 Tsujimoto
ファイル名 Memory#9
試料名 2'-N-(4-Fluorobenzoyl) DiAllyl Et 770
コメント

No.	nm	Mol. CD	No.	nm	Mol. CD	No.	nm	Mol. CD
1	292	-75.2294	2	255	149.457	3	229	-150.432
4	225	-80.8216	5	220	1.35551	6	218	-49.1606
7	217	-16.0485	8	214	-43.4453	9	213	-65.7885
10	210	-0.266825	11	208	-7.69699	12	205	-41.5909
13	204	-36.6641						

Figure 50. The CD spectrum of 18,6'-*O*-bisallyl-2'-*N*-(4''-fluorobenzoyl) Et 770.

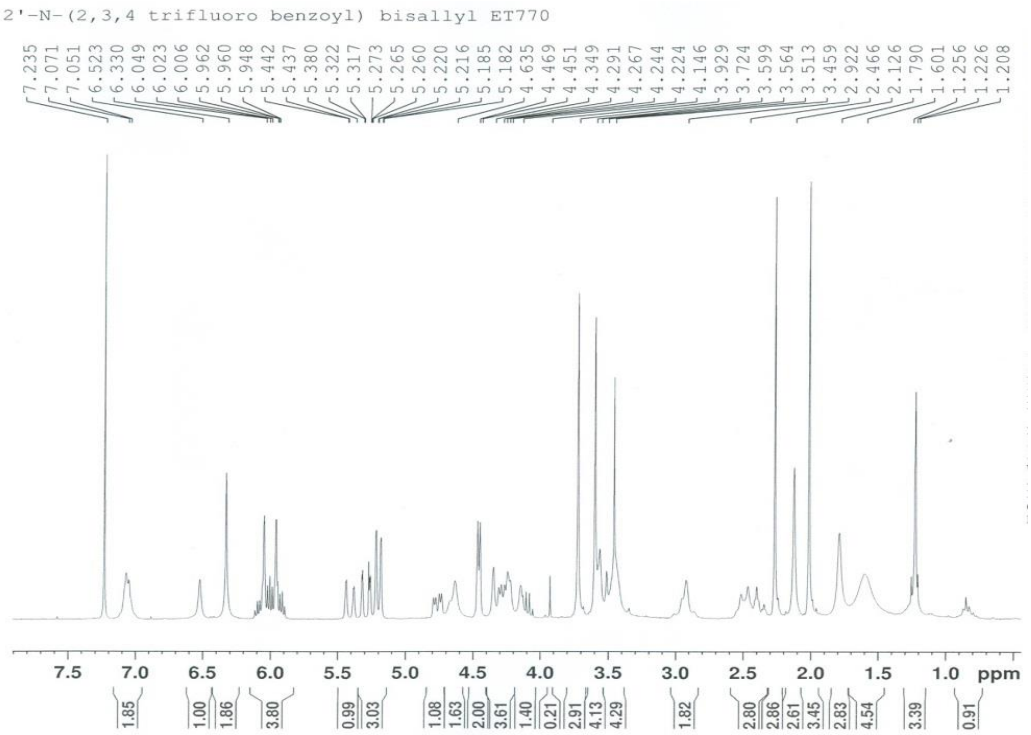

Figure 51. The ^{1}H-NMR spectrum of 18,6'-*O*-bisallyl-2'-*N*-(2'',3'',4''-trifluorobenzoyl) Et 770 (300 MHz, $CDCl_3$).

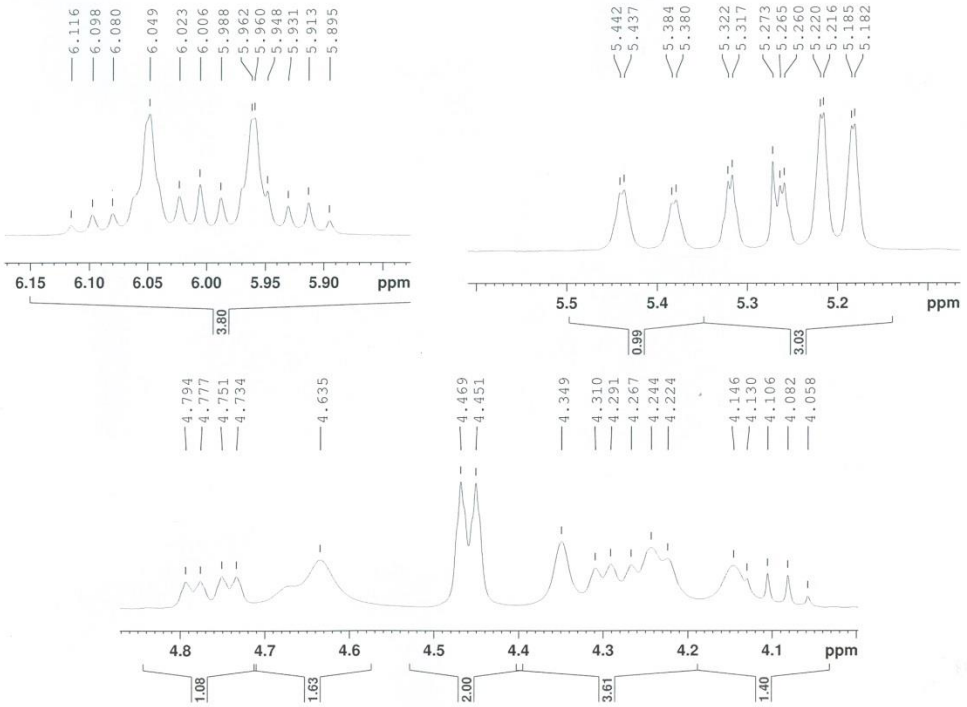

Figure 52. The ^{1}H-NMR spectrum of 18,6'-*O*-bisallyl-2'-*N*-(2'',3'',4''-trifluorobenzoyl) Et 770 (expansion between δ_H 4.0-6.2 ppm, 300 MHz, $CDCl_3$).

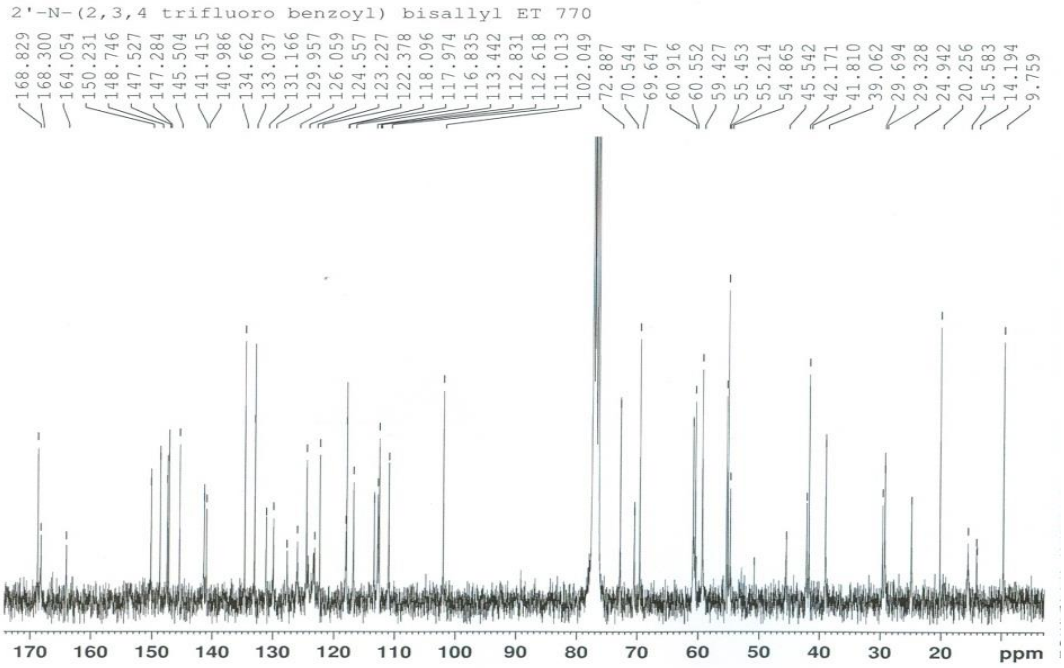

Figure 53. The ^{13}C-NMR spectrum of 18,6'-*O*-bisallyl-2'-*N*-(2,3,4-trifluorobenzoyl) Et 770 (75 MHz, $CDCl_3$).

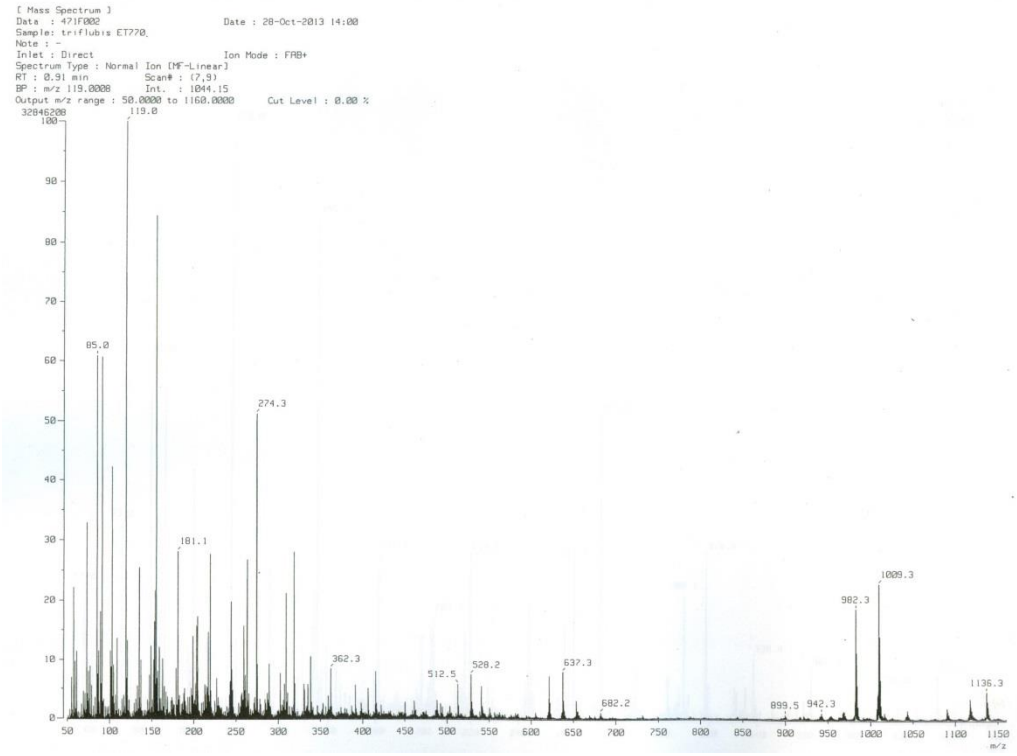

Figure 54. The FAB-Mass spectrum of 18,6'-*O*-bisallyl-2'-*N*-(2,3,4-trifluorobenzoyl) Et 770.

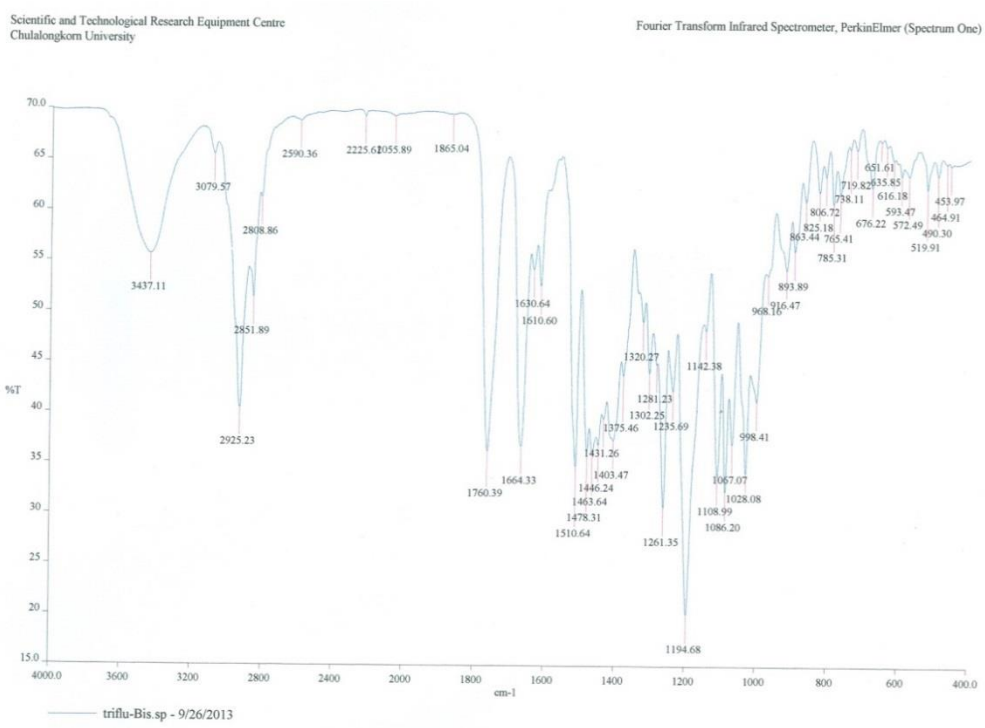

Figure 55. The IR spectrum (in KBr) of 18,6'-*O*-bisallyl-2'-*N*-(2,3,4-trifluorobenzoyl) Et 770.

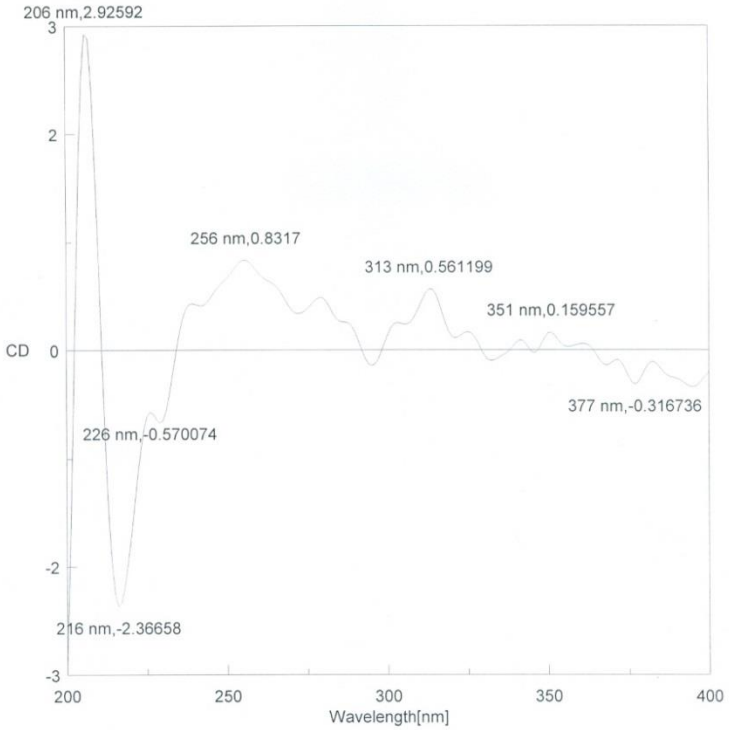

Figure 56. The CD spectrum of 18,6'-*O*-bisallyl-2'-*N*-(2,3,4-trifluorobenzoyl) Et 770.

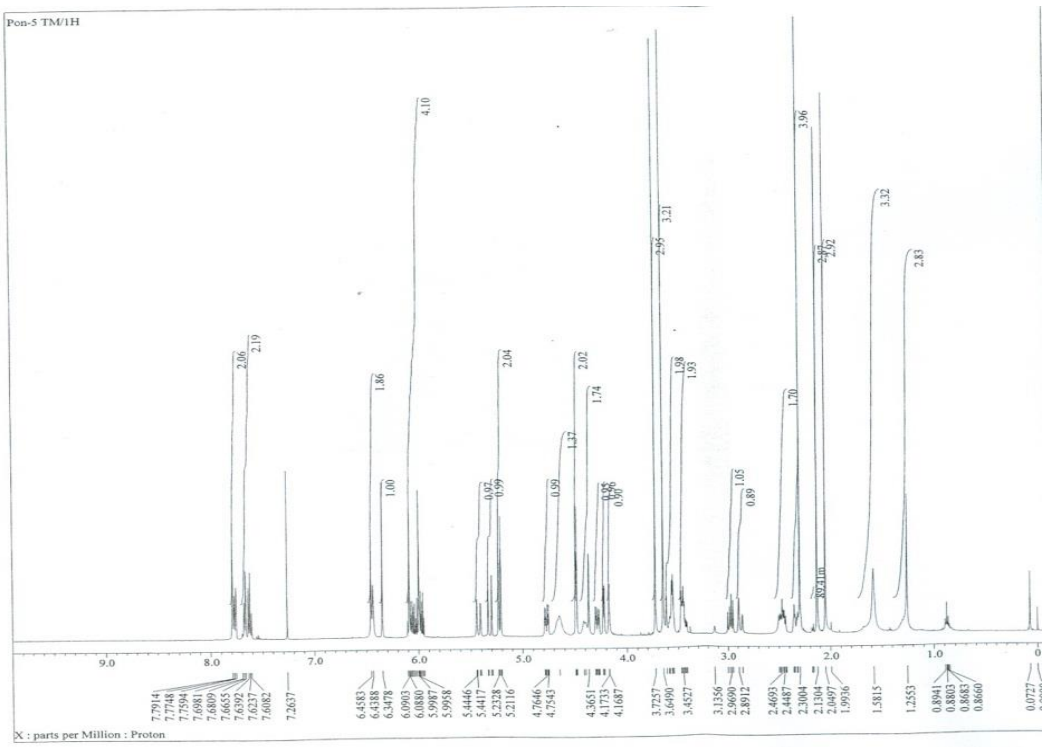

Figure 57. The ^{1}H-NMR spectrum of 18,6'-*O*-bisallyl-2'-*N*-(3''-trifluoromethylbenzoyl) Et 770 (500 MHz, $CDCl_3$).

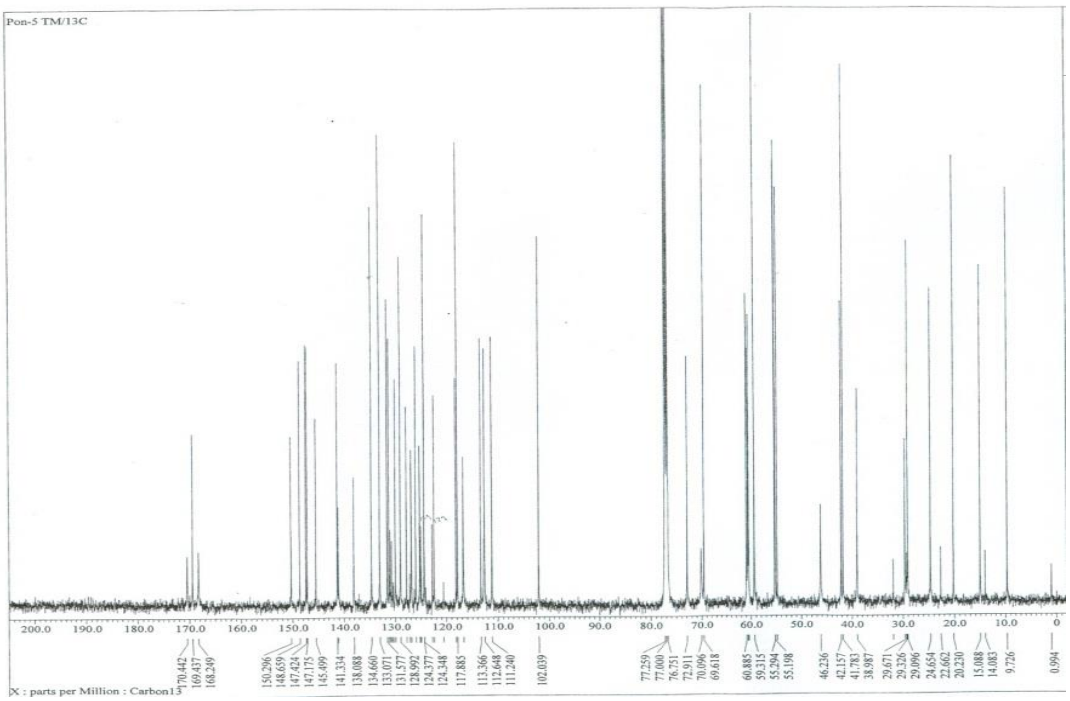

Figure 58. The ^{13}C-NMR spectrum of 18,6'-*O*-bisallyl-2'-*N*-(3''-trifluoromethylbenzoyl) Et 770 (125 MHz, $CDCl_3$).

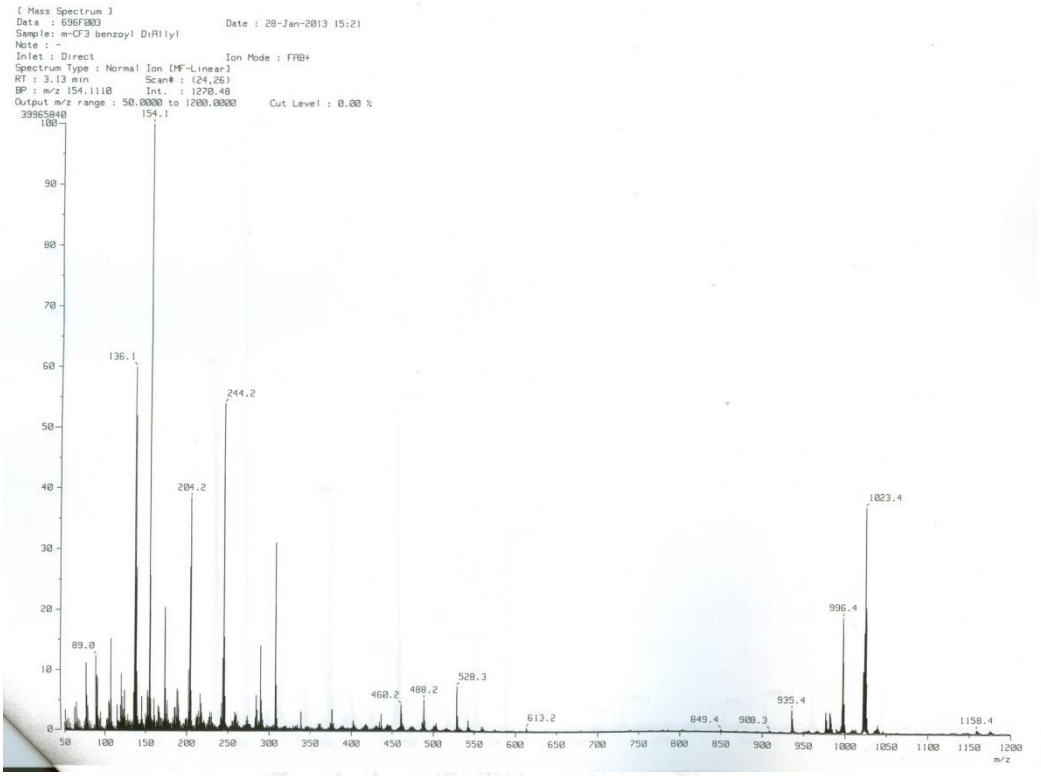

Figure 59. The FAB-Mass spectrum of 18,6'-*O*-bisallyl-2'-*N*-(3''-trifluoromethylbenzoyl) Et 770.

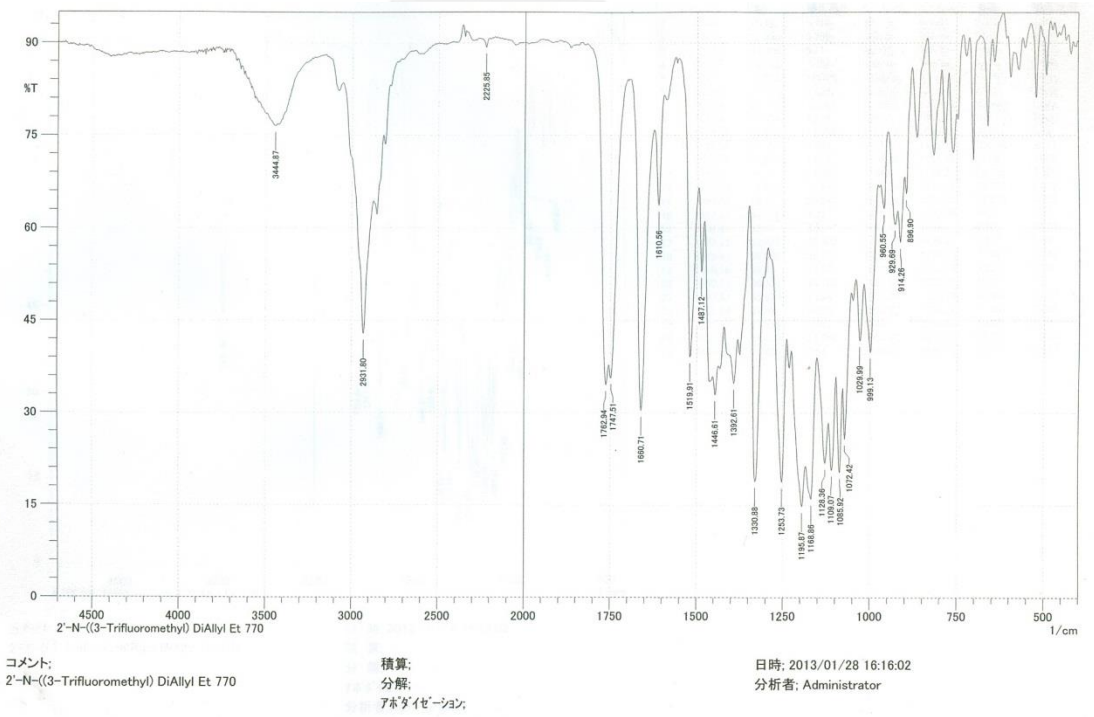

Figure 60. The IR spectrum (in KBr) of 18,6'-*O*-bisallyl-2'-*N*-(3''-trifluoromethylbenzoyl) Et 770.

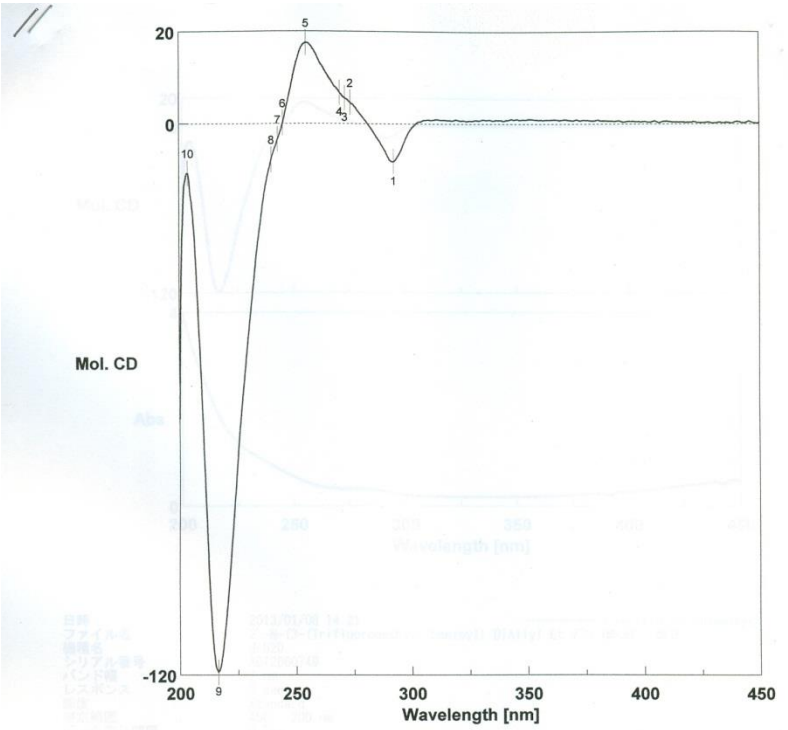

日時 2013/01/08 14:21
測定者 Nanae Mori
ファイル名 2'-N-(3-(Trifluoromethyl) benzoyl) DiAllyl Et 770 (MeOH) 修正
試料名 2'-N-(3-(Trifluoromethyl) benzoyl) DiAllyl Et 770 (MeOH)
コメント

No.	nm	Mol. CD	No.	nm	Mol. CD	No.	nm	Mol. CD
1	292	-8.23857	2	274	4.60315	3	271	5.57649
4	269	6.76375	5	255	17.6011	6	245	0.214413
7	242	-3.32081	8	240	-7.7357	9	216	-119.377
10	204	-10.6866						

Figure 61. The CD spectrum of 18,6'-*O*-bisallyl-2'-*N*-(3''-trifluoromethylbenzoyl) Et 770.

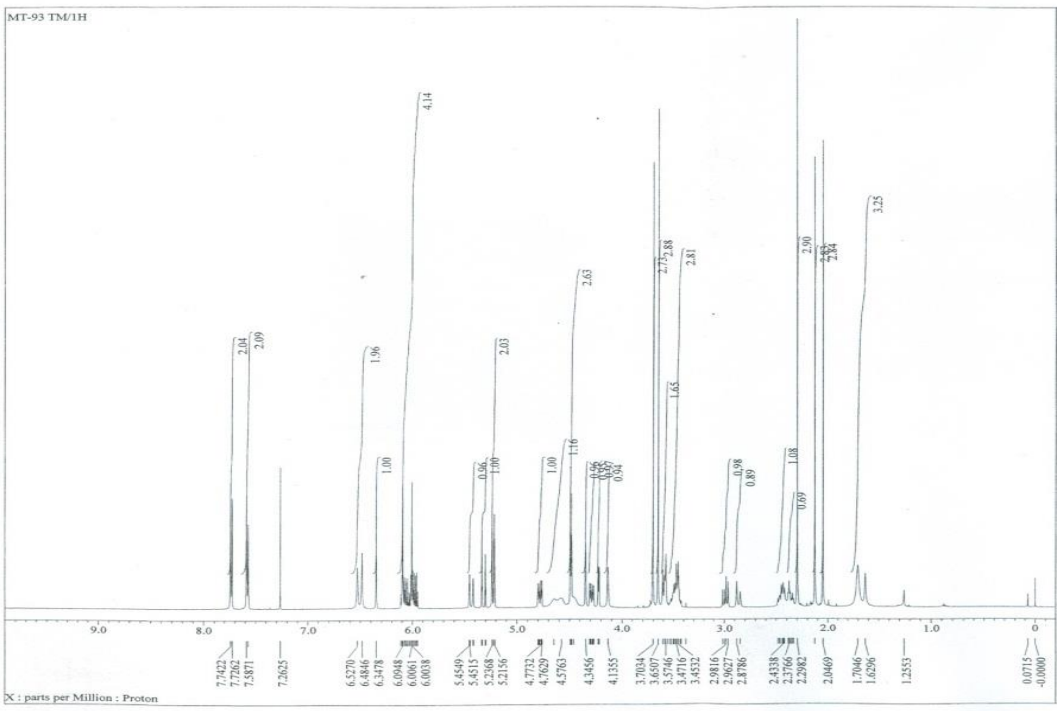

Figure 62. ^{1}H-NMR spectrum of 18,6'-*O*-bisallyl-2'-*N*-(4''-trifluoromethylbenzoyl) Et 770 (500 MHz, $CDCl_3$).

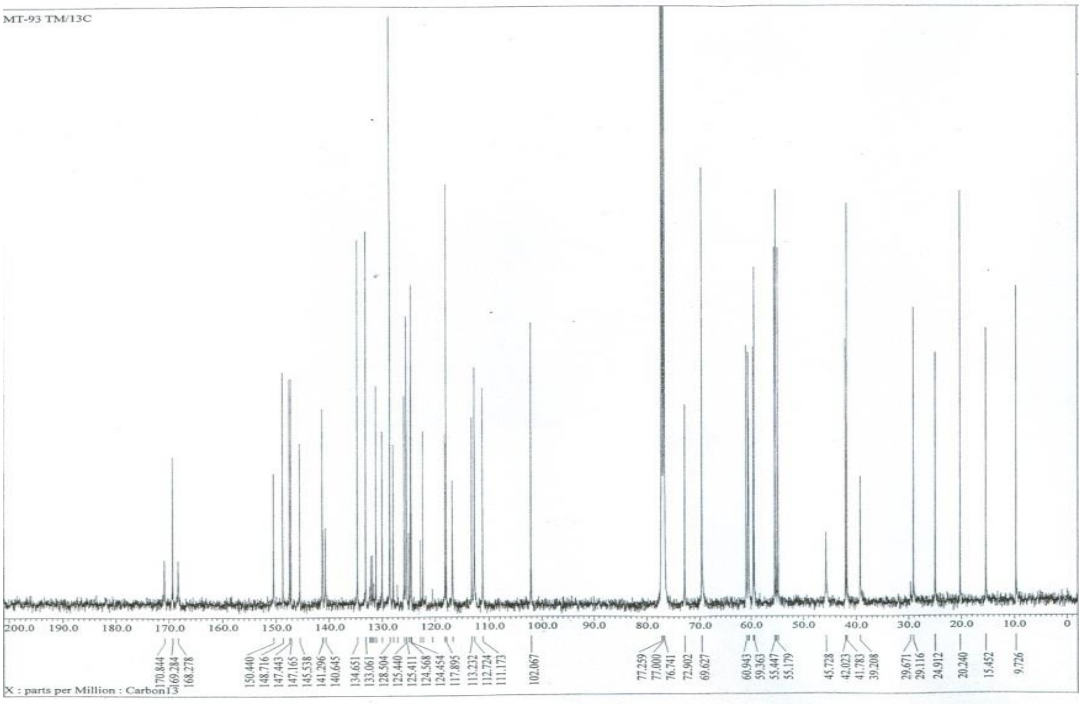

Figure 63. The ^{13}C-NMR spectrum of 18,6'-*O*-bisallyl-2'-*N*-(4''-trifluoromethylbenzoyl) Et 770 (125 MHz, $CDCl_3$).

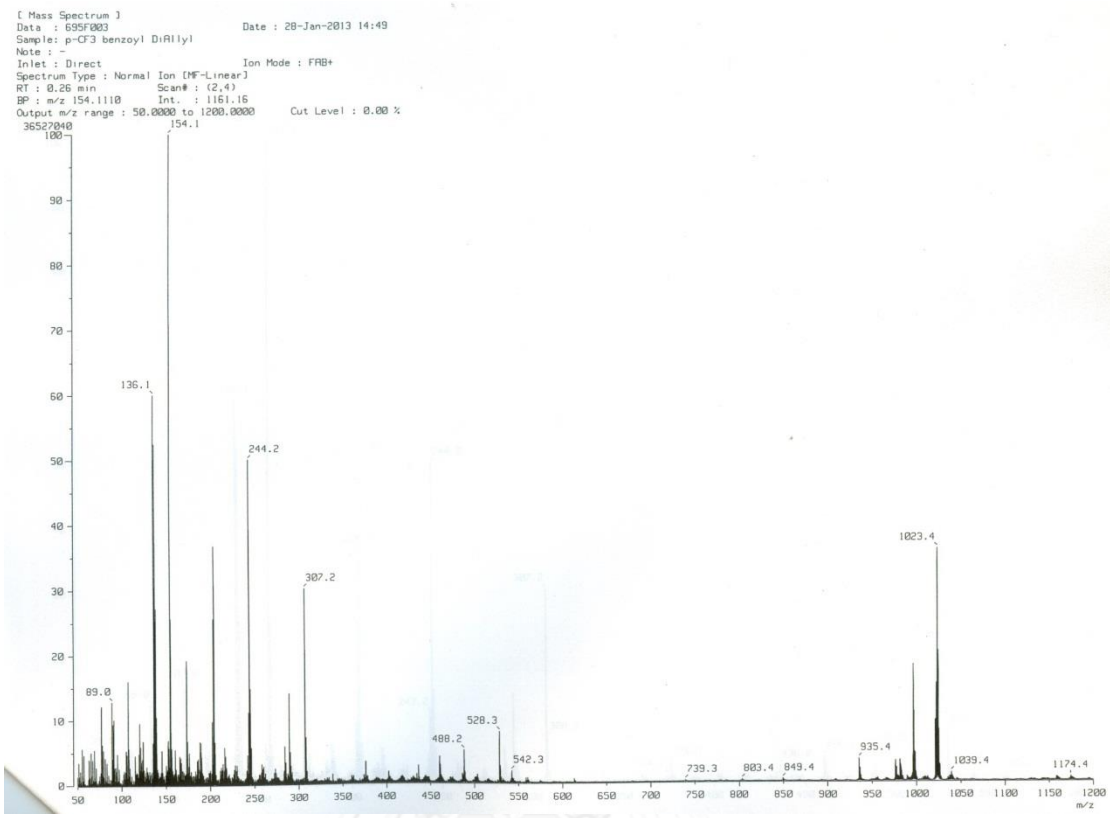

Figure 64. The FAB-Mass spectrum of 18,6'-*O*-bisallyl-2'-*N*-(4''-trifluoromethylbenzoyl) Et 770.

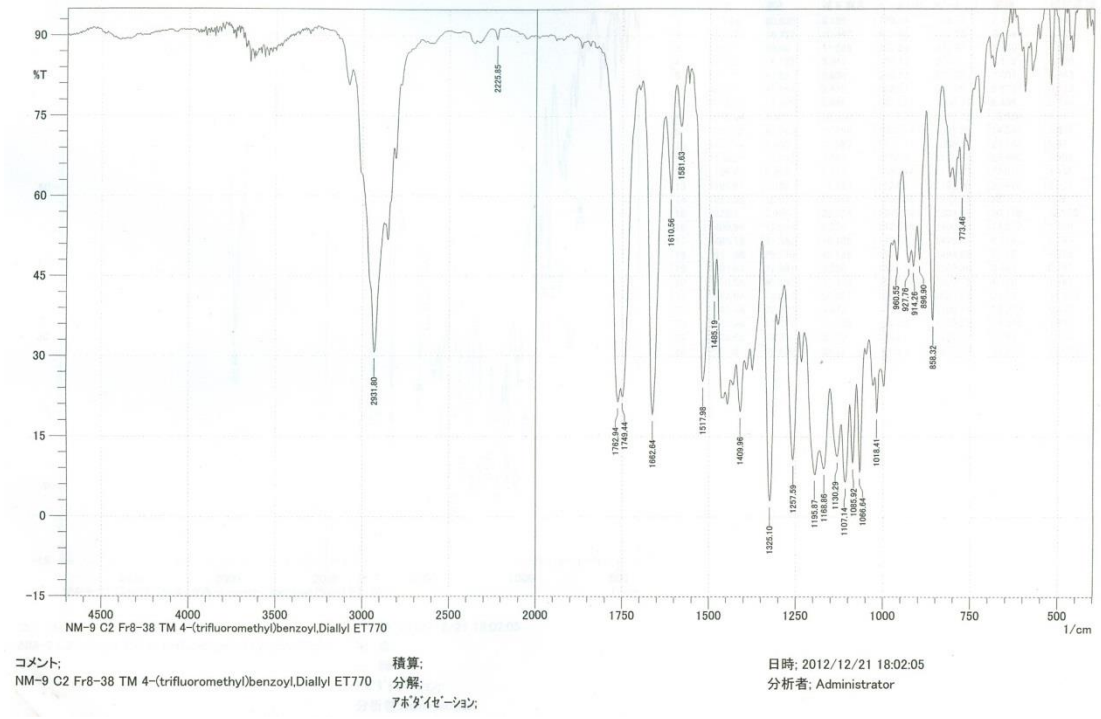

Figure 65. The IR spectrum (in KBr) of 18,6'-*O*-bisallyl-2'-*N*-(4''-trifluoromethylbenzoyl) Et 770.

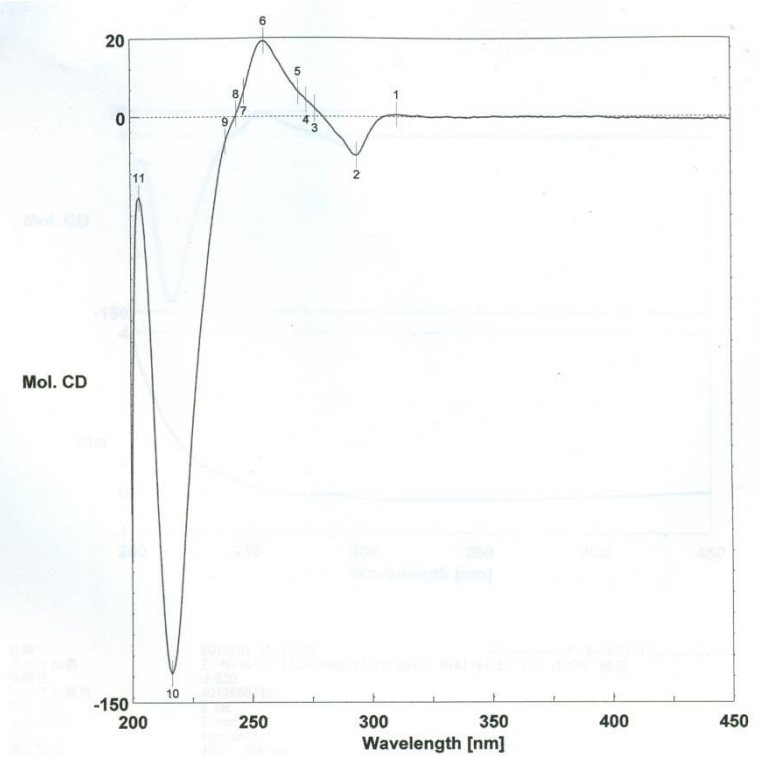

日時	2013/01/29 12:26
測定者	Tsujimoto
ファイル名	2'-N-(4-Trifluoromethyl benzoyl) DiAllyl Et 770 (MeOH) 修正
試料名	2'-N-(Trifluoromethyl benzoyl) DiAllyl Et 770 (MeOH)
コメント	2'-N-(Trifluoromethyl benzoyl) DiAllyl Et 770 (MeOH)

No.	nm	Mol. CD	No.	nm	Mol. CD	No.	nm	Mol. CD
1	311	0.495308	2	294	-9.8194	3	277	2.09278
4	273	4.18858	5	270	6.38244	6	256	19.2691
7	247	6.43987	8	244	0.650946	9	240	-6.42038
10	216	-142.531	11	204	-20.5588			

Figure 66. The CD spectrum of 18,6'-*O*-bisallyl-2'-*N*-(4''-trifluoromethylbenzoyl) Et 770.

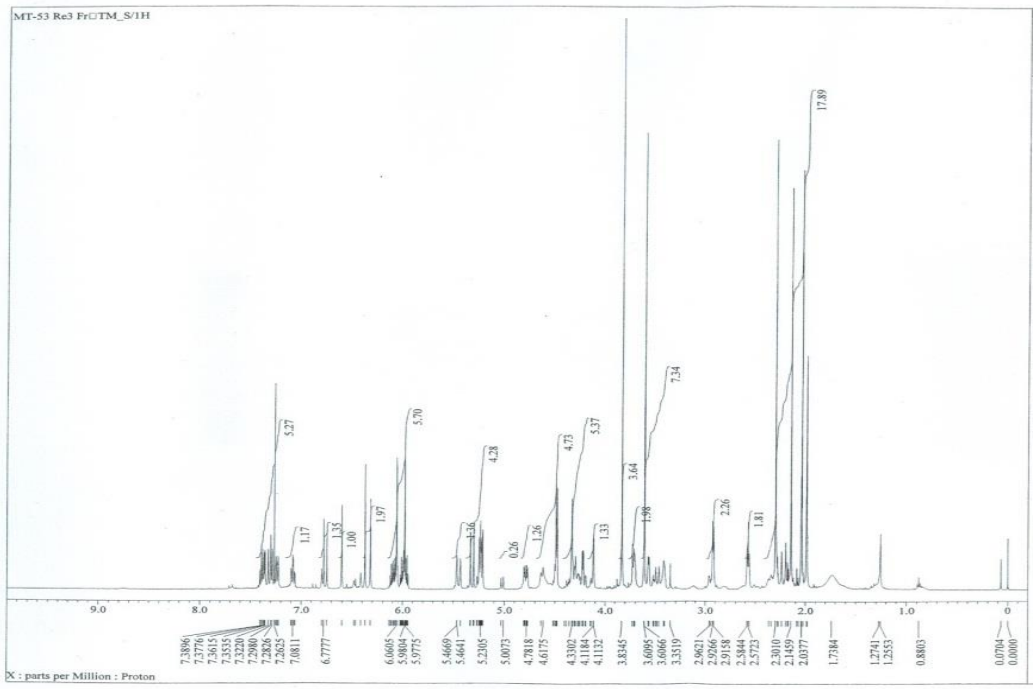

Figure 67. The ^{1}H-NMR spectrum of 18,6'-*O*-bisallyl-2'-*N*-(3"-fluorocinnamoyl) Et 770 (500 MHz, $CDCl_3$).

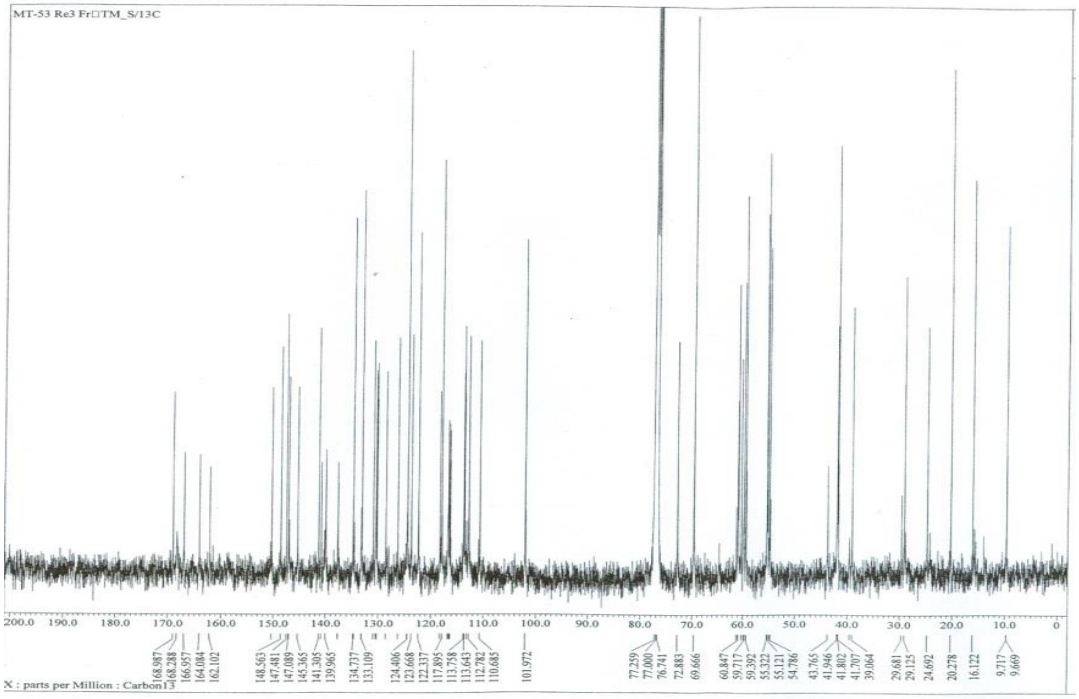

Figure 68. The ^{13}C-NMR spectrum of 18,6'-*O*-bisallyl-2'-*N*-(3"-fluorocinnamoyl) Et 770 (125 MHz, $CDCl_3$).

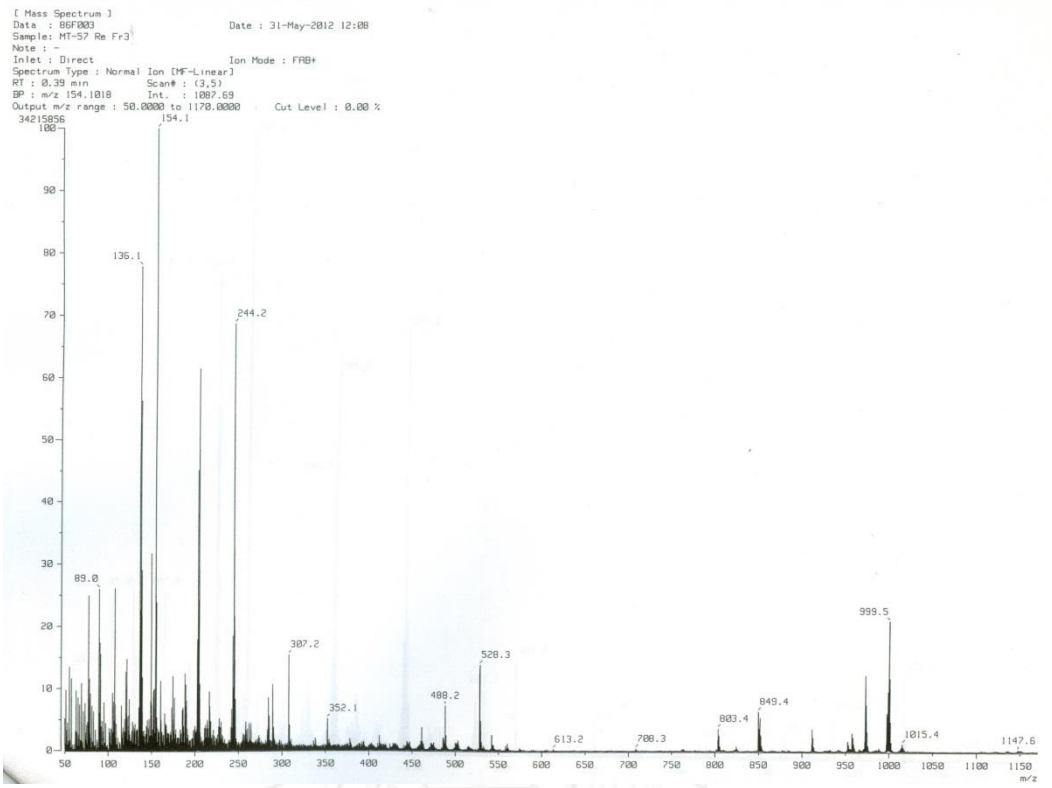

Figure 69. The FAB-Mass spectrum of 18,6'-*O*-bisallyl-2'-*N*-(3''-fluorocinnamoyl) Et 770.

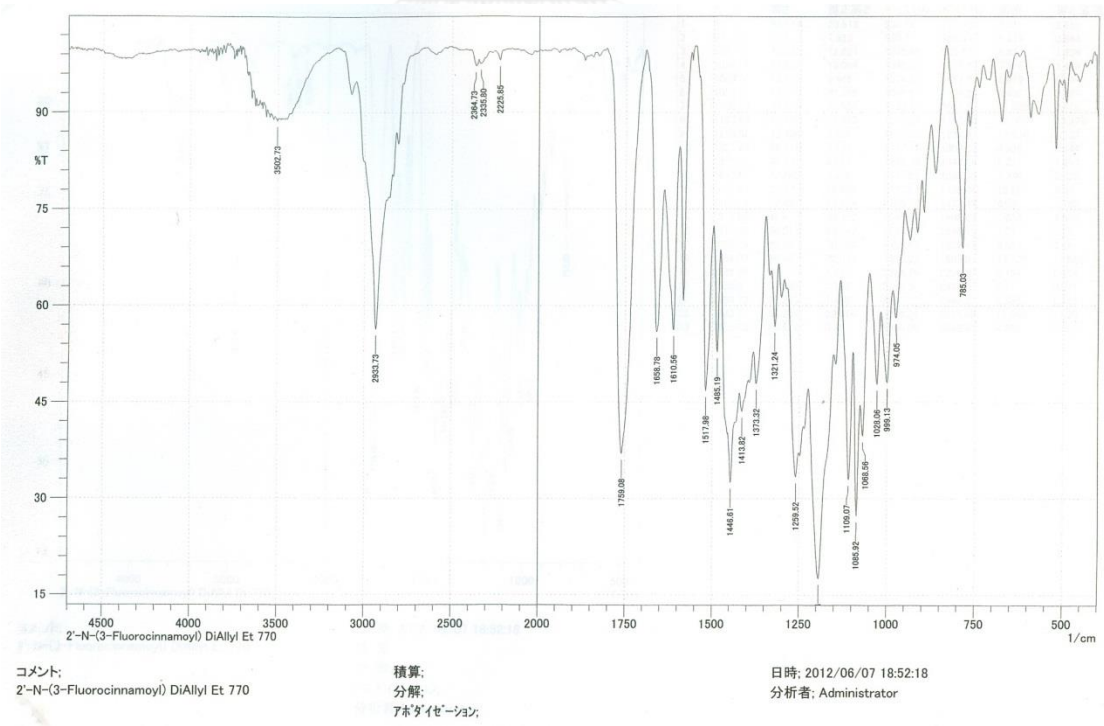

Figure 70. The IR spectrum (in KBr) of 18,6'-*O*-bisallyl-2'-*N*-(3''-fluorocinnamoyl) Et 770.

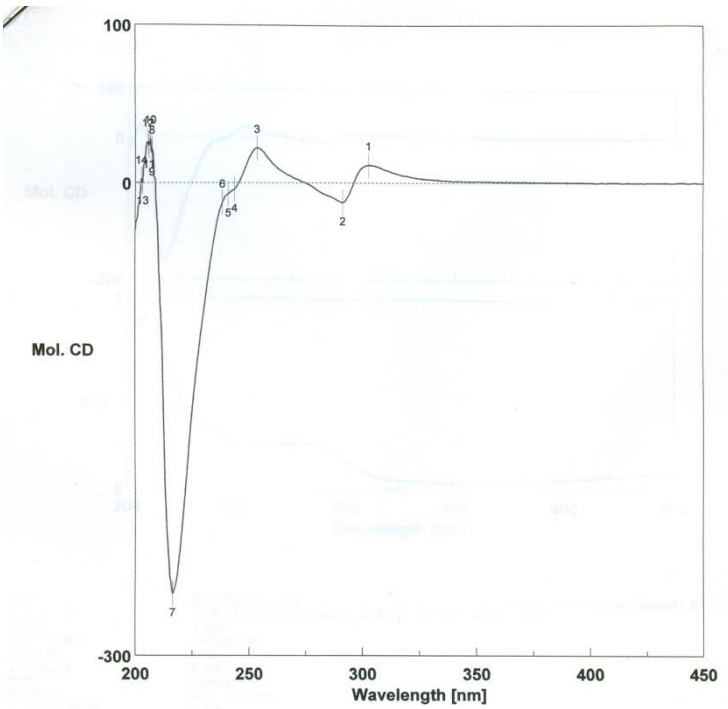

日時 2012/06/08 12:34
測定者 Tsujimoto
ファイル名 2'-N-(3-Fluorocinnamoyl) DiAllyl Et 770 (MeOH) 修正
試料名 2'-N-(3-Fluorocinnamoyl) DiAllyl Et 770 (MeOH)
コメント 2'-N-(3-Fluorocinnamoyl) DiAllyl Et 770 (MeOH)

No.	nm	Mol. CD	No.	nm	Mol. CD	No.	nm	Mol. CD
1	303	11.2789	2	291	-12.6002	3	254	22.1084
4	244	-4.16312	5	241	-7.11845	6	238	-12.6347
7	216	-260.556	8	207	21.2256	9	207	18.8012
10	207	27.7598	11	206	23.6356	12	206	25.8412
13	203	0.578141	14	203	2.28287			

Figure 71. The CD spectrum of 18,6'-*O*-bisallyl-2'-*N*-(3"-fluorocinnamoyl) Et 770.

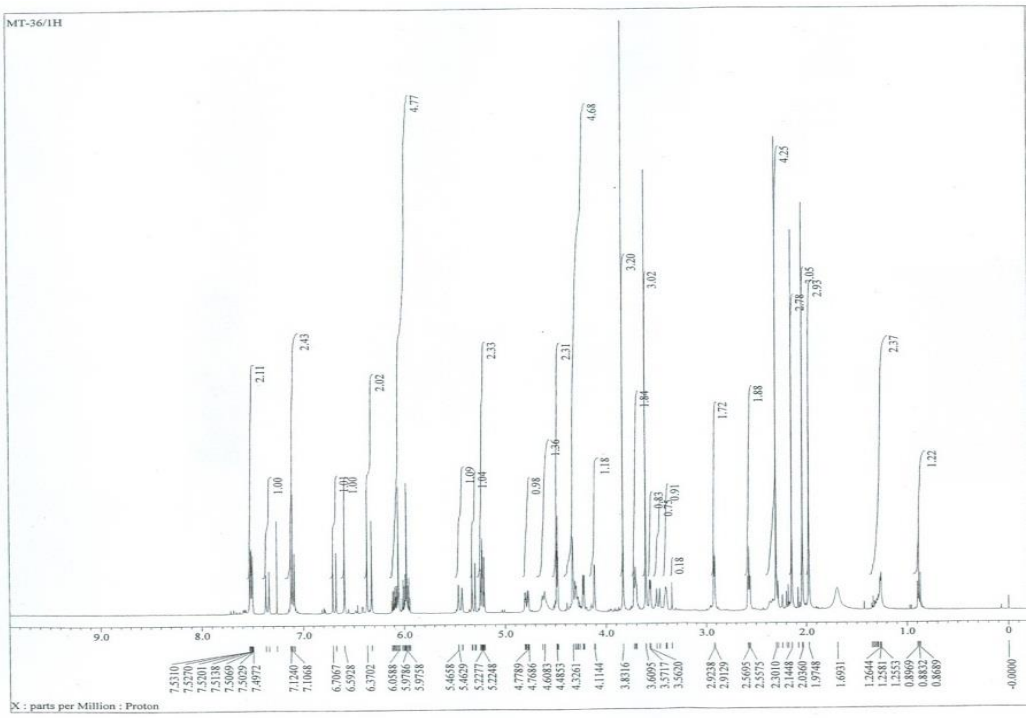

Figure 72. The ^{1}H-NMR spectrum of 18,6'-*O*-bisallyl-2'-*N*-(4''-fluorocinnamoyl) Et 770 (500 MHz, $CDCl_3$).

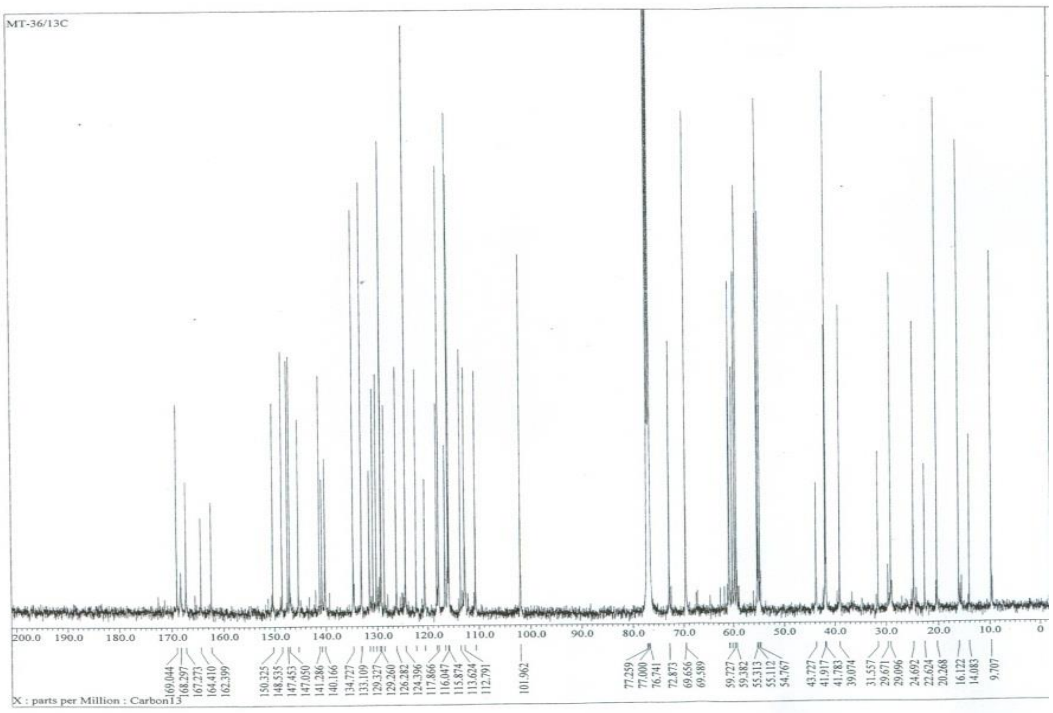

Figure 73. The ^{13}C-NMR spectrum of 18,6'-*O*-bisallyl-2'-*N*-(4''-fluorocinnamoyl) Et 770 (125 MHz, $CDCl_3$).

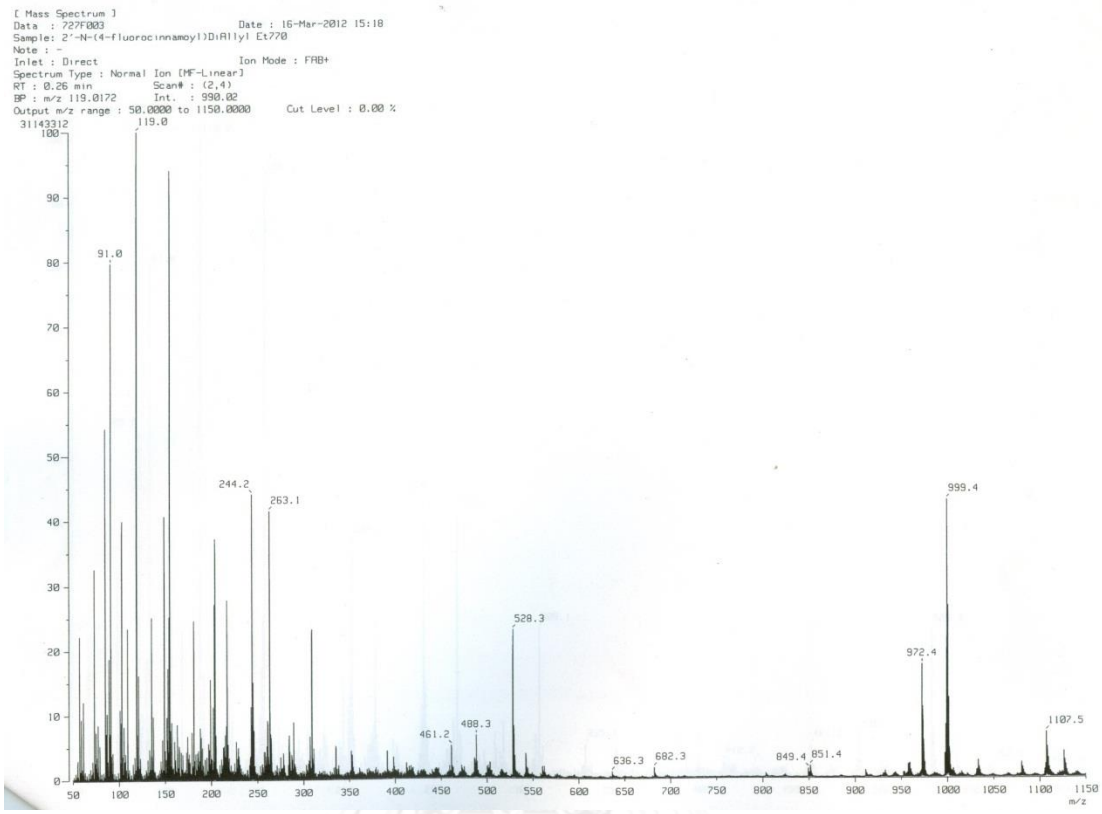

Figure 74. The FAB-Mass spectrum of 18,6'-*O*-bisallyl-2'-*N*-(4''-fluorocinnamoyl) Et 770.

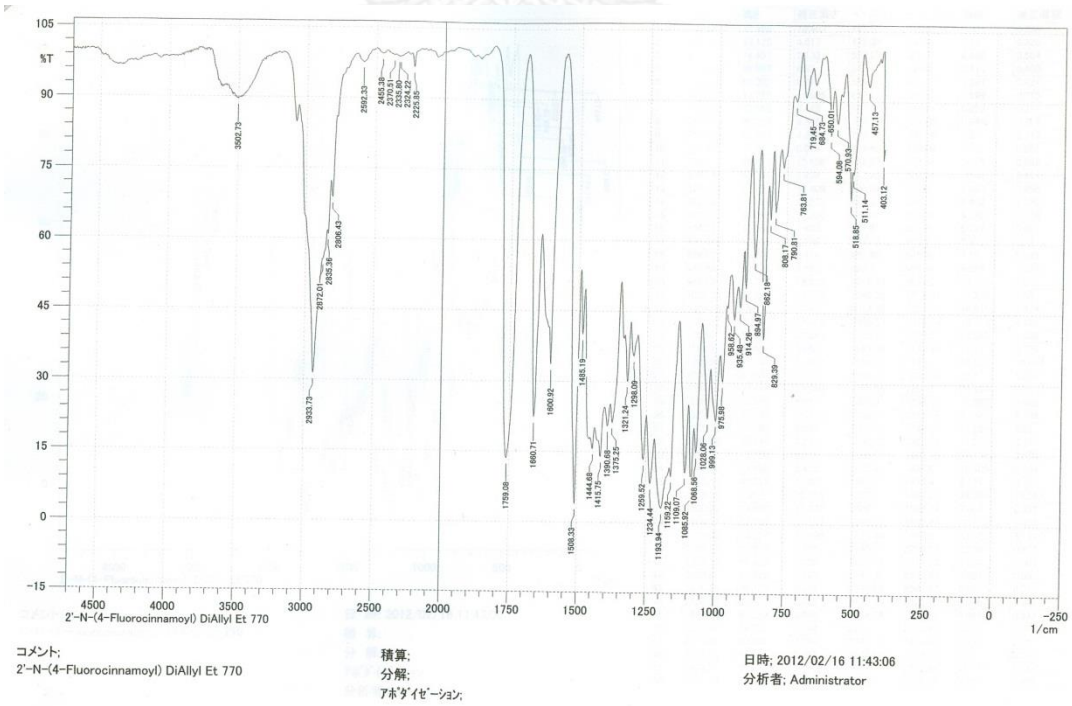

Figure 75. The IR spectrum (in KBr) of 18,6'-*O*-bisallyl-2'-*N*-(4''-fluorocinnamoyl) Et 770.

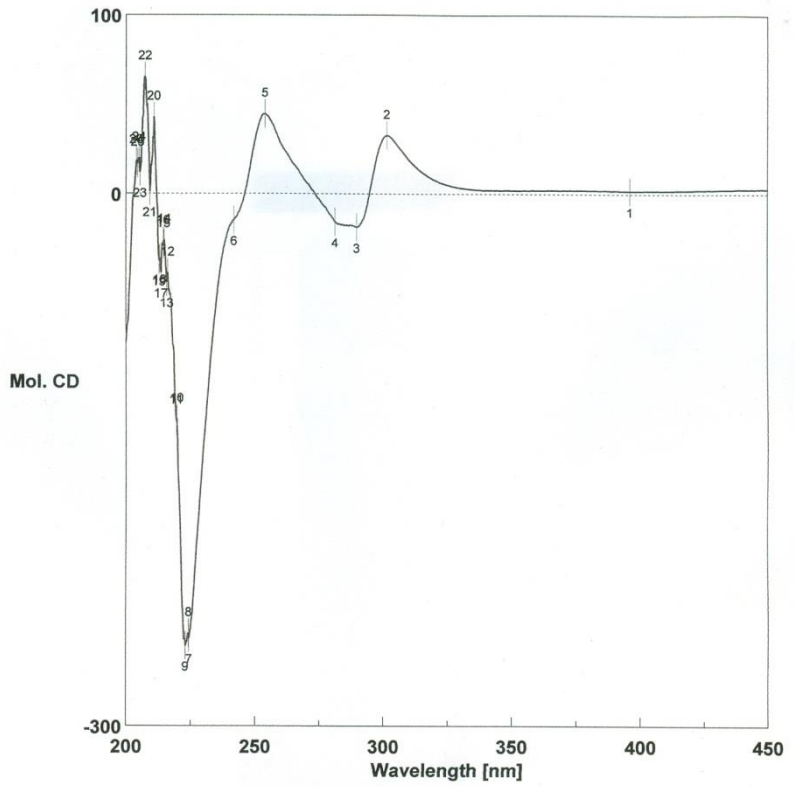

日時 2012/03/08 12:20
測定者 Tsujimoto
ファイル名 2'-N-(4-Fluorocinnamoyl) DiAllyl Et 770 (Methanol) 修正後
試料名 2'-N-(4-Fluorocinnamoyl) DiAllyl Et 770 (Methanol)
コメント 2'-N-(4-Fluorocinnamoyl) DiAllyl Et 770

No.	nm	Mol. CD	No.	nm	Mol. CD	No.	nm	Mol. CD
1	396	1.63976	2	302	32.5784	3	290	-18.9404
4	281	-15.9044	5	254	44.5852	6	242	-14.8204
7	224	-250.373	8	224	-247.511	9	223	-254.576
10	220	-126.678	11	220	-127.747	12	216	-44.5405
13	216	-49.6743	14	215	-26.1101	15	215	-28.6528
16	214	-26.9494	17	214	-44.1248	18	213	-36.4543
19	213	-37.587	20	211	42.8145	21	209	1.27106
22	207	65.3929	23	205	12.0762	24	205	19.9091
25	204	16.9367	26	204	18.4269			

Figure 76. The CD spectrum of 18,6'-*O*-bisallyl-2'-*N*-(4"-fluorocinnamoyl) Et 770.

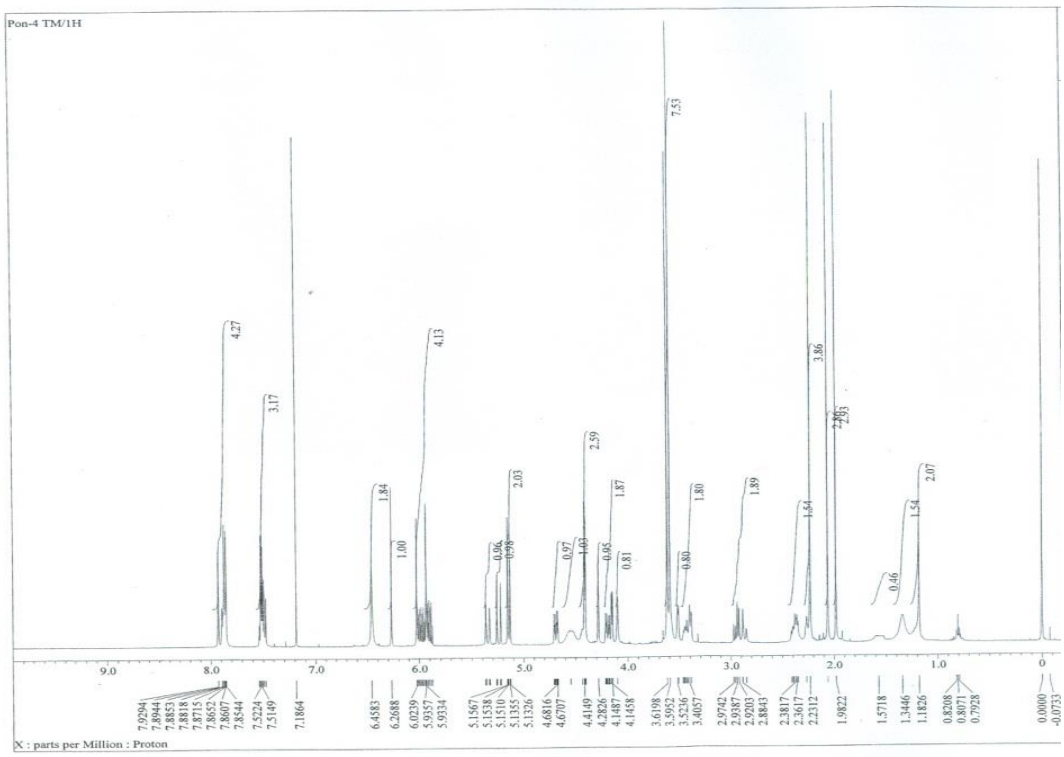

Figure 77. The ^{1}H-NMR spectrum of 18,6'-*O*-bisallyl-2'-*N*-(2''-naphthoyl) Et 770 (500 MHz, $CDCl_3$).

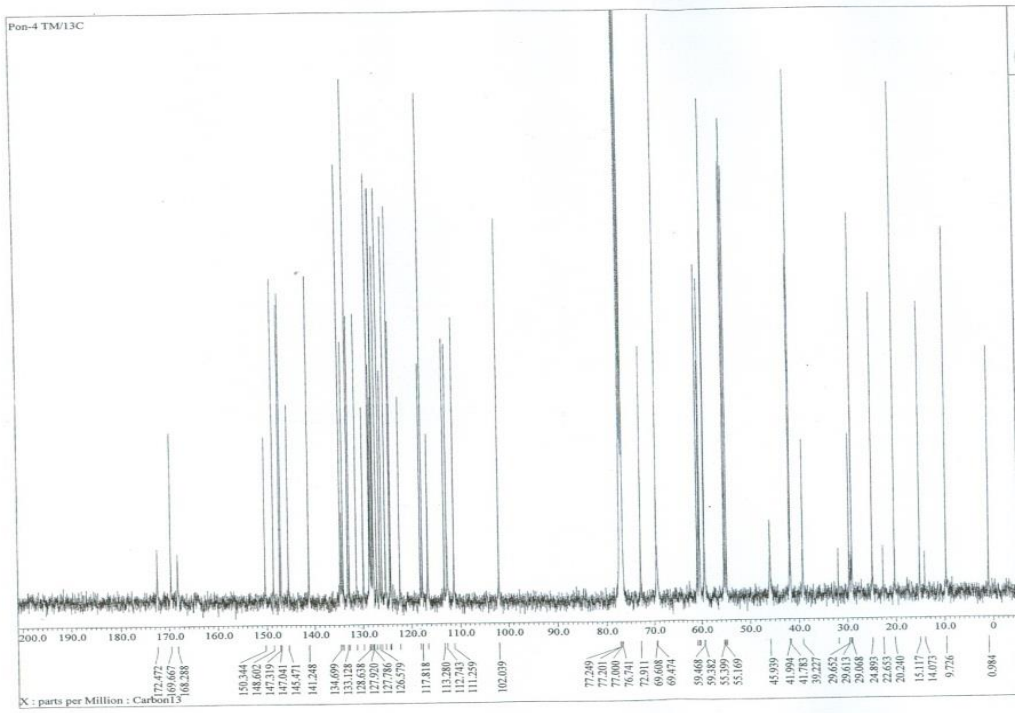

Figure 78. The ^{13}C-NMR spectrum of 18,6'-*O*-bisallyl-2'-*N*-(2''-naphthoyl) Et 770 (125 MHz, $CDCl_3$).

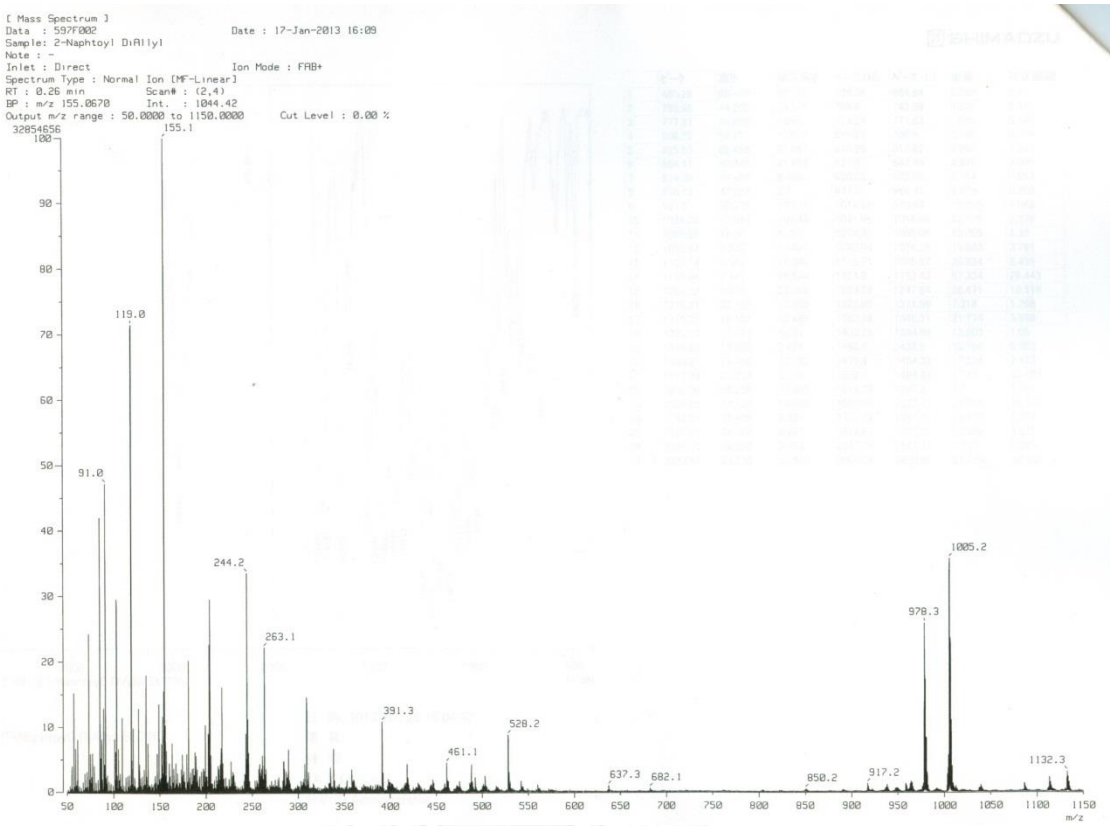

Figure 79. The FAB-Mass spectrum of 18,6'-*O*-bisallyl-2'-*N*-(2"-naphthoyl) Et 770.

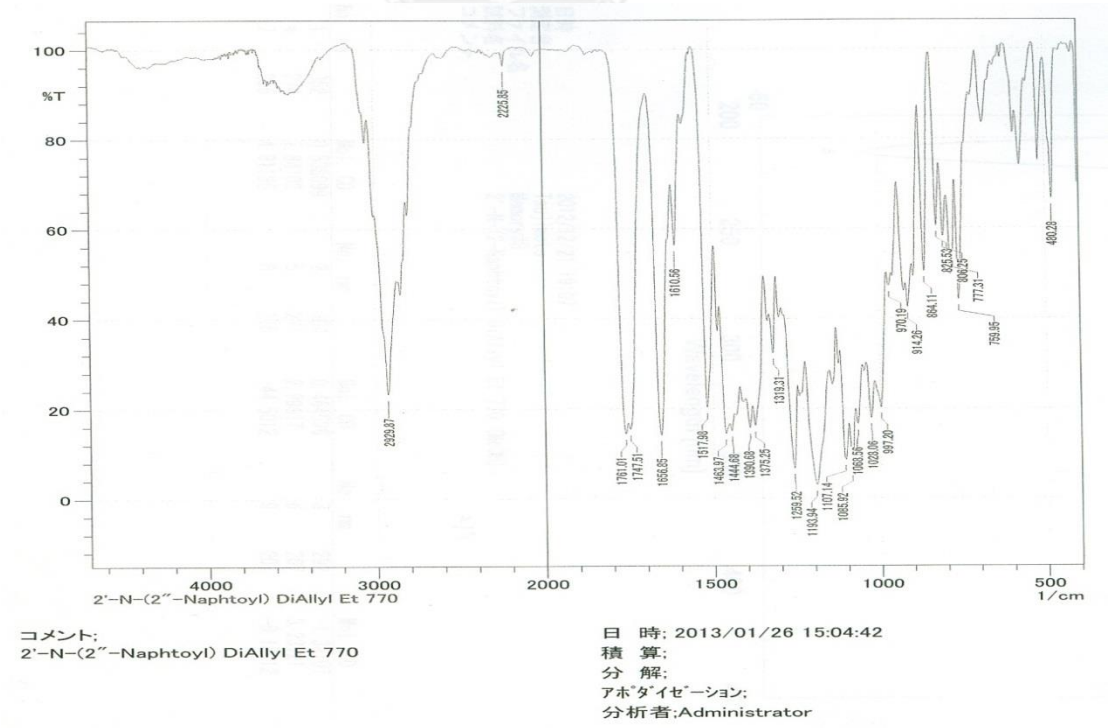

Figure 80. The IR spectrum (in KBr) of 18,6'-*O*-bisallyl-2'-*N*-(2"-naphthoyl) Et 770.

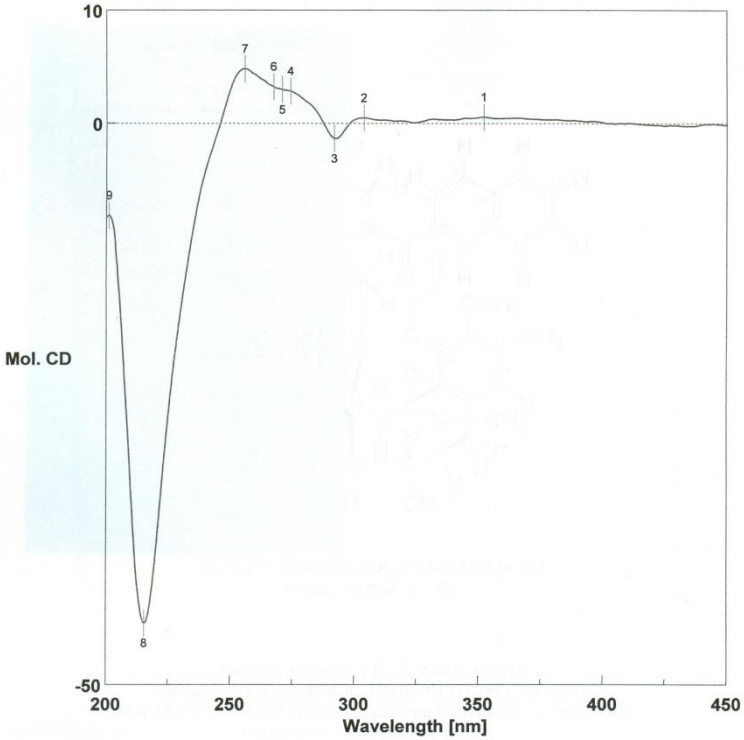

日時 2012/12/21 19:07
測定者 Tsujimoto
ファイル名 Memory#8
試料名 2'-N-(2-Naphtoyl) DiAllyl Et 770 (MeOH)
コメント 23°c

No.	nm	Mol. CD	No.	nm	Mol. CD	No.	nm	Mol. CD
1	352	0.538099	2	304	0.464596	3	292	-1.35107
4	274	2.84102	5	271	2.99617	6	267	3.23721
7	256	4.81186	8	215	-44.5012	9	201	-8.18012

Figure 81. The CD spectrum of 18,6'-*O*-bisallyl-2'-*N*-(2''-naphthoyl) Et 770.

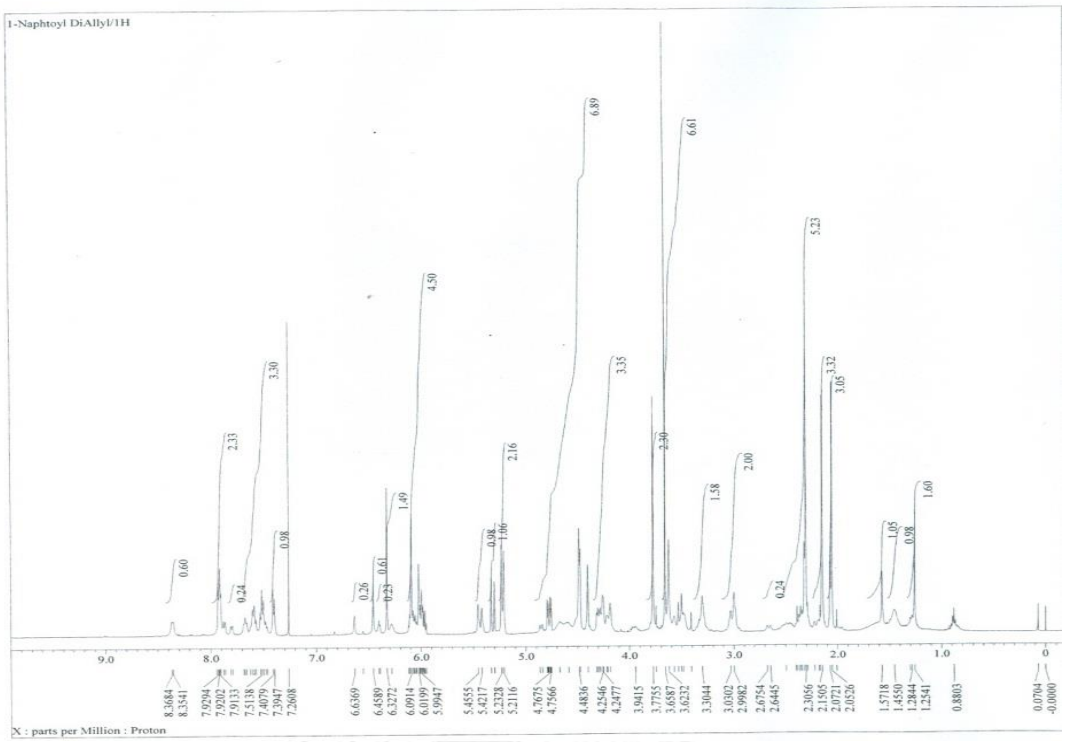

Figure 82. The ^{1}H-NMR spectrum of 18,6'-*O*-bisallyl-2'-*N*-(1''-naphthoyl) Et 770 (500 MHz, $CDCl_3$).

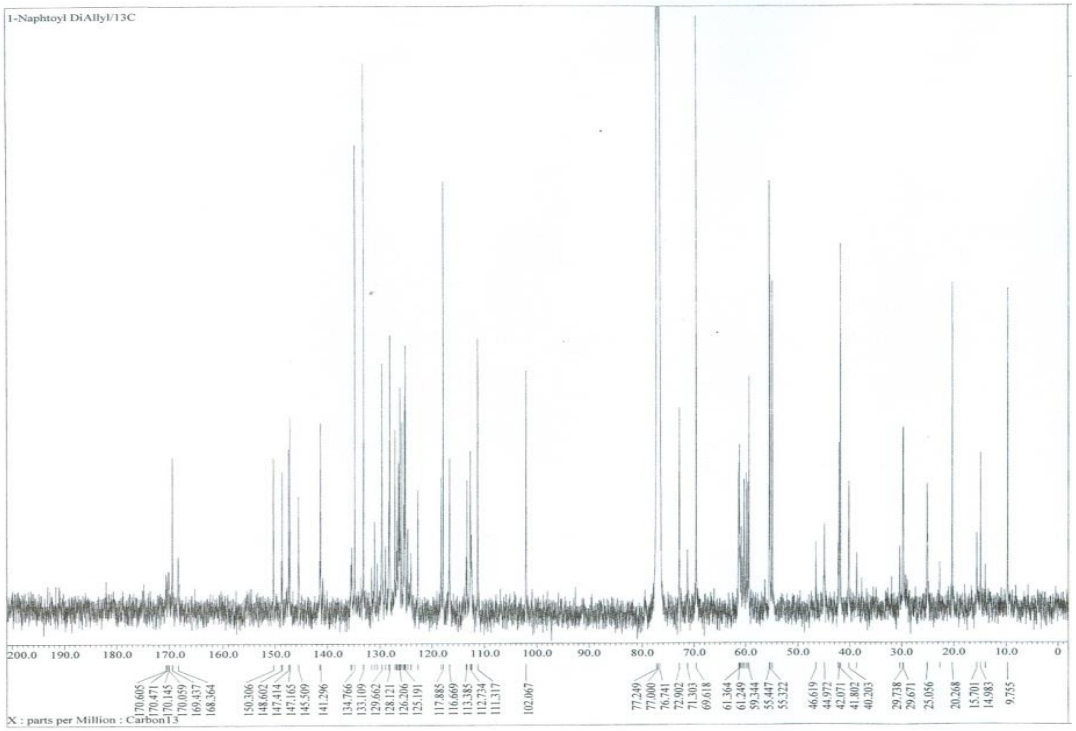

Figure 83. The ^{13}C-NMR spectrum of 18,6'-*O*-bisallyl-2'-*N*-(1''-naphthoyl) Et 770 (125 MHz, $CDCl_3$).

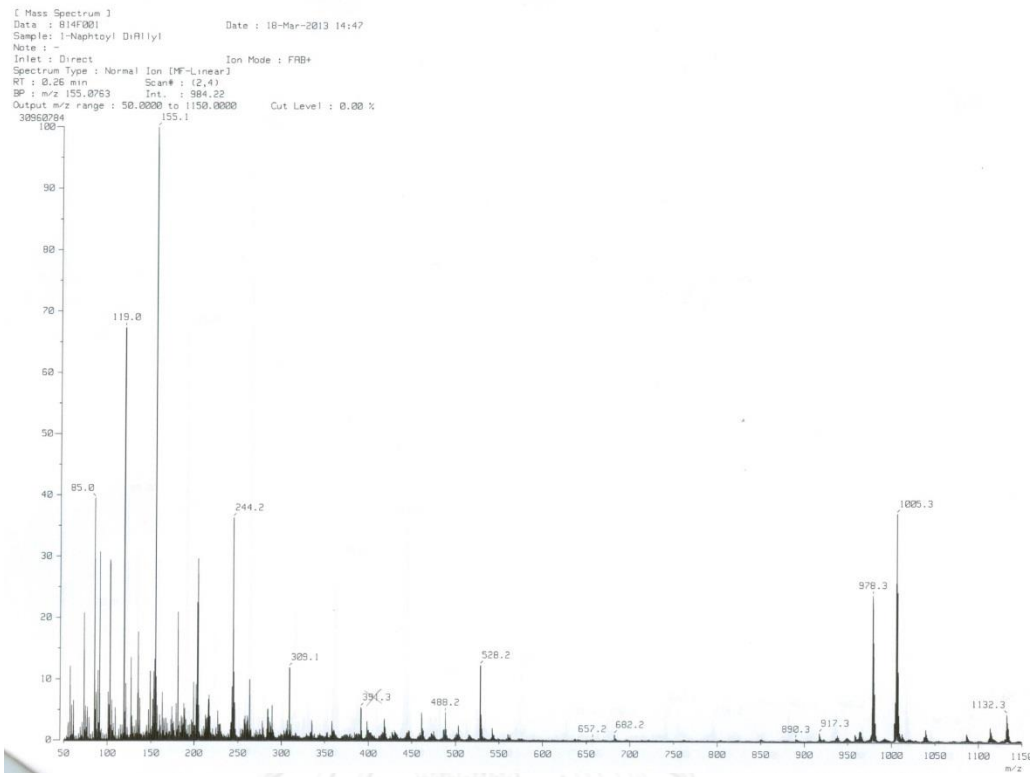

Figure 84. The FAB-Mass spectrum of 18,6'-*O*-bisallyl-2'-*N*-(1"-naphthoyl) Et 770.

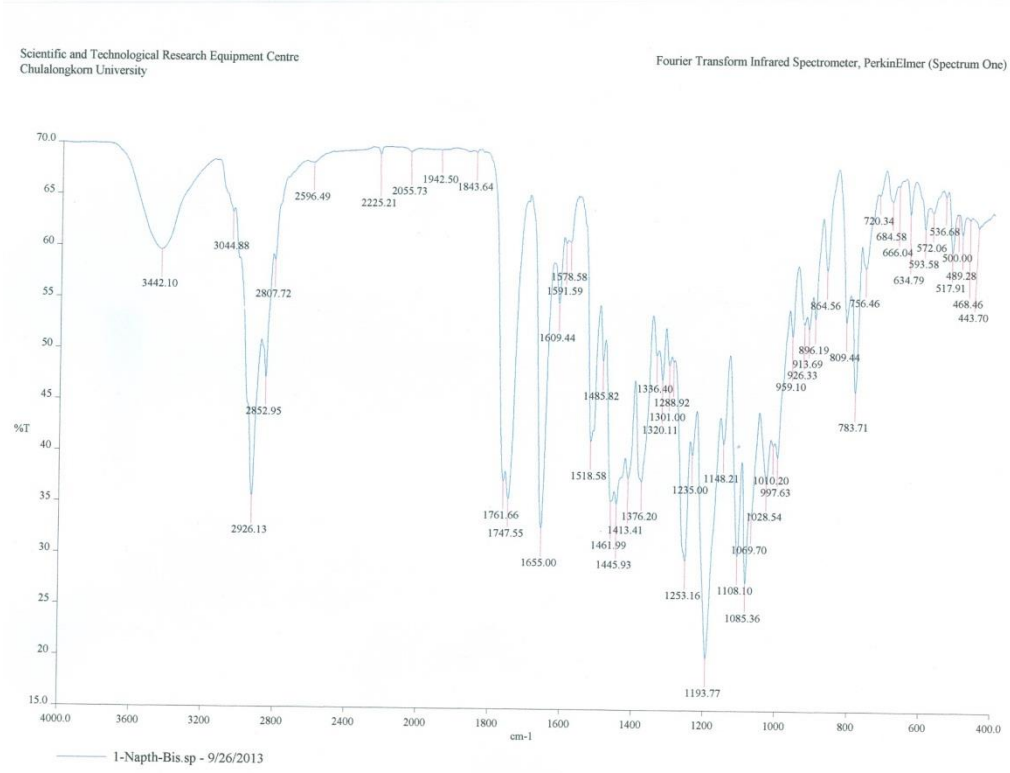

Figure 85. The IR spectrum (in KBr) of 18,6'-*O*-bisallyl-2'-*N*-(1"-naphthoyl) Et 770.

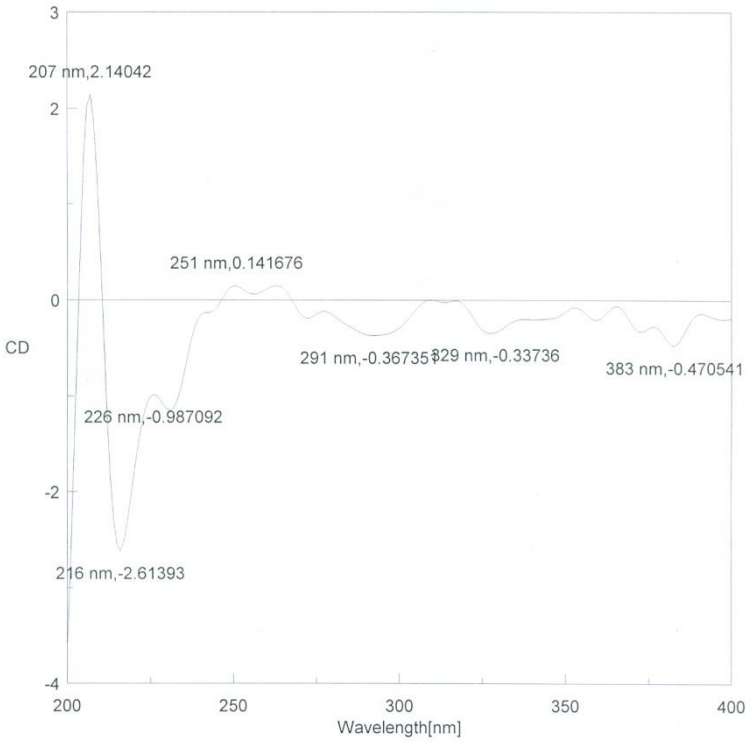

File Name :	1napbis.jws		
Date :	19/09/2013 2:56PM [19/09/2013 2:28PM]		
Sample :	2'-N-1-Naptho-bisallyl ET770		
Cell Length :	0.1 cm		
Concentration :	1.6 mg		
Solvent :	MeOH		
Temperature :	22 C		
Operator :	Pon		
Organization :			
Comment :			
Data mode :	CD		
Ch2-mode :	HT		
Range :	400 - 200 nm		
Band width :	1.0 nm	Sensitivity :	100 mdeg
Resolution :	1 nm	Response :	1 sec
Accumulation :	5	Speed :	100 nm/min

Figure 86. The CD spectrum of 18,6'-*O*-bisallyl-2'-*N*-(1''-naphthoyl) Et 770.

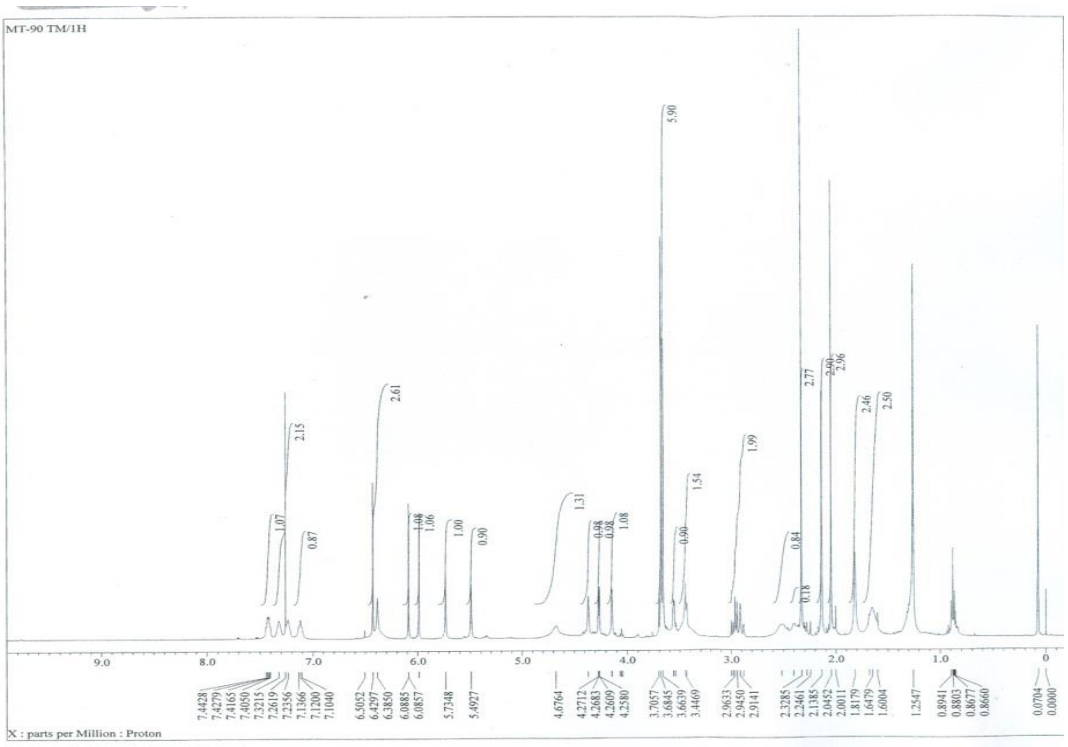

Figure 87. The ^{1}H-NMR spectrum of 2'-*N*-(2''-fluorobenzoyl) Et 770 (500 MHz, $CDCl_3$).

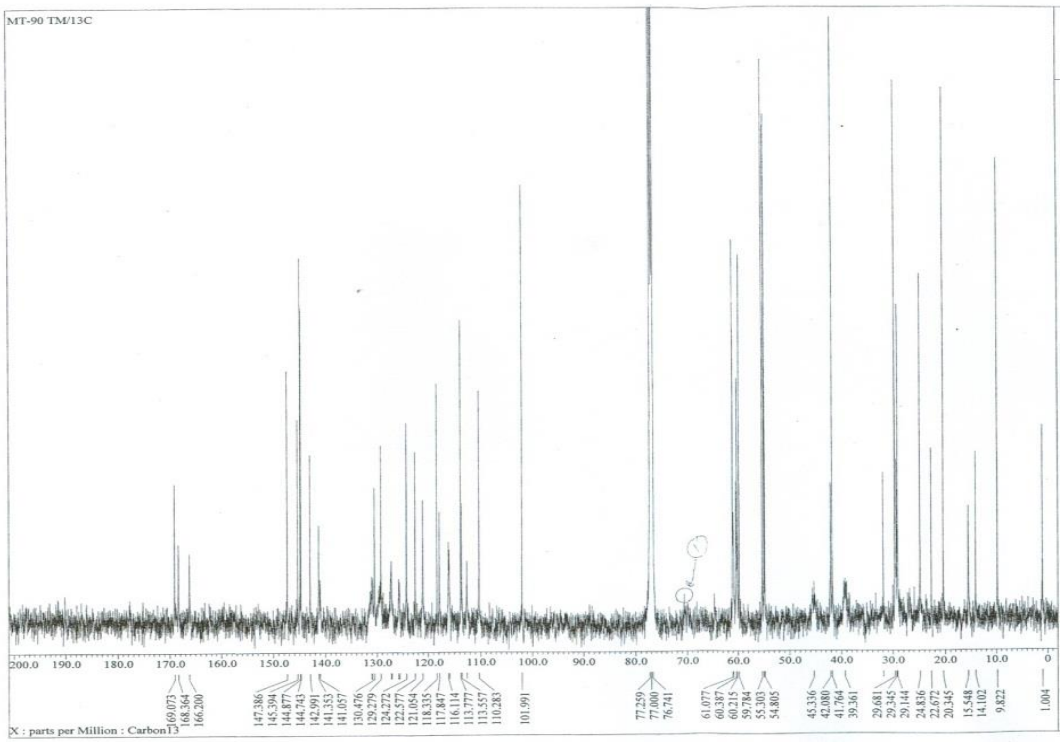

Figure 88. The ^{13}C-NMR spectrum of 2'-*N*-(2''-fluorobenzoyl) Et 770 (125 MHz, $CDCl_3$).

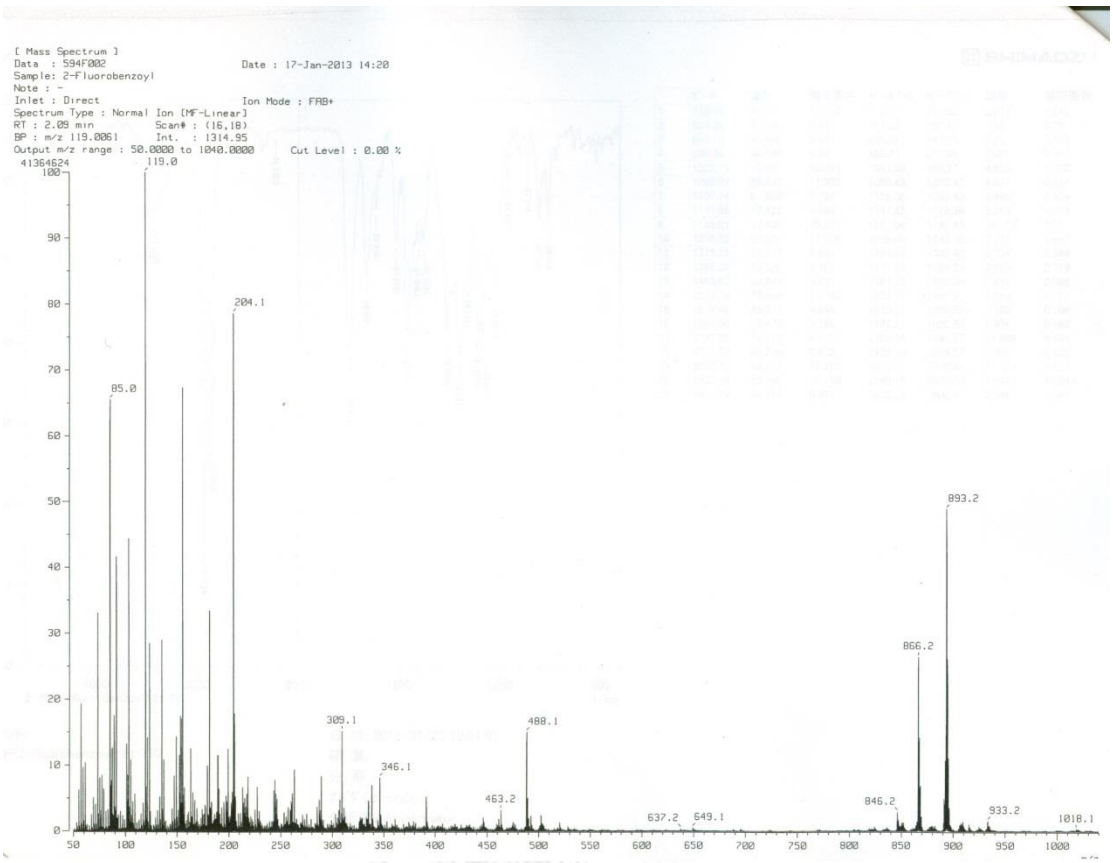

Figure 89. The FAB-Mass spectrum of 2'-*N*-(2''-fluorobenzoyl) Et 770.

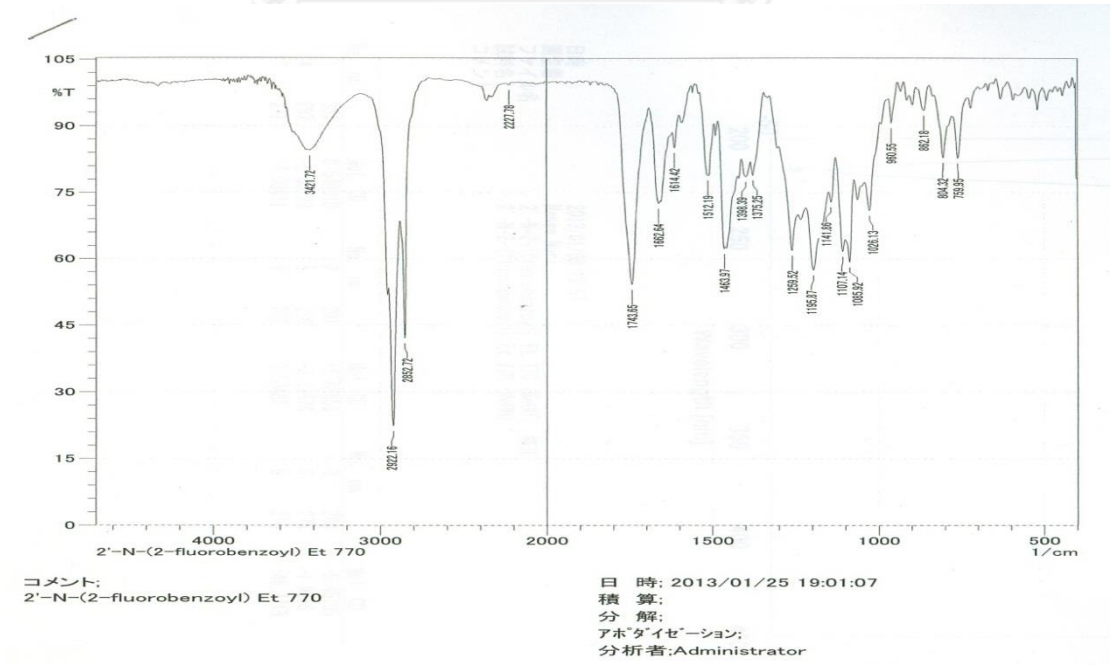

Figure 90. The IR spectrum (in KBr) of 2'-*N*-(2''-fluorobenzoyl) Et 770.

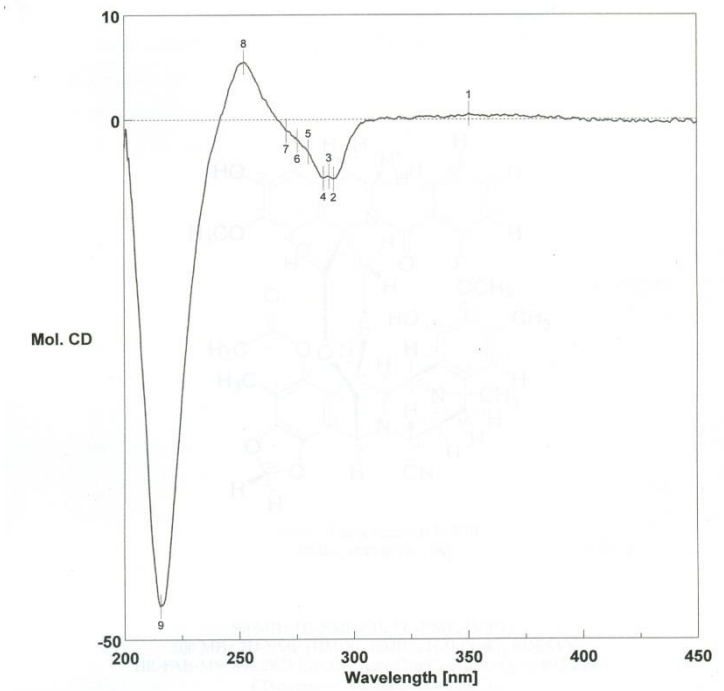

日時 2013/01/08 19:57
測定者 Nanae Mori
ファイル名 2'-N-2-(fluorobenzoyl) Et 770 (MeOH) 修正
試料名 2'-N-2-(fluorobenzoyl) Et 770 (MeOH)
コメント

No.	nm	Mol. CD	No.	nm	Mol. CD	No.	nm	Mol. CD
1	351	0.548018	2	291	-5.68653	3	289	-5.45705
4	287	-5.63229	5	280	-3.11576	6	276	-1.9816
7	271	-1.03611	8	252	5.50483	9	216	-46.7718

Figure 91. The CD spectrum of 2'-*N*-(2''-fluorobenzoyl) Et 770.

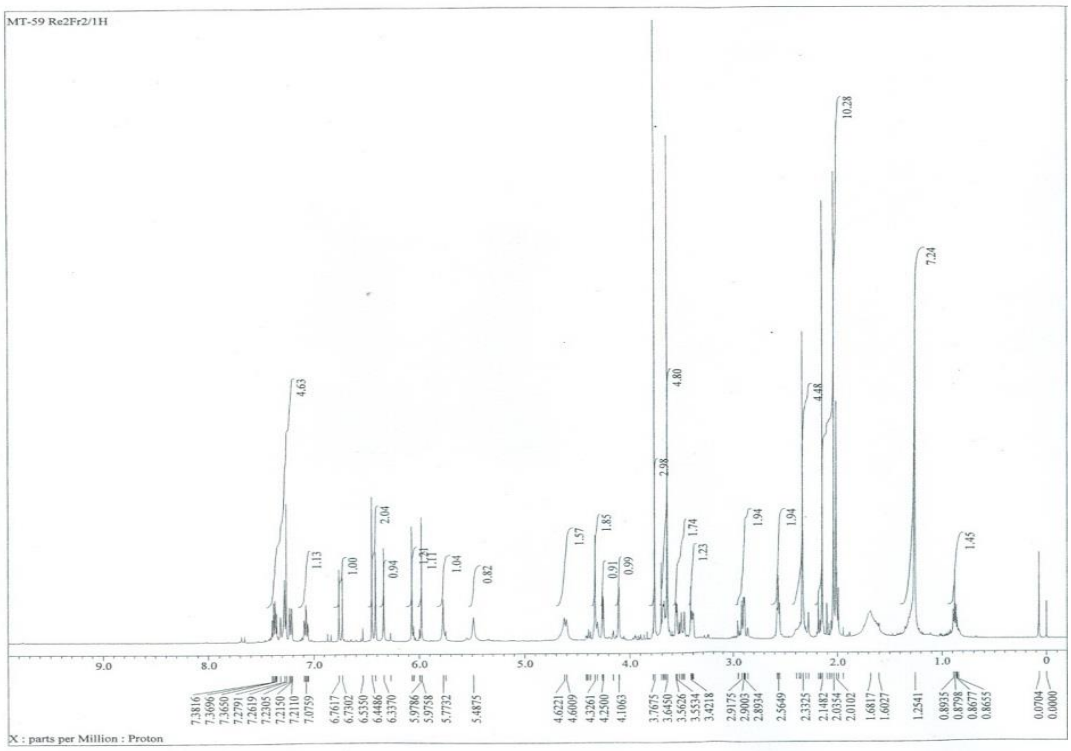

Figure 92. The ^{1}H-NMR spectrum of 2'-*N*-(3''-fluorobenzoyl) Et 770 (500 MHz, $CDCl_3$).

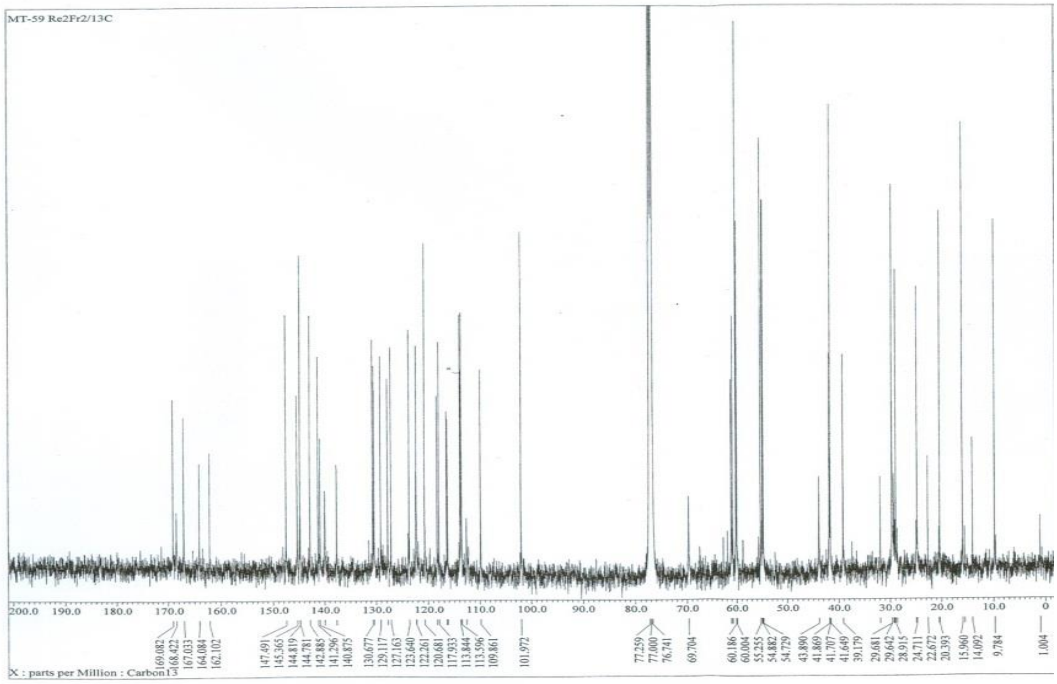

Figure 93. The ^{13}C-NMR spectrum of 2'-*N*-(3''-fluorobenzoyl) Et 770 (125 MHz, $CDCl_3$).

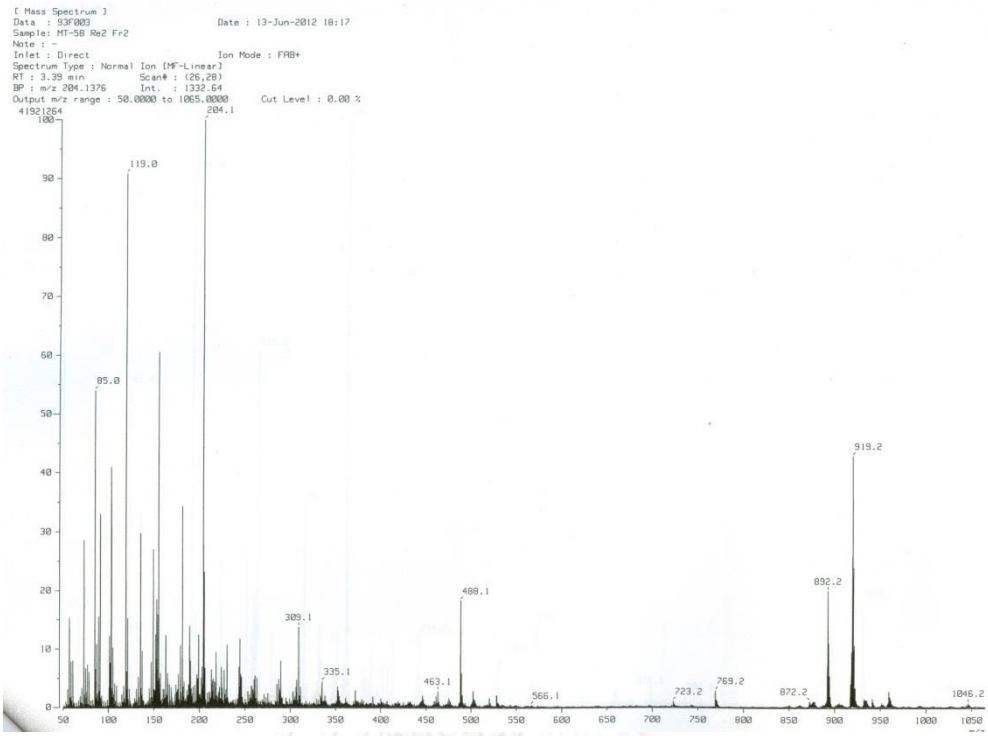

Figure 94. The FAB-Mass spectrum of 2'-*N*-(3''-fluorobenzoyl) Et 770.

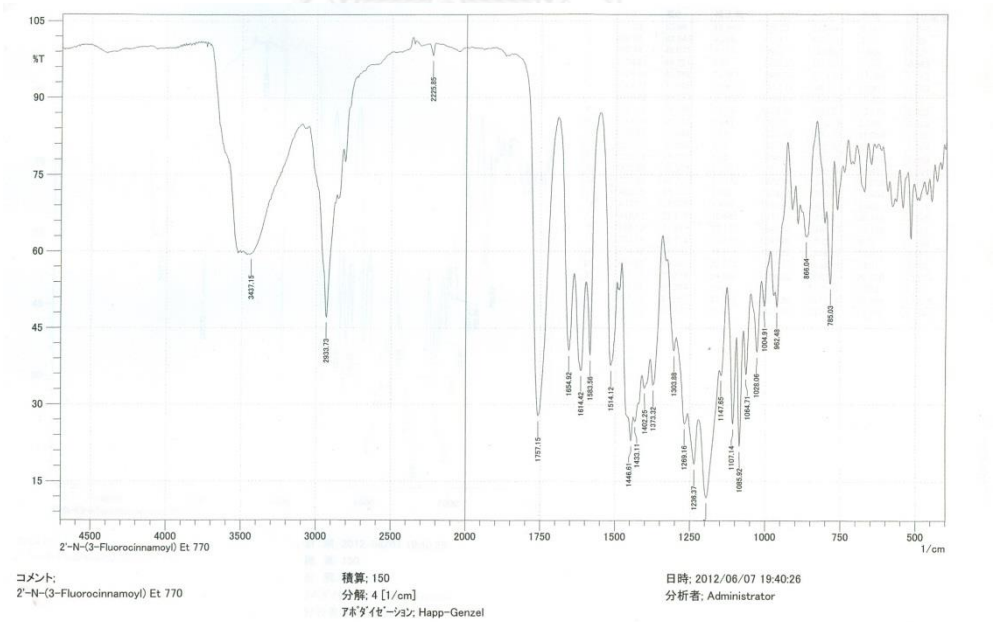

Figure 95. The IR spectrum (in KBr) of 2'-*N*-(3''-fluorobenzoyl) Et 770.

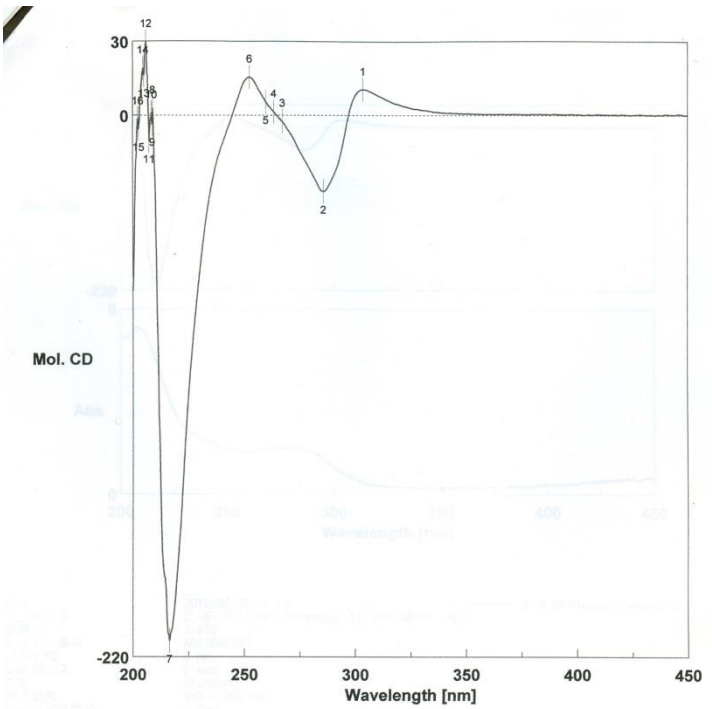

日時	2012/06/08 16:06
測定者	Tsujimoto
ファイル名	2'-N-(3-Fluorocinnamoyl) Et 770 (MeOH) 修正
試料名	2'-N-(3-Fluorocinnamoyl) Et 770 (MeOH)
コメント	2'-N-(3-Fluorocinnamoyl) Et 770 (MeOH)

No.	nm	Mol. CD	No.	nm	Mol. CD	No.	nm	Mol. CD
1	304	10.5458	2	286	-30.8707	3	267	-2.4943
4	263	1.38839	5	260	5.45037	6	252	15.5609
7	216	-213.42	8	209	2.86649	9	209	-3.42947
10	208	1.01145	11	207	-10.3281	12	206	29.8277
13	205	16.4117	14	205	19.0787	15	203	-5.46007
16	202	-1.52574						

Figure 96. The CD spectrum of 2'-*N*-(2''-fluorobenzoyl) Et 770.

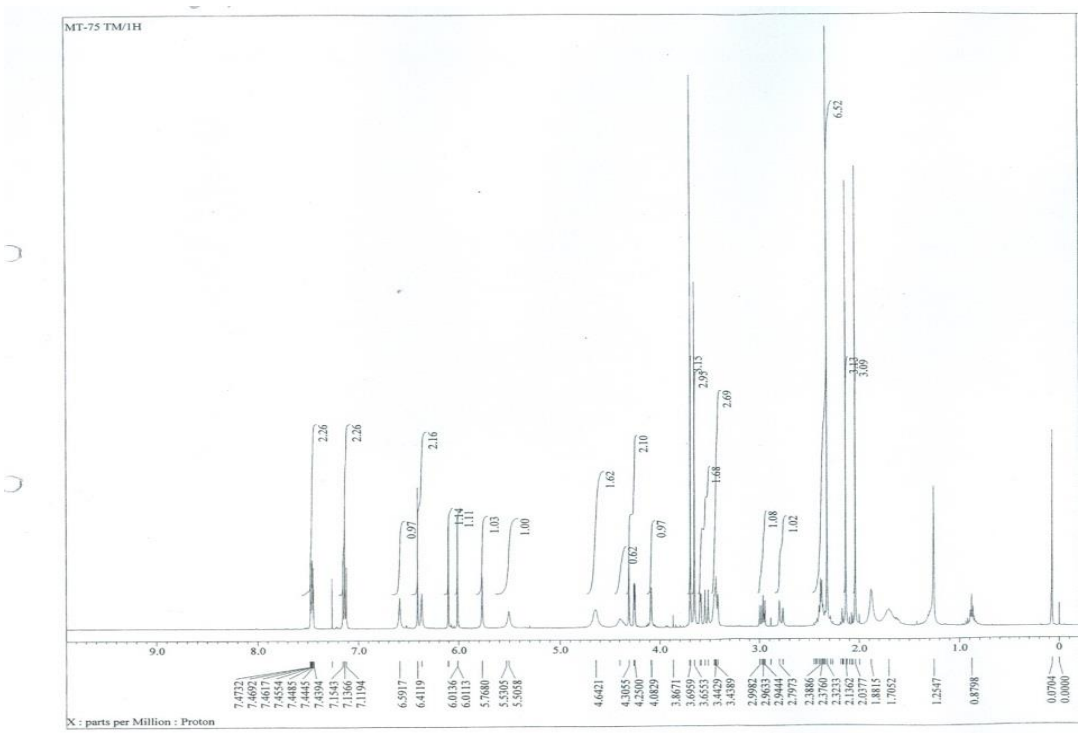

Figure 97. The ^{1}H-NMR spectrum of 2'-*N*-(4''-fluorobenzoyl) Et 770 (500 MHz, $CDCl_3$).

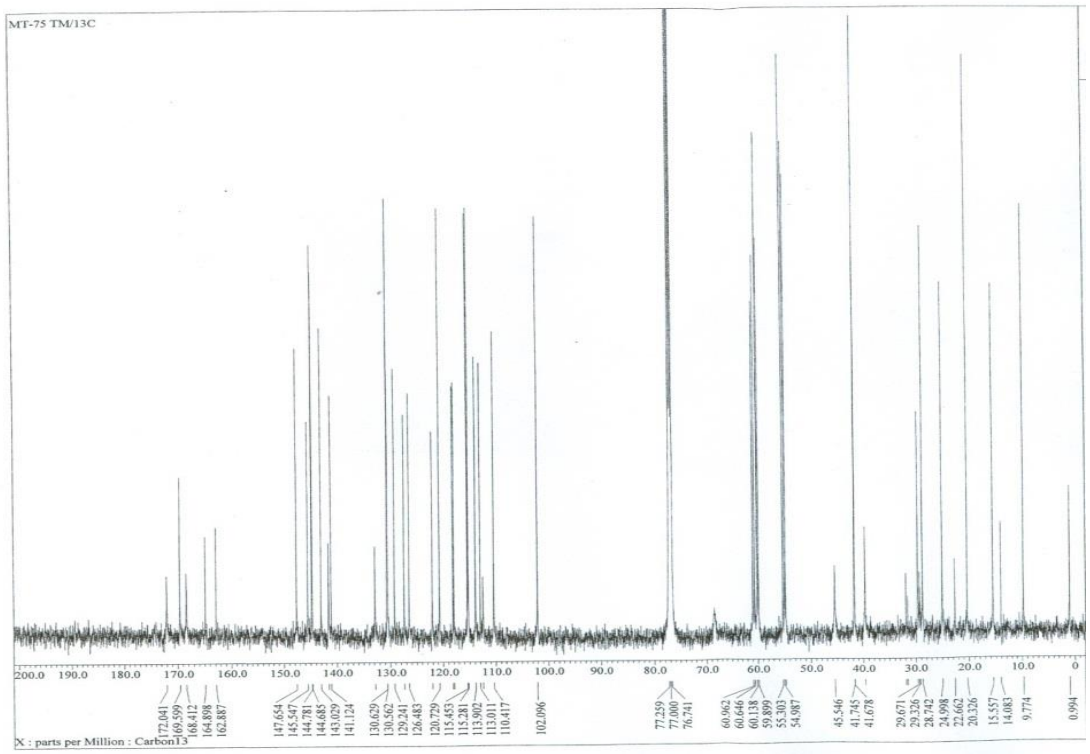

Figure 98. The ^{13}C-NMR spectrum of 2'-*N*-(4''-fluorobenzoyl) Et 770 (125 MHz, $CDCl_3$).

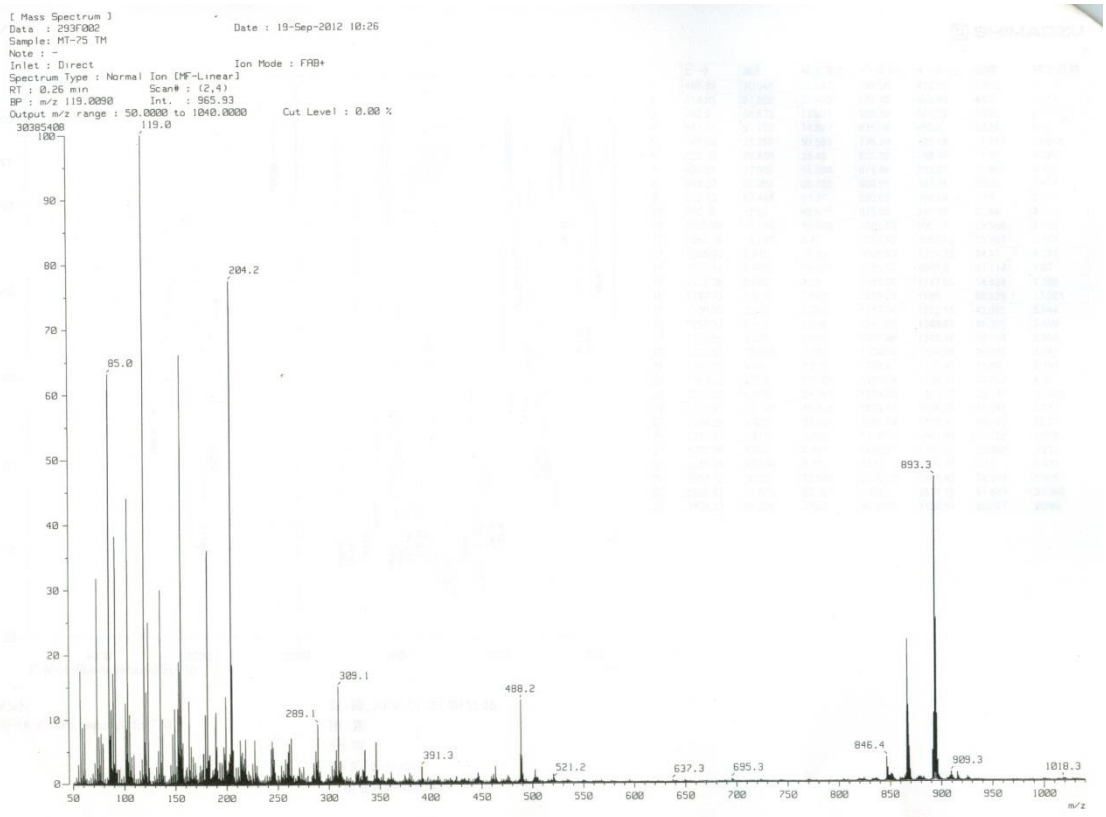

Figure 99. The FAB-Mass spectrum of 2'-*N*-(4''-fluorobenzoyl) Et 770.

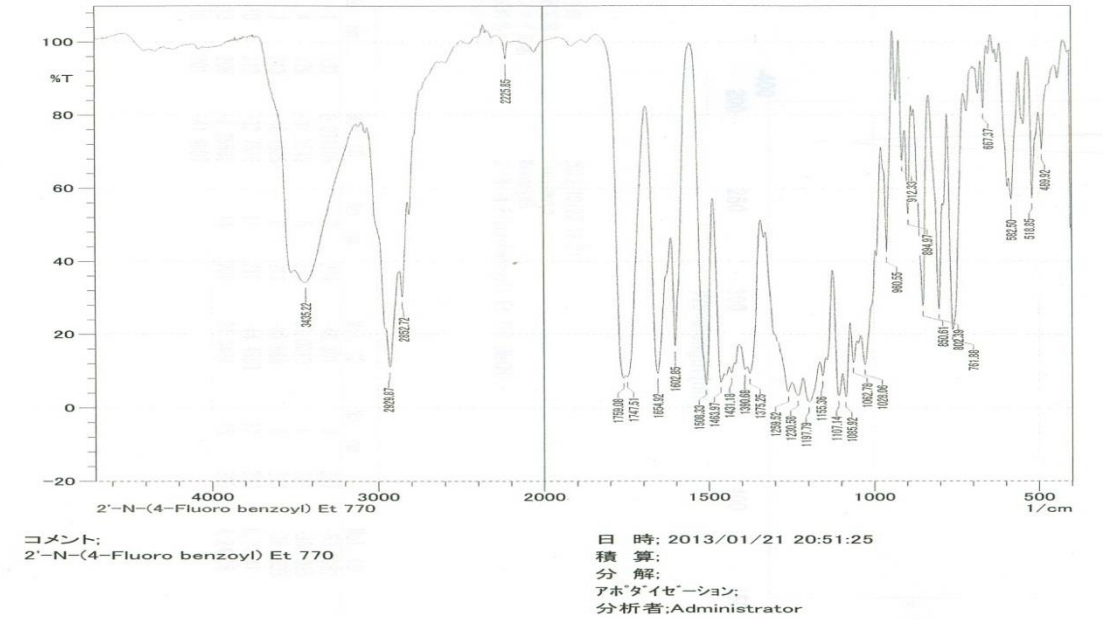

Figure 100. The IR spectrum (in KBr) of 2'-*N*-(4''-fluorobenzoyl) Et 770.

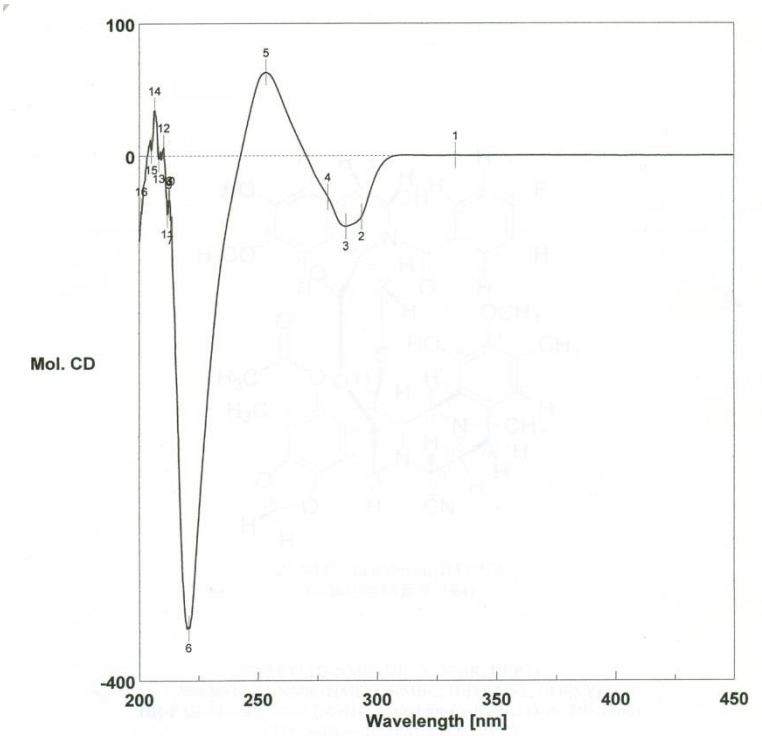

日時	2012/10/23 12:21
測定者	Tsujimoto
ファイル名	Memory#6
試料名	2'-N-(4-Fluorobenzoyl) Et 770 (MeOH)
コメント	

No.	nm	Mol. CD	No.	nm	Mol. CD	No.	nm	Mol. CD
1	333	0.073405	2	294	-46.301	3	287	-53.6062
4	279	-31.3549	5	253	63.0013	6	221	-360.035
7	213	-48.7865	8	213	-33.568	9	213	-36.7335
10	212	-33.7536	11	212	-44.4553	12	210	6.24541
13	208	-2.35588	14	206	34.3424	15	205	4.24116
16	201	-41.9907						

Figure 101. The CD spectrum of 2'-*N*-(4''-fluorobenzoyl) Et 770.

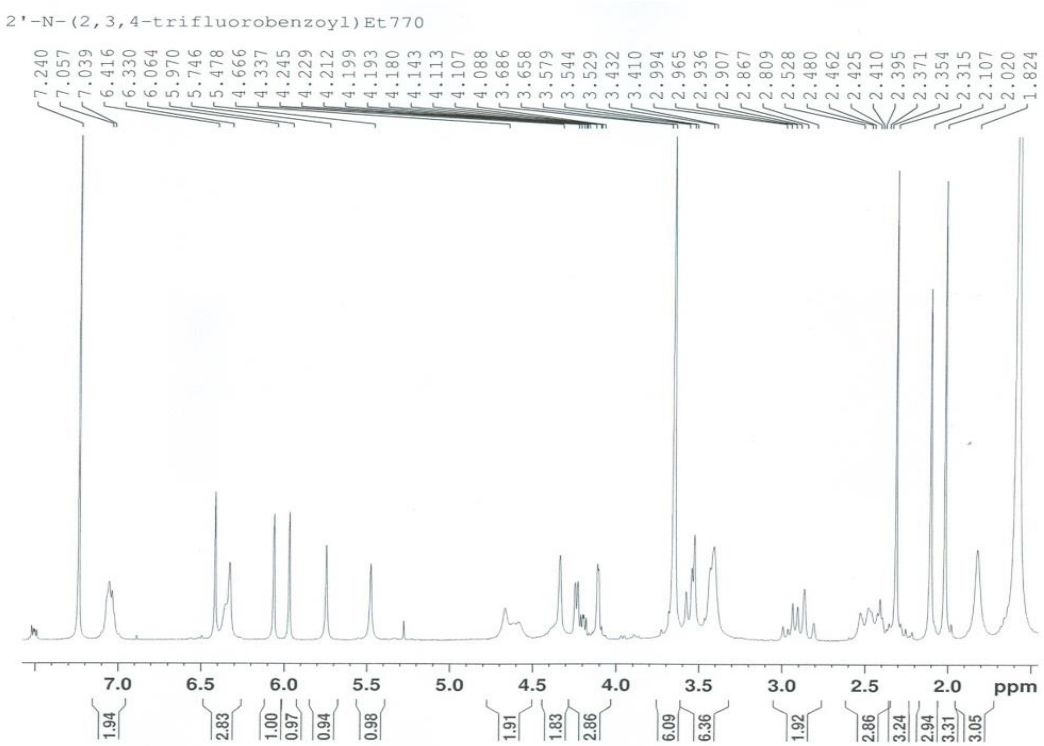

Figure 102. The ^{1}H-NMR spectrum of 2'-*N*-(2'',3'',4''-trifluorobenzoyl) Et 770 (300 MHz, $CDCl_3$).

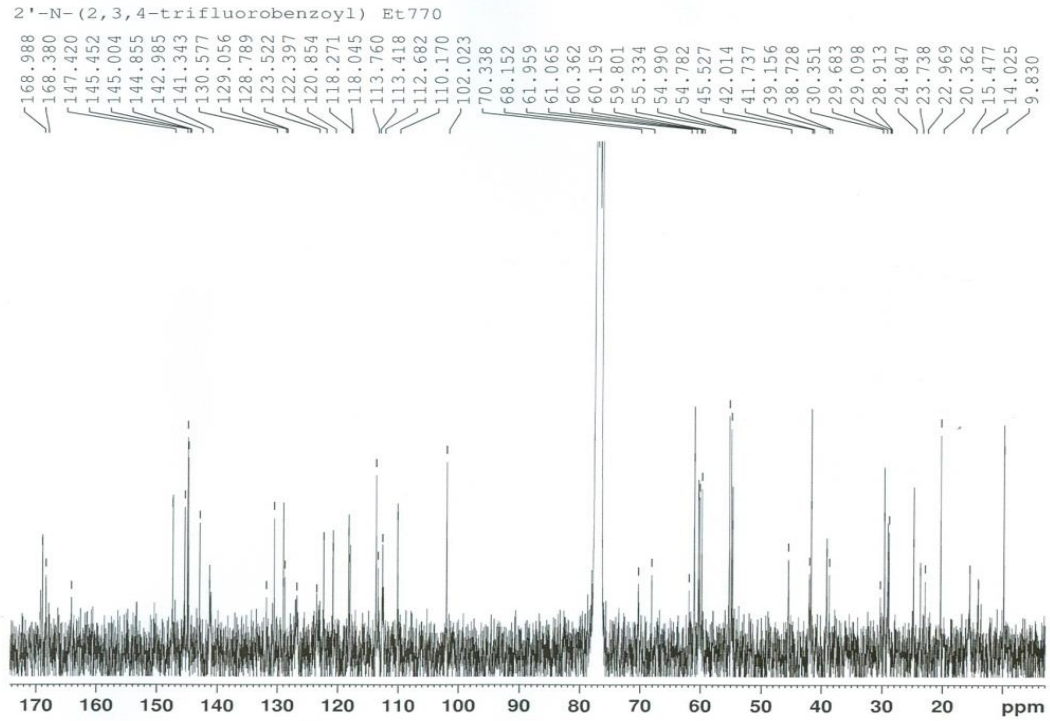

Figure 103. The ^{13}C-NMR spectrum of 2'-*N*-(2'',3'',4''-trifluorobenzoyl) Et 770 (75 MHz, $CDCl_3$).

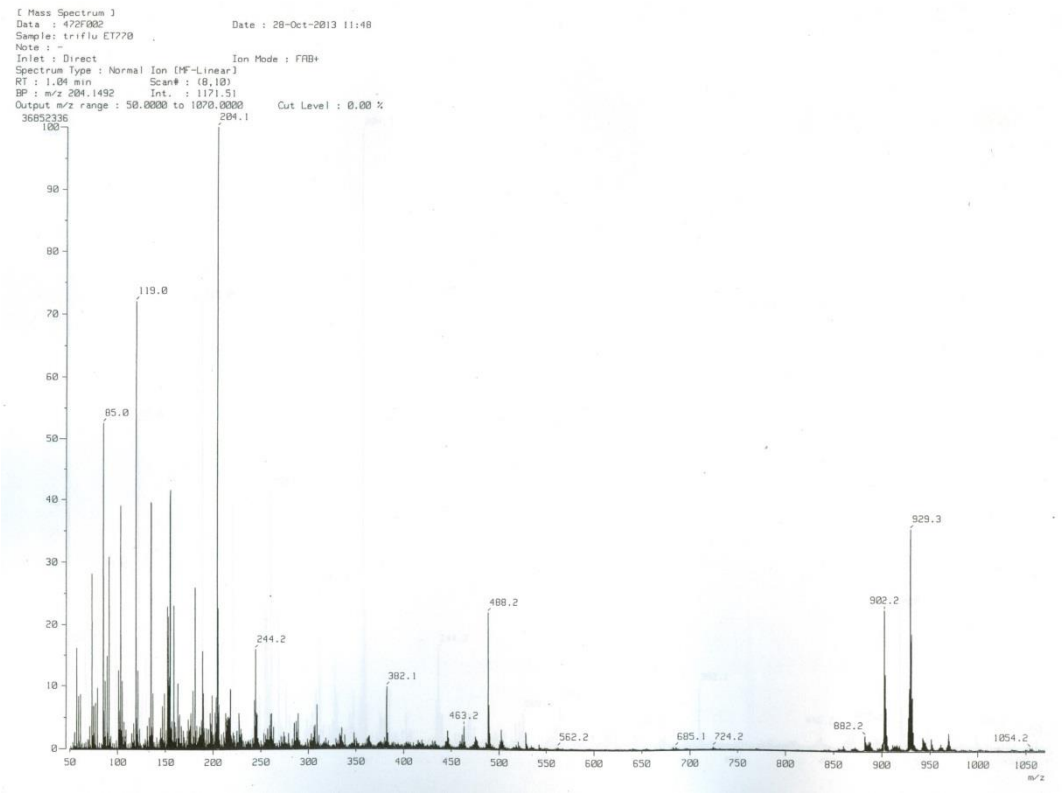

Figure 104. The FAB-Mass spectrum of 2'-*N*-(2,3,4-trifluorobenzoyl) Et 770.

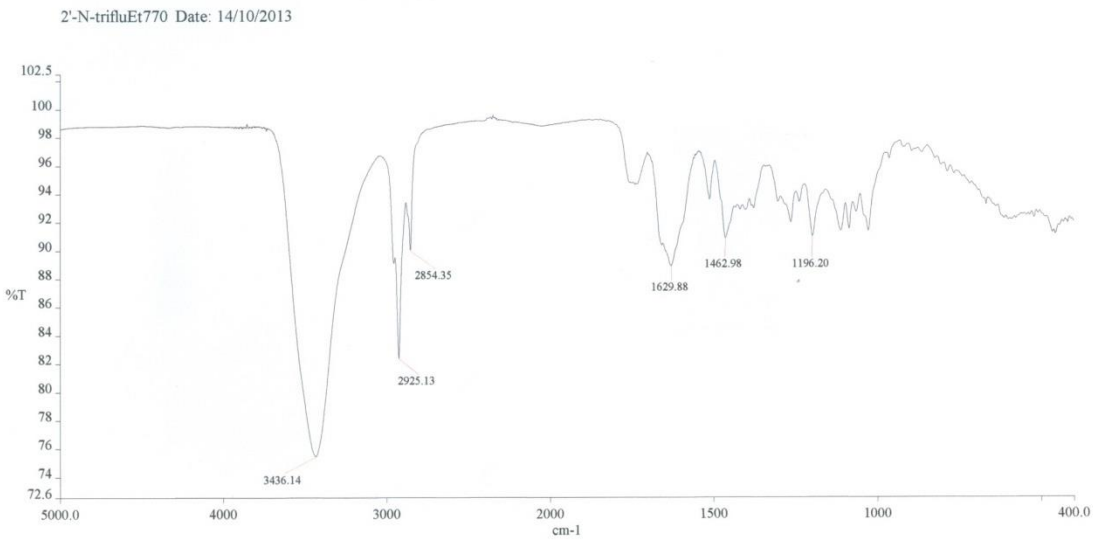

Figure 105. The IR spectrum (in KBr) of 2'-*N*-(2,3,4-trifluorobenzoyl) Et 770.

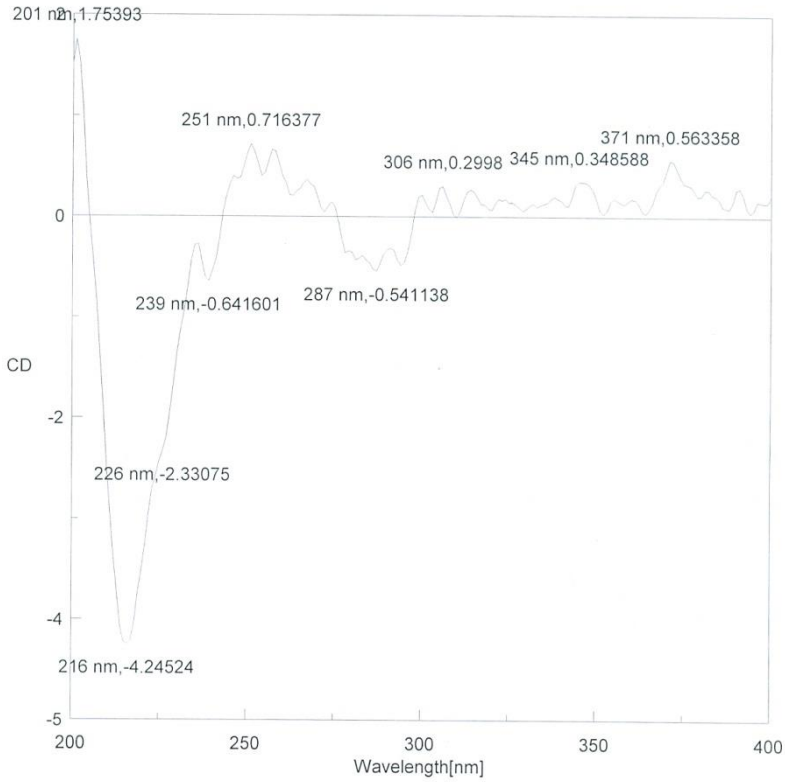

File Name :	trifluet.jws		
Date :	11/10/2013 11:08AM [11/10/2013 11:04AM]		
Sample :	2'-N-trifluoroBz ET770		
Cell Length :	0.1 cm		
Concentration :			
Solvent :	MeOH		
Temperature :	22 C		
Operator :	Pon		
Organization :			
Comment :			
Data mode :	CD		
Ch2-mode :	HT		
Range :	400 - 200 nm		
Band width :	1.0 nm	Sensitivity :	100 mdeg
Resolution :	1 nm	Response :	1 sec
Accumulation :	5	Speed :	100 nm/min

Figure 106. The CD spectrum of 2'-*N*-(2,3,4-trifluorobenzoyl) Et 770.

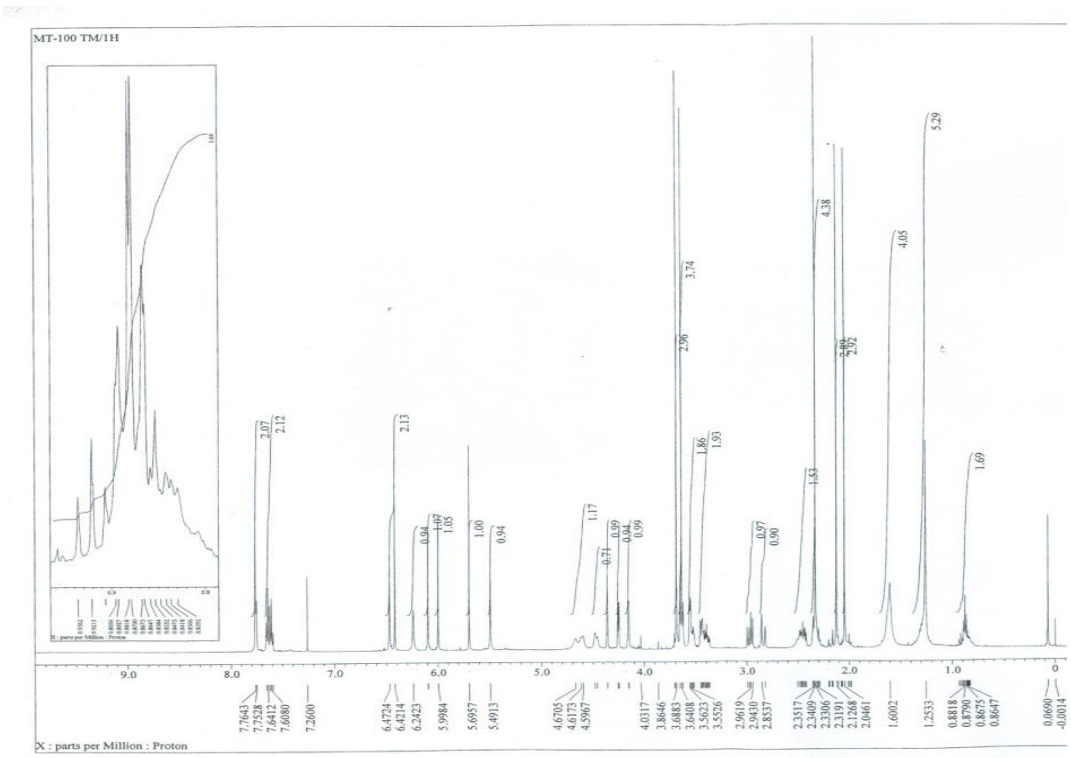

Figure 107. The ^{1}H-NMR spectrum of 2'-*N*-(3''-trifluoromethylbenzoyl) Et 770 (500 MHz, $CDCl_3$).

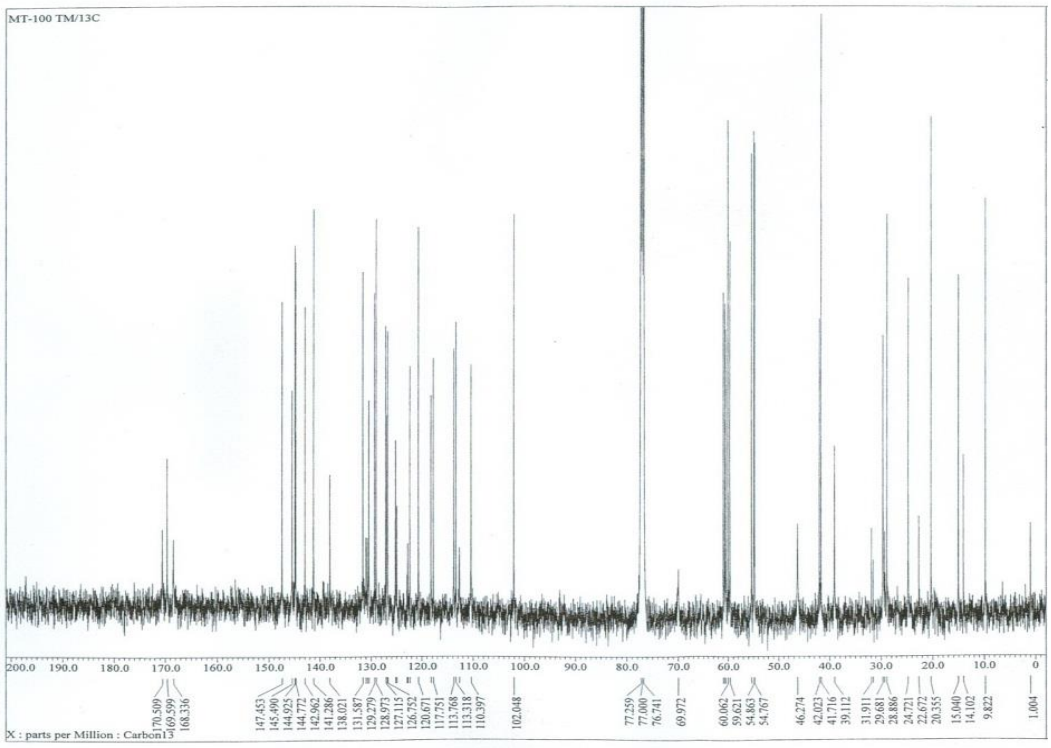

Figure 108. The ^{13}C-NMR spectrum of 2'-*N*-(3''-trifluoromethylbenzoyl) Et 770 (125 MHz, $CDCl_3$).

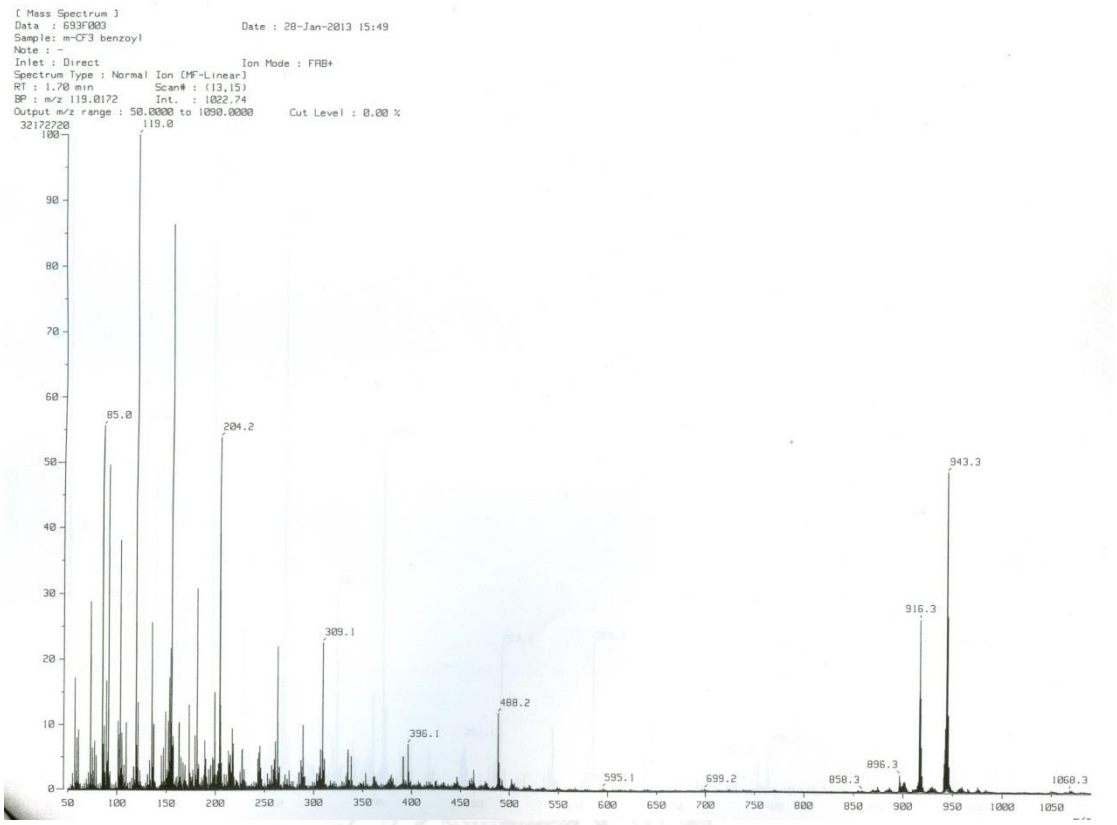

Figure 109. The FAB-Mass spectrum of 2'-*N*-(3''-trifluoromethylbenzoyl) Et 770.

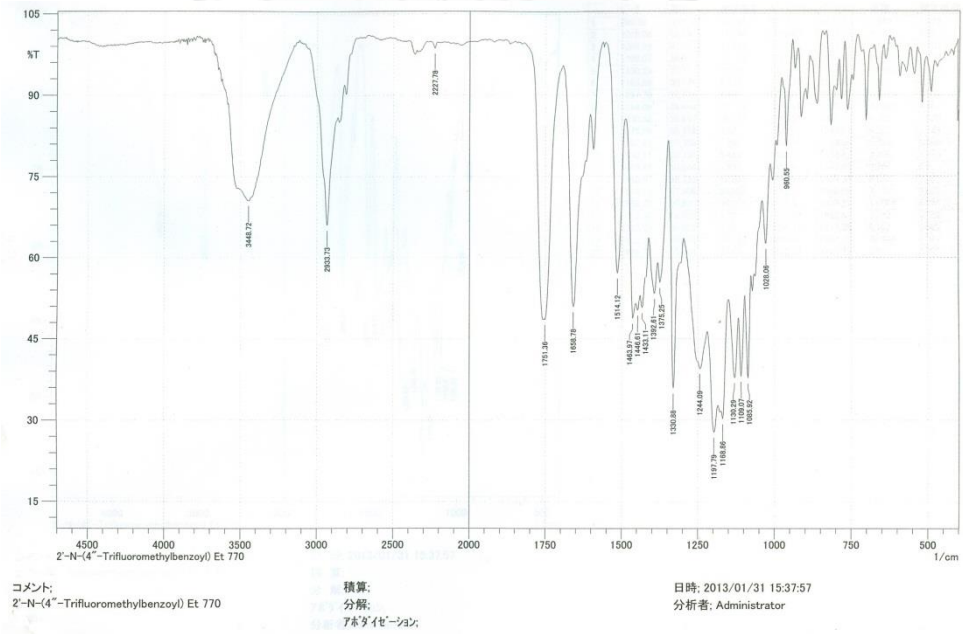

Figure 110. The IR spectrum (in KBr) of 2'-*N*-(3''-trifluoromethylbenzoyl) Et 770.

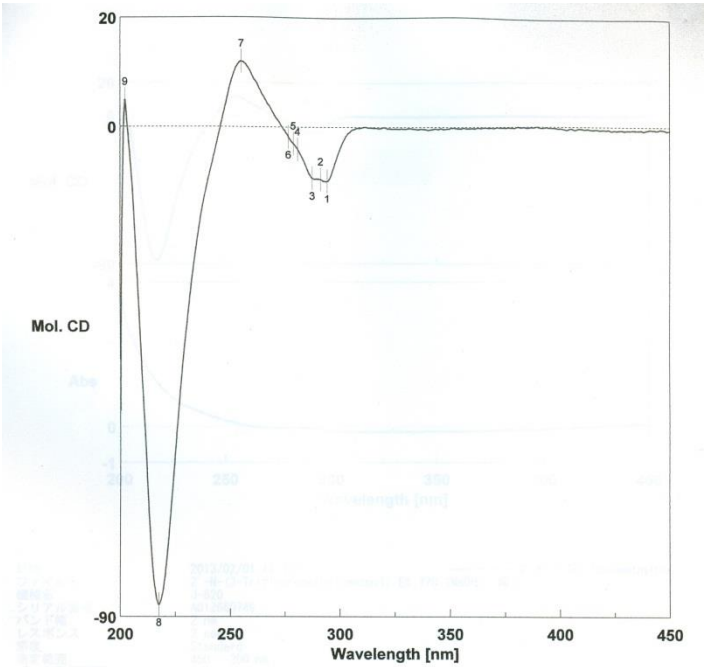

日時	2013/02/01 12:19
測定者	Tsujimoto
ファイル名	2'-N-(3-Trifluoromethylbenzoyl) Et 770 (MeOH) 修正
試料名	2'-N-(3-Trifluoromethylbenzoyl) Et 770 (MeOH)
コメント	2'-N-(3-Trifluoromethylbenzoyl) Et 770 (MeOH)

No.	nm	Mol. CD	No.	nm	Mol. CD	No.	nm	Mol. CD
1	294	-9.9604	2	291	-9.6669	3	287	-9.4262
4	281	-4.15059	5	279	-3.059	6	277	-1.86866
7	255	11.9597	8	218	-87.7787	9	202	4.93945

Figure 111. The CD spectrum of 2'-*N*-(3''-trifluoromethylbenzoyl) Et 770.

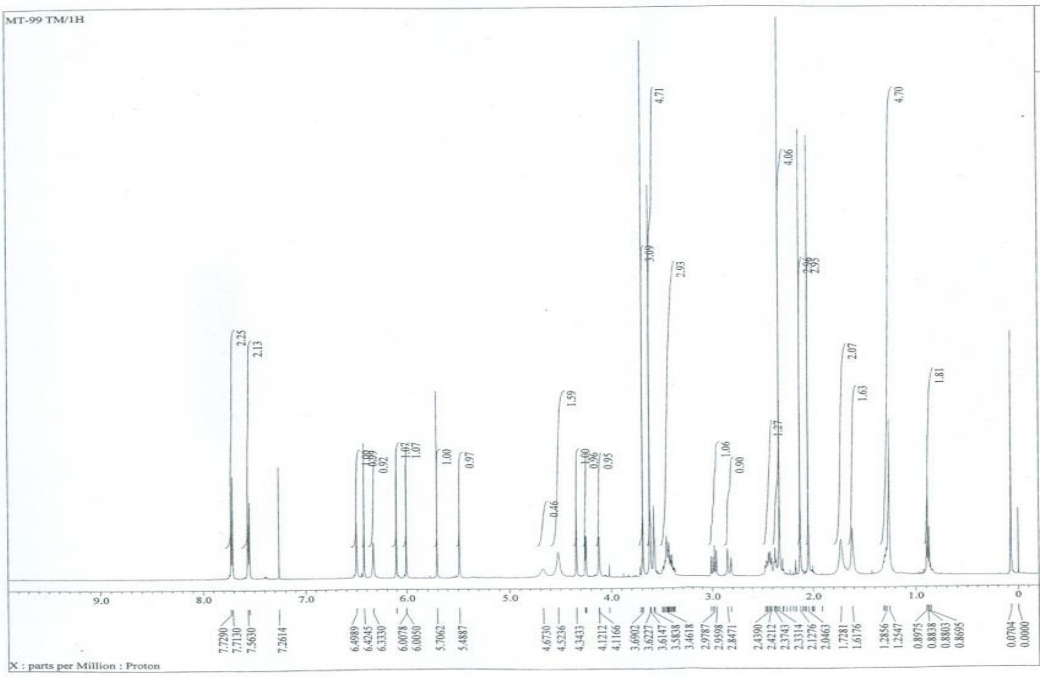

Figure 112. The ^{1}H-NMR spectrum of 2'-*N*-(4''-trifluoromethylbenzoyl) Et 770 (500 MHz, $CDCl_3$).

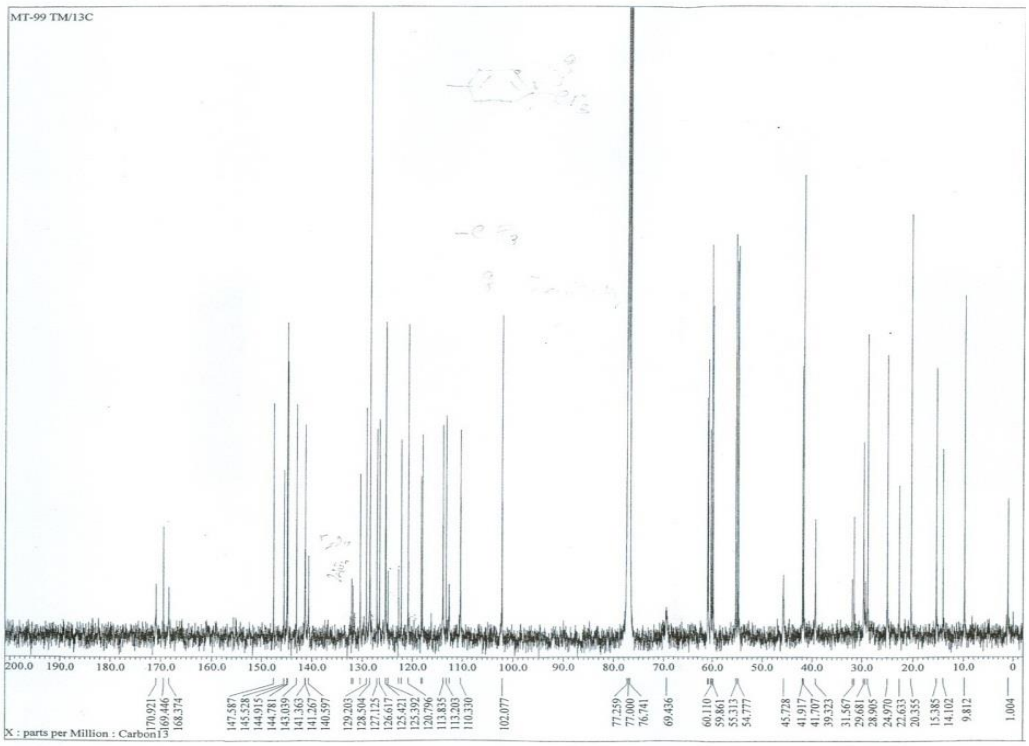

Figure 113. The ^{13}C-NMR spectrum of 2'-*N*-(4''-trifluoromethylbenzoyl) Et 770 (125 MHz, $CDCl_3$).

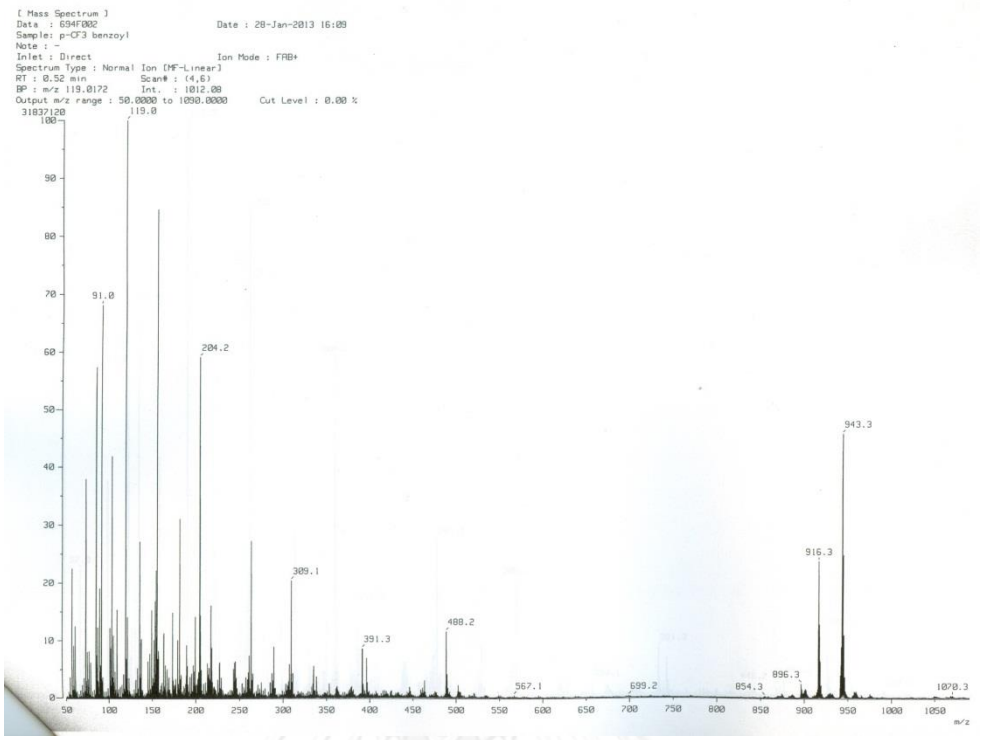

Figure 114. The FAB-Mass spectrum of 2'-*N*-(4''-trifluoromethylbenzoyl) Et 770.

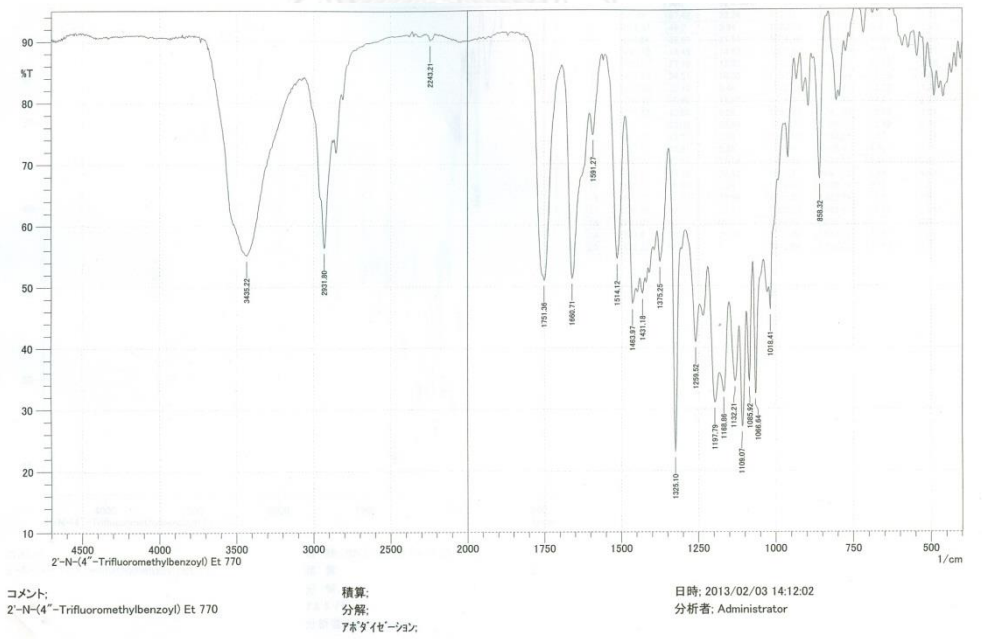

Figure 115. The IR spectrum (in KBr) of 2'-*N*-(4''-trifluoromethylbenzoyl) Et 770.

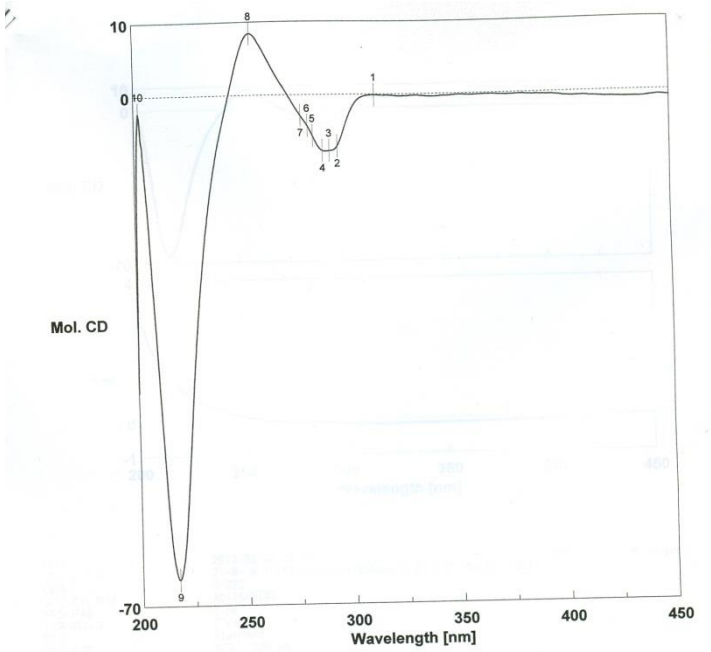

日時 2013/02/02 16:06
測定者 Tsujimoto
ファイル名 2'-N-(4-Trifluoromethylbenzoyl) Et 770 (MeOH) 修正
試料名 2'-N-(4-Trifluoromethylbenzoyl) Et 770 (MeOH)
コメント 2'-N-(4-Trifluoromethylbenzoyl) Et 770 (MeOH)

No.	nm	Mol. CD	No.	nm	Mol. CD	No.	nm	Mol. CD
1	313	-0.109553	2	295	-7.06631	3	291	-7.71238
4	288	-7.67955	5	284	-5.66806	6	281	-4.26594
7	278	-2.85524	8	255	8.43122	9	217	-66.3496
10	202	-2.31418						

Figure 116. The CD spectrum of 2'-*N*-(4''-trifluoromethylbenzoyl) Et 770.

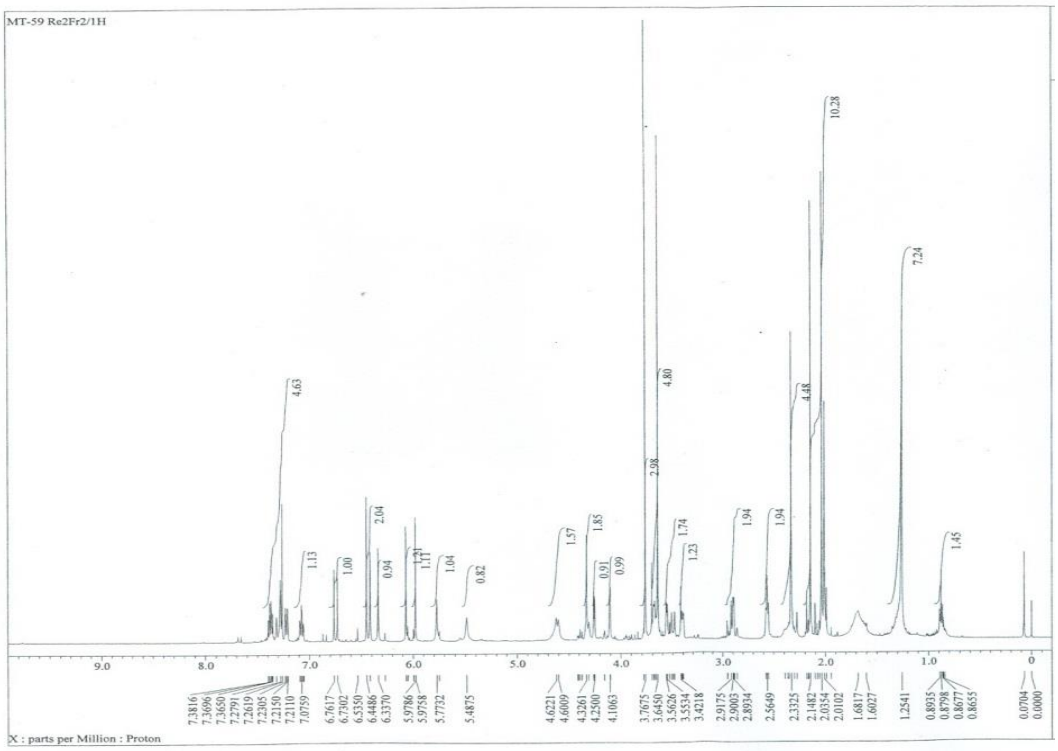

Figure 117. The ^{1}H-NMR spectrum of 2'-*N*-(3''-fluorocinnamoyl) Et 770 (500 MHz, $CDCl_3$).

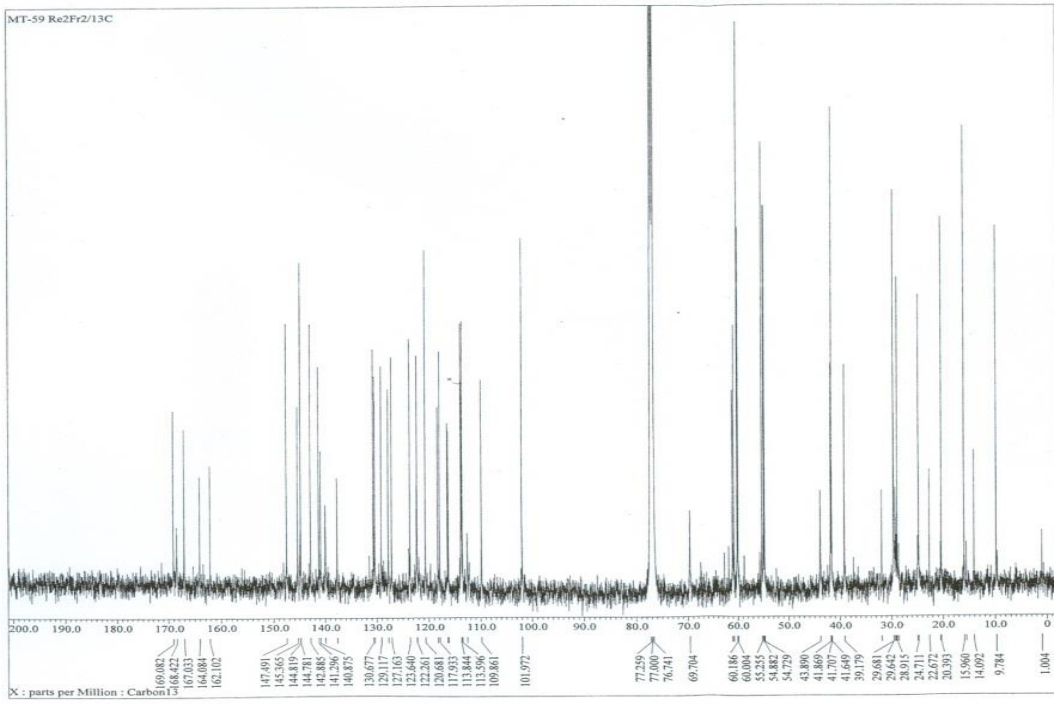

Figure 118. The ^{13}C-NMR spectrum of 2'-*N*-(3''-fluorocinnamoyl) Et 770 (125 MHz, $CDCl_3$).

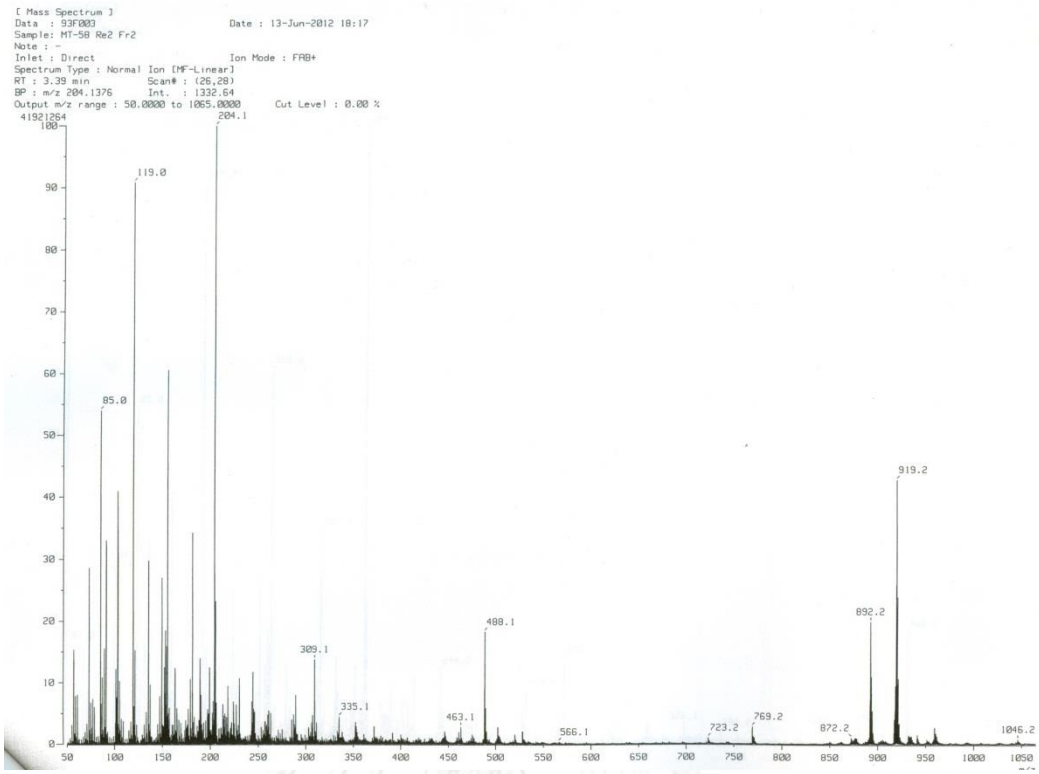

Figure 119. The FAB-Mass spectrum of 2'-*N*-(3"-fluorocinnamoyl) Et 770.

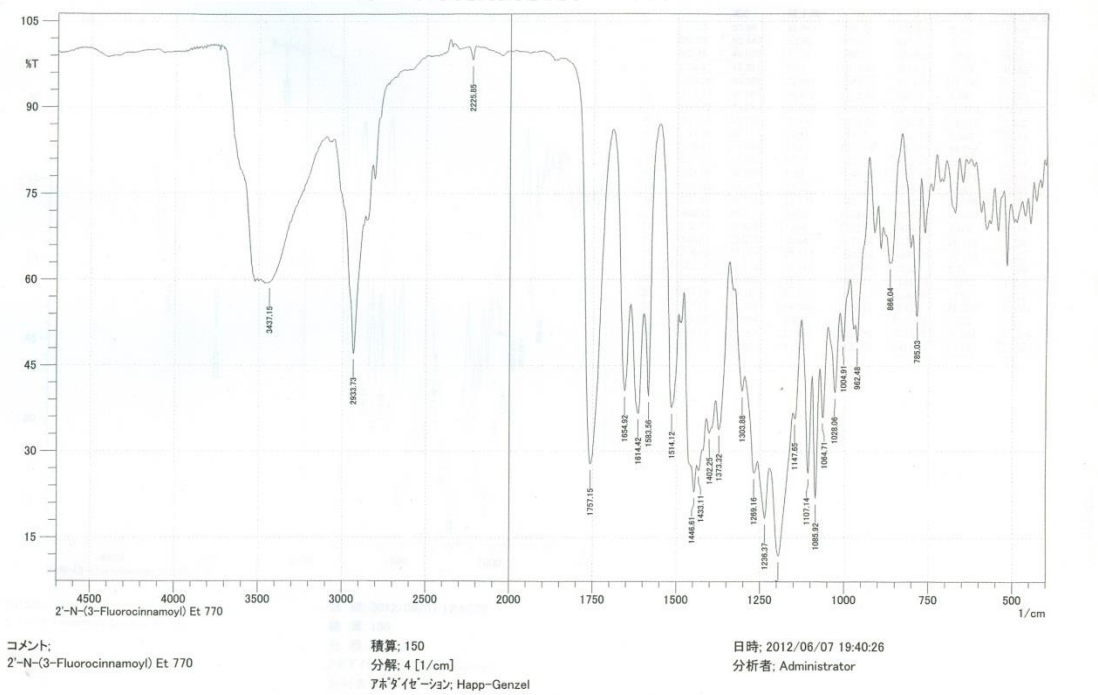

Figure 120. The IR spectrum (in KBr) of 2'-*N*-(3"-fluorocinnamoyl) Et 770.

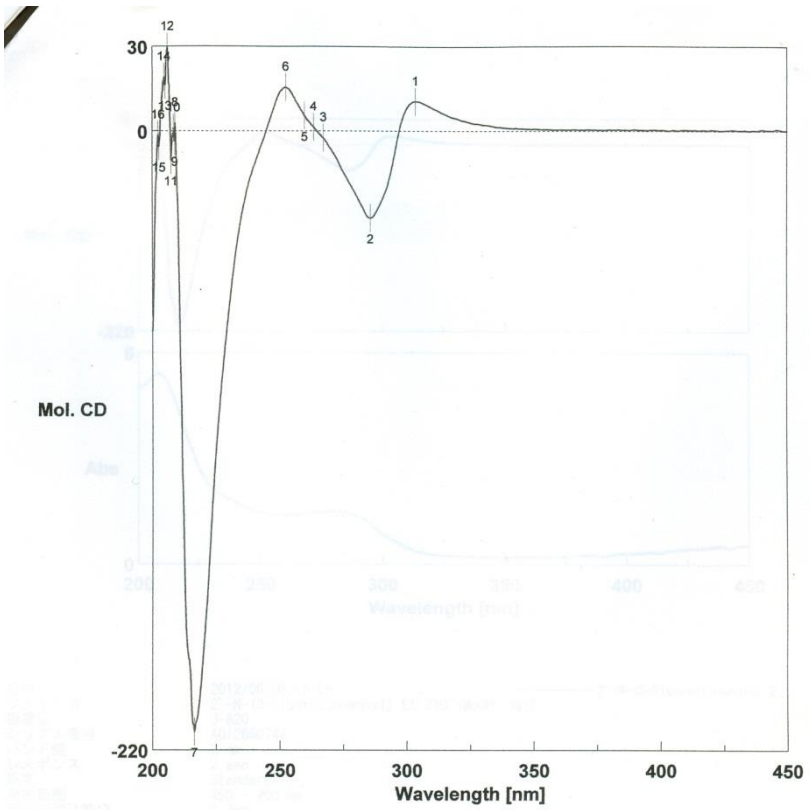

日時 2012/06/08 16:06
測定者 Tsujimoto
ファイル名 2'-N-(3-Fluorocinnamoyl) Et 770 (MeOH) 修正
試料名 2'-N-(3-Fluorocinnamoyl) Et 770 (MeOH)
コメント 2'-N-(3-Fluorocinnamoyl) Et 770 (MeOH)

No.	nm	Mol. CD	No.	nm	Mol. CD	No.	nm	Mol. CD
1	304	10.5458	2	286	-30.8707	3	267	-2.4943
4	263	1.38839	5	260	5.45037	6	252	15.5609
7	216	-213.42	8	209	2.86649	9	209	-3.42947
10	208	1.01145	11	207	-10.3281	12	206	29.8277
13	205	16.4117	14	205	19.0787	15	203	-5.46007
16	202	-1.52574						

Figure 121. The CD spectrum of 2'-*N*-(3''-fluorocinnamoyl) Et 770.

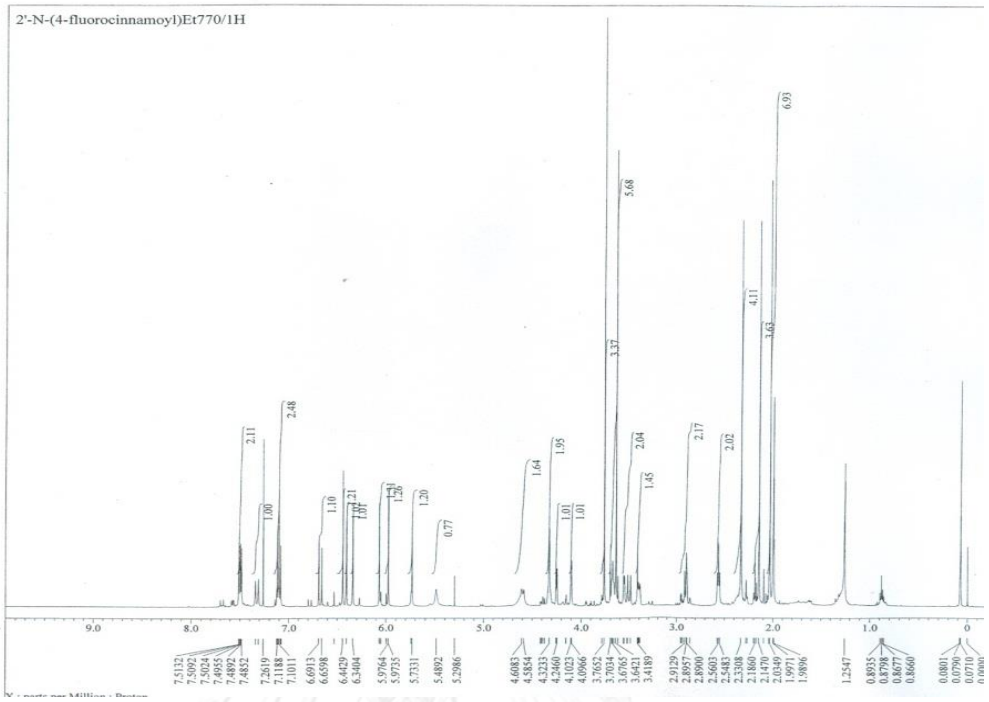

Figure 122. The ^{1}H-NMR spectrum of 2'-*N*-(4''-fluorocinnamoyl) Et 770 (500 MHz, $CDCl_3$).

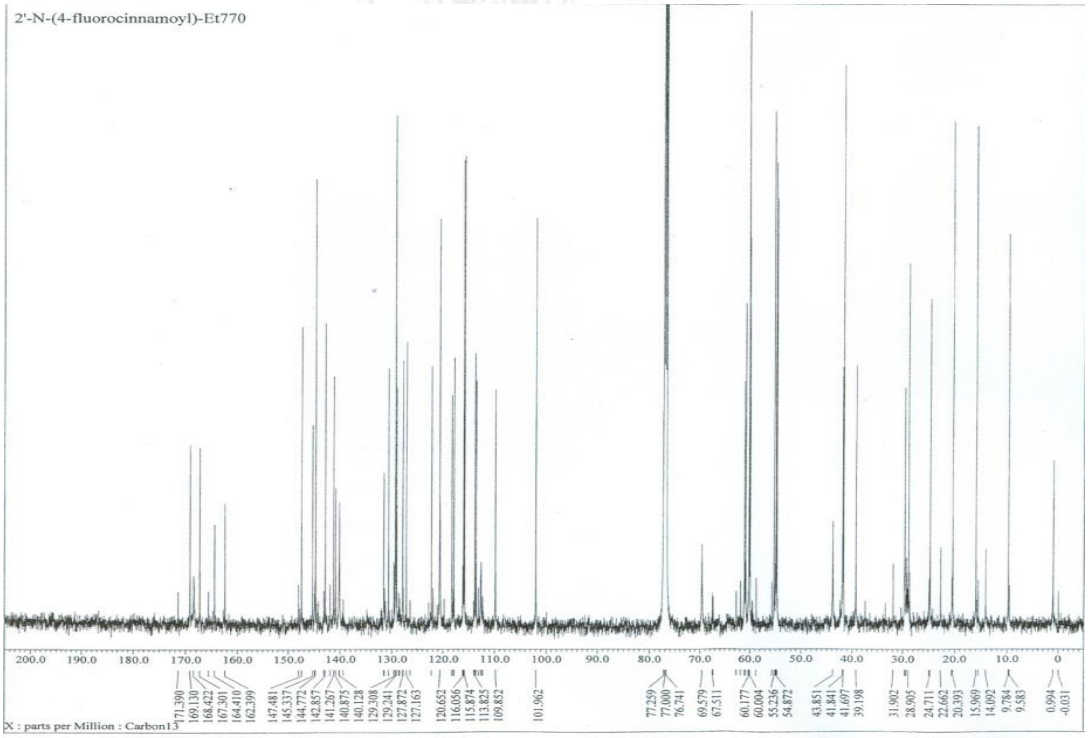

Figure 123. The ^{13}C-NMR spectrum of 2'-*N*-(4''-fluorocinnamoyl) Et 770 (125 MHz, $CDCl_3$).

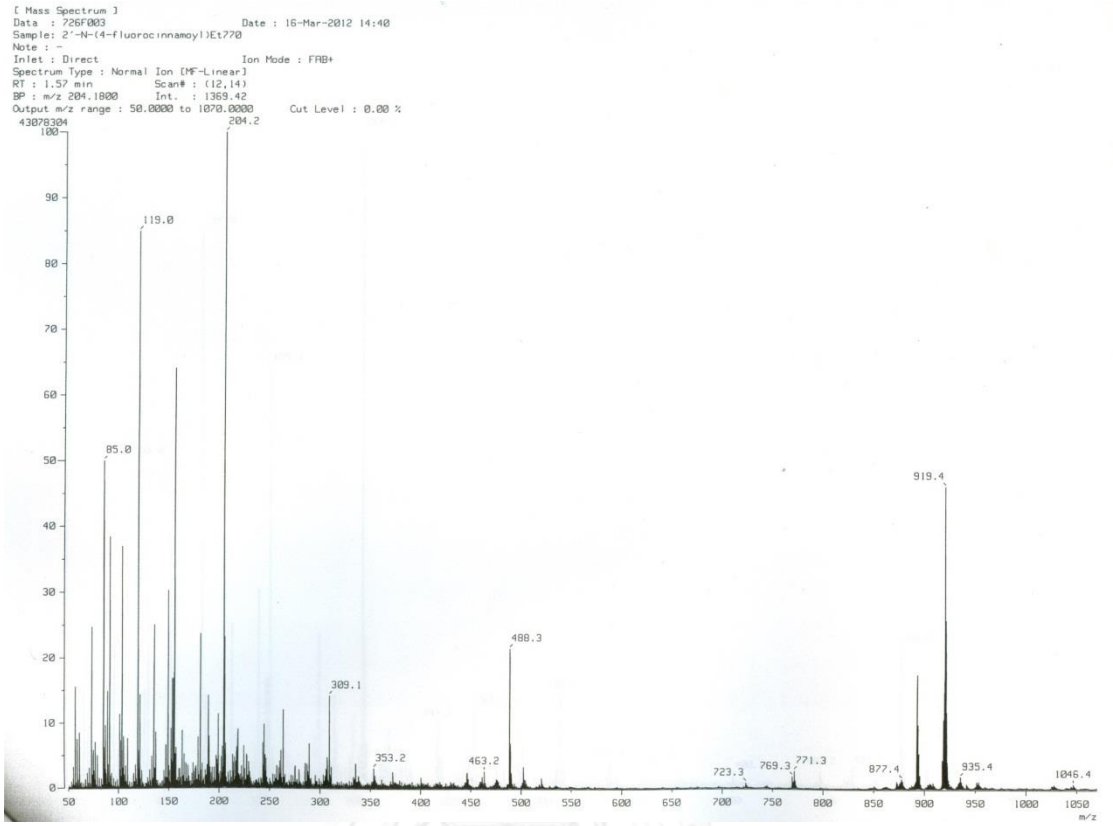

Figure 124. The FAB-Mass spectrum of 2'-*N*-(4"-fluorocinnamoyl) Et 770.

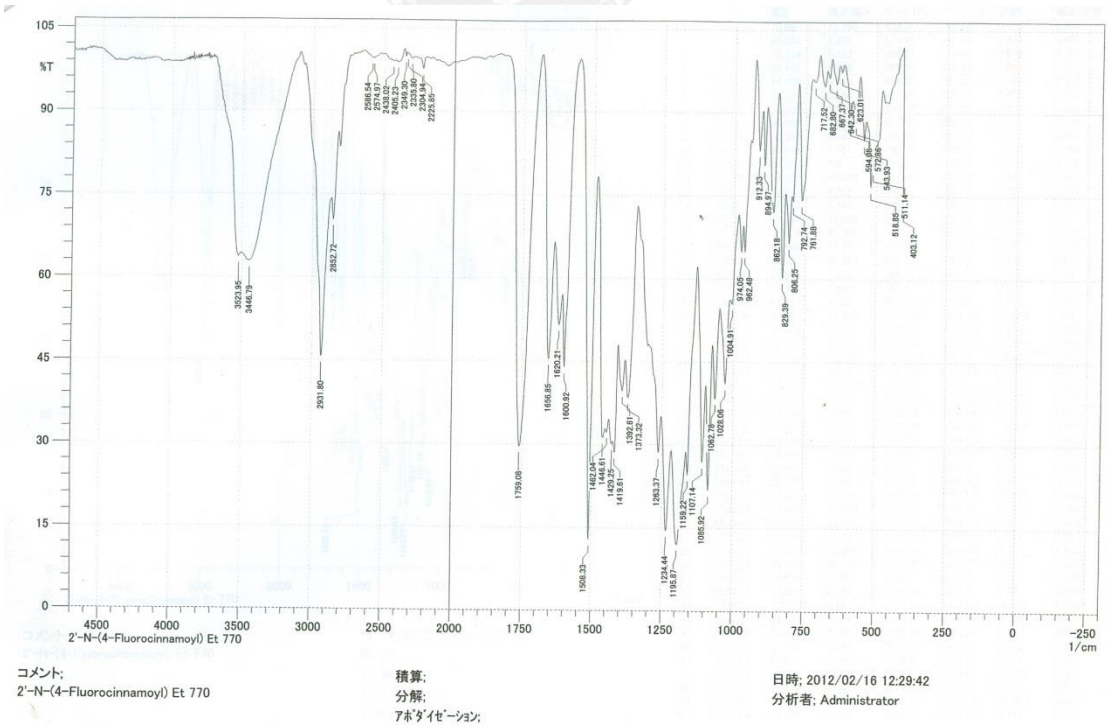

Figure 125. The IR spectrum (in KBr) of 2'-*N*-(4"-fluorocinnamoyl) Et 770.

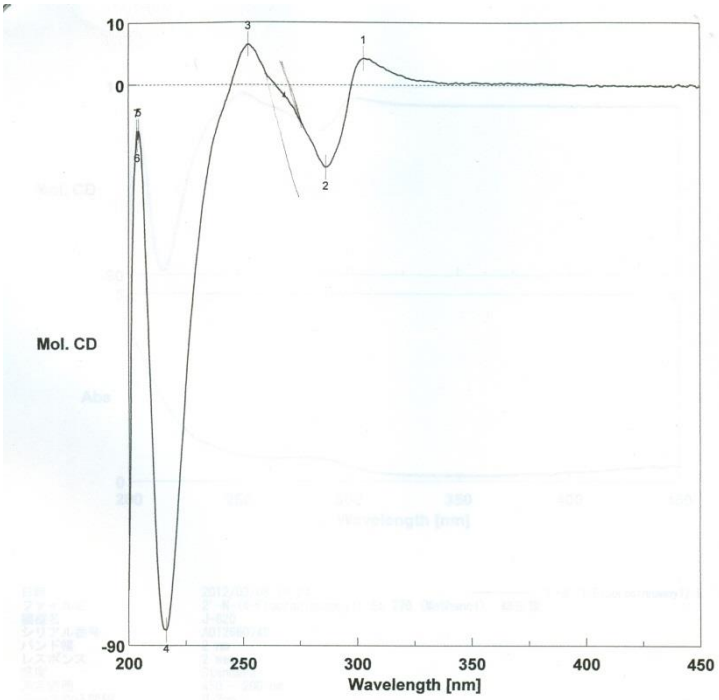

日時 2012/03/08 16:24
測定者 Tsujimoto
ファイル名 2'-N-(4-Fluorocinnamoyl) Et 770 (Methanol) 修正後
試料名 2'-N-(4-Fluorocinnamoyl) Et 770 (Methanol)
コメント 2'-N-(4-Fluorocinnamoyl) Et 770 (Methanol)

No.	nm	Mol. CD	No.	nm	Mol. CD	No.	nm	Mol. CD
1	303	4.2664	2	286	-13.1569	3	252	6.50125
4	216	-87.5135	5	204	-7.37106	6	204	-8.76946
7	204	-7.51892						

Figure 126. The CD spectrum of 2'-*N*-(4''-fluorocinnamoyl) Et 770.

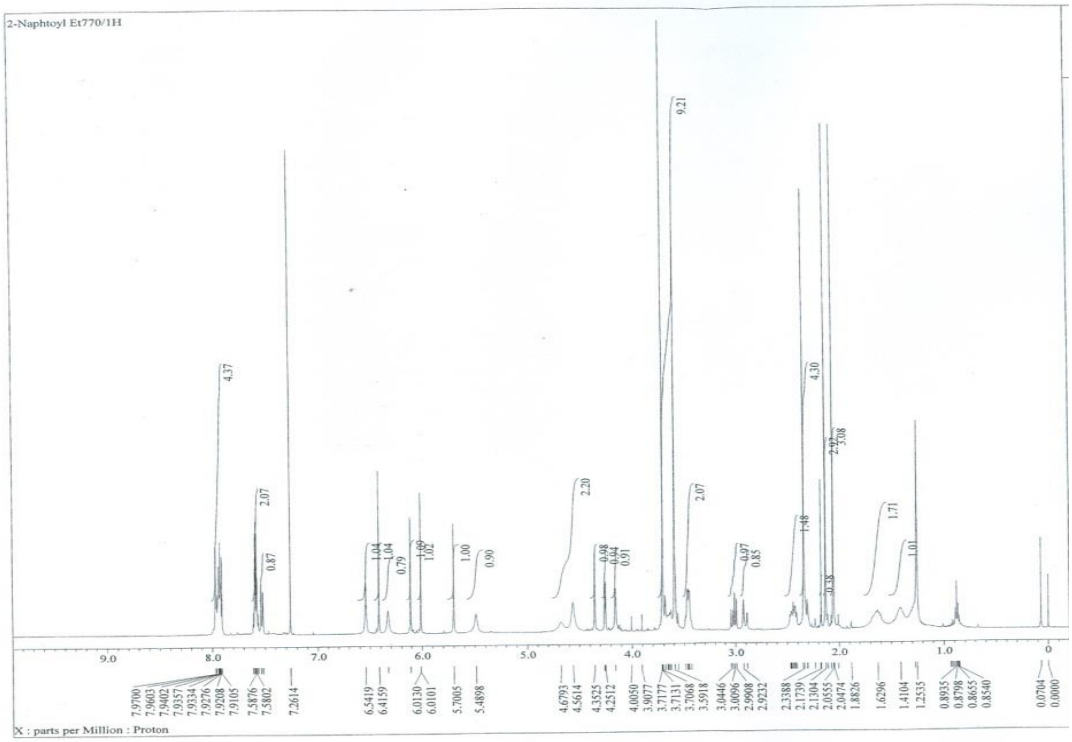

Figure 127. The ^{1}H-NMR spectrum of 2'-*N*-(2"-naphthoyl) Et 770 (500 MHz, $CDCl_3$).

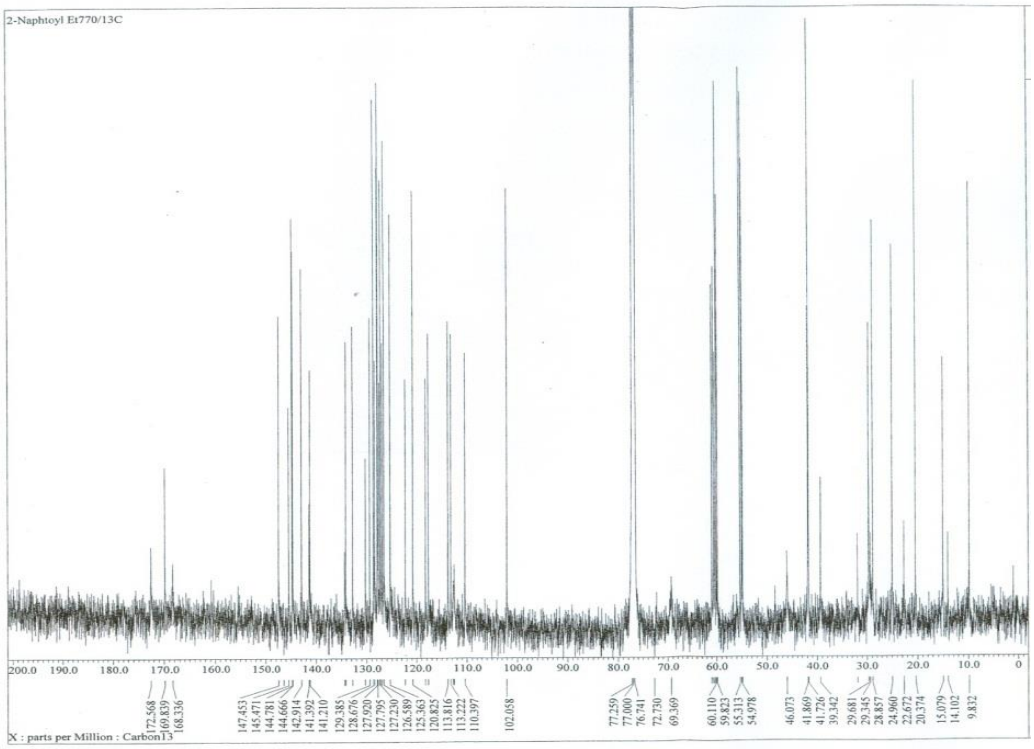

Figure 128. The ^{13}C-NMR spectrum of 2'-*N*-(2"-naphthoyl) Et 770 (125 MHz, $CDCl_3$).

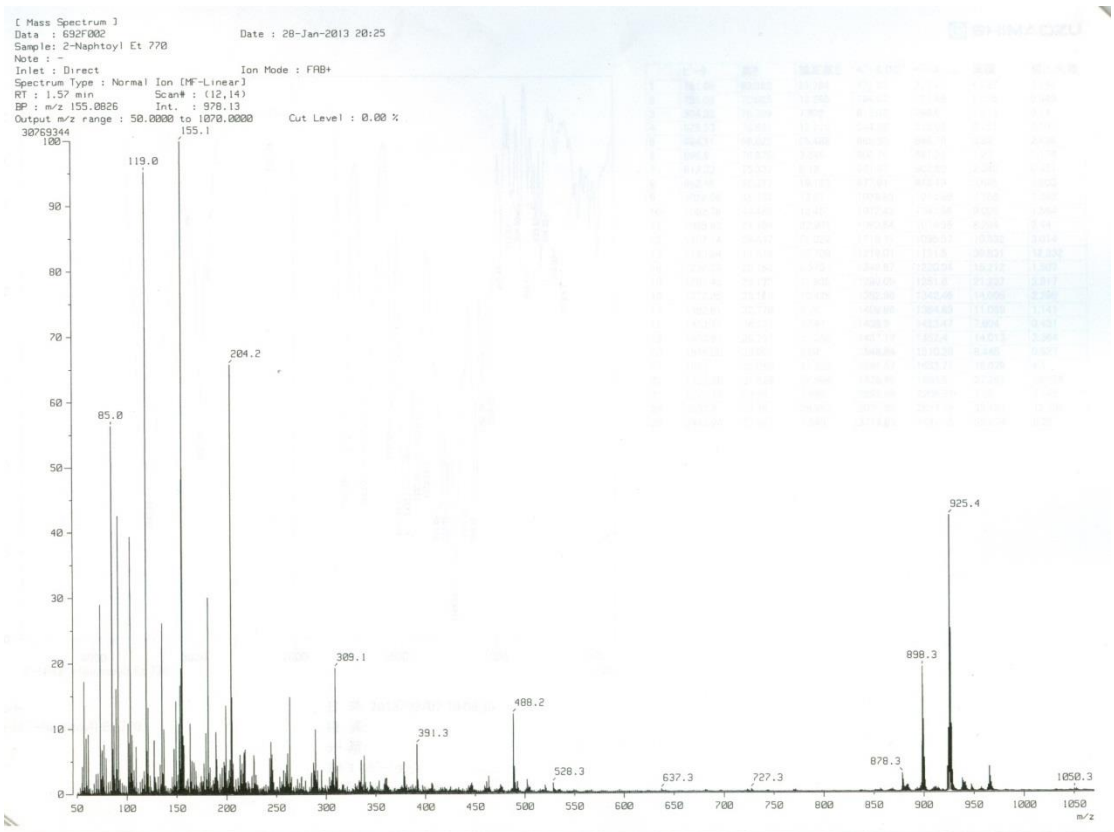

Figure 129. The FAB-Mass spectrum of 2'-*N*-(2''-naphthoyl) Et 770.

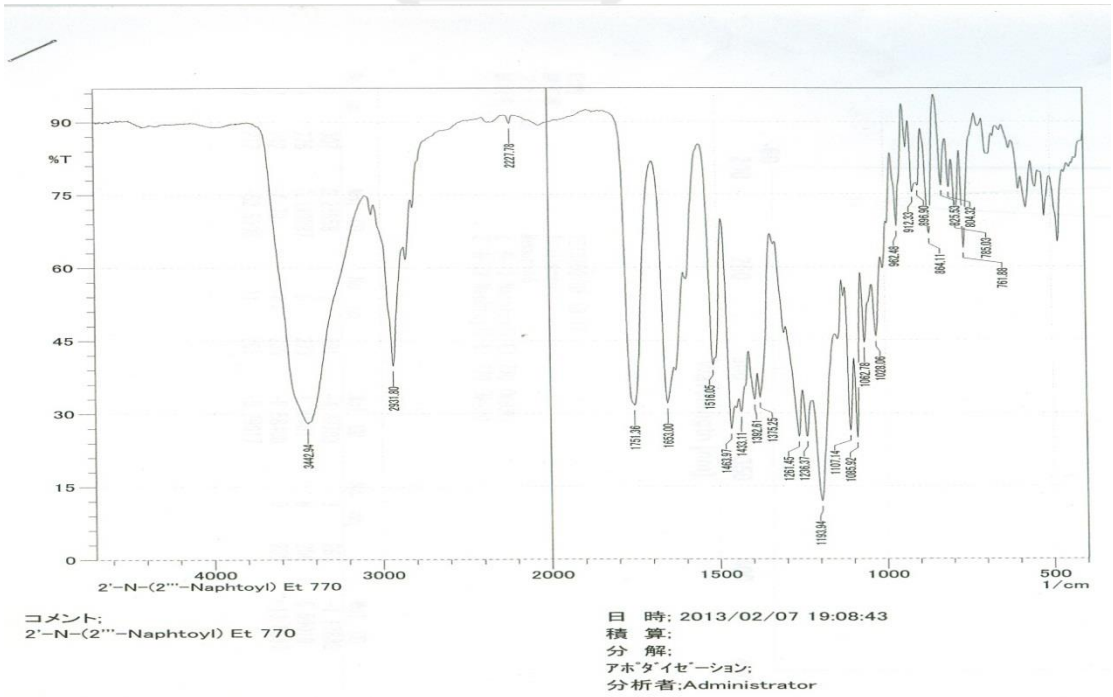

Figure 130. The IR spectrum (in KBr) of 2'-*N*-(2''-naphthoyl) Et 770.

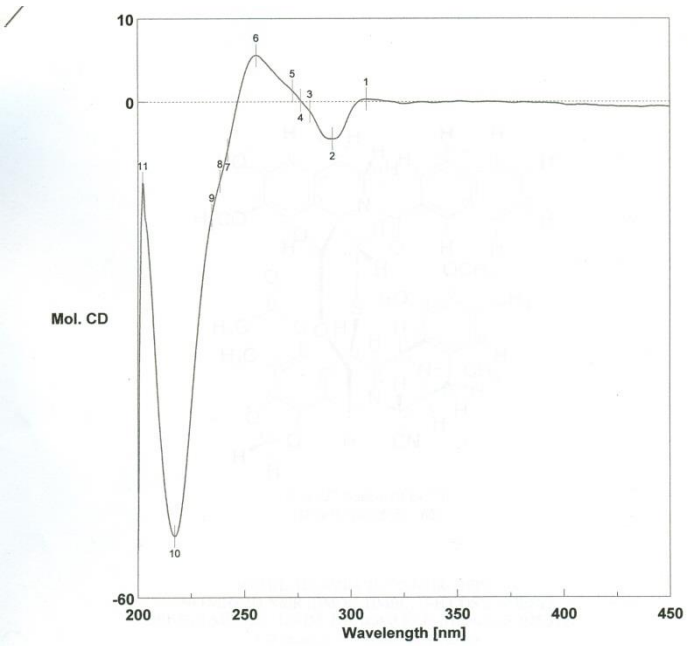

日時 2013/02/01 18:11
測定者 Tsujimoto
ファイル名 Memory#6
試料名 2'-N-(2-Naphtoyl) Et 770 (MeOH)
コメント 2'-N-(2-Naphtoyl) Et 770 (MeOH)

No.	nm	Mol. CD	No.	nm	Mol. CD	No.	nm	Mol. CD
1	307	0.28858	2	291	-4.48783	3	281	-1.17888
4	276	0.149287	5	273	1.30461	6	256	5.59019
7	242	-5.79	8	239	-9.58408	9	235	-13.6587
10	217	-52.5303	11	202	-9.79917			

Figure 131. The CD spectrum of 2'-*N*-(2''-naphthoyl) Et 770.

VITA

Mr. Witaya Lowtangkitcharoen was born on October 7, 1987 in Bangkok, Thailand. He received his Bachelor of Science in Pharmacy from the Faculty of Pharmaceutical Sciences, Khon Kaen University in 2010.

Publication

Mitsuhiro Tsujimoto, Witaya Lowtangkitcharoen, Nanae Mori, Waree Pangkruang, Ploenthip Puthongking, Khanit Suwanborirux, and Naoki Saito. (2013). Chemistry of Ecteinascidins. Part 4: Preparation of 2'-N-acyl ecteinascidin 770 derivatives with improved cytotoxicity profiles. Chemical and Pharmaceutical Bulletin 61(10): 1052-1064.

Poster presentations

Witaya lowtangkitcharoen, Taksian Chuanasa, Naoki Saito, and Khanit Suwanborirux. Preparationn of 2'-N-2,3,4-trifluorobenzoyl derivative of cytotoxic ecteinascidin 770 from the Thai tunicate Ecteinascidia thurstoni. Proceedings of the 30th Annual Research Conference in Pharmaceutical Sciences. December 6-8, 2013. Faculty of Pharmaceutical Sciences, Chulalongkorn University, Bangkok, Thailand. P.8-11.